A STUDY OF ELLIPTICAL AND CIRCULAR JETS AT THERMODYNAMIC SUBCRITICAL AND SUPERCRITICAL CONDITIONS

A Thesis submitted
in partial fulfillment for the Degree of

Doctor of Philosophy

by

C. K. MUTHUKUMARAN

Department of Aerospace engineering

INDIAN INSTITUTE OF SPACE SCIENCE AND TECHNOLOGY

THIRUVANANTHAPURAM

AUGUST, 2016

To my parents

CERTIFICATE

This is to certify that the thesis entitled **A Study of Elliptical and Circular Jets at Thermodynamic Subcritical and Supercritical Conditions**, submitted by **C. K. Muthukumaran**, to the Indian Institute of Space Science and Technology, Thiruvananthapuram, in partial fulfillment for the award of the degree of **Doctor of Philosophy**, is a *bonafide* record of the research work done by him under my supervision. The contents of this thesis, in full or in parts, have not been submitted to any other Institute or University for the award of any degree or diploma.

Dr. Aravind Vaidyanathan
Supervisor
Department of Aerospace
engineering

Place: Thiruvananthapuram
August, 2016

Counter signature of Head,
Department of Aerospace engineering with seal

DECLARATION

I declare that this thesis entitled **A Study of Elliptical and Circular Jets at Thermodynamic Subcritical and Supercritical Conditions** submitted in partial fulfillment of the Degree of Doctor of Philosophy is a record of original work carried out by me under the supervision of **Dr. Aravind Vaidyanathan**, and has not formed the basis for the award of any other degree or diploma, in this or any other Institution or University. In keeping with the ethical practice in reporting scientific information, due acknowledgements have been made wherever the findings of others have been cited.

C. K. Muthukumaran

SC10D005

Place: Thiruvananthapuram
31/08/2016

ACKNOWLEDGEMENTS

First I express my sincere gratitude to my research supervisor Dr. Aravind Vaidyanathan for his valuable guidance and infinite patience on the path towards my Ph.D. His moral support and encouragement during the ups and downs of my research time were very helpful. Also, I would like to thank him for introducing me to PLIF and various optical diagnostic techniques that I needed for this work and future works.

I am highly indebted to my doctoral committee members Prof. Job Kurien, IIT Madras, Dr. P. Balachandran, LPSC-ISRO, Valiyamala, Prof. K. Kurien Issac, IIST, Prof. A. Salih, HOD, Dept. of Aerospace engineering, IIST, Dr. M. Deepu, IIST for reviewing and providing suggestions to improve my work. I also thank Department of Space, Government of India, for providing me IIST-ISRO Research Fellowship.

I am very thankful to late Shri. M. K. A. Kurup and Shri. Thomas Varghese for providing me valuable suggestions regarding the construction of the experimental facility. I thank APLD lab technician and my friend Shri. R. R. Vinilkumar for helping me during the design and construction of experimental facility. I also thank the technicians of manufacturing lab, IIST for their help during the construction of the experimental facility.

I am grateful to all my teachers who laid the foundation of knowledge and interest in science which are fundamental to pursue my research work. My special thanks to all my friends who made this long stay at IIST a fruitful one. I thank my friends Dr. M. Srinivasa Raju and Shri. Rahul Waghmare for their suggestions in Matlab and thesis writing. At this point, I am highly thankful to the friends who stood beside me during the critical times of my Ph.D.

More importantly, I acknowledge my parents and my sisters for their love and care. The support and strength provided by my father (C Krishnan) and mother (K Chitra) during my personal difficulties are invaluable. Their motivation was essential at some point in time during my research period without which I would not have survived and progressed to the present level.

C K Muthukumaran

ABSTRACT

The study of fluid jet is one of the interesting areas in the field of fluid mechanics. The study finds various applications in engineering field such as spray painting, ink-jet printing and spray combustion. Early studies on the fluid jet are focused on understanding the fluid dynamic behavior of the jet with the injection and the ambient conditions being atmospheric, and the thermophysical properties are constant throughout the process. In some applications, the chamber conditions are quite different than that of the injectant conditions, more often it is at high temperature and pressure. In diesel and rocket engines, the chamber conditions are often supercritical for the fuel to be used. This requires understanding of the fluid jet behavior at higher pressure and temperature conditions.

Below the critical temperature, the fluid exists in liquid and vapor phases. As the temperature and pressure reach the critical point, the distinction between the liquid and vapor phase disappears, and the fluid exists in single homogeneous fluid phase known as the supercritical fluid. Various thermodynamic anomalies such as the absence of surface tension, larger heat capacity and very low thermal diffusivity exist near the critical point. The liquid jet injected into supercritical chamber condition is subjected to large changes in thermophysical properties; hence the study involves the strong dependence between the fluid dynamic and thermodynamic processes.

The surface tension is considered to be the most important property that decides the two phase and single phase mixing characteristics of the fluid jet. The presence of surface tension in the case of liquid-gas interface leads to a distinct interface of the liquid jet, and the mixing occurs through atomization process followed by evaporation. In the case of gas-gas mixing, there is no distinct interface due to the absence of interface tension and results in diffusional mixing.

In the present work, the investigation is carried out with the elliptical jet as well as the circular jet at subcritical to supercritical conditions. In the past, most of the studies on the fluid jet at supercritical condition is carried out with the circular jet. The studies revealed the absence of droplet formation as the liquid jet is injected into its supercritical environment. The droplet formation in the case of circular jet involves the combined influence of surface tension as well as aerodynamic shear stresses. The elliptical liquid jet at atmospheric condition exhibits axis-switching characteristics only due to the effect of surface tension. To isolate and study the effect of surface tension, the experiments are carried out with the elliptical jet at supercritical condition in binary component system (N_2 or He environment) as well as in single component system (own environment). In N_2 environment, the fluoroketone elliptical liquid jet is investigated at chamber conditions that vary from subcritical to supercritical condition. In the N_2 environment, it is observed that the fluoroketone elliptical jet exhibits axis switching even at supercritical conditions. However, at its own supercritical environment, the injected jet does not exhibit axis switching.

For supercritical injection conditions, the density map of the 2-d center plane of the jet is obtained using Planar Laser Induced Fluorescence (PLIF) technique. The injec-

tion pressure plays a major role in the thermodynamic transition of near critical jet at subcritical chamber condition. At subcritical pressure, the near critical jet is comprised of a few droplets and vapor. As the pressure become supercritical, the jet behaves as a liquid jet but without axis switching. The supercritical jet injection into subcritical chamber condition results in fewer droplet formation at high chamber pressure due to the higher injectant density of about 550 kg/m^3. At subcritical pressure, the injectant supercritical jet behaves like a gaseous jet. However, above the critical injectant temperature condition, the elliptical jet does not undergo axis-switching. The injection of the supercritical jet into supercritical chamber condition exhibit the behavior similar to that of variable density gaseous jet.

The study is also carried out with a circular liquid jet to investigate the interfacial disturbance wavelength, breakup characteristics and mixing behavior for the fluoroketone liquid jet that is injected into N_2 environment as well as into its own vapor at subcritical and supercritical chamber conditions. At subcritical chamber condition, the injected liquid jet exhibits classical liquid jet characteristics with Rayleigh breakup at lower Weber number and Taylor breakup at higher Weber number for both N_2 and its own environment. In its own environment at supercritical pressure and temperature conditions, the injected liquid jet undergoes a gradual thermodynamic transition to supercritical fluid phase with single phase mixing characteristics. However, the supercritical chamber condition with N_2 as ambient fluid does not have a significant effect on the thermodynamic transition of the injected liquid jet. The fractal dimension of the jet is examined to study the interfacial corrugations that are responsible for the mixing process. The fractal dimension of the jet exceeds the value of 1.3 as the chamber pressure and temperature becomes supercritical for the pure component system.

The study is also performed for near critical and supercritical circular jets injected into subcritical to supercritical chamber condition using PLIF technique to obtain the density and density gradient field of the jet. The thermodynamic transition of the jet is analyzed using density and density gradient field maps. The fractal analysis of the supercritical jet is also performed to investigate the evolution of the jet boundary in detail. The results indicated that the thermodynamic transition of the injected supercritical jet to liquid phase under subcritical chamber conditions never occurred in both nitrogen and helium chamber environments; the reason is attributed to the lower injectant density of the supercritical jet. The fractal nature of the jet is also investigated and the jet boundary possesses fractal dimensions between 1.25 and 1.35.

TABLE OF CONTENTS

DESCRIPTION **PAGE NUMBER**

LIST OF FIGURES

LIST OF TABLES

ABBREVIATIONS

CCD	Charge Couped Device
FK	Fluoroketone
IC	Internal Combustion
ID	Inner diameter
K-H	Kelvin-Helmholtz
LED	Light Emitting Diode
Nd-YAG	Neodymium-doped Yttrium Aluminium Garnet
NI	National Instruments
NPT	National Pipe Thread Taper
OD	Outer diameter
PID	Proportional-Integral-Derivative
PRSV	Peng-Robinson-Stryjek-Vera
PLIF	Planar Laser Induced Fluorescence
SS	Stainless steel
UV	Ultraviolet
VDC	Volts Direct Current

NOMENCLATURE

a	Radius of the jet
Co_2	Carbon dioxide
D	Diameter, m
D_{eq}	Equivalent Diameter, m
D_f	Fractal Dimension
Fr	Froude number
He	Helium
I	Modified Bessel function of the first kind
J	Joule
K	Modified Bessel function of the second kind
k	Complex non-dimensional wave number
k_r	Non-dimensional spatial oscillation
k_i	Non-dimensional spatial growth rate
m	meter
mm	millimeter
ms	millisecond
$mrad$	milli radians
μs	microsecond
N_2	Nitrogen
ns	nanosecond
M	Mass flow rate, g/s
n	Number density of molecule
Oh	Ohnesorge number
P	Pressure, bar
P_c	Critical pressure, bar
P_r	Reduced chamber pressure, $P_r = P_{chamber}/P_c$

P_i	Reduced injection pressure, $P_i = P_{injection}/P_c$
psi	pounds per square inch
Q	Ratio of Ambient fluid density to Injectant fluid density
Re	Reynolds number
T	Temperature, $Kelvin$
T_c	Critical temperature, $Kelvin$
T_r	Reduced chamber temperature, $T_r = T_{chamber}/T_c$
T_i	Reduced injection temperature, $T_i = T_{injection}/T_c$
V	Velocity, m/s
L_b	Breakup length, m
We	Weber number
We_p	Calculated Weber number based on λ_m

Greek symbols

λ	Wavelength, m
λ_m	Measured wavelength, m
λ_{as}	Axis switching wavelength
μ	Viscosity, Ns/m^2
ρ	Density Kg/m^3
ρ_{grad}	Density gradient, Kg/m^4
ρ_g	Density of gas or vapor, Kg/m^3
ρ_l	Density of liquid, Kg/m^3
σ	Surface tension, N/m
ω	Complex non-dimensional temporal oscillation
ω_r	Non-dimensional temporal oscillation
ω_i	Non-dimensional temporal growth rate

Subscripts

c	critical condition
r	reduced chamber condition
i	properties at injection
0	Zeroth order
1	First order

CHAPTER 1

INTRODUCTION

In this chapter, a brief introduction to the mechanism of liquid jet breakup process, the associated instability and various regimes of breakup process are presented. The thermodynamic supercritical condition is introduced. The necessity for the experiments on the liquid jet at the thermodynamic supercritical condition is discussed in the context of rocket and diesel engine applications. Finally, the motivation for carrying out the current study is also presented.

1.1 Introduction

The study of fluid jet disintegration or breakup has been an interest to the researchers of fluid mechanics for more than a century. There are various fluid dynamic forces that are responsible for the breakup of the liquid jet. Understanding of the liquid jet dynamics is very important in various engineering fields. The conventional liquid jet breakup and the atomization process lead to spray formation which enables uniform spreading and distribution of the fine sized droplets. This meets the requirement of many applications such as spray painting, distribution of insecticide in the agricultural field, etc. In some applications like Ink-jet printing process, the liquid jet is externally subjected to an instability and results in monodisperse droplet formation which meets the requirement of quality printing. In the above-mentioned applications, the injection and the ambient temperature conditions are quite similar and the flow physics involved pertains to the fluid dynamic processes.

The pressure and temperature conditions in which a process takes place are very important in deciding the nature of the interfacial instability as well as the universal behavior of jet mixing. In certain applications such as in the field of automobile engineering, atomizers are used to form a fuel-air mixture of specified ratio, necessary for the operation of IC engines. The goal of spray formation is the production of a large surface area to aid in higher evaporation rate. The mixing of fuel jet in the ambient gas relies on the evaporation process. At subcritical temperature and pressure conditions, there exists a sharp distinction between the liquid and the vapor phases; the interface is characterized by the presence of surface tension. The physical processes of the droplet interior and the ambient gases are evaluated separately and then matched at the interface by requiring liquid-vapor phase equilibrium and continuities of mass and energy fluxes (Yang, 2000). This procedure eventually determines the droplet surface conditions and the evaporation rate.

The aforementioned processes take place under the temperature and pressure conditions that are well below the thermodynamic critical point of the injected fluid. The situation, however, becomes qualitatively different in the supercritical regime. In certain applications like those in diesel and rocket combustion chambers, the pressure and temperature conditions often reach the supercritical state for the fuel under consideration. Beyond the critical point, the liquid-vapor distinction ceases to exist, and the state of the fluid is neither a gas nor a liquid and is termed as the supercritical fluid. At this state, the effect of surface tension is absent and the process associated with evaporation is non-existent. Under such condition, the mass transport occurs purely through the mass diffusion process. Also, there are various anomalies that exist in the vicinity of the critical point and need to be understood for efficient design of the injectors at supercritical conditions.

Many of the earlier studies conducted on the liquid jets are mostly at subcritical conditions where the studies focused on understanding the jet behavior in which the thermophysical properties are constant. However, in certain application such as in rocket engines, the injectant state of the fuel is subcritical whereas the chamber condition is supercritical to the injectant fluid. The injectant fuel/fluid is continuously subjected to variations in the thermophysical properties such as surface tension, viscosity and thermal conductivity. Hence, there is a strong coupling between the fluid dynamic and the thermodynamic processes.

In order to efficiently design an injector and the combustion chamber of the rocket engines, a thorough understanding of the fluid dynamic as well as the thermodynamic aspect of the jet behavior is mandatory. Also, the investigation on the liquid jet dynamics at supercritical conditions is necessary for enhancing the design database of the combustion chamber. Many of the previous works were related to the studies on droplet at supercritical conditions (Givler and Abraham, 1996). Understanding the behavior of droplets at supercritical conditions is necessary since the spray formation results in fine sized droplets. Later the experiments are also initiated with the study of liquid jet behavior at the supercritical chamber conditions (Givler and Abraham, 1996). The modeling of the jet at supercritical conditions is always challenging and it requires experimental data (Bellan, 2000). The injection of a liquid jet into the supercritical conditions involve large changes in the thermophysical properties. Due to the various anomalies that exist near the thermodynamic critical point, studies involving comprehensive and detailed experimentation are necessary.

Early studies on jet injection into supercritical condition were initiated by Newman and Brzustowski (1971). The authors performed studies on the injection of liquid CO_2 into the thermodynamic critical conditions with surrounding gas as the mixture of N_2 and CO_2 at various compositions. As the temperature reached the critical point, finer spray with smaller droplets is observed. Mayer et al. (2000) investigated the behavior of single and coaxial jet from subcritical to supercritical conditions and found that beyond the critical pressure, the interface of the jet exhibited streaky-like appearance and a change in the atomization process was also observed. Several notable investigations are carried out by Chehroudi et al. (2002b), Chehroudi et al. (2002a) to understand the physical mechanism as well as the characteristic feature of the supercritical jet. Their study focused on the injection of liquid N_2 into gaseous N_2 at subcritical and supercritical conditions. Their research work revealed that the supercritical jet exhibited characteristic features similar to the variable density gaseous jet. To examine the mixing layers in detail, the fractal nature of the jet was also studied by Chehroudi et al. (1999) . An extensive review on various models utilized for drops and jets at supercritical conditions is presented by Bellan (2000) and it is found that there are insufficient experimental data available to have complete understanding and achieve accurate modeling of the jet behavior at supercritical conditions. A detailed discussion on the key experimental findings is carried out by many researchers, and they focused on the behavior and the structure of the single and coaxial jet at supercritical conditions (Oschwald et al., 2006) (Chehroudi, 2012). The discussion also brought out major experimental efforts in the recent decades in characterizing supercritical jets. Some of the recent works were carried out by applying planar laser induced fluorescence (PLIF) technique to study the mixing characteristics of a supercritical jet. The notable studies investigated the behavior of a subcritical fluoroketone round jet injected into chamber conditions that varied from subcritical to supercritical (Segal and Polikhov, 2008) (Roy and Segal, 2010). The studies indicated that beyond the critical pressure and temperature, the jet exhibited supercritical behavior with the absence of droplet formation.

Initial studies on fluid jet at supercritical conditions considered the chamber conditions to be supercritical and the injectant conditions were at liquid state. The need for the study of a jet at supercritical injected condition and the subcritical chamber condition has become an increasingly important area of research work. In emerging technologies such as those involving heat transfer from the airframe of supersonic ramjet and hypersonic flights, the endothermic fuel is under consideration as a heat absorbing medium (Wu et al., 1999). In rocket engines, the hydrogen after passing through the regeneration coolant passage becomes supercritical and gets injected into supercritical chamber conditions. Also, the application of formation of solute nano-particles from the rapid expansion of supercritical fluid solution (RESS) into subcritical condition is of great interest since the process utilizes the dramatic change in the dissolving power of the solvent (Lin et al., 2006) (Matson et al., 1987). Recently, the investigation of supercritical jet injected into subcritical conditions using PLIF is conducted by Roy et al. (2013). This study revealed the presence of formation of droplets at the jet interface and it indicated that the effect of surface tension becomes obvious at subcritical chamber conditions. .

Much of the studies in the past were focused on the circular jet at supercritical conditions. There is hardly any study that is conducted to understand the behavior of the non-circular jets at supercritical chamber conditions. However, under atmospheric condition, several studies were focused on fluid jet issued from a non-circular orifice to investigate the effect of asymmetry on the entrainment and the mixing characteristics of the jet. Next to circular jets, the elliptical jets are well explored for both the single phase and two phase cases. For the case of two phase elliptical jet, in which a liquid jet is issued into the ambient gas, there exists a distinct interface that is characterized by the presence of surface tension. The behavior of the liquid elliptical jet was earlier studies by Plateau (1873) and Rayleigh (1889). The elliptical jet is found to exhibit axis switching phenomenon and it is found to be due to the effect of surface tension (Bohr, 1889). Hoyt and Taylor (1978) performed experimental investigation on axis-switching phenomenon for a high speed elliptical liquid jet at high Reynolds number. There are several studies which relate the axis-switching length to the surface tension of the liquid jet (Bohr, 1889), (Bechtel et al., 1995). The axis switching characteristics of the liquid jet at low velocity under atmospheric condition is investigated experimentally by Kasyap et al. (2009). The authors related the axis switching length with the Weber number (We) of the jet. Later, Amini and Dolatabadi (2012) made temporal stability analysis on elliptical jet of small aspect ratio, and found a linear relationship between the axis switching length and the square root of Weber number. The analysis of Amini and Dolatabadi (2012) agreed well with the experiments of Kasyap et al. (2009).

The studies of gas jet emanating from the elliptical orifice also have been carried out by many researchers because of its application in the high performance aircrafts due to its advantage in noise reduction. The elliptical gas jet possesses enhanced entrainment and mixing characteristics as compared to that of a circular jet (Abdel-Hameed and Bellan, 2002). It is experimentally observed that the gaseous jet could also exhibit axis-switching even though the mechanism is quite different from that of liquid jets. It is observed that the incompressible elliptical gaseous jets exhibit axis switching due to azimuthal curvature variation of the vortical structure (Hussain and Husain, 1989). However, for the gaseous jets where the surface tension is absent, the axis switching occurs only once, after which the jet flattens into a sheet perpendicular to the major axis of the orifice (Bechtel, 1989).

It could be understood that the existence of secondary flows in non-circular jets such as the existence of the axis switching phenomenon of the elliptical jet would further reveal the thermodynamic transitional characteristics of the jet at supercritical conditions. The fundamental difference in the mixing characteristics of the two phase jets from a single phase jets is due to the presence of the effect of surface tension. The transition in the surface tension of the elliptical jet could be revealed more clearly than that of the circular jet due to the existence of axis switching phenomena. Though the fluid dynamics associated with the elliptical jet is more complex than that in the circular jets, the axis switching phenomenon of the elliptical jet would reveal the transitional nature of the surface tension effects. However, the circular jet is axi-symmetric and there is hardly any secondary flow characteristics; hence it would be difficult to study any transition related to the surface tension effects in isolation. Therefore in the present experimental work, it is proposed to carry out the investigation of the axis switching characteristics of the elliptical jet in precedence to the detailed investigation of the circular jets.

1.2 Motivation

The present work aims at understanding the transition in the characteristics of the fluid jet at subcritical to supercritical condition. In order to investigate the onset of interfacial instability and the mixing characteristics of the injected jet, the experiments are conducted at laminar regime and the regime closer to turbulent. The term supercritical is defined with respect to the temperature condition of the injectant fluid.

For a single component system, for a given mass of fluid substance to occupy a constant volume, the supercritical pressure and temperature conditions can be achieved from a subcritical pressure and temperature condition, only by increasing the temperature of the fluid. When the temperature is increased, the pressure gets increased and the fluid transform from the liquid-vapor coexistence state to a supercritical state. Thus for this reason, throughout the thesis, the chamber or the injected jet state is referred to supercritical when the temperature is supercritical. However, the complete supercritical condition implies that the both the temperature and the pressure are supercritical. In the present work, since the behavior of the injected jet is investigated at varied chamber conditions, supercriticality is defined with respect to the temperature condition of the injected jet fluid.

Experiments are performed for single component as well as binary component system. For the case of single component system, the injected jet and chamber fluids are similar; fluoroketone. Whereas for the binary component system, the injected fluid is fluoroketone and the chamber fluid is either N_2 or He. The transitional nature of the injected jet is studied through investigating the visual structure of the jet, obtaining the density map of the jet and performing linear stability analysis and fractal analysis of the jet. The experiments utilise backlighting technique as well as PLIF technique for visualising the jet. The axis switching length of the elliptical jet is analyzed to understand the nature of transition of the jet; using PLIF technique the two dimensional center plane of the jet is captured along with density details. Through linear stability analysis the transition in the surface tension property of the circular jet is investigated. The single phase and the two phase mixing characteristics of the jet is studied by performing the fractal analysis of the jet; also the interfacial corrugations of the jet is studied in detail using fractal analysis.

1.3 Thesis outline

A brief introduction to the jet mixing at supercritical condition was presented in this chapter (1) along with the motivation for the current study.

In chapter 2, the detailed literature review pertaining to the study of jet at subcritical and the supercritical condition is discussed. The various anomalies related to the supercritical jet mixing are discussed in detail. Also the challenges that are presently existing in modeling of the supercritical jet mixing is explained. Finally the scope and the objective of the current study is presented.

In chapter 3, the experimental details are presented. Various components of the experiments such as high pressure chamber, heating system, pressure and temperature sensors, mass flow measurement system and the data acquisition system are discussed in detail. Also the visualisation techniques like backlight imaging and PLIF measurements are described in detail.

In chapter 4, the detailed investigation of the elliptical jet at subcritical to supercritical condition is presented. Experiments are carried out to investigate the axis switching characteristics of an atmospheric-condition elliptical liquid jet injected into supercritical chamber conditions. The study is performed for single component system as well for binary component system. Also the study is carried out with supercritical and near-critical jet injected into subcritical and supercritical chamber condition to obtain density field of the jet using PLIF technique.

In chapter 5, the detailed investigations on the various regimes of breakup characteristics of circular jet are carried out. The liquid jet from a circular orifice is injected into subcritical or supercritical chamber filled with N_2 or its own vapor. The disturbance generated on the jet by the injection produces a wave at the jet interface; the jet interface is analysed in detail to understand the jet behavior. Also, the fractal dimension of the jet is analysed to investigate the mixing nature of the jet. For near-critical and supercritical injection condition, the experiment is performed using PLIF technique to obtain the density and the density gradient field of the jet.

In chapter 6, the major conclusions from the current study are presented.

CHAPTER 2

LITERATURE REVIEW

In this chapter, a detailed introduction to literature related to the study of liquid jets at atmospheric condition is discussed. The topic includes the different regimes of jet breakup and the mechanism of instability of the jet. Subsequently, the thermodynamic supercritical condition is introduced along with the various anomalies in fluid properties. The need for the experimental investigation at supercritical condition is explained. A detailed literature review on the studies related to the droplets, and behavior of the jet at supercritical condition is also carried out. Finally, the scope of the work and objectives are presented.

2.1 Introduction

When a liquid jet emanates from an orifice into a quiescent gaseous environment, as it travels downstream it preserves the shape of the orifice exit with a distinct interface for a certain distance. The interface separates the injected liquid from the ambient medium; the interface exists because of the surface tension. Subsequently, the jet breaks up.

The study of liquid jet finds its application in various areas ranging from spray painting to rocket engines. In the case of spray painting process, the liquid jet is injected at very high velocity, thereby resulting in breakup of bulk liquid into fine droplets. The spray painting necessitates the droplet formation to be of fine sized as well as homogeneously distributed in space. However, in some applications such as in crop spraying, the small droplets must be avoided as their settling velocity is very low and it can drift considerably far away in downwind.

The understanding of the liquid jet breakup process is very crucial in certain application like ink-jet printing process. The breakup process of the ink-jet determines the quality of the printing process. The generation and manipulation of the ink drops has fascinated scientists for centuries (Martin et al., 2008). For ink-jet printers using continuous jets, satellite formation must be controlled to avoid disruption of the printing process. For a given ink, satellite formation is normally controlled pragmatically by changing the amplitude of the driving disturbance. This amplitude will change the satellite behaviour, and also changes the distance over which the jet forms into drops, the break-up length. However some non-conventional metal cutting process uses water jet as a tool to cut hard metals. In such applications, the water jet needs to be intact despite high Reynolds number.

The breaking of liquid jet into fine droplets is a purely fluid dynamical process and it tends to increase the surface area of the injectant fluid material. In the case of rocket and diesel engines, the liquid fuel jet is atomized to fine droplets, thereby increasing the surface area for effective combustion process. Thus the study on fluid dynamics of liquid jets not only possess some fundamentally interesting characteristics but is also driven by the requirement to understand the process in numerous engineering applications. Thus the understanding of the fundamental process of liquid jet breakup is important in the field of engineering.

Though there are several studies on the characteristics of the liquid jet from various orifice geometries, the breakup of a liquid jet from a circular orifice has been studied most frequently. There are various fluid dynamic forces that are responsible for the instabilities and breakup mechanism of the liquid jet and are discussed in the following sections. In this chapter, the various regimes of the circular jet breakup and the studies related to the instability analysis of the circular jet are discussed first. Following the discussions on the circular jet, the non-circular jet is introduced and the elliptical jet characteristics are discussed in detail. Then, the supercritical jets are discussed in detail.

2.2 Regimes of circular liquid jet breakup

The fluid dynamic forces play an important role in determining the mechanism of breakup of liquid jets. There are various regimes of circular jet behavior. The flow parameters such as the momentum of the jet and the fluid properties such as viscosity, surface tension and density of the fluid determine the fluid dynamic forces acting on the jet. There are four forces that are acting on the liquid jet. They are: inertial force ($\rho L^2 V^2$), surface tension force (σL), viscous force (μLV), gravity force ($\rho L^3 g$), and are responsible for the breakup of the liquid jets. The ratios of four forces are typically represented as three independent non-dimensional groups: they are Reynolds number Re, Weber number We and Froude number Fr. The other non-dimensional number that is subsequently used is Ohnesorge number Oh which is the ratio of the square root of Weber number to the Reynolds number (Sirignano and Mehring, 2000).

The initial studies on liquid jet breakup date back to Plateau (1873) who conducted his experiments on the instability of liquid cylinder under static condition. He identified the force responsible for such instability as that due to surface tension. The analysis of the liquid jet instability was later performed by Rayleigh (1878) and he pointed out that only the disturbances of certain wavelength possess the maximum growth rate and are enhanced by surface tension. Later Taylor (1940) incorporated the effect of aerodynamic force acting on the interface of the liquid jet. He observed that as the velocity of the jet is increased, the short wavelength disturbance possessed the maximum growth rate. The significant role of ambient gas density in determining the wavelength of the disturbances on the surface of the jet is also identified. There are various non-dimensional numbers that are used in the study of liquid jets to understand the relative magnitude between the various forces (Chigier and Reitz, 1996). The We is meaningful when the effect of viscosity is not significant and the breakup mechanism is only determined by the surface tension and the inertial force. The Weber number (We) is the ratio of the inertial force to

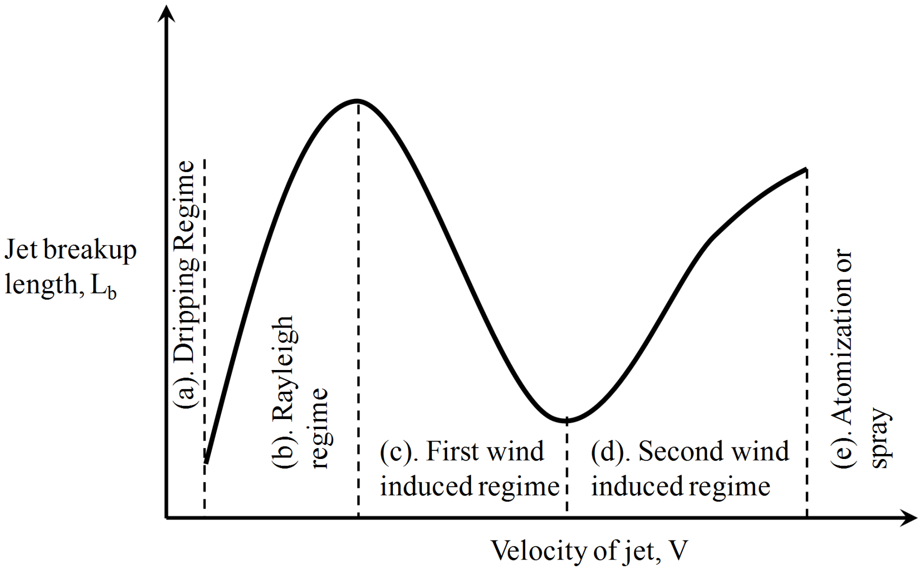

Figure 2.1 Various regimes of circular liquid jet breakup based on velocity and breakup length of the jet.

the surface tension force. The We is defined in eq. 2.1.

$$We = \frac{\rho V^2 a}{\sigma} \tag{2.1}$$

where ρ is the jet density, V is the velocity of the jet, a is the radius of the jet and σ is the surface tension of the jet.

In a viscous jet, the viscosity has the effect of damping the growth rate, and the disturbance wavelength of maximum growth rate tend to be longer than that of the inviscid liquid jet. The viscous jet is characterised by Reynolds number (Re) which is the ratio of the inertial force to the viscous force and is defined in eq. 2.2.

$$Re = \frac{\rho V a}{\mu} \tag{2.2}$$

where μ is the viscosity of the jet fluid.

In order to understand the time scale of a jet breakup, the Ohnesorge number is also used (McKinley and Renardy, 2011). The Ohnesorge number is the ratio

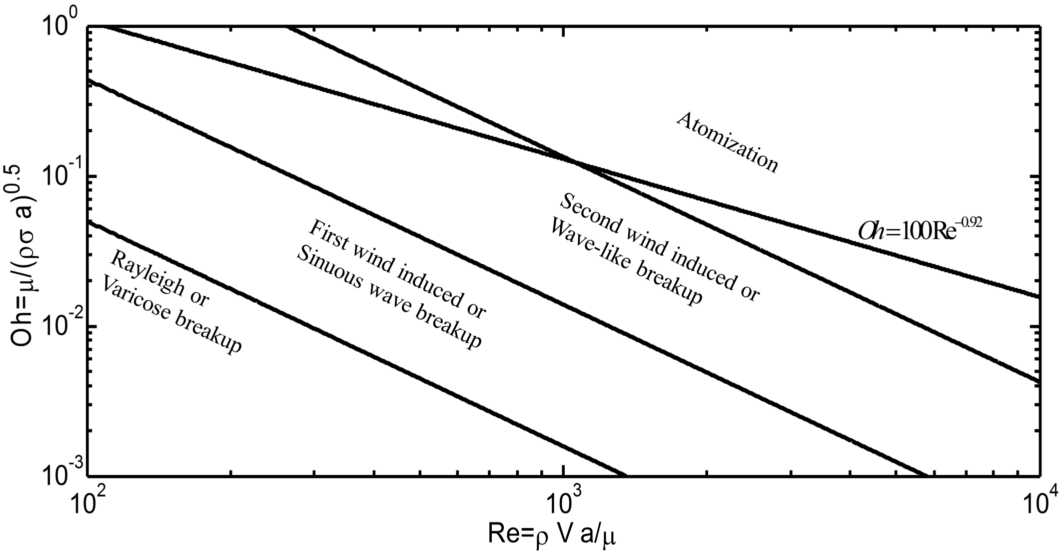

Figure 2.2 Various regimes of circular liquid jet breakup delineated in Re-Oh phase space.

of the viscous force to the product of the inertial force and the surface tension. In other words, the Ohnesorge number is a ratio of the visco-capillary time scale to the Rayleigh time scale which characterises the thinning dynamics of viscous threads. The expression of Ohnesorge number is:

$$Oh = \frac{\mu}{\sqrt{\rho a \sigma}} = \frac{\sqrt{We}}{Re} = \frac{\mu a/\sigma}{\sqrt{\rho a^3/\sigma}} \tag{2.3}$$

For given fluid properties such as viscosity and surface tension, the injected jet velocity determines the regime of jet characteristics. Fig. 2.1 illustrates the various regimes of jet characteristics based on the breakup length and the injectant velocity. Fig. 2.2 describes the various regimes based on the non-dimensional numbers, Re and Oh.

2.2.1 Dripping regime

Dripping is a phenomena in which the individual liquid drops emanate from the nozzle exit. This occurs when the surface tension force is greater than the inertia possessed by the liquid stream. As the liquid mass flow is increased from zero, the dripping of the liquid drops could be observed at the orifice exit. The dripping pattern can be observed only at very low Weber number or injectant velocity as indicated in fig. 2.1. Below a certain critical Weber number, the momentum possessed by the liquid mass flowing inside the nozzle is very low. Once the flowing liquid mass reaches the exit of the nozzle, it starts accumulating and forms a drop. Beyond the critical Weber number the transition from dripping to jetting process occurs (Ambravaneswaran et al., 2004).

2.2.2 Rayleigh regime

At low Weber number, the liquid jet is subjected to an instability as it emanates from the nozzle. In the case of a circular orifice, the liquid jet is initially cylindrical and at a certain downstream distance it is subjected to the growth of unstable waves at the jet surface. These unstable waves are axisymmetric and generally occur in the longitudinal direction, grow in the downstream direction and eventually lead to the formation of drops with sizes of the order of jet diameter. The first theoretical analysis of the instability of the circular liquid jet was performed by Rayleigh (1878). The analysis of Rayleigh indicates that among all unstable disturbances, the jet is more susceptible to the disturbance with wavelength 143.7 times the circumference, and finally causes the liquid jet to breakup into droplets. This phenomena occurs only at sufficiently small We and is termed as the Rayleigh regime. Within the Rayleigh regime, the breakup length of the jet is observed to increase as the Weber number increases (Lin and Reitz, 1998) as shown in figs. 2.1 and 2.2.

2.2.3 First wind induced regime

Further increase in the We results in the decrease in the breakup length of the jet as shown in fig. 2.1, and is termed as the first wind induced regime. Even in this regime, the resultant drop formation is of the order of the jet diameter. The decrease in the breakup length (L_b) is attributed to the effect of the flow on the growing disturbances at the jet surface. Further increase in the We results in the pinching of small droplets from the surface of the jet. This regime of jet breakup is termed as the second wind induced jet breakup. In this regime, the droplets are formed at the jet interface due to the strong shear stress caused by the aerodynamic effect.

In the first wind induced regime, the asymmetric perturbation growth becomes possible due to the significant aerodynamic effect on the jet. The surrounding gas effect produces irregular weaving on the jet surface and results in decrease in the breakup length of the jet as the velocity is increased. The size of the droplets produced is not organised as observed in Rayleigh regime and the drops are slightly smaller than those in the Rayleigh regime.

The first wind-induced regime occurs when the surrounding gas inertia force is approximately one-tenth of the surface tension force; these two forces are of the same order of magnitude in the second wind-induced regime. Lin and Creighton (1990) calculated the energy budget of a disintegrating liquid jet based on the spatial linear stability theory. It was revealed that in the Rayleigh and the first wind-induced regimes, the capillary pinching still remains the governing mechanism of jet breakup, and the term associated with surface tension is always dominant.

2.2.4 Second wind induced regime

In the second wind induced regime, the inertia of the jet overcomes the aerodynamic shear and the jet breakup length again increases with jet velocity. In addition to the liquid flow turbulence, the aerodynamic effect results in higher growth rate of occurring perturbations. The liquid jet shape is chaotic from the nozzle exit and the droplets are pinched from the surface of the jet. Farther downstream, the intact core of the jet breaks down into large fragment of liquid that further undergo secondary breakup.

2.2.5 Taylor regime or atomization

At higher We, the jet breakup into fine droplets occurs immediately as the jet exits the orifice. Due to the strong flow effects, the jet breaks into fine droplets whose size is much smaller than the jet diameter. This regime is referred to as the Taylor mode of breakup and is typically associated with atomization or spray formation. The atomization regime is characterized by primary and secondary breakup processes. In the primary breakup process, the liquid jet is distorted as it leaves the nozzle exit and the liquid fragments are pinched from the main jet. These fragments further undergo distortion due to the aerodynamic effects and break down into smaller fragments. The fragmentation continues until the surface tension is strong enough to overcome the distortion due to the aerodynamic effects, and eventually fine-sized stable droplets are produced, having sizes much smaller than the jet diameter.

The nozzle that injects the liquid at such high velocity is generally designated as an atomizer. The function of an atomizer is to disintegrate the bulk liquid into fine droplets. However the spray characteristics also include cone angle, penetration, radial liquid distribution and circumferential liquid distribution. In many applications, the primary purpose of the atomization is to increase the surface area and thus enhance the evaporation process. The ensemble of drops resulting from atomization is termed as a spray. The minimum energy required for an atomization process can be expressed as a product of the surface tension and the increase in surface area. In the atomization process the Weber number is an important non-dimensional number to characterize the drop size data (Lefebvre, 1988).

The effect of viscosity is not only to affect the drop size distribution but also the spray pattern. An increase in viscosity lowers the Reynolds number and hinders any natural instability formation on the liquid jets. The combined effect of increased surface tension and the increased viscosity leads to increased size of the droplets in the spray. Extensive amount of research has been carried out in this area to understand the aforementioned phenomena (Lin and Reitz, 1998). The regimes

Disintegration regime	**We criteria**
Dripping regime	$We < 4$
Rayleigh regime	$We < 4, QWe < 0.6 + 2.5Oh^{0.9}$
First wind induced regime	$0.6 + 2.5Oh^{0.9} < QWe < 6.5$
Second wind induced regime	$6.5 < QWe < 20.15$
Atomization regime	$QWe > 20.15$

Table 2.1 Criteria for obtaining various regimes of jet breakup Dumouchel (2008).

of jet breakup process and their associated criteria were investigated experimentally by Dumouchel (2008) based on We, as it is presented in table 2.1.

2.3 Instability analysis of circular liquid jets

The study on liquid jets dates back to Plateau when he observed a cylindrical liquid column becoming unstable and finally breaking into an array of droplets. Plateau (1873) performed the experiments in a static condition by placing the olive oil between two disks that are immersed in a mixture of water and alcohol to neglect the effect of gravity, and the distance between the disks was increased in the horizontal direction so that a liquid cylinder of olive oil was formed between the disks. He observed that as the disks are moved apart, the length of the liquid cylinder increases. He found that as the length of the liquid cylinder exceeds three times of its diameter, the liquid cylinder becomes unstable. He also explained that the static instability phenomena is similar to the liquid jet instability when the effect of gravity is neglected (Plateau, 1873). Later Rayleigh (1878) performed an extensive theoretical analysis on liquid jet instability. He described that the instability of the liquid jet leads to droplet distribution along its length, and the droplet size depends on the peculiarities of the small displacements in the radial direction of the liquid cylinder. He explained that the driving force of the instability is the potential energy of the capillary force, as it tends to minimize the surface area by forming droplets. Rayleigh's insight into the problem is profound, such that he could relate the acoustic disturbances to the various modes of liquid jet instability (Rayleigh, 1878). He demonstrated using instability analysis that only the disturbances of certain wavelength amplify rapidly. He could show theoretically that the wavelength of disturbance with maximum growth rate corresponds to 1.437 times the circumference of the liquid jet. Rayleigh performed temporal instability analysis on the nature of instability by only considering the effect of surface tension and by neglecting the effect of viscosity, ambient medium and gravity.

The effect of viscosity on the stability of the liquid jet is first investigated by Rayleigh (1892). Tomotika (1935) reported that an optimal ratio of viscosities of the jet and the ambient fluid exists for which a disturbance of finite wavelength attains the maximum growth rate. The effect of viscosity is considered mathematically by Chandrasekhar (1970) and his analysis showed that the viscosity tends to decrease the jet breakup length, and also increases the resultant droplet size. The effect of the density of the ambient gas on the liquid jet stability was studied by Weber (1931); however, his theoretical prediction did not match with the experiments and the predictions were later improved by Sterling and Sleicher (1975). As the jet Reynolds number increases, there will be aerodynamic shear force that may assist the instability and breakup of the jet. Taylor (1940) also showed that the inertial force of the ambient gas has the profound effect on liquid-gas interface and results in formation of fine droplets.

An extensive set of experiments on liquid jet instability was performed by Donnelly and Glaberson (1966) with water and glycerine mixture as liquid jet. Audio disturbances of various frequencies were induced and the growth rate of the disturbances were obtained. Their experimentally obtained dispersion relation agreed well with the theoretical prediction of Rayleigh (1879) and Chandrasekhar (1970). When a jet is subjected to a broad range of disturbance frequencies with equal amplitudes, only a particular mode with maximum growth rate causes the formation of droplets. The jet left to itself does not typically exhibit a completely regular breakup corresponding to maximum instability. The satellite droplets formed from the ligament between two main drops are not predicted by linear theories; however the mechanism of the satellite formation is still considered to be caused by capillary pinching of the Rayleigh mode (Donnelly and Glaberson, 1966).

Following Rayleigh's work numerous studies were performed to understand the mechanism of instability of the circular liquid jets and its breakup characteristics. Keller et al. (1973) performed spatial instability analysis of the liquid jet in air where the disturbance spatially grows along the jet downstream, and also reported the absence of temporal growth rate. The authors found from their spatial instability analysis that the jet has an infinity of unstable modes for the axially symmetric case. Also, it is found that both spatial and temporal instability yield similar results for $We >> 1$. The effect of viscosity on the capillary instability of the liquid jet is examined in detail by Leib and Goldstein (1986). Their analysis resulted in identifying the critical Weber number above which the jet exhibited convective instability that depended on the Reynolds number of the jet. Later, the effect of ambient gas on the absolute instability of a viscous liquid jet was examined by Lin and Lian (1989). The critical Weber number above which the instability is convective and below which it is absolute was determined as a function of Reynolds number and density ratio. The mechanism of atomization of liquid jet is studied by Reitz and Bracco (1982) and the investigation suggests that at high Reynolds number the atomization is affected by the combined action of the liquid-gas interaction and nozzle geometry. Lin and Kang (1987) extended the analysis made by Taylor (1940) for the spatially growing disturbances. In their analysis, the authors found that the atomized droplet size is inversely proportional to the square root of the jet velocity. Also, a sufficiently large initial amplitude disturbance at the nozzle exit is essential for the onset of atomization process. A review on jet breakup by Chigier and Reitz (1996) brought out the presence of various regimes of jet breakup and the underlying physical mechanism. Earlier attempts on growth rate of the asymmetric mode on the liquid jet was carried out by Levich (1962). Later Yang (1992) extended the analysis of Levich (1962) by considering the effect of asymmetric modes in both liquid-gas aerodynamic interaction, and also incorporating the effect in surface curvature term.

2.4 Elliptical liquid jets

The non-circular jets possess several advantages over the circular jets because of its enhanced mixing characteristics. The non-circular orifice geometries that caught the interest of the researchers were the ellipse and various other corner containing geometries such as square, triangle, etc. There are several studies on non-circular jets that are related to both two phase and single phase jet cases. The single phase jets or gaseous jets from a non-circular orifice possess secondary flow features that result in increased entrainment and better mixing. One of the applications of non-axisymmetric nozzles employed in high performance aircrafts leads to noise reduction that is attributed to the flat surface of the jets (Crighton, 1973). Among the non-circular jets, the simple asymmetric jet that is studied extensively in the past is the elliptical jet.

The notable studies on elliptical liquid jet are performed by Rayleigh (1889), Bohr (1889), Taylor (1960), Hoyt and Taylor (1978), Bechtel et al. (1995), Kasyap et al. (2009) and Amini and Dolatabadi (2012) where the investigation was primarily focused on axis switching characteristics of the jet. The axis switching is a result of the secondary flow characteristics that is exhibited due to the effect of geometry on the flow field.

The experimental studies on elliptical gaseous jets performed by Gutmark and Ho (1986), Ho and Gutmark (1987), Hussain and Husain (1989), Zaman (1996) and Gutmark and Grinstein (1999) investigated numerous flow features of non-circular gaseous jets that are fundamentally interesting and find applications in the engineering field. In the following section 2.4.1, the axis switching characteristics of the liquid jets and the gaseous jets are discussed in detail. Also the fundamental difference in the mechanism of axis switching exhibited by the liquid and the gaseous jets are brought out.

2.4.1 Axis switching characteristics in elliptical liquid jets

The fundamental fluid dynamic characteristics of the elliptical jet are different from that of the circular jet. The schematic of a circular and an elliptical jet is presented in fig. 2.3. The liquid jet emanating from the elliptical orifice possesses some interesting geometrical features that caught the attention of some researches. The investigation on liquid jet that emanates from the elliptic orifice dates back to Rayleigh (1889) where he observed the axis switching phenomenon exhibited by the jet as it moves downstream. The axis-switching of the jet is mainly due to the dynamic counteracting effects between the surface tension and lateral inertia of the jet. When the cross-section of the elliptical jet at various downstream distances is investigated, the physical process could be understood. As the elliptical jet leaves the orifice, the cross-section at the exit is elliptical and the surface tension tends to minimize the surface area of the jet. As a result, the elliptical cross-section tends to become circular as it moves downstream. At a particular downstream distance the jet become circular; however, because of lateral inertia the cross-section becomes elliptical with its minor axis being switched to major axis. This phenomenon repeats itself till the jet breakup occurs. This axis switching phenomena is a purely fluid dynamic process that is solely determined by the density and surface tension of the fluid. Rayleigh (1889) developed a mathematical model to calculate the dy-

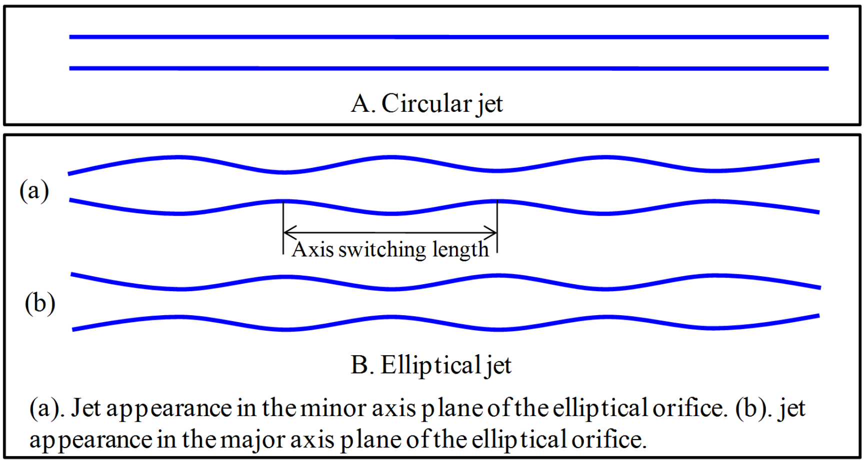

Figure 2.3 Circular and elliptical jet.

namic surface tension of liquids from the axis-switching wavelength of the elliptical liquid jets. This model was further improved by Bohr (1889). Later Taylor (1960) performed experiments with impinging circular jet to produce elliptic sheets and the change in the shape of the jet was nicely sketched by him to illustrate the spatial evolution of the free surface of the jet. Geer and Strikwerda (1983) performed analytical and numerical studies on jets issued from elliptic, square and triangular orifice to understand the evolution of free surface with and without the effect of surface tension. There are several attempts that are carried out to establish the relation between the surface tension and the axis switching wavelength. Bechtel et al. (1995) proposed an inverse model to relate the surface tension and axis switching of the jet using oscillating jet technique.

Recently, the axis switching and breakup of low speed elliptic liquid jet has been investigated by Amini and Dolatabadi (2012). Based on their temporal analysis, the stable modes that cause the axis switching are identified as asymmetric and those corresponding to unstable modes as symmetric. Their analyses show that the axis switching mode or stable mode is propagated at the same phase velocity as breakup mode, i.e., the axis switching of the jet gets altered with the frequency that is equal to the natural frequency of free oscillations. The authors also noted that their theoretical prediction of axis switching is in good agreement with the experimental results of Kasyap et al. (2009). Kasyap et al. (2009) made experimental investigations on flow from an elliptical orifice. They observed a linear relationship between the square root of Weber number and the axis switching wavelength.

The elliptical gaseous jet also exhibit the axis switching behavior, however, the mechanism is quite different from that of the liquid jets. The azhimuthal curvature variation of the vortical structure due to the geometry of the jet causes its non-uniform self induction that results in axis switching phenomenon (Hussain and Husain, 1989), (Zaman, 1996). For the case of gaseous elliptical jets, without the effect of surface tension, the axis switching occurs only once and after this the jet flattens into a sheet that is perpendicular to the major axis of the orifice (Bechtel, 1989). The analysis of Bechtel (1989) predicted that in the presence of surface tension, the elliptical liquid jets undergo axis switching several times before the occurrence of jet breakup. In elliptical gaseous jets, the spreading occurs in both the major axis plane and the minor axis plane. However, the spreading rate in the minor axis plane is larger than that of the major axis plane. This is mainly due to the occurrence of self-induction at the flat surface of the minor axis plane that is typically larger than those in the major axis plane. Due to this, the elliptical geometry of the axis switched cross section of the jet possesses different shape and size as compared to the orifice geometry. In the case of liquid jets, the shape and size of the elliptical geometry is preserved in successive axis switching processes until the disturbances are generated and are also fully evolved at the jet surface.

2.5 Gaseous jets

The mixing behavior of a gaseous jet is fundamentally different from that of the liquid jets. When the injectant and the ambient fluid are of the same phase then the mixing characteristics is termed as single phase mixing characteristics. The interface of the gas jets do not possess surface tension. The diffusion process

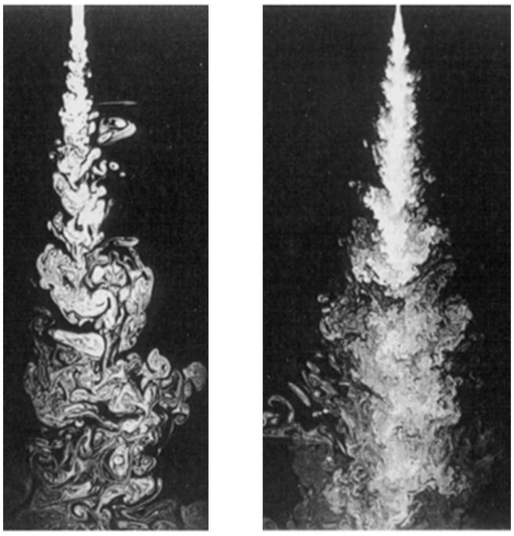

(a) (b)

Figure 2.4 The geometry of low and high Reynolds number turbulent gaseous jets (Davidson, 2015).

is primarily responsible for mixing of the jet fluid medium with that of the ambient medium. When a gaseous jet emanates from a nozzle, the interface of the jet experiences shear stress and it undergoes Kelvin-Helmholtz instability that is characterized by roll-up vortices. The instability leads to the formation of turbulent structures on the interface as shown in fig. 2.4. The size of the vortical structures/eddies formed at the interface of the turbulent flow depends on the Reynolds number as observed in fig. 2.4. The turbulent structure increases the interfacial area between the injectant fluid and the ambient fluid drastically. The length scales of the turbulent structures are related to the momentum possessed by the jet (Chaté et al., 2012). However, the complete mixing of the jet fluid medium depends on the diffusion process that occurs at the molecular level.

2.6 Fluid jets at supercritical conditions

In some applications like rocket and diesel engines, the liquid jet upon injection is exposed to extreme pressure and temperature conditions. Under such condition, the thermodynamic properties of the injectant fluid undergo continual variation, and it could affect the fluid dynamic process associated with the mixing of the injectant fluid and the ambient fluid. The understanding of the behavior of the injectant fluid at such extreme condition is necessary for an engineer to design the injectors and other components of the engines (Anderson and Yang, 1995).

However, in many practical applications, the environment often reaches the critical point of the jet fluid. In the case of liquid propellant rocket engines, the mixing of the liquid fuel and the oxidizer prior to combustion is important as the combustion chamber condition often reaches the supercritical state of the propellants where the surface tension is expected to be absent and droplet formation could be significantly affected. Under such state, the mixing process that takes place could be significantly different from those that take place at conventional subcritical conditions due to the existence of various critical anomalies. There are numerous experimental and theoretical studies, that are related to the laminar liquid jet instability and breakup characteristics at thermodynamic subcritical conditions.

However, there is a lack of theoretical modeling that deal with the instability and mixing behavior of liquid jets at supercritical chamber conditions.

2.6.1 Thermodynamic supercritical state

At temperatures below the thermodynamic critical point, the fluid exist in liquid and vapor state. At subcritical conditions, the liquid and its vapor coexist with a distinct interface that is characterised by surface tension. As the temperature of the liquid-vapor system increases, the vapor pressure of the system also increases, and the density of the liquid phase keeps decreasing. When the temperature is just below the critical point, the vapor pressure of the system approaches critical pressure with vapor density being almost equal to the density of the liquid phase, and there is a drastic reduction in the surface tension (Anderson and Yang, 1995). At the critical point, the surface tension becomes zero and the distinct interface between the liquid and the vapor phase ceases to exist as identified in fig. 2.5. The fluid exists in a homogeneous state with the physical properties like viscosity and density that lie in between the liquid and vapor state; the phase is referred to as supercritical state. In this phase, the density is nearly half that of the liquid, with some properties similar to that of vapor (Zappoli, 2003). Also at the critical point, the fluid exhibits certain anomalies such as infinite heat capacity and decrease in thermal conductivity, and also non-existence of latent heat of evaporation (Sengers, 1985). The injection of a subcritical jet into supercritical chamber condition causes the injected fluid at some point to reach the thermodynamic critical regime. Since there are various anomalies in the thermodynamic properties of the fluid near the critical point, it is very challenging to model the jet dynamics at supercritical conditions.

2.6.2 Studies on droplets at supercritical condition

In the due course of atomization, the jet undergoes breakup and result in the formation of fine droplets, and in some applications such as in combustion chamber, the droplet evaporation is very important for efficient combustion. Hence the droplet evaporation in the spray process at high temperature caught the attention of

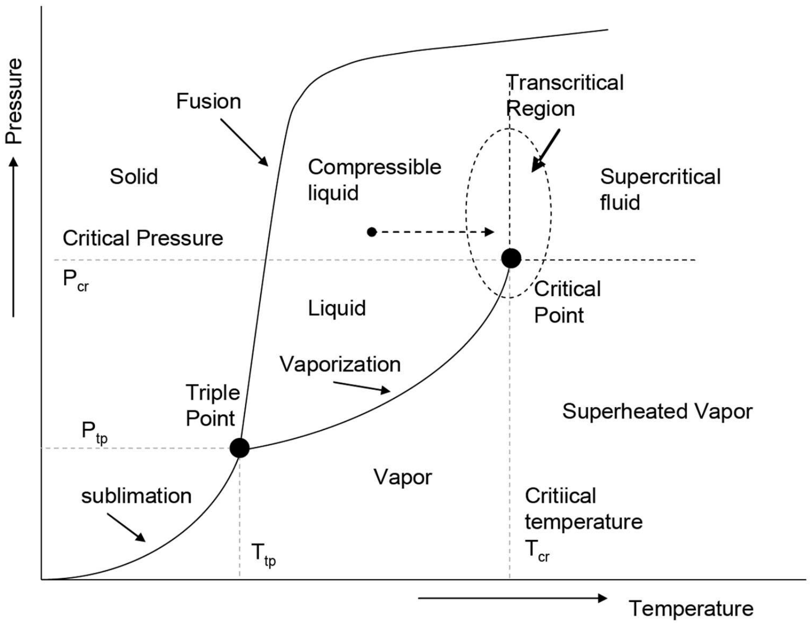

Figure 2.5 Thermodynamic phases of a pure component in Pressure-temperature phase diagram.

some researchers while they were trying to understand the physical and chemical processes associated with the combustion chamber (Manrique and Borman, 1969). Such understanding is essential for the design consideration of combustion chamber. The authors observed that under subcritical conditions, the physical process inside the droplet and the ambient gas could be treated separately and could be matched at the interface by imposing liquid-vapor equilibrium condition. Also the spray at subcritical temperature and pressure condition is considered as a turbulent two phase mixing process. However, at supercritical conditions, the situation is quite different. Droplet vaporization and combustion lifetime is significantly influenced by the ambient pressure and temperature condition (Givler and Abraham, 1996).

The sharp distinction between liquid and vapor ceases to exist and there is no abrupt phase change as involved in vaporization. During combustion process, the flame envelops the droplets and so the temperature is supercritical. The pressure dependence of the burning rate of the droplet is mainly due to the pressure dependence of the latent heat of vaporization (Rosner, 1967). It has to be highlighted that Manrique and Borman (1969) initiated the systematic investigation of droplet evaporation in the near critical regions using a quasi-steady model. The authors concluded that the vaporization process in the supercritical environment is significantly different due to the thermodynamic non-idealities. The droplets in the spray are initially at subcritical temperature and their temperature increases as they move downstream, and hence some of the studies on spray combustion suggested the consideration of temperature variation in thermodynamic properties in the modeling process (Law, 1982) (Faeth, 1977). Following the studies carried out by Faeth (1977), a series of experimental and theoretical studies are carried out by researchers to model the droplet behavior at supercritical conditions.

The numerical simulation of droplet vaporization at zero gravity environment for an axisymmetric case is carried out by considering high pressure transient effects and variable thermo-physical properties (Zhang et al., 2009) (Balaji et al., 2011). The study reveals that the droplet lifetime decreases with increase in pressure at supercritical pressure conditions. The various discrepancies existing between the numerical simulation and the experimental data are discussed by Zhang et al. (2009). These discrepancies are mostly attributed to the lack of sufficient knowledge on conduction in the droplet at critical and supercritical condition (Harstad and Bellan, 2001), (Yang and Wong, 2001). Most of the numerical studies are carried out with one or few droplets and in those cases, the values of droplet lifetime determined from numerical simulations vary only slightly from their experimental counterparts. However, in certain practical applications such as in spray formation, the droplets occur as clusters or clouds, and in that case, the D^2 law is not valid since the neighboring droplet prevent the droplet clouds in attaining the critical mixing state (Sirignano and Delplanque, 1999).

2.6.3 Studies on liquid jets at supercritical conditions

The thermodynamic analysis of liquid rocket engine thrust chambers indicates higher specific impulse and increased efficiency of the rocket engines for higher chamber pressures. At such extreme condition, the state of the injected fuel is typically beyond its critical point. Thus, the need for any improvement in the design of rocket engines requires an understanding of the liquid jets at supercritical condition. Most of the studies in Air Force Research Laboratory(AFRL) and German Aerospace center (DLR) were initiated to understand the complete behavior of the jet. Most of the early works were focused on static droplet at supercritical conditions. Only in the past few decades has the study on the fluid jets at supercritical condition been initiated. The study on fluid jet at supercritical condition involves more complex phenomena than the study of droplets. The study of fluid droplets at supercritical condition is one aspect of the study of jets at such conditions. There are several characteristics of the jets such as shear layer geometry, spreading angle, and transition to supercritical behavior that determine the mixing characteristics. The pressure in the rocket or the diesel engines often reaches twice the critical pressure of the fuel. The injected fuel/fluid continually undergoes changes in its thermodynamic properties that equally affects the fluid dynamic behavior of the jet. Below the critical condition, the thermodynamics of the fluid is well understood and its properties like viscosity and surface tension do not change significantly over a wide range of pressure and temperature conditions.

The necessity for the study of jet dynamics under supercritical conditions is of interest to the researchers to understand the mixing of propellant in rocket engines, as there is a transition in the thermodynamic properties of the jet when it is injected from subcritical to the supercritical chamber conditions. Furthermore, understanding the fluid dynamics of high Reynolds number jets is itself difficult. The early studies on jet under such conditions were investigated by Newman and Brzustowski (1971). The authors studied the characteristics of liquid CO_2 at the near critical condition with chamber gas as CO_2/N_2 mixture at various compositions. The effect of partial pressure of CO_2 in the environment is found to influence the evaporation rate of the liquid CO_2 jet; the lower partial pressure in the environment results in higher evaporation rates. Also, finer spray with smaller droplets is observed as the conditions reach the critical temperature. Shen and Poulikakos (1998) studied the impinging jet atomization of liquid nitrogen injected into a supercritical

N_2 environment using two reference beam holography technique. In their study, it is shown that the droplet formation is nearly absent as the pressure reaches the critical state inside the chamber that is already at supercritical temperature. The effect of the ambient gas composition is also studied by heating and pressurizing the chamber to the supercritical conditions with N_2 ans He mixture as the ambient fluid. Their observation revealed that the liquid nitrogen/gas helium binary system has higher critical state than liquid nitrogen/ gas nitrogen system.

Mayer et al. (2000) investigated the characteristics of single and coaxial jet at supercritical conditions, and found that beyond the critical pressure, the interface of the jet exhibits streaky like behavior. The authors attributed this effect to the continual decline of the surface tension of the liquid jet. Extensive experiments to understand the jet mixing at supercritical condition were initiated by Chehroudi et al. (2002b) Chehroudi et al. (2002a) at Air Force Research Laboratory (AFRL). The authors investigated the visual characteristics of the liquid jet injected into supercritical temperature with pressure varying from the subcritical to supercritical conditions. At low subcritical chamber pressure the jet surface exhibited surface irregularities similar to the turbulent jet that amplified downstream. In their study, as the pressure reaches the critical conditions, turbulent gas/gas like mixing behavior is observed. The first quantitative growth rate measurement of a jet mixing layer was performed and it is found to agree with the mixing layer theory of the incompressible variable density gaseous jet (Chehroudi et al., 2002a). Oschwald et al. (2006) summarized the investigation made by AFRL and DLR (German Aerospace Center) on the single jet and coaxial jet, and it revealed that there is enhancement in jet mixing at the supercritical conditions.

Recently, the experimental techniques have been improved with the application of Laser and intensified CCD camera. Segal and Polikhov (2008) have investigated the subcritical fluoroketone round jet injected into the supercritical conditions with N_2 as the ambient fluid using PLIF technique. Their observation reveals the absence of droplet formation as the chamber condition reaches the supercritical state. Instead, the cluster or finger-like structures being pinched out from the jet is observed. Roy and Segal (2010) investigated the jet structure at supercritical condition in detail and it is found that there is a decrease in potential core length of the jet as the chamber to injectant density ratio is increased. An extensive review on various models utilized for drops and jets at supercritical conditions is presented by Bellan (2000) and it is found that the available experimental data is insufficient to have complete understanding and modeling of the jet behavior at supercritical conditions. A detailed discussion on the key experimental findings in the recent decades is carried out by Chehroudi (2012) and it focused on the behavior and the structure of single and coaxial jets at supercritical conditions. The review also brought out some of the major experimental efforts that are involved in characterizing liquid jets injected into its supercritical conditions.

The study of the supercritical jet injected into subcritical conditions has become an increasingly important area of research work. In emerging technologies such as those involving heat transfer from the airframe of supersonic ramjet and hypersonic flights, endothermic fuel is under consideration as a heat absorbing medium (Wu et al., 1999). In rocket engines, hydrogen after passing through the regeneration coolant passage becomes supercritical and gets injected into supercritical chamber conditions. Also the application of formation of solute nano-particles from rapid expansion of supercritical fluid solution (RESS) into subcritical condition is of great interest since the process utilizes the dramatic change in the dissolving power of the solvent (Lin et al., 2006), (Matson et al., 1987). Recently, the investigation of supercritical jet injected into subcritical conditions using PLIF is conducted by Roy et al. (2013) This study revealed the presence of formation of droplets at the jet interface and it indicated the presence of surface tension.

2.6.4 Fractal geometry of supercritical jets

Fractals are objects which are self-similar under a wide range of scales. The study of fractals is a branch of mathematics where the fractal objects possess self-similarity in infinite range of scales. However, the application of fractal concept to the physical objects has its own limitation such as the existence of self-similarity only over certain range of scales. For example, the turbulent boundaries are fractal objects only up to Kolmogorov scale. The fractal objects possess a fractal dimension unlike integer dimension possessed by classical objects. Topologically, curve is a one-dimensional object and when the curve is space filling, its fractal dimension depends on the degree of space filling nature. Hence a fractal curve possess a dimension between one and two. The evaluation of the fractal nature of the injected jet finds its significance in practical applications where the high fractal dimensions correspond to the larger interfacial area that enhances the mixing process. The fractal nature of the fluid dynamic phenomena such as turbulence is discussed by Mandelbrot in his studies (Mandelbrot, 1983) (Mandelbrot and Blumen, 1989). There are several fluid dynamic characteristics that may exhibit fractal nature, and the turbulence is one among them (Turcotte, 1988).

Sreenivasan and Meneveau (1986) applied the concept of fractals to turbulent jets, wakes, and clouds. In their studies, the authors found that an axisymmetric turbulent jet surface in three dimensional space possess a fractal dimension of 2.33. Later Chehroudi et al. (1999) found out the fractal dimensions of liquid N_2 injected into ambient N_2 in which the pressures vary from subcritical to supercritical condition. It is found that below the critical pressure the fractal dimension (D_f) of the jet boundary is found to be less than 1.2 and it becomes $D_f > 1.3$ as the pressure becomes supercritical. In the study by Chehroudi et al. (1999), the liquid jet exhibited two phase mixing characteristics until the chamber pressure was below the critical point. In his study, as the chamber reached the critical pressure, the liquid N_2 jet instantly underwent mixing that resembled gas-gas like mixing; however it must be noted that liquid N_2 injected into chamber with nitrogen environment represents a single component system. The fractals dimensions of the jet at various chamber conditions are presented by Chehroudi et al. (1999). At supercritical chamber temperature, the fractal dimension of the jet exhibits a strong dependence on the chamber pressure.

2.7 Inferences from literature

To the present date, the investigation at supercritical state was performed using circular orifices. The use of non-circular jet will help reveal further flow physics involved in the transition of the fluid jet behavior near the critical regime. In the case of circular jet, the thermodynamic transition is investigated by observing the presence or absence of droplets. The formation of droplets in the case of circular jet breakup is a combined action of the surface tension as well the shear force acting on the jet surface. However, for the case of elliptical jet at low velocity, the axis switching is directly related to the Weber number of the jet due to the negligible shear force and thus by knowing the density and the velocity of the jet, the surface tension of the jet fluid can be calculated. As the surface tension force could significantly be reduced at near critical conditions, the axis switching phenomena should also get affected.

The study on the behavior of liquid jet at supercritical condition is initiated in the year 1971 by Newman and Brzustowski (1971). Much of the researches in the past are conducted to understand the mixing of the jet at rocket engine conditions. The liquid jets at supercritical condition is studied at high Reynolds number $Re > 10000$ (Chehroudi et al., 2002a), (Segal and Polikhov, 2008). Since the jets are studied using visualisation technique through the optical access system, the residence time of the injectant jet is very minimum at such high Re of jet to observe the thermodynamic transition. In order to study the effect of transition in thermodynamic properties like surface tension on the jet behavior, the jet must be studied at low Re. The disintegration of supercritical jet at subcritical environments is performed by Roy et al. (2013) with velocity ranging from 7 to 30 m/s, and the jet is investigated for a length of 40 mm downstream of the jet inlet. At such high velocity, the droplet formation could be observed only at the shear layer. Studies in the past were performed to understand the supercritical jet behavior with injectant condition at atomization regime. The low velocity jet could reveal further insight into the transitional nature and the behavior of the jet could be analyzed in more detail.

The studies in the past at supercritical condition were conducted either in a binary component system (injectant and ambient fluids are different) or in a single component system (injectant and ambient fluids are same). Also there are notable contradictions existing in the past investigations. Some studies performed by Chehroudi et al. (2002b) indicate that the jet in a binary component system does not undergo transition to supercritical state even at supercritical chamber condition. However, the recent studies conducted by Segal and Polikhov (2008) and Roy and Segal (2010) suggest that the jet in a binary component system undergoes transition and exhibits gaseous jet-like behavior at supercritical chamber condition.

The visualisation technique is the most effective methodology in studying the kinematics of the jets. Almost all the studies in the past were carried out by employing different methods of jet visualisation. Much of the experimental studies related to fluid jets at supercritical condition in the past is carried out using cryogenic fluids like N_2, He. The main components in the experiment were the high pressure chamber and optical access system. The visualisation technique used in the past was simple backlighting technique. Only recently, the studies were performed using PLIF technique since the injectant fluid, fluoroketone possess good spectroscopic properties. Using PLIF studies, the investigation of density field of the jet became possible (Segal and Polikhov, 2008) (Roy et al., 2013). The structure of the shear layer of a jet possess certain interesting features, such as fractal geometry, that determine the mixing characteristics of the jet.

2.8 Scope and objective

The jet dynamics at supercritical condition involves strong coupling between fluid dynamic and the thermodynamic processes. When the injectant and the chamber conditions are different, the injected jet must undergo changes in some important thermodynamic properties such as surface tension and the viscosity of the fluid. The changes in the thermodynamic properties in turn alter the fluid dynamic processes. In the past, most of the studies were carried out with the circular orifice and the absence of droplet formation was attributed to the absence of surface tension.

The use of an elliptical jet at supercritical condition is thought to reveal the changes in the surface tension. The axis-switching length is an indicator of the amount of surface tension present; the transitional nature of the injected jet at supercritical environments could be investigated in a precise manner. Performing the experiment using a low speed jet may reveal several fundamental characteristics in phase transition and regimes of jet behavior at supercritical condition. Also using the PLIF technique, the density and the density gradient could be obtained. The interfacial geometry will be studied in detail using fractal analysis.

The liquid elliptical jet exhibits axis-switching due to the counteracting balance between the surface tension force and the lateral inertia. If there is no axis-switching it can be inferred that there is no surface tension and the jet is no longer a liquid. The circular jets do not exhibit axis-switching and hence it is difficult to ascertain the presence of surface tension. For example, because some instability such as Kelvin-Helmholtz can occur between two gases as well as at a gas/liquid interface, when this instability occurs, the thermodynamic state of the fluid in the jet is not clear. Thus, for the circular jets the situation is less clear as compared to that of elliptic jets. Due to the above mentioned reasons, the study on elliptical jet precedes that of circular jet in the current investigation.

The main objective of the present work is to understand the thermodynamic transition of the jet as well the changes in the geometry/structure of the jet at chamber and the injectant supercritical conditions. The circular and the elliptical orifice are chosen for the study. The injected jet fluid for all the experiments carried out is fluoroketone and the chamber fluid is either N_2 or He or fluoroketone. The objectives are listed as follows:

1. The first objective of the present work is to perform the experiments with

elliptical orifice at supercritical conditions and this work is further divided into two parts

   - The first part of the work is performed to understand the axis-switching behavior of the subcritical elliptical jet at subcritical to supercritical chamber condition for both binary as well as the pure component system (own environment).
   - The second part of the work is performed to investigate the characteristics of the supercritical elliptical jet injected into the subcritical chamber conditions. In this study, the density measurements are obtained for the supercritical jet injected into subcritical as well as the supercritical conditions using PLIF technique. The N_2 as well as He are chosen as the chamber environments respectively.

2. The second objective of the work is to conduct the experiment with circular jet. The N_2 or He is used as the chamber fluid for the binary component system and its own vapor is used as the chamber environment for the pure component system.

   - The first part of the second objective of the work is to understand the nature of the instability waves that develop in a circular jet as it is injected from subcritical condition to chamber conditions that vary from subcritical to supercritical. This experiment is conducted with N_2 as ambient gas for the binary component system and its own vapor as ambient fluid for single component system. Also the fractal dimension of the jet boundary is investigated.
   - The second part is to study the supercritical circular jet at subcritical and supercritical chamber condition for the binary component system with N_2 or He as the ambient fluid using PLIF technique. The density as well as the density gradient measurements are utilized to investigate the mixing characteristics of the jet. The fractal geometry of the supercritical circular jet is also evaluated to analyze the interface in detail.

CHAPTER 3

EXPERIMENTAL METHODS

In this chapter, the setting up of the experimental facility for conducting experiments at supercritical condition is discussed in detail. Various components such as high pressure chamber facility, liquid and gas heater systems and various measurement technique are described. The experiment relies on the visualization technique and hence the details of the various techniques utilised in the current study is described. To obtain density field of the jet, the PLIF technique has been employed and the image of the jet is captured using charge coupled device (CCD) camera.

3.1 Experimental facility

The experiments are performed to comprehend the jet behavior at thermodynamic supercritical conditions. To conduct the experiments in laboratory, the high pressure and temperature environment has to be created to simulate the supercritical conditions. An experimental facility with high pressure chamber is required along with provision for heating the chamber to the desired temperature. This facility has been built in Advanced Propulsion and Laser Diagnostics (APLD) lab, IIST to conduct the experiments at supercritical conditions. The schematic of the overall experimental facility is shown in fig. 3.1. The facility primarily consists of a high pressure chamber, liquid and gas heaters and supply lines. The chamber is generally pressurized with nitrogen/helium gas to the desired level prior to conducting the experiment. There are two supply lines. They are: 1. liquid supply line and 2. gas supply line. The gas supply line constitutes of a nitrogen cylinder, ball valves, metering valve, pressure transducer and gas heater. The pressure downstream of the nitrogen cylinder is controlled using a pressure regulator. The mass flow of the gas to the high pressure chamber is controlled using the SWAGELOK metering valve.

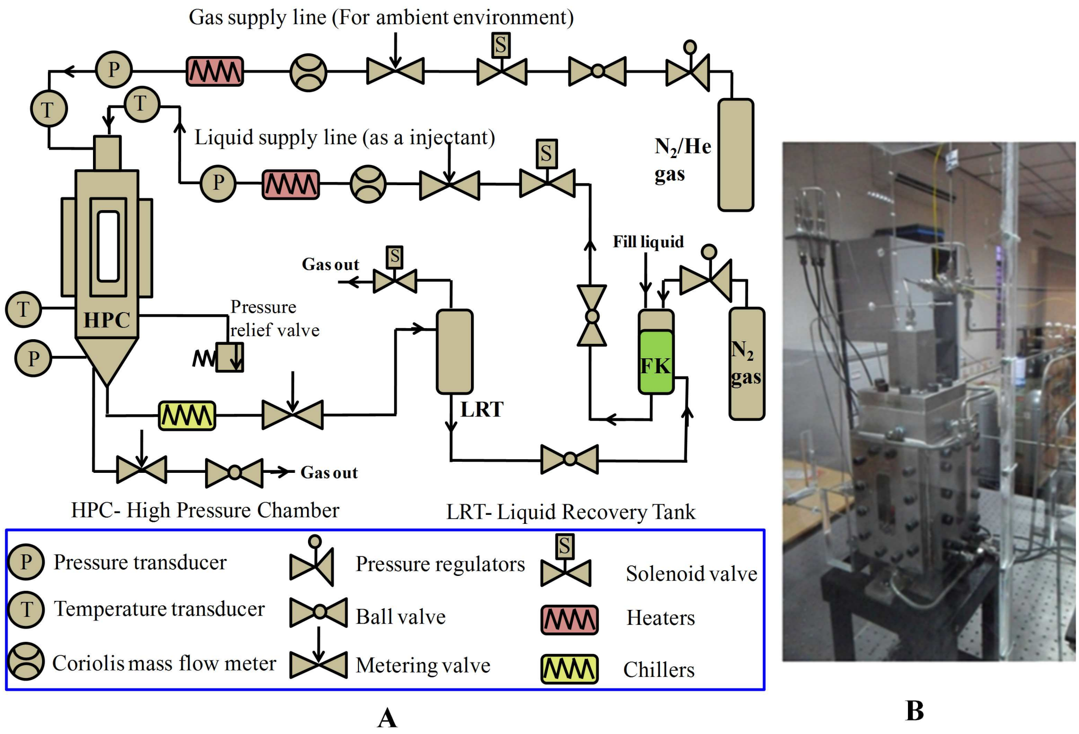

Figure 3.1 Schematic of the experimental facility and the high pressure chamber.

In the case of the liquid supply line, the liquid to be used as an injectant fluid is stored in a storage tank and is pressurized to the desired pressure level using gas from the nitrogen cylinder through pressure regulator.

3.1.1 High pressure chamber

A high pressure chamber has been designed to withstand a pressure of 70 bar and a temperature of 700 K to carry out the experiments as shown in fig. 3.1. The high pressure chamber is provided with quartz optical access at its four sides for the visualization of the jet. The chamber consists of the main chamber body, top head of the chamber, bottom portion and four side flanges. The main chamber body shown in fig. 3.1 has four rectangular slots in its sides to accommodate the optical windows. The top head of the chamber is designed to accommodate various types of injector like circular, elliptical and coaxial injectors. The quartz window is fixed onto the flanges by means of O-rings and high temperature RTV silicones. The side

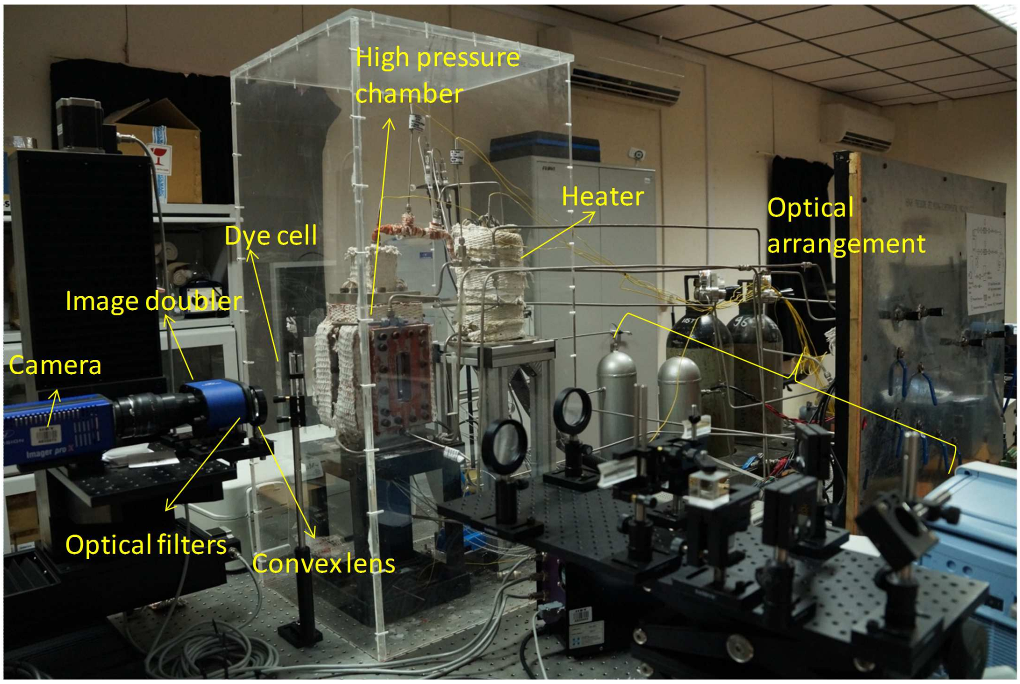

Figure 3.2 Photograph of the experimental facility.

flanges are fixed to the main chamber body by means of bolts, and also gaskets are provided to ensure leak proof operation. For the supply of liquid and gas, 1/4" NPT (National Pipe Thread Taper) ports are provided in required places.

The central top of the chamber is provided with an elliptical/circular orifice through which the liquid is injected. To heat the chamber to the desired temperature condition, it is provided with cartridge heaters that can be inserted into the through holes on its four corners. To measure the temperature of the chamber, thermocouples are inserted into the chamber. One thermocouple is installed to measure the temperature of the chamber near the injection orifice exit, and the other thermocouple is installed at the bottom side of the chamber. To ensure the uniformity of the temperature distribution inside the chamber, the difference between the thermocouple readings is monitored and the maximum deviation amounted to 1.6% with respect to the absolute scale. The chamber temperature is maintained at desired level through the use of PID controller. The PID controller maintains the temperature of the chamber with errors less than 0.5%. The chamber is insulated with asbestos except in the place of optical access to avoid the heat loss from the chamber and maintain uniform temperature distribution. The field of view of optical access of 30 mm × 90 mm is only 7% and constitutes only a small fraction of the surface area of the chamber. As the quartz windows are poor conductors, the heat loss through the optical access is assumed to be negligible.

3.1.2 Optical access

The optical access is provided using Quartz window at all the four sides of the high pressure chamber. Quartz is chosen because of its excellent physical, chemical and optical properties. It has high softening temperature and thermal resistance, low thermal expansion and high resistance to thermal shock. More importantly, it has high optical transparency from ultraviolet to infrared range.

In order to provide a maximum field of view, the optical access is designed to be rectangle. The edges of the quartz window are chamfered to minimize the stress concentration. The provision is made in side flanges to fix the quartz window and is sealed using Viton O-rings. The detailed design and dimension are provided in the appendix C. In the present study, the field of view is 30 mm × 90 mm.

3.1.3 Heating system for chamber, liquid and gas

For experiments that require preheating of the liquid jet prior to injection into the chamber, a liquid heater is employed just upstream of the injection point. The design of the liquid and the gas heaters are similar. The construction of the heater has two main parts. They are: 1. The inner cylindrical core and the outer casing. The inner core of the heater is made of brass material and its central portion is provided with blind holes for inserting cartridge heaters. The outer casing of the heater is made of stainless steel for having high strength at high temperatures. Also the outer casing is provided with two 1/4" NPT ports each at two ends of the outer casing. These ports serve as the inlet and outlet for the liquid or the gas.

The surface of the inner core cylinder is provided with a helical thread of square pitch to enhance the surface area. As the inner core is assembled with the outer casing, the interface between the inner core and the outer casing provides helical pathway for circulating the fluid circumferentially from the inlet port at the bottom side of the heater to the outlet at the top side of the heater. The heater is placed vertically with cold dense fluid entering the inlet port, and gets heated along the thread like structure; the hot less dense supercritical/high subcritical jet leaves through the outlet port. The measurement of the temperature of the preheated liquid is carried out just prior to the injection point. The heater temperature is monitored and controlled using PID controller.

3.1.4 Liquid and gas supply lines

The liquid and gas supply lines are detailed in fig. 3.1. The purpose of the liquid and gas supply line is to supply injectant fluid and ambient gas into the chamber. The 6 mm OD stainless steel tube with a wall thickness of 1.5 mm and intenal diameter of 3 mm is used as the supply line for liquid and the gas. The tube has a burst pressure of 250 bar.

The gas is supplied from the N_2/He cylinder as shown in fig. 3.1 at desired pressure using pressure regulators. The pressure downstream of the pressure regulator is kept in the range of 25 to 30 bar and the gas is introduced into the chamber in required amounts by monitoring the pressure in the chamber using pressure sensors. The ball valve is used whenever it is required to mechanically shut off the flow to the chamber. During the experiment, the electrically operated solenoid valve is used for supply/shut off instead of the ball valve. After the solenoid valve, the gas is made to pass through metering valve for the finer adjustment in the flow rate. The gas is then passed through the gas flow meter if the flow rate is required to be measured. For the current set of experiments, only the injectant liquid flow rate is measured and the gas flow is not measured. For the experiments at high subcritical and supercritical chamber condition, the gas is preheated to the required temperature and introduced into the chamber. All the connections to various components are made using ferule fitting from SWAGELOK. All the components are provided with either 1/4" or 1/2" NPT port and the supply tube is connected to the components using corresponding ferule fittings.

For the case of liquid supply, the injectant fluid fluoroketone is stored in a 6 litres capacity stainless steel tank. The liquid tank is pressurised using the nitrogen cylinder as shown in fig. 3.1 at pressures of 25 to 30 bar using pressure regulator. The storage tank is provided with 1/4" NPT port at the top, bottom and the side of the tank. The top 1/4" NPT port is connected to the N_2 cylinder for pressurising the tank. The side port 1/4 " is used for pressure relief and is connected to the atmosphere through a ball valve and an electrically operated solenoid valve. Through the other 1/4" NPT port, the liquid is supplied and the supply line is similar to that of the gas line. The liquid is passed through the ball valve, solenoid valve, SWAGELOK metering valve and is fed into the EMERSON coriolis mass flow meter. The flow rate is monitored in real time and fine adjustments are made using the metering valve. The liquid is subsequently passed through the liquid heater to preheat to high subcritical or supercritical temperatures for the experiments that necessitate the required conditions.

The fluid injected into the chamber is recovered back at the recuperation tank through the supply lines as shown in fig. 3.1. The design of the recuperation tank is similar to the storage tank. Between the chamber and the recuperation tank, the chiller is used to cool down the hot injectant fluid to room temperature. The injected fluid is fed to the storage tank and is reused for the experiment. This could be perceived from fig. 3.1.

3.2 Measurement system

The pressure and temperature are the important physical parameters to be measured. Since the experimental facility is designed to carry out experiments at high pressure and temperature conditions in the laboratory, the measurement of the pressure and temperature at various important points in the experimental facility is required for the operation of the facility as well as for safety reasons.

The pressure is measured using the OMEGA dyne PX309-1KGV steady pressure transducer (Product information, High performance pressure transducer, Omega engineering). The measurement is highly accurate with an error less than 0.25 % of the full scale reading with the pressure ranges up to 500 psi gauge. The transducer is excited with 5 VDC, and the output of 4-20 mA corresponding to the pressure is accordingly measured. The output of the transducer is connected to the NI PXIe-6363 card of National Instruments (NI) for acquiring the pressure data. One pressure transducer is fitted to the chamber through a coiled stainless tube and ferule fitting to avoid direct contact with the chamber. Two pressure transducers in liquid and gas supply lines are provided. Also, the pressure transducers are fitted to the storage tank and the recuperation tank and the pressure levels are constantly monitored.

The temperature is measured using the OMEGA K-type thermocouple having the temperature range from -100 to 1200^o C with a maximum error of 1.1^o C. The thermocouple is connected to the NI system to acquire the temperature readings. The chamber is provided with two thermocouples: one at the top and another at the bottom to ensure the uniformity in the temperature distribution. Also the thermocouple is placed in the core of the gas and liquid heaters as well as downstream of both the gas and liquid heaters. The temperature of the injectant liquid and the gas is measured by fitting the thermocouple near the entrance of the liquid and the gas supply line into the chamber. The thermocouple is fitted to the supply line using a T-ferule connection which is placed 100 mm upstream of the injector exit. It is assumed that the disturbances generated by the thermocouple in the flow may not sustain for a length of about 70 mm in a 3 mm diameter supply tube which further constricts into a smaller diameter elliptical or circular cross section tube of 30 mm length just prior to the injector exit.

Another important parameter to be measured in the experiment is the mass flow rate of injectant fluid. The EMERSON Coriolis mass flow meter is used for this purpose (Instruction Manual, Micromotion Coriolis Elite sensor, Emerson process management). The mass flow meter uses the Coriolis principle to measure the flow rate. The measuring range of the flow meter is from 0.2 to 10 g/s. The error involved in measuring the flow rate is less than 1%.

3.3 Data acquisition

All the pressure, temperature and the mass flow readings are fed to the National Instruments (NI) data acquisition system (Instruction Manual, National Instruments). Using LABVIEW software, the hardware/software interface is made. The LABVIEW is a visual programming language from National Instruments (NI) commonly used for data acquisition and instrumentation control. The programs in LABVIEW are based on graphical block diagrams in which the programs/subroutines represent virtual instruments (Essick, 2012). For the present experiments, the pressure, temperature and the mass flow readings are acquired and monitored by employing LABVIEW programs. The output signal of 4-20 mA from the pressure transducer is connected to the NI PXIe-6363 card. The thermocouple output signal is connected to the NI PXIe-4353 card. The current signal from the mass flow meter is connected to NI PXIe-6239 card.

Before the start of the experiment, the pressure, temperature and the mass flow reading are monitored in real time. Once the steady state condition is attained, the experimental run is initiated. To ensure data acquisition in steady state flow conditions, the images are captured along with pressure, temperature, and mass flow measurements only after 5 s from the start of the injection. In the present study, for the range of mass flow rates between 0.2 and 2 g/s, the jet images exhibited transients in the characteristics only for a time period of around 3 s after the start of injection of liquid jet from the orifice. The jet reached steady state beyond 5 s from the start of injection. During the experimental run, the images and the pressure and temperature data are acquired simultaneously for a time period of 10 s after 5 s from the start of injection.

In the present study, the experimental runtime for data acquisition is set for 10 seconds and the corresponding data is acquired and stored in a MICROSOFT excel file during the experiment. The pressure and mass flow data is obtained at the rate of 100 sample/sec and the temperature data at 500 samples /sec. Since all the experiments are conducted at steady state conditions any small scale fluctuations in pressure, temperature and mass flow rate reading is considered to be due to the random nature of the signal, and only the mean of the reading is considered for data processing.

3.4 Injected fluid, Fluoroketone

Recently, a compound referred to as fluoroketone is used by some researchers to study the jet dynamics at supercritical conditions owing to its desirable critical and thermal properties (Segal and Polikhov, 2008). In the current study, fluoroketone is used as the injected fluid and it has the critical pressure (P_c) of 18.6 bar and critical temperature (T_c) of 441.8 K. The maximum pressure and temperature condition of the experiments correspond to 25 bar and 500 K respectively. Based on the data available from the literature, it is found that the fluoroketone has thermal stability up to 773 K and this ensures that it is chemically stable under the current set of experimental conditions.

3.5 Ambient fluid

The N_2 or He is used as the ambient fluid for the binary component system. However, in the case of single component system, the fluoroketone vapor is used as the ambient fluid. The N_2 or He is chosen as the ambient fluid because of their difference in the critical pressure. The N_2 has a critical pressure of 33 bar whereas the He has a critical pressure of 2.27 bar.

3.6 Flow visualisation

The study on the jet characteristics primarily relies on the visualisation technique. Most of the studies in the past are carried out through visualisation because of its non-intrusive nature. The geometry and the kinematics of the jet could be studied in detail using this technique. In the present experiment, the backlighting technique as well as the PLIF technique are used as diagnostic tools. The details of the techniques are provided in the following sections.

3.7 Visualising using backlighting method

The most simple visualisation technique is backlighting that constitutes Light Emitting Diode (LED) as the light source, ground glass to form diffused light and a camera for capturing the image of the jet. In the present study, a Charge Coupled Device (CCD) camera is used. Using this technique, the structure of the jet can be visualised and the distinct boundary of the jet is obtained from which several structural and kinematic features associated with the fluid mechanics of the jet can be analysed in detail. Several measurements such as droplet size, wavelength of the instability, spreading angle of atomizing jet, breakup length of a jet, transition from single-phase jet to two-phase mixing behavior can be evaluated in detail using this technique.

In the past, several experimental studies on fluid jet visualisation at supercritical condition were performed using the backlighting technique (Chehroudi, 2012) (Oschwald et al., 2006). In the present study, the experiment is conducted at a low velocity of less than 2 m/s and the camera exposure is 150 μs. There are some limitations to this technique because the image captured in the camera is an integration of the fluid dynamic processes in the direction of light, and much of the finer details are masked due to its own shade. To overcome this limitation, the PLIF technique is used and is discussed in next section. 3.8.

3.8 Visualising using PLIF technique

To obtain detailed information of the two dimensional density map of the jet, the PLIF technique has been utilised. The optical arrangement of the PLIF technique is quite complex and it requires to be very precise to have accurate density determination. The PLIF technique is used to investigate the detailed structure of the jet along the two dimensional center plane. The Spectra-physics Nd-YAG laser with repetition rate of 10 Hz and Imager pro X 4M CCD camera from Lavision are utilized in the current study. The camera is synchronized with the laser pulse and the images are captured with an exposure time of 400 ns. The jet medium is excited with the third harmonics (355 nm) of the Nd-YAG laser. The study from Gustavsson and Segal (2007) revealed that the emission spectrum of fluoroketone is shifted to visible range with its peak at 420 nm. The detailed description of the experimental arrangement for PLIF technique is presented in the section 3.8.6

3.8.1 Fluorescence

The fluorescence process occurs at an electronic level and it involves two steps: the first step is the excitation of the molecules and the second step is the emission of photons. When a molecule absorbs photons, the ground state electrons in the outer orbit of a molecule is excited to the higher energy state. Depending on the energy levels of the photons, the excited electrons occupy one of the higher electronic states. Each of the electronic states has a number of ro-vibrational levels superimposed on it. Collisions among the molecules cause the excited molecules to

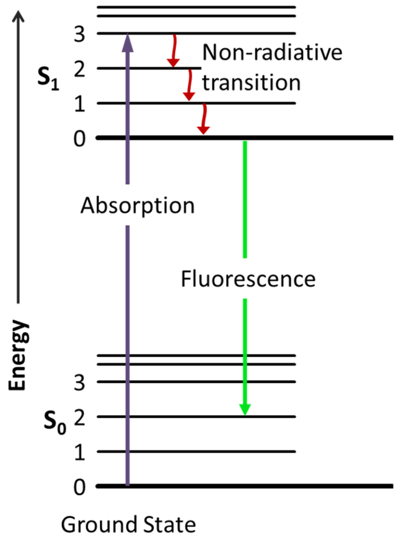

Figure 3.3 Jablonski diagram describing fluorescence process.

lose the ro-vibrational energy and return to one of the lower ro-vibrational levels of the same excited state. The excited state of the molecule is very unstable and the molecules while returning to the ground state emit photons of energy that are lower than the absorbed energy. This process is explained well using Jablonski diagram and is shown in fig. 3.3 (Valeur and Berberan-Santos, 2012). Since there is a certain loss of energy due to the relaxation of vibrational levels, the photons are emitted at lower energy and the corresponding wavelength is slightly higher than the absorbed wavelength. Since the fluorescence intensity is directly proportional to the number density of molecules, the spatial density map is easily determined (Roy et al., 2011).

3.8.2 Spectroscopic properties of fluoroketone

The injectant fluid, fluoroketone, possesses certain spectroscopic properties that are favorable for conducting experiments using the Laser Induced Fluorescence (LIF) technique. The ultra violet (UV) absorption spectrum of fluoroketone was measured by Taniguchi et al. (2003) and it is found that the UV light from 220 nm to 370 nm is absorbed by fluoroketone. According to Taniguchi et al. (2003), the peak absorption exists at 305 nm with maximum molecular absorption cross section of $\alpha = 6.81 \times 10^{-20}\ cm^2$, while α is $1.78 \times 10^{-20}\ cm^2$ at 266 nm and $0.12 \times 10^{-20}\ cm^2$ at 355 nm. The third harmonic of the Nd-YAG LASER is found to possess good liquid penetration of approximately 3 mm. Gustavsson and Segal (2007) investigated the emission spectrum of fluoroketone that is excited with 355 nm in the presence of argon. The experiment was conducted to measure the variations in the emission spectrum for the pressure and temperature conditions that vary from atmospheric condition to the thermodynamic supercritical conditions of the fluoroketone. A wide range of vapor conditions were tested with $1 < P < 23.6$ bar and $22.5 < T < 179.6^oC$ and their investigation revealed that the emission shows minor variation for changes in temperature and pressure with its peak emission at 420 nm.

3.8.3 CCD Camera

The Charge Coupled Device(CCD) camera is used for acquiring the image of the jet. The CCD camera possesses several advantages to be used in quantitative imaging. The CCD detector provides the highest level of sensitivity and high dynamic range that are required to fulfil the most demanding requirements of spectroscopic experiments. In the present experiment, LAVISION Imager proX 4M camera has been used and the pixel resolution is 2040×2040. The image could be acquired at the rate of 10 Hz with the minimum exposure of 1 μs. The camera has an inherent delay of 10 μs when triggered (Instruction Manual, Imager Pro X 4M CCD camera, Lasion).

3.8.4 Laser system

The high energy Nd-YAG laser system from spectra-physics having fundamental wavelength of 1064 mm is used (Instruction Manual, Pulsed Nd-YAG laser for PIV, Spectra-Physics). The laser operates in Q-switch mode with the frequency of 10 Hz and having pulse duration of about 8-12 ns. The beam diameter is less than 10 mm and the beam divergence is less than 0.5 mrad. The system is provided

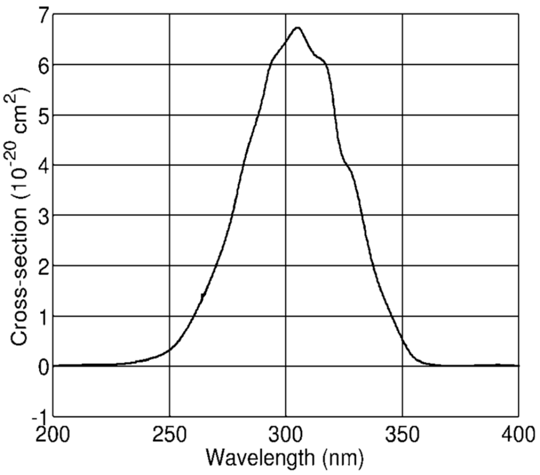

Figure 3.4 Absorption spectrum of fluoroketone (Gustavsson and Segal, 2007).

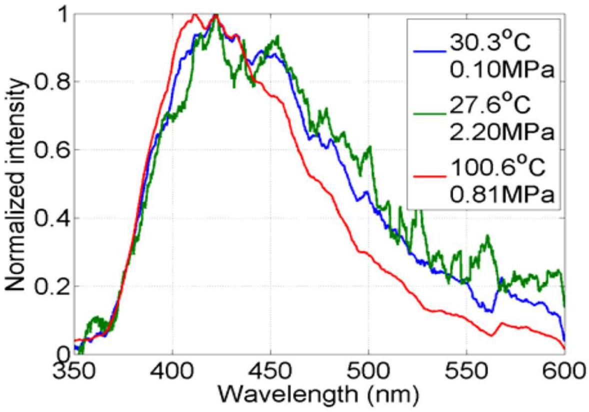

Figure 3.5 Emission spectrum of fluoroketone at various pressure and temperature condition (Gustavsson and Segal, 2008).

with inbuilt harmonic generator using KDP crystals that converts the fundamental 1064 nm wavelength into other wavelength of 532 nm, 355nm, and 266 nm. In the present study, the 355 nm wavelength is used to excite the fluoroketone with the pulse energy of 20 mJ.

3.8.5 Synchronisation of camera and laser

The laser system and the CCD camera must be synchronised for conducting the experiment. The camera and the laser are operated externally using trigger signal from STANFORD delay/pulse generator (Instruction Manual, DG535 digital delay generator, Stanford research systems). The delay generator could produce four signals, each of different delay time that can be set in the device. Using YOKOGAWA DG535 oscilloscope, the trigger signals of pulse generator as well as the acquired signals from the camera are monitored (Instruction Manual, Mixed signal oscilloscope DLM2000 Yokogawa). The schematic of the synchronisation operation is detailed in fig. 3.6.

3.8.6 Optical arrangement

The optical arrangement of the experimental setup to obtain the two-dimensional density field map from the fluorescence of the jet is demonstrated in fig.

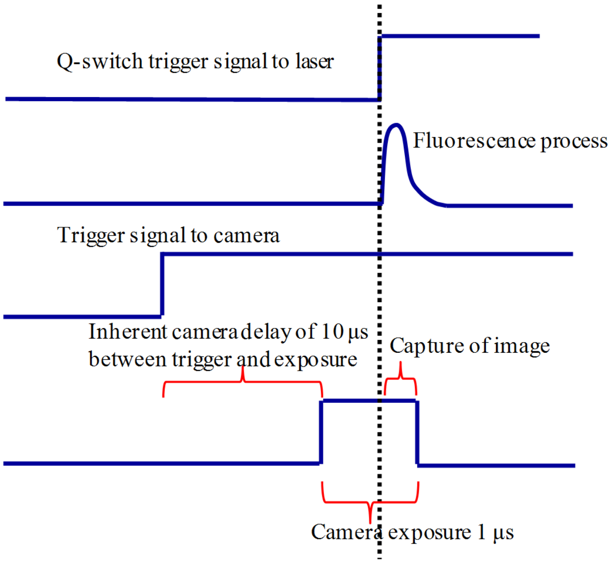

Figure 3.6 Schematic of trigger signals from pulse generator and camera, illustrating the synchronisation between the laser and the camera operation.

3.7 and 3.8. The quantitative measurement of the concentration of the species using PLIF technique is initiated by Hanson et al. (1990). The study also addresses the various errors and image corrections to be employed for minimizing the uncertainty from PLIF measurements.

There are certain uncertainties that are inherent in the PLIF technique which can lead to errors in density measurement. The sources of the uncertainties are identified as: 1) shot-to-shot fluctuations in laser beam, 2) variation in laser sheet intensity due to Gaussian nature of the beam, 3) variations in laser sheet profile shape, and 4) the attenuation of the laser sheet in fluid jet due to absorption.

Due to the shot-to-shot fluctuations in the laser intensity, the fluorescence jet image does exhibits fluctuations in its fluorescence intensity and it would cause an uncertainty in the density measurement. In order to eliminate this uncertainty, the reference dye cell is utilised. The reference dye cell is a quartz cuvette filled with liquid fluoroketone at 300 K and 1 atm. In the current experiment, the laser beam from Nd-YAG laser is split into two beams of equal energy using polarizing cubic beam splitter and a half wave plate as shown in fig. 3.7. Employing cylindrical concave lens and spherical convex lens, two laser sheets of wavelength 355 nm are formed. One laser sheet is used to excite the fluid jet injected into the chamber, and the other is used to excite the fluoroketone in the reference dye cell. The fluorescence image of fluid jet as well as the dye cell is captured in the same camera sensor using LAVISION image doubler simultaneously. The fluorescence from the dye cell which is filled with fluoroketone liquid at atmospheric temperature is utilised as the reference signal to account for the uncertainty due to the shot-to-shot fluctuations in the laser.

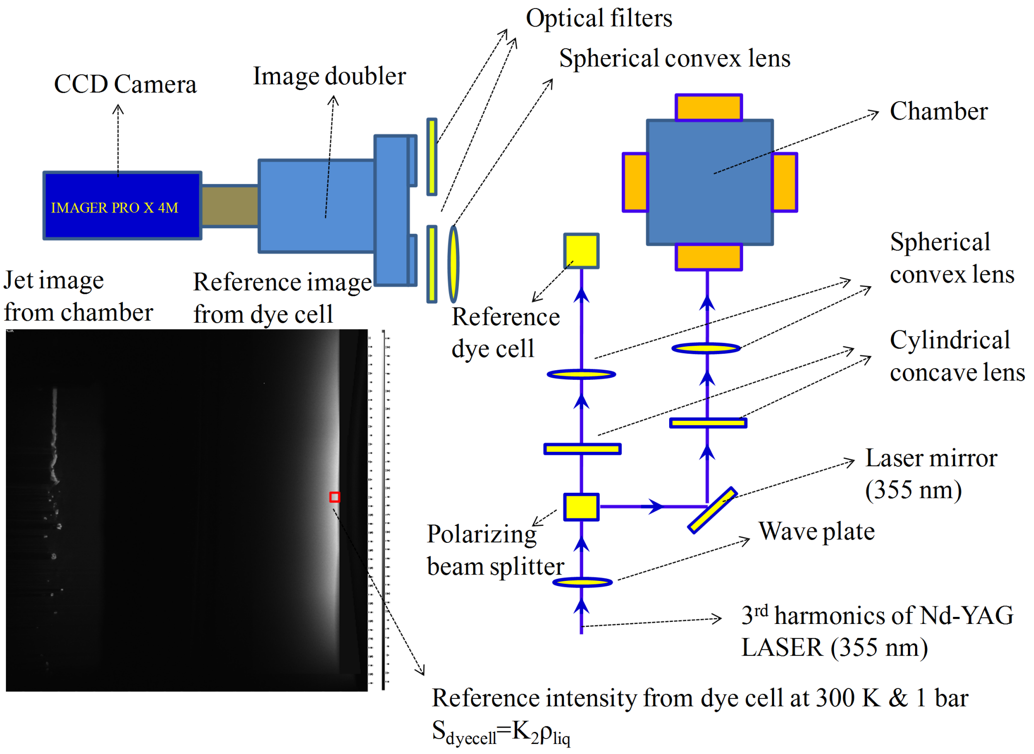

Figure 3.7 Schematic of the top view of optical arrangement for the PLIF experiment.

As the laser beam profile is Gaussian in nature, the laser sheet formed from the beam has variations in intensity along the vertical direction and needs to be corrected. In order to correct for the spatial variations in the laser sheet, the normalized laser sheet profile is utilized and the same is obtained from the fluorescence of fluoroketone vapour that is uniformly filled inside the chamber. The 2D-fluorescence

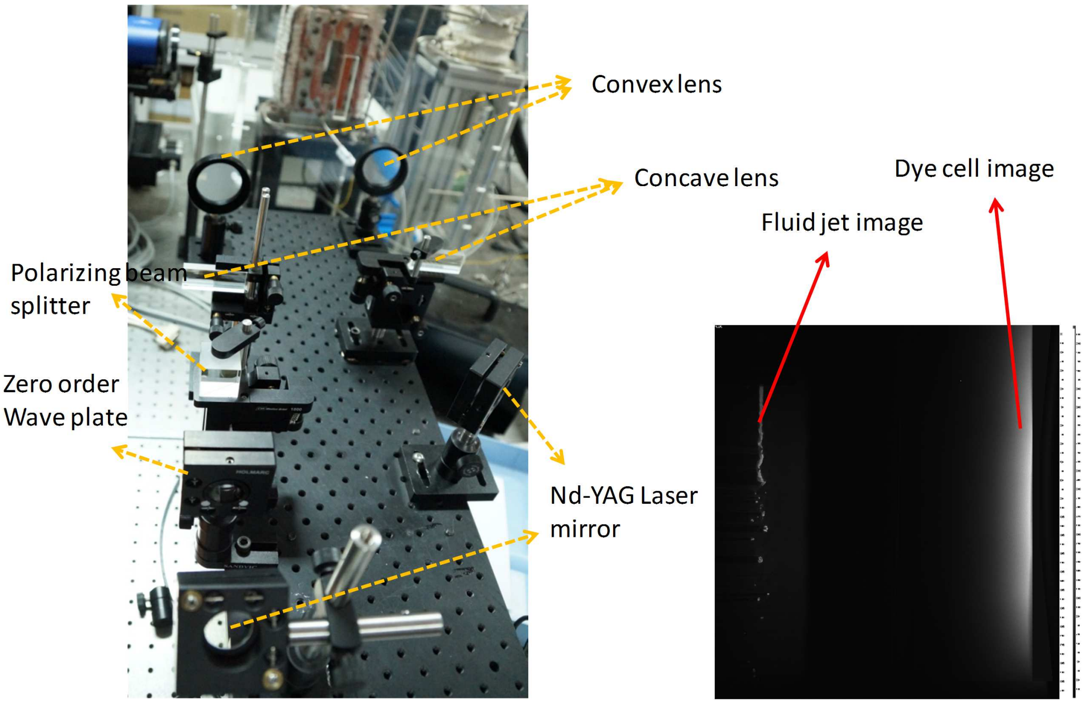

Figure 3.8 Photograph of the optical arrangement for the PLIF experiment.

signal is collected by effectively blocking the elastic scattering using UV filters.

The variation in the intensity of the laser sheet profile along the vertical direction must be corrected. The laser sheet is sent through the chamber filled with fluoroketone vapor. The 2D-fluorescence signal is collected by effectively blocking the elastic scattering using UV filters. The laser sheet profile correction is performed to account for the variation in the intensity along the height of the sheet. The expression for the laser sheet profile correction utilized by Vaidyanathan et al. (2009) is used in the current study. The normalized laser sheet intensity variation along the jet center plane is shown in fig. 3.9. It is observed that the intensity varies from 50% at the jet inlet to nearly 100% at a distance of 30 and 50 mm from the jet inlet. The intensity again decreases gradually to about 50% at around 85 mm distance from the jet inlet. The error due to the intensity variation in the vertical direction is corrected using equation 3.1.

$$S_{corrected}(m,n) = S_{uncorrected}(m,n)\frac{max(S_{profile})}{S_{profile}(m)} \tag{3.1}$$

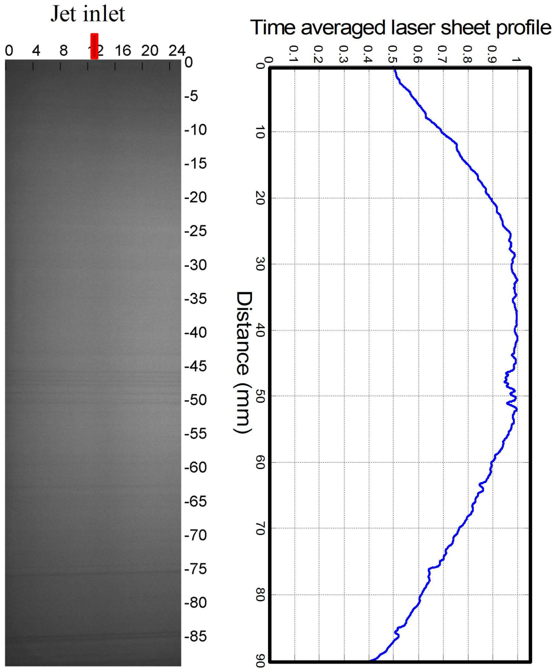

Figure 3.9 Variation in laser intensity along the jet axis.

The $S_{uncorrected}(m,n)$ is the fluorescence signal obtained from the 2-d jet plane, $S_{profile}(m)$ is the variation of fluorescence signal of the fluoroketone vapor along the jet axis and the $S_{corrected}(m,n)$ represents the corrected intensity of the jet plane, and accounts for the changes in the laser intensity along the vertical direction. It is to be noticed that there exists an uncertainty due to shot-to-shot fluctuations of the laser sheet profile and the uncertainty contributes to random error. The 50 images selected are normalized with the maximum intensity and the standard deviation is computed for each pixel along the vertical direction. The mean percentage deviation in the normalized laser sheet intensity along the profile height is found to be 2.8%. From the laser sheet fluorescence signal, it is found that the maximum percentage deviation in the fluorescence signal due to shot-to-shot fluctuation in laser intensity is around 5.5%.

The attenuation of the laser sheet passing through the liquid medium with density of 1600 kg/m^3 is measured and it is found that for about 1 mm distance, the intensity of the laser is reduced by 35% as evident from fig. 3.10. For the case of

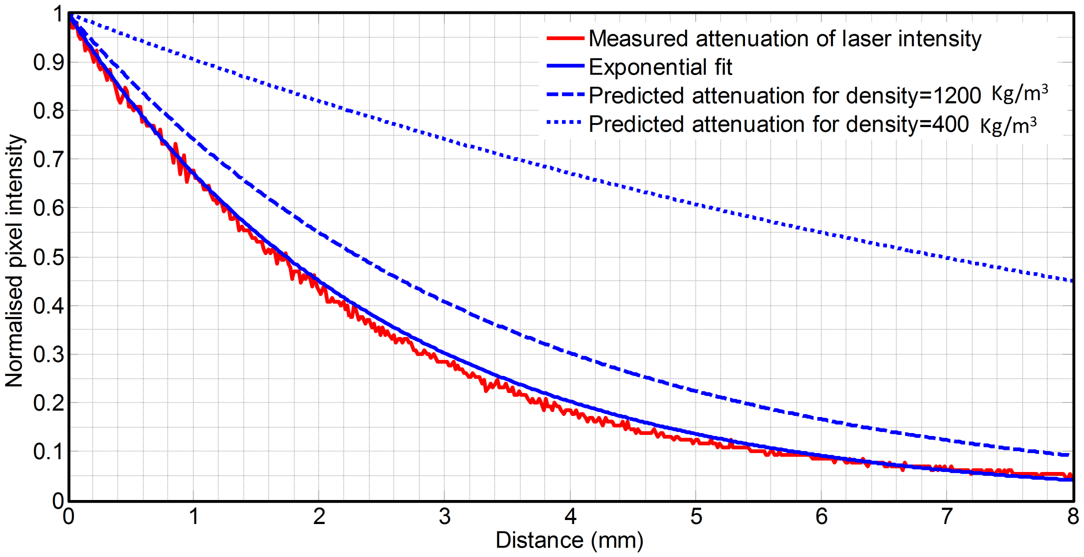

Figure 3.10 Attenuation of the laser intensity along the direction of propagation inside the liquid.

supercritical jet injection, the density of the injected jet is below one-third of liquid density and is around 400 kg/m^3. The maximum deviation in the measurement of the density is found to be about 9% for the supercritical injection density of 400 kg/m^3 and 12.5% for that of 550 kg/m^3. Hence in the current study, the calculation of density values from the fluorescence measurement are carried out for only those cases corresponding to jets injected at supercritical conditions where the injectant density ranges between 220 and 575 kg/m^3.

The errors due to the aforementioned uncertainties could be significantly different for each experiment, depending on the setting up of various optical configurations for the PLIF measurements. The uncertainties associated with the density measurement are discussed in the respective chapters 4 and 5.

3.8.7 Determination of density map of the jet

Roy et al. (2011) obtained the relation for fluorescence as

$$S(x,y) = F\rho\varphi\left[1 - e^{-\alpha(\frac{\lambda}{hc})I(0,y)e^{-\sigma n x}}\right] \tag{3.2}$$

where S is the flurorescence signal recorded at various positions (x, y). The factor F constitutes of optical efficiency, fractional solid angle and other constants. ρ is the mass density of the medium and φ is the fluorescence yield.

$I(0, y)$ is the incident intensity of the laser sheet and term $I(0, y)e^{-\alpha nx}$ is intensity at various positions (x, y) due to the absorption of the laser which depends on absorption cross section (α) and number density of the molecules (n). In the current experiment, the laser intensity is fixed and the attenuation of the laser intensity due to absorption is estimated to cause a maximum uncertainty of 12.5% in density measurements. Based on the assumption of constant laser intensity, the expression could be written as,

$$S(x, y) = F\rho\varphi \left[1 - e^{-k}\right] = C\rho \tag{3.3}$$

From the equation 3.3, it is clear that the fluorescence is directly proportional to the mass density. One of the uncertainties involved in the measurement of density is the shot to shot fluctuations in the laser intensity. This is eliminated by employing a reference dye cell as shown in fig. 3.7. In the current set of experiments conducted as part of the study, the image doubler has been used to capture the two different images simultaneously: one is the jet image and the other is that from the reference dye cell filled with the liquid fluoroketone at 300 K and 1 bar.

It has to be noted that the injected jet and the reference dye cell are kept at two different image planes. To account for the difference in optical efficiency, fractional solid angles and other factors that contribute to the fluorescence signal collected from the image plane of the jet and the dye cell, calibration is carried out by collecting the fluorescence signal simultaneously from the jet plane and the dye cell at atmospheric condition at 1 bar and 300 K. Thus the fluorescence signal could be modeled as

$$S_{liqjet(300K,1bar)} = K_1\rho_{liq(300K,1bar)} \tag{3.4}$$

$$S_{dyecell(300K,1bar)} = K_2\rho_{liq(300K,1bar)} \tag{3.5}$$

Here $S_{liqjet(300K,1bar)}$ and $S_{dyecell(300K,1bar)}$ refer to the fluorescence signal collected from the jet image plane and the dye cell respectively. K_1 and K_2 represents two different constants that include the contribution from the optical efficiency, solid angles and other factors for the jet and the dye cell respectively. Since density of fluoroketone at 300 K and 1 bar for both the jet and the dye cell are the same, the ratio of the signals, $S_{liqjet(300K,1bar)}/S_{dyecell(300K,1bar)}$, will represent the ratio of the factors K_1 and K_2 of the jet and dye cell respectively. Thus

$$\frac{S_{liqjet(300K,1bar)}}{S_{dyecell(300K,1bar)}} = \frac{K_1}{K_2} \tag{3.6}$$

This will take into the account the variation in the fluorescence signal at image plane and dye cell due to all the factors other than density variations. The next step is to calculate the density values of the jet injected at supercritical conditions with reference to the density values corresponding to 300 K and 1 bar of the fluoroketone liquid in the dye cell. The fluorescence signal from a supercritical jet, S_{jet}, injected into chamber could be related to density of the supercritical jet as

$$S_{jet} = K_1 \rho_{jet} \tag{3.7}$$

The ρ_{jet} can be determined by using eq. (3.5) and (3.7) as

$$\rho_{jet} = \frac{K_2}{K_1} \frac{S_{jet}}{S_{dyecell(300K,1bar)}} \rho_{liq}(300K, 1bar) \tag{3.8}$$

The expression for (K_2/K_1) from equation (3.6) could be substituted in equation (3.8) to get,

$$\rho_{jet} = \left[\frac{S_{dyecell(300K,1bar)}}{S_{liqjet(300K,1bar)}}\right]_{\text{Calibration shot}} \left[\frac{S_{jet}}{S_{dyecell(300K,1bar)}}\right]_{\text{Experimental shot}} \rho_{liq}(300K, 1bar) \tag{3.9}$$

Note that the fluorescence signals from the dye cell during the calibration shot and the experimental shot are different due to the fluctuation in the incident laser intensities corresponding to the two different laser shots. However for the jet and the dye cell the fluorescence signal is captured for the same shot in which the incident laser intensity is same. Thus using equation (3.9), the error due to the fluctuation of the incident laser intensity is eliminated in determining the density of the supercritical jet.

3.9 Equation of state of fluoroketone

The fluoroketone has been used in our study as the jet fluid because of its desirable properties. The density of the fluoroketone at various pressure and temperature conditions can be obtained using Peng-Robinson-Stryjek-Vera (PRSV) equation of state (Peng and Robinson, 1976) (Stryjek and Vera, 1986). The PRSV equation of state is used for predicting the thermodynamic state of the fluoroketone as suggested by Owens (2002). The parameters involved in the PRSV equation 3.10 are adopted from Gustavsson and Segal (2008). All the parameters involved in the equation are expressed in terms of critical properties and acentric factor. This model is found to provide reasonably accurate values of density near the critical point.

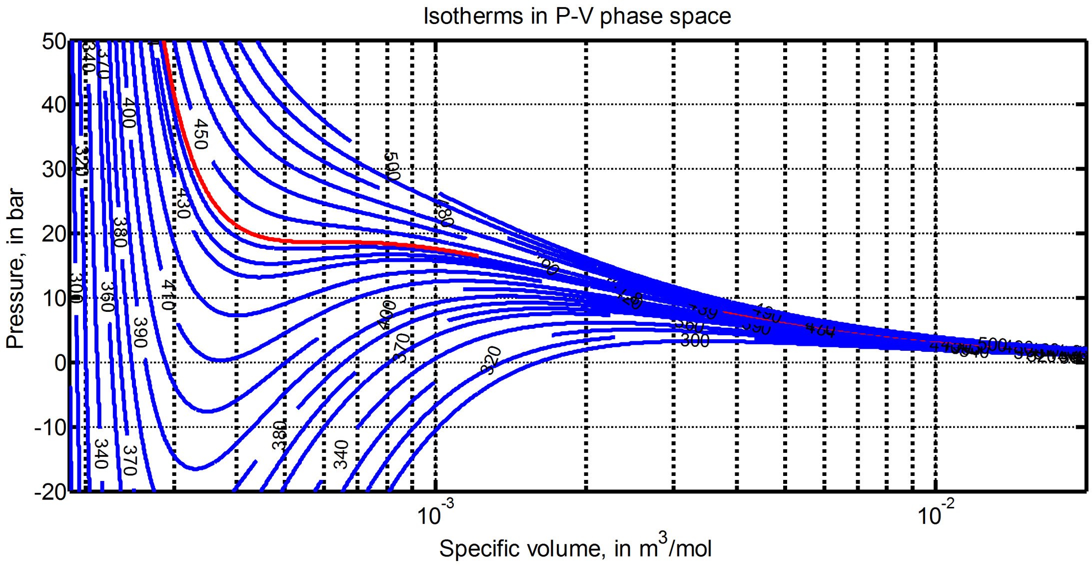

Figure 3.11 Pressure-molar volume phase space of fluoroketone obtained using Peng-Robinson-Stryjek-Vera equation of state.

$$P = \frac{RT}{V-b}\frac{a}{V^2+2bV-b^2} \tag{3.10}$$

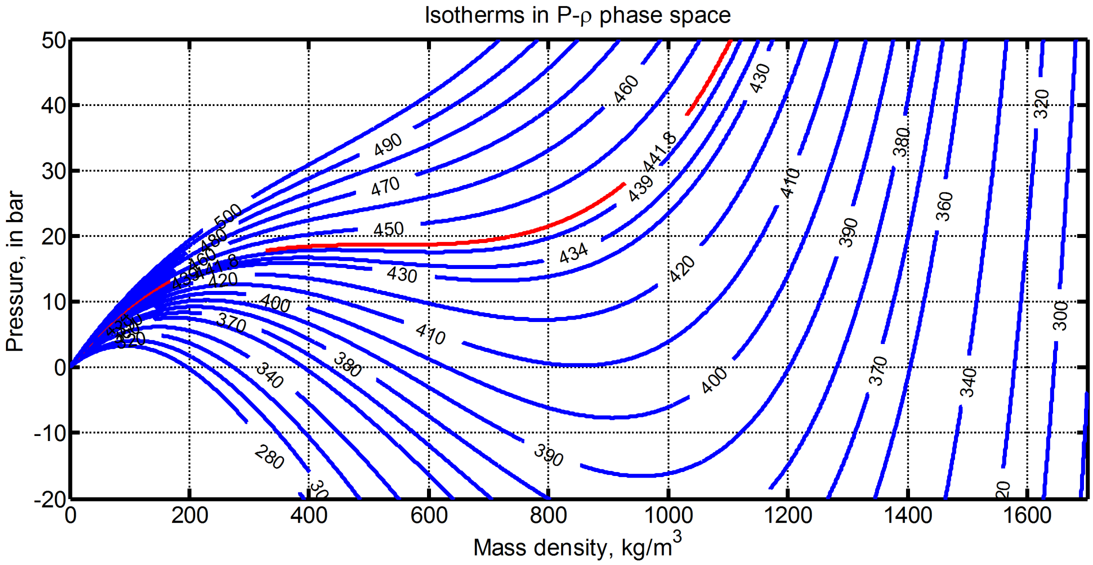

Figure 3.12 Pressure-density phase space of fluoroketone obtained using Peng-Robinson-Stryjek-Vera equation of state.

The parameters involved are:

$$a = \left[0.457235 \frac{R^2 {T_c}^2}{P_c}\right] \alpha$$

$$b = \left[0.077796 \frac{R T_c}{P_c}\right]$$

$$\alpha = \left(1 + \kappa(1 - \sqrt{T_R})\right)^2$$

$$\kappa = \kappa_0 + \kappa_1 (1 + \sqrt{T_R})(0.7 - T_R)$$

$$\kappa_0 = 0.378893 + 1.4897153\omega - 0.17131848\omega^2 + 0.0196554\omega^3$$

$\omega = 0.471$ and $\kappa_1 = 0.052$

Here P_c and T_c are the critical pressure and critical temperature respectively and the correction term (α) in the attraction parameter (a) is a function of acentric factor (ω) and adjustable pure component factor (κ_1).

The isotherms that range between 300 K and 500 K are plotted in P-V and P-ρ phase space. The red line in figs. 3.11 and 3.12 indicates the critical isotherm (T_c) of 441.8 K. At supercritical temperatures, it is observed in fig. 3.11 that the pressure of the fluid increases monotonically when subjected to isothermal compression. However at subcritical temperatures, it is observed from fig. 3.11 that during the compression process, the pressure first increases along the isotherm, then decreases and it again increases; this depicts an unrealistic physical process. Hence the PRSV equation can be directly utilized at supercritical temperature conditions only. However for the case of subcritical temperature, the Maxwell construction for PRSV equation can be performed to determine the state of the fluid precisely.

3.9.1 Maxwell construction of PRSV equation

The three isotherms: subcritical, critical and supercritical isotherms are plotted and are presented in fig. 3.13. On the critical isotherm and above the critical isotherm, the pressure is monotonically decreasing with increasing volume. However, below the critical temperature, the isotherm has negative pressure regions and mechanically unstable regions ($\frac{\partial P}{\partial V} = 0$) where the fluid tries to compress itself, and thus these regions are unphysical as shown in figs. 3.11 3.12 and 3.13. It can also be noticed that for a given pressure on subcritical isotherms, the curve has three solutions. However, physics requires that there should be only two solutions, corresponding to the liquid and the vapor phase to coexist in equilibrium, and this can be resolved using the Maxwell construction. Clerk-Maxwell (1875) constructed a horizontal line of constant pressure in the $P - V$ phase space for an isotherm to satisfy the equilibrium condition where the Gibbs free energy (G) of the liquid and the gas phases becomes equal (Clerk-Maxwell, 1875) (Greiner et al., 1995). The equilibrium pressure can be obtained by requiring the area under the curve $abcde$ and area under coexistence line to be same or in other words the areas $A1$ and $A2$ formed by the intersection of isotherm with Maxwell line to be equal. This is shown in fig. 3.13, mathematically represented in equation 3.11, and is referred to as Maxwell equal area construction.

$$\int_{V_{liq}}^{V_{vap}} \left(P - P_{eq}\right) dV = 0 \tag{3.11}$$

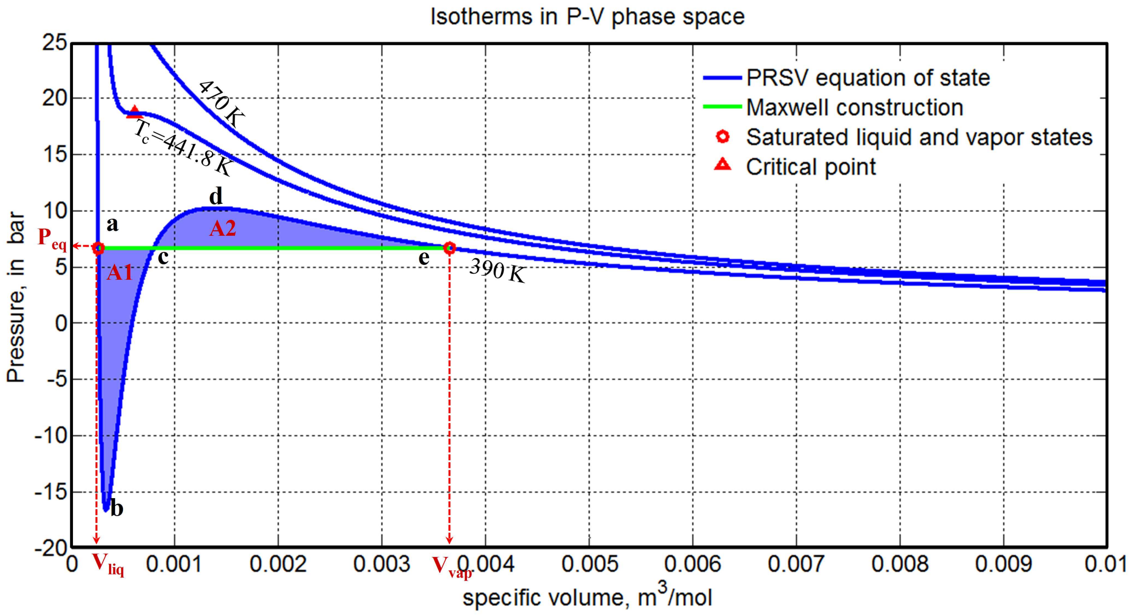

Figure 3.13 Maxwell construction of PRSV equation of state.

Thus in the current study, an algorithm is developed in MATLAB to apply the Maxwell equal area rule to the set of isotherms that ranges from the subcritical to the supercritical state in p-v phase space as shown in figs. 3.14, 3.15 (Clerk-Maxwell, 1875). The Maxwell equal area rule is generally accepted and used to determine the saturated liquid and vapor properties as mentioned by Davis and Scriven (1982). However, under certain circumstances, the Maxwell equal area rule cannot be generalized and may not be used unless certain special conditions are satisfied (Aifantis and Serrin, 1983). Hence the Maxwell construction of the PRSV equation of state needs to be validated. The liquid and vapor saturation states are presented in figs. 3.14, 3.15 and the saturated vapor pressure obtained from the Maxwell construction is validated against the Antoine model (Thomson, 1946) for vapor pressure.

To compute the vapor pressure of the fluoroketone, the Antoine model is used by Gustavsson and Segal (2007). The Antoine equation for fluoroketone is detailed in equation (3.12). The vapor pressure of the fluoroketone obtained from the Antoine model and the Maxwell construction of PRSV equation is plotted against the temperature as shown in fig. 3.16. The Maxwell construction of PRSV equation agrees well with the Antoine equation at temperatures below 400 K. The deviation between them increases monotonically with temperature and the maximum deviation is observed near the critical point and it is found to be about 5.5%. To predict the density of the fluoroketone vapor, the PRSV equation with Maxwell construction is utilized in the present work.

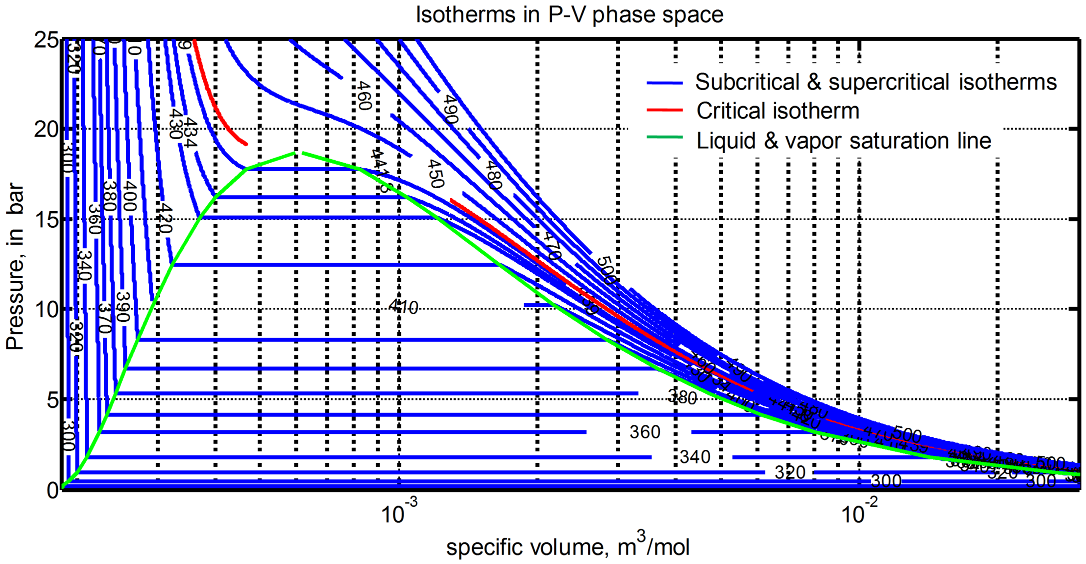

Figure 3.14 Pressure-molar volume phase space of fluoroketone obtained using Maxwell constructed PRSV equation of state.

$$Log_{10}P = 10.205 - \frac{1861.01}{T + 34.883} \tag{3.12}$$

It can be observed from fig. 3.15 that at subcritical isotherms, there is a sudden transition between the liquid and vapor phase with respect to the occurrence of changes in pressure. This transition is the so called first order transition. At the critical point, the liquid-vapor coexistence ceases to exist and this transition is said to be in continuous phase transition. Along the critical isotherm, the point of inflection is perceived at the critical point and is characterized by:

$$\left(\frac{\partial P}{\partial V}\right)_T = \left(\frac{\partial^2 P}{\partial V^2}\right)_T = 0 \tag{3.13}$$

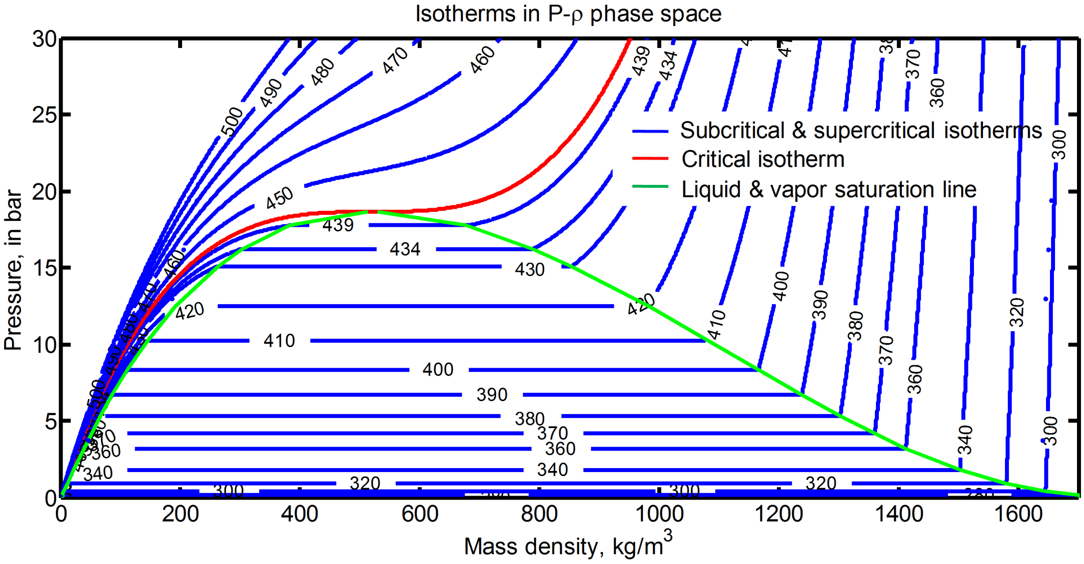

Figure 3.15 Pressure-density phase space of fluoroketone obtained using Maxwell constructed PRSV equation of state.

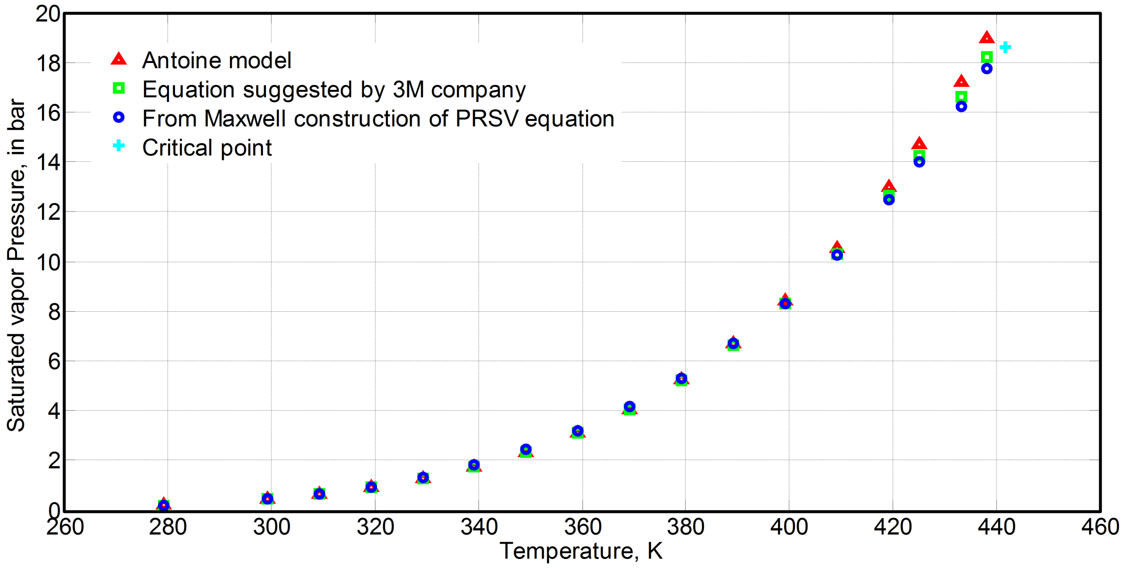

Figure 3.16 The comparison of the saturated vapor pressure of the fluoroketone obtained using Maxwell constructed PRSV with the Antoine model and those suggested by 3M company.

Also near the critical point, isothermal compressibility is perceived to be practically very large. This means that even a very small change in pressure could cause large changes in specific volume or the density of the fluid. This can be noticed and is evident from figs. 3.12, 3.13 and 3.15.

$$\beta_T = -\frac{1}{V}\left(\frac{\partial V}{\partial P}\right)_T \rightarrow \infty \tag{3.14}$$

For the supercritical isotherm, the pressure monotonically decreases with increasing volume. In the current study, the effect of pressure on the behavior of the jet is studied. The change in the pressure has direct effect on the density of the injected jet and it is expected to alter the behavior of the jet. The density of the injected fluid is found to be one of the parameters that determine the thermodynamic transition of the supercritical and the near critical jet in subcritical environments. The equation of state used in the present study is utilized to identify the conditions of the fluoroketone jet just prior to the point of injection. However, the equation of state cannot be used to predict the state of the fluoroketone jet once it is injected into the chamber with nitrogen or helium as the ambient fluid; this is because the thermo-physical properties of the jet fluid mixing with chamber fluid require complete knowledge of the properties of the binary component system.

CHAPTER 4

ELLIPTICAL JET AT THERMODYNAMIC SUBCRITICAL AND SUPERCRITICAL CONDITIONS

In this chapter, the investigation of the elliptical jet at subcritical to supercritical condition is carried out in detail. The elliptical jet at atmospheric condition exhibits axis-switching due to dynamic imbalance between the lateral inertia and the surface tension force. The work constitutes two parts: 1. Investigating elliptical liquid jet at supercritical chamber condition and 2. Investigating supercritical elliptical jet injected at subcritical and supercritical chamber condition using PLIF technique.

4.1 Introduction

Much of the studies in the past are carried out with circular jet and are mainly focused on understanding the thermodynamic transition of the jet fluid and its effect on the jet mixing characteristics. From the literature, it is well known that a liquid jet injected into supercritical chamber condition undergoes thermodynamic transition akin to a gaseous jet, without droplet formation. Most of the previous investigations on transition to supercritical behavior were carried out only through visual observation of presence/absence of droplets. The droplet formation at the shear layer of the injected liquid jet occurs due to the combined effect of surface tension as well as the shear shear force due to aerodynamic effects. The droplet formation could only reveal the presence of surface tension and the amount of surface tension could not be perceived.

However, the elliptical liquid jet exhibits axis-switching behavior due to the counteracting balance between the lateral inertia and the surface tension. This axis-switching phenomenon is a direct indicator of the presence of surface tension, and the axis-switching length is directly proportional to the surface tension present (Bohr, 1889). Any change in the surface tension could be perceived directly through the measurement of the axis-switching length (Kasyap et al., 2009), (Amini and Dolatabadi, 2012). Among the asymmetric liquid jets, the elliptical jet is the well studied, however, there was no study on elliptical jets at supercritical conditions.

The investigation of the elliptical jet at supercritical conditions could reveal further insight into the transition in surface tension as the jet encounters supercritical chamber conditions. The surface tension is the most important property and its presence or absence results in the two phase or single phase mixing characteristics of the fluid jet. The measurement of the axis-switching length of the jet could reveal further insight on the changes in surface tension of the jet. The detailed literature review on the elliptical jet is discussed in section 2.4 of chapter 2.

Hence, the changes in the surface tension of the liquid jet into a supercritical state could be directly understood from the axis switching phenomenon of the elliptical jet which would not be so straight forward if the circular jet is to be used at the supercritical state. This is the reason that the chapter on elliptical jet is preceding the chapter on circular jet.

4.2 Experimental conditions for subcritical jet injection using back-lighting visualisation

The chamber conditions for performing the experiments are detailed in table 4.1. The subcritical, critical and the supercritical chamber temperature conditions have been employed to study the effect of sub to supercritical pressures on the elliptical jet for the case of binary component system with nitrogen as the chamber fluid. For the case of single component system, fluoroketone itself is the chamber environment with chamber temperature at supercritical state and the pressure being varied from the subcritical to supercritical state. The term subcritical, critical

Chamber temperature conditions	**Chamber pressure P_r** $\frac{P_{chamber}}{P_c}$	**Chamber temperature T_r** $\frac{T_{chamber}}{T_c}$	**Injection temperature T_i** $\frac{T_{injection}}{T_c}$	**Chamber environment**	**Corresponding figures**	**Chamber conditions for N_2**	
						$\frac{P_{chamber}}{P_{c,N_2}}$	$\frac{T_{chamber}}{T_{c,N_2}}$
Atmospheric	0.054	0.68	0.68	N_2	Fig. 4.1	0.0295	2.38
Subcritical	0.913	0.96	0.68	N_2	Fig. 4.3	0.500	3.361
	1.012					0.554	
	1.37					0.750	
Critical	0.89	1.01	0.68	N_2	Fig. 4.4	0.487	3.536
	1.03					0.564	
	1.29					0.706	
Supercritical	0.875	1.12	0.68	N_2	Fig. 4.5	0.479	3.921
	1.05					0.575	
	1.32					0.723	
Supercritical	1.20	1.10	0.76	N_2	Fig. 4.6	0.657	3.851
	1.26	1.11	0.90			0.690	3.886
Supercritical	0.24	1.12	0.68	FK	Fig. 4.7		
	0.87						
	1.02						
	1.39						

Table 4.1 The pressure and temperature condition chosen for the experiment. FK denotes fluoroketone. The T_c and P_c are the critical properties of fluoroketone.

or supercritical is defined with respect to the chamber temperature to describe the chamber condition.

4.3 Jet behavior at atmospheric chamber condition

The experiment is performed with the elliptical jet to study the axis switching phenomena at atmospheric condition. The orifice is oriented with its major axis parallel to the line of sight of the camera. The equivalent diameter of the elliptical orifice employed in the present work is D_{eq}=2mm with aspect ratio of 4:1. The chamber and the liquid to be injected are at atmospheric temperature. Each experiment is repeated atleast 2 to 3 times to ensure repeatability. The 10 images from each experiment are selected and the axis switching wavelength is measured. The important flow parameter includes the velocity of the jet, and the jet characteristics are mainly determined from the fluid properties such as density, viscosity and the surface tension. The flow conditions of the jet are expressed in terms of the non-dimensional numbers such as Weber number (We) and Reynolds number (Re) that are determined from the flow and fluid properties.

$$Re = \frac{\rho V D_{eq}}{\mu} \tag{4.1}$$

$$We = \frac{\rho V^2 D_{eq}}{\sigma} \tag{4.2}$$

Here ρ is the density, V is the jet velocity, D_{eq} is the equivalent diameter of the orifice, σ is the surface tension of the fluoroketone and μ is the viscosity of the fluoroketone. The experimental data obtained for the liquid jets discharging from the elliptical orifice reveals that the jet exhibits distinct flow features at various flow conditions. Since the axis switching phenomenon arises due to the counteracting effect between the inertial force and the surface tension force, the Weber number is used to determine the flow characteristics of the elliptical jet. The axis switching phenomenon of the elliptical jets at various Weber number and Reynolds number corresponding to the laminar and transition regime is as shown in fig. 4.1.

It can be perceived from fig. 4.1 that for Reynolds number much below 2000, the flow is laminar with surface of the jet being smooth, and as the Reynolds number increases to the transition regime, ruffles on the jet surface begin to appear. This also indicates that for low Re cases, the effect of viscosity smoothens out the ruffles on the jet surface. It is found from the experimental data that the measured axis switching wavelength increases linearly with the velocity of the jet.

In fig. 4.2, the non-dimensional axis switching wavelength $\frac{\lambda_{as}}{D_{eq}}$ obtained from the current study is plotted against $\sqrt{We}$, and a similar relationship is also reported by Kasyap et al. (2009) and Amini and Dolatabadi (2012). The plot shows the linear dependence between λ_{as} and $\sqrt{We}$ with a slope of 1.11. Recently the

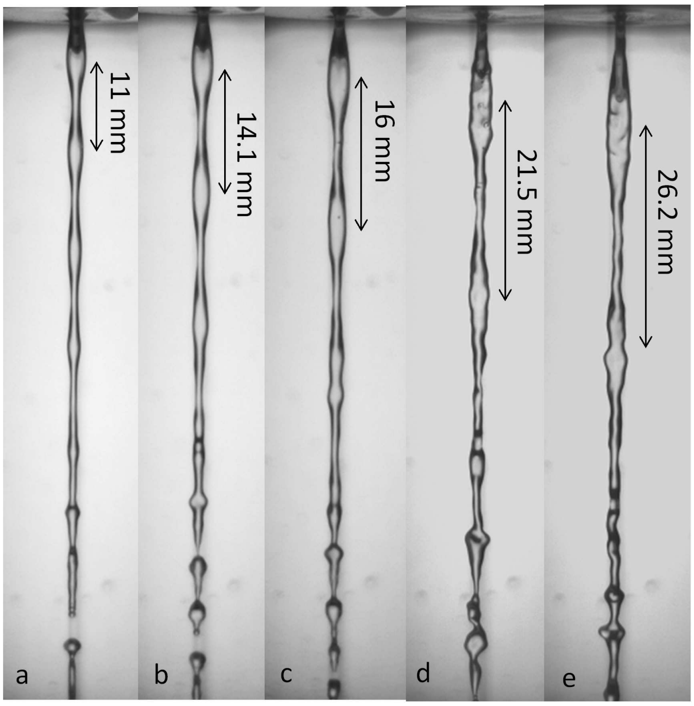

Figure 4.1 Variation of axis switching length with Weber number a) Re=667, We=5.42 b) Re=950, We=11 c) Re=1211, We=17.8 d) Re=1954, We=46.5 e) Re=2434, We=72.2.

relation between axis-switching wavelength and Weber number was proposed for small aspect ratio by Amini and Dolatabadi (2012), using a temporal mode analysis, as in equation 4.3.

$$\frac{\lambda_{as}}{D_{eq}} = \frac{\pi}{\sqrt{6}}\sqrt{\frac{We}{2} - 2} \tag{4.3}$$

which approximately yields,

$$\frac{\lambda_{as}}{D_{eq}} = 0.91\sqrt{We} \tag{4.4}$$

For high Weber number flow, the above equation can be approximated as $\frac{\lambda_{as}}{D_{eq}} = 0.91\sqrt{We}$. From fig. 4.2, it is evident that the slope obtained in the current study is in reasonably good agreement with the trends observed by Kasyap et al. (2009). The slight variation in the value of the slope could be attributed to the high aspect ratio elliptical orifice employed in the current study.

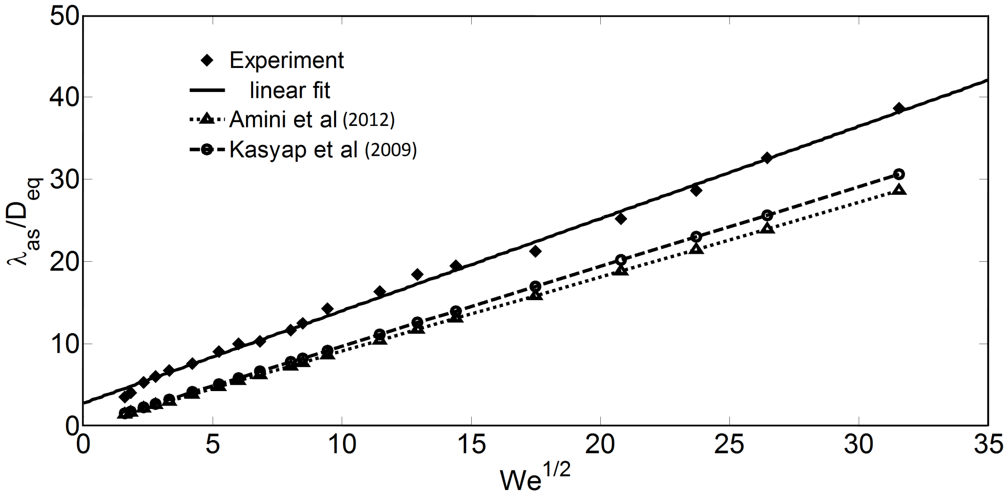

Figure 4.2 Variation of non-dimensional axis-switching wavelength with Weber number.

4.4 Liquid jet injected into supercritical chamber condition

As previously discussed, around the critical point, the fluid properties vary drastically. The surface tension effect becomes nearly extinct and there exists no distinction between the liquid and its vapor. The experimental conditions involved the jet at atmospheric temperature condition being injected into chamber conditions as detailed in table 4.1. The chamber conditions vary from the subcritical to supercritical conditions of the fluoroketone. The maximum chamber pressure is 26 bar and the maximum temperature is 500 K. The corresponding reduced pressure and temperature conditions are $P_r = 1.40$ and $T_r = 1.13$. The effect of pressure on the jet behavior has been studied for temperature conditions ranging from the subcritical to supercritical conditions of fluoroketone. The thermodynamic transition of the surface tension property of the fluoroketone is investigated based on the (1) axis switching phenomena and (2) jet characteristics, as it is injected into the supercritical chamber conditions. The experiments are performed with nitrogen as the ambient environment for binary component system, and fluoroketone as the ambient environment for single component system.

4.4.1 Nitrogen environment

The results of the low speed elliptical jet with axis switching behavior in a supercritical chamber conditions should provide physical insight about the changes in the surface tension. The N_2 gas is used to pressurize the chamber to desired condition before the start of the experiment. To ensure that the chamber is filled with N_2 gas, the chamber is repeatedly purged with N_2 gas before pressurization for each experiment. Since the injected jet is initially at the atmospheric conditions, the Reynolds number and Weber number are calculated based on the properties at the inlet condition and are abbreviated as Re_i and We_i.

The chamber is kept just below the critical temperature of fluoroketone, $T_r = 0.913$, and the pressure is varied from the subcritical to supercritical condition to investigate the corresponding effect on the fluoroketone jet behavior. Two different flow rates are employed and the jet behavior is investigated. Fig. 4.3 shows the effect of subcritical to supercritical pressures on the behavior of the jet at subcritical temperature condition. It is evident that there is no significant effect of the pressure on the axis-switching or the breakup of the jet. The measurement of the first and second axis switching wavelength of 4.3 show that the effect of surface tension of the jet does not vary over the large downstream distances. This also indicates that the time taken for the fluid to attain the thermal equilibrium with the surroundings and for the surface tension effects to get reduced is slower than which is typically expected.

Similar studies are performed with the chamber at the critical temperature $T_r = 1.01$ of the fluoroketone and the pressure is varied from the sub to supercritical conditions with $P_r = 0.89$ to $P_r = 1.35$. The effect of pressure on the axis switching behavior of the jet is shown in fig. 4.4. The jet surface remains smooth and the effect of surface tension is dominant for the large downstream distance without affecting the axis switching wavelength significantly. This indicates that the jet has not thermally equilibrated with the chamber condition.

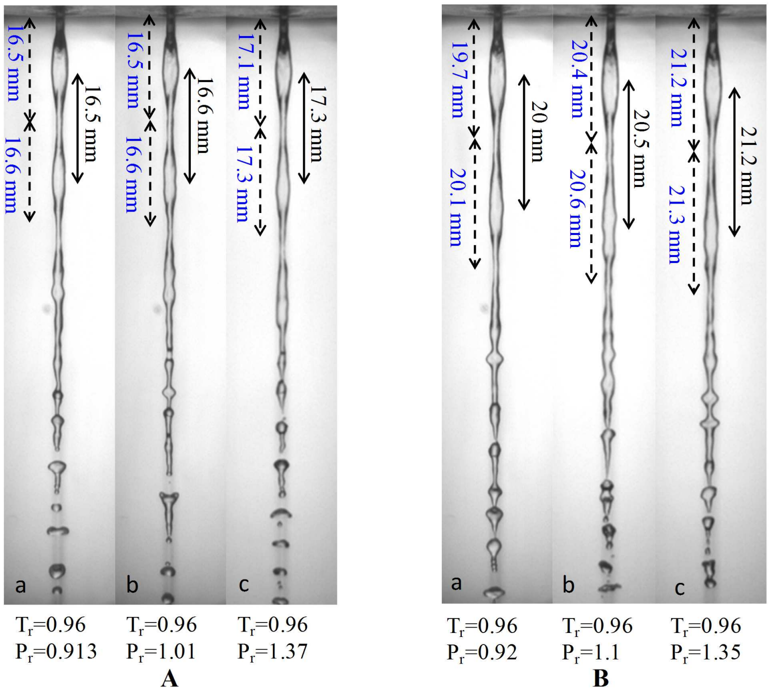

Figure 4.3 Fluoroketone injected into Nitrogen environment. Injection from subcritical temperature to high subcritical temperature condition. The pressures range from sub to supercritical conditions.
A) a) $\frac{\lambda_{as}}{D_{eq}}$=8.25 b) $\frac{\lambda_{as}}{D_{eq}}$=8.3 c) $\frac{\lambda_{as}}{D_{eq}}$=8.65, V=0.17 to 0.18 m/s, Re_i=1250, We_i=18
B) a) $\frac{\lambda_{as}}{D_{eq}}$=10 b) $\frac{\lambda_{as}}{D_{eq}}$=10.25 c) $\frac{\lambda_{as}}{D_{eq}}$=10.6, V= 0.33 to 0.36 m/s, Re_i=1930, We_i=46.3.

The investigation at the supercritical chamber temperature is carried out by increasing the chamber temperature to 490 K for which the corresponding reduced temperature is $T_r = 1.13$. The pressure of the chamber is varied from the $P_r = 0.87$ to 1.36. From fig. 4.5 it is clear that the first axis switching phenomena is still predominant for the pressure conditions ranging from the sub to supercritical condition. The measurement of the axis switching wavelength based on the first switching for this case is in good agreement with that of the atmospheric condition for the same velocity of the jet. This shows that the surface tension effect is still dominant even for the chamber at supercritical condition. At subcritical pressure, the formation of surface disturbances and distinct breakup modes are observed even at far down-

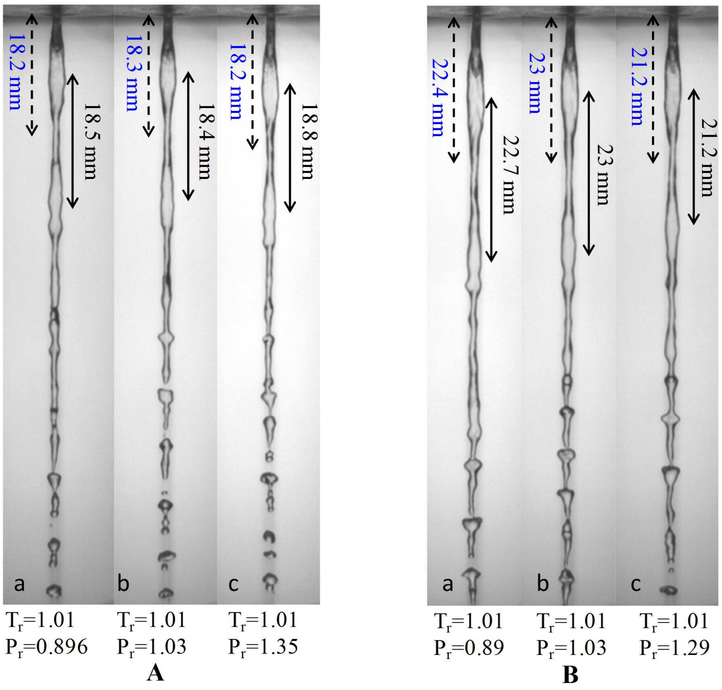

Figure 4.4 Fluoroketone injected into Nitrogen environment. Injection from subcritical temperature to critical temperature condition. The pressures range from sub to supercritical conditions.
A) a) $\frac{\lambda_{as}}{D_{eq}}$=9.25 b) $\frac{\lambda_{as}}{D_{eq}}$=9.2 c) $\frac{\lambda_{as}}{D_{eq}}$=9.4, V=0.19 to 0.20 m/s, Re_i=1490, We_i=27.6.
B) a) $\frac{\lambda_{as}}{D_{eq}}$=11.35 b) $\frac{\lambda_{as}}{D_{eq}}$=11.5 c) $\frac{\lambda_{as}}{D_{eq}}$=10.6. V=0.36 to 0.39 m/s, Re_i=1960, We_i=46.5.

stream distances. This behavior is observed even as the pressure is increased to near critical conditions. As the pressure is further increased to the supercritical condition of $P_r = 1.36$, the conventional breakup mode is not observed. This behavior is clearly observed in fig. 4.5.A.c and 4.5.B.c. Beyond a certain downstream distance, the breakup of the jet resulted in the formation of small droplets. Also, large amount of ruffles are formed at the jet surface at larger downstream distances. Similar observation is also reported by Chehroudi et al. (2002b) Chehroudi et al. (2002a). According to their study, the formation of ruffles on the surface of the jet indicates the marked decrease in surface tension force of the jet. Due to the restrictions on the optical access in the current study, the jet could be visualized only up

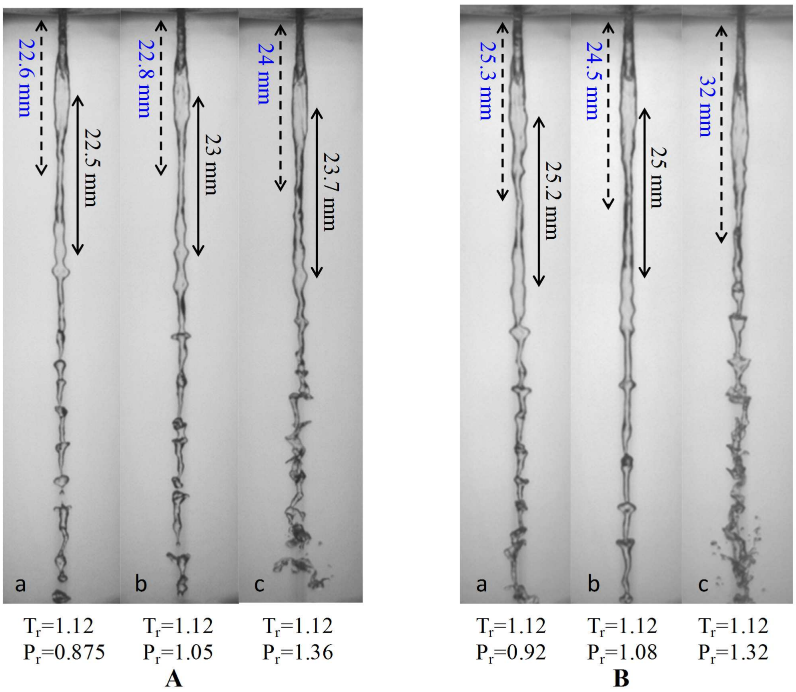

Figure 4.5 Fluoroketone injected into Nitrogen environment. Injection from subcritical temperature to supercritical temperature condition. The pressures range from sub to supercritical conditions. A) a) $\frac{\lambda_{as}}{D_{eq}}$=11.25 b) $\frac{\lambda_{as}}{D_{eq}}$=11.5 c) $\frac{\lambda_{as}}{D_{eq}}$=11.85, V=0.21 to 0.23 m/s, Re_i=1940, We_i=46.4 B) a) $\frac{\lambda_{as}}{D_{eq}}$=12.6 b) $\frac{\lambda_{as}}{D_{eq}}$=12.5 c) $\frac{\lambda_{as}}{D_{eq}}$=16, V=0.5 to 0.6 m/s, Re_i=2300, We_i=64.3.

to the limited downstream distance.

From 4.3, 4.4 and 4.5, the jet exhibits axis-switching phenomenon and a distinct interface of the jet is visible. The axis switching wavelength of the jet appears to be independent of the chamber pressure and the temperature conditions, and it only depends on Re and We of the injected jet. However, at supercritical chamber conditions, the fluoroketone jet at larger downstream distance experiences large amount of interfacial corrugations and the formation of fine droplets at the jet interface. As observed in fig. 4.5.A.c and 4.5.B.c, the fine droplet formation at supercritical pressure and temperature condition is attributed to the significant

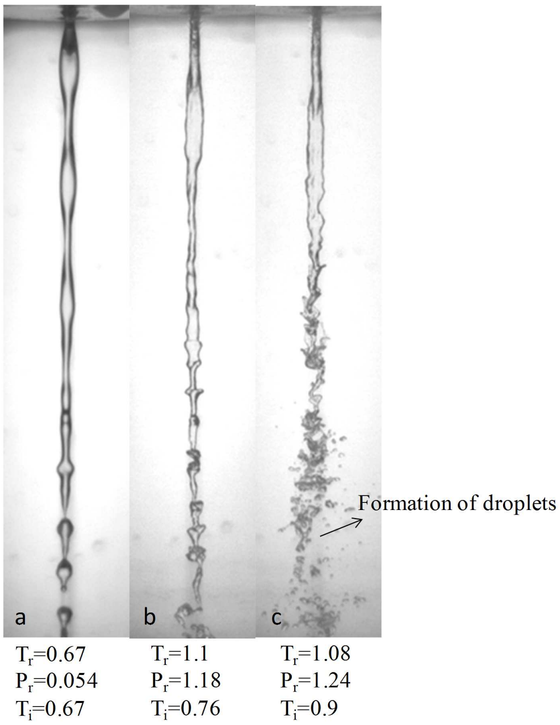

Figure 4.6 Fluoroketone injected into Nitrogen environment. Effect of preheating of jet prior to injection a) At atmospheric condition V=0.18 m/s, Re=950, We=11 b) V=0.183 m/s c) V=0.22 m/s. T_i is the reduced injection temperature that varies from atmospheric temperature to high subcritical temperature condition.

reduction in the surface tension of the jet at large downstream distance. It is also reported by (Chehroudi, 2012) and (Oschwald et al., 2006), that the solubility rate of the ambient gas in the jet fluid increases as the pressure is increased and this effect needs to be explored in more detail.

Attempts are also made to preheat the fluid before injecting into the chamber. The chamber is already at supercritical conditions and the jet is preheated prior to injection. The effect of preheating of the fluid on axis switching and breakup behavior is shown in fig. 4.6. The preheating seems to affect the axis-switching of the jet. The preheating of the jet to reduced temperature $(T_i = T/T_c)$ of 0.76 is performed prior to the injection of the jet into the chamber. The jet exhibits the same axis switching behavior but with an increased wavelength. This implies that the preheating temperature has the effect of decreasing the surface tension, thus increasing the axis switching wavelength for the same jet velocity. For this case, it can be seen that with the decreased effect of surface tension, the second axis switching event is significantly subdued.

When the jet is preheated to 122^oC $(T_i = 0.90)$ prior to the injection, the effect of surface tension considerably decreases and this results in increased axis switching length as this can be clearly seen in fig. 4.6c. Beyond the non-dimensional downstream distance about $L/D_{eq} = 14$, the jet breaks up. This breakup could be due to the sufficiently strong aerodynamic drag on the jet surface that is already having reduced surface tension. As the jet at reduced injection temperature $T_i = 0.90$ approaches near critical temperature, the effect of surface tension to sustain axis switching is significantly reduced. However, the effect of surface tension cannot be completely neglected as there are evidences of droplet formation at the downstream side of the jet.

4.4.2 Fluoroketone environment

The temperature of the chamber is kept well above the critical point with reduced temperature $T_r = 1.12$. The nitrogen supply to the chamber is shut off and the fluoroketone is injected into the chamber. Due to the high temperature of the chamber, the fluoroketone evaporates and its vapor occupies the chamber volume. Moreover there is an increase in the pressure of the chamber. The chamber is then opened to the atmosphere and is followed by injection of fluoroketone into the chamber. After purging the chamber with fluoroketone for 3 to 4 times in the aforementioned manner, the chamber is used for carrying out experiments with fluoroketone as the chamber environment. The chamber is already at supercritical temperature and the experiment is conducted for subcritical, critical and the supercritical pressures. The fluoroketone is introduced into chamber and the change in the pressure is monitored.

Once the chamber pressure reaches the desired subcritical pressure $P_r =$

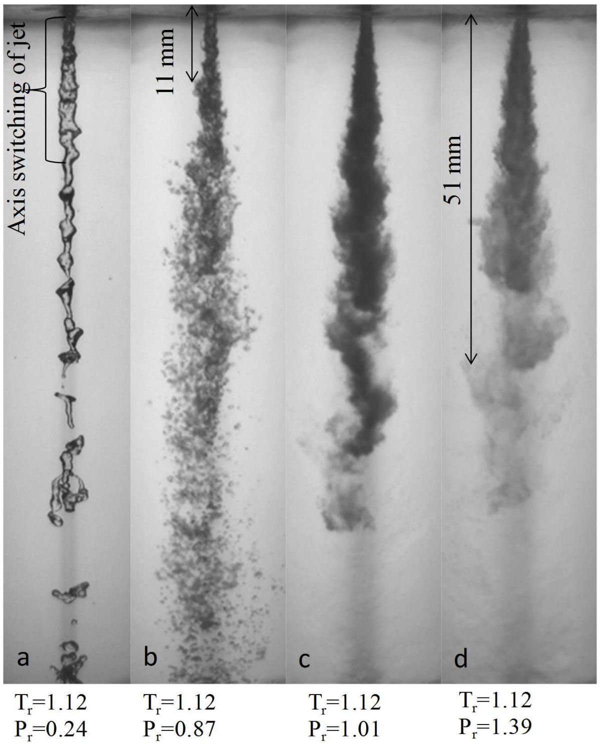

T_r=1.12 P_r=0.24

T_r=1.12 P_r=0.87

T_r=1.12 P_r=1.01

T_r=1.12 P_r=1.39

Figure 4.7 Fluoroketone injected into itself. Variation in the elliptical jet characteristics from sub to supercritical pressure conditions at T_i=0.68, V=0.21 m/s to 0.23 m/s, Re_i=1210, We_i=17.8.

0.24, the experiment is performed. The jet at atmospheric temperature with $T_i = 0.68$ is then injected into the chamber. It is observed in 4.7a that the elliptical jet exhibits the axis switching behavior, with large scale of ruffles on the surface. The ambient fluid to injecting fluid density ratio is 0.022, with the ambient fluid density being 35 kg/m^3. From fig. 4.7a, it is clear that the formation of the surface ruffles could be attributed to the aerodynamic drag that is induced on the surface of the jet due to the ambient fluid. A further increase in the chamber pressure to $P_r = 0.87$ causes the jet to disintegrate without exhibiting axis switching behavior; see 4.7b. The jet is intact only for few downstream distances of about $L/D_{eq} = 5.5$; thereafter it immediately breaks down into droplets, this effect indicates the presence of surface tension. The disintegration of the jet could be due to the aerodynamic force experienced by the jet as it enters the dense fluoroketone vapor. From the phase diagram of fluoroketone, the density of the vapor corresponds to 120 kg/m^3. The droplet formation is evident as the jet disintegrates and it is evident that the surface tension cannot be considered insignificant. As the pressure is increased to the critical value, see fig. 4.7c, it is observed that the opaqueness of the jet is significantly higher as compared to those in fig.4.7a and 4.7b. One of the reasons could be attributed to the high level of internal scattering of light and this could be either due to the presence of large number of very fine sized droplets or due to the high levels of fluctuation in the density of the fluid. On further increasing the chamber pressure to the supercritical regime, the jet becomes relatively transparent as compared to fig. 4.7c and exhibits behavior similar to gas-gas like mixing without significant droplet formation; a similar mixing behavior is also reported by Chehroudi et al. (2002a) for the case of circular jets. This indicates that the effect of surface tension is nearly absent and the transport process is governed by mass diffusion processes that dominate the gaseous jet mixing. From fig. 4.7d, it can also be observed that the jet mixing and diffusion rate is very high as it is hardly possible to distinctly identify the jet at downstream distances of $L/D_eq > 25.5$.

It is clear from fig. 4.5 and fig. 4.7 that the compositional effect of environment plays a significant role in the mixing process of the jet at sub to supercritical conditions. For the case of single component system as the pressure reaches the critical state, the surface of the jet reaches the critical mixing point and hence the distinct boundary between the liquid phase and the supercritical fluid phase does not exist. Similar behavior is observed for the case of liquid droplet in the supercritical environment without distinct boundary (Yang, 2000) (Manrique and Borman, 1969). For the case of binary component system, the solubility of the gas in the liquid is another important phenomenon that determines the thermodynamic transition of the jet to supercritical behavior. For a case of binary component system a distinct boundary could be perceived even when the pressure and the temperature of the chamber are well above the critical point of the jet fluid, and the reason could be attributed to solubility effects, resulting in the delayed transition of the jet interface to the thermodynamic critical state of the mixture.

4.5 Investigation using PLIF technique

Experiments are also performed with the PLIF technique to obtain a detailed two dimensional structure of the centreline of the jet. The details of the PLIF technique and the method of determination of density field of the jet are discussed in detail in section 3.8 of chapter 3. The density field of the jet at its centreline could be obtained only using PLIF technique. Since the attenuation of laser is around 35% for 1 mm distance for subcritical jets with density as high as 1300 kg/m^3, the density determination of supercritical jets is carried out as discussed in section 3.8.7.

4.5.1 Uncertainties in density measurement for supercritical injectant condition

The uncertainties associated with the determination of the density are listed in table 4.2 and it is evident that the largest source of uncertainty of 46% arises due to the variation of laser intensity along the sheet height. This is attributed to the

Uncertainty source	**Percentage error**	**Correction/remarks**
Intensity variation along laser sheet profile	46% deviation	Corrected as detailed in section 3.8.6 using a normalized laser sheet profile
Shot-to-shot fluctuation	5.5% deviation	Corrected as detailed in section 3.8.7
Laser sheet profile shape variation	2.8%	Corrected using average laser sheet profile. However shot to shot profile variation will contribute to random error
Laser attenuation	12.5%	Due to absorption by density up to 575 kg/m3
Root Square uncertainty in density prediction	**12.81%**	Due to profile variation and laser attenuation

Table 4.2 List of uncertainties and the possible errors in predicting the density field of supercritical jets.

Gaussian nature of the intensity distribution of laser beam and is corrected using a normalized laser sheet profile along the length of the jet. However, the normalized sheet profile is only an average representation of 50 laser shots and it must be highlighted that there will be minor shot to shot laser sheet profile variations; the uncertainty due to minor deviation from the averaged profile amounts to 2.8$\%$. Similar to the laser sheet profile variation in space, the shot to shot fluctuation in the intensity of the laser sheet amounts to 5.5$\%$; this is eliminated by simultaneously imaging the dye cell fluorescence and jet fluorescence using image doubler. Finally the uncertainty in the laser attenuation due to absorption by fluoroketone with a density of 575 kg/m^3 is estimated to be 12.5$\%$; it is nearly impossible to perform corrections without major assumptions. Based on the error analysis, the two factors that contribute to the uncertainty in density measurements include (1) laser sheet profile shape variation of 2.8$\%$ and (2) laser attenuation of 12.5$\%$, and the corresponding root square uncertainty in density is determined as 12.81$\%$.

4.6 Experimental conditions for subcritical and supercritical jet injection using PLIF visualization

In table. 4.3 the conditions employed for the subcritical to supercritical experiment with helium as the ambient medium are presented. In the current study, the helium is used for its much lower critical pressure as compared to fluoroketone whereas nitrogen has critical pressure greater than that of fluoroketone. It can be noted from table. 4.3 that the subcritical fluoroketone jet is injected into a high subcritical or supercritical environment with helium as the ambient fluid.

Table 4.3 shows the various experimental conditions that are selected to investigate the effect of ambient fluids: nitrogen or helium. The conditions correspond to (1) high subcritical to supercritical fluoroketone jet injected into subcritical conditions, and (2) supercritical fluoroketone jet injected into supercritical conditions. All the chamber and the injection conditions shown in table 4.3 are reduced with respect to critical pressure and temperature of fluoroketone. Also the chamber

Injection temperature to chamber temperature conditions	**Chamber pressure P_r**	**Chamber temperature T_r**	**Injection temperature T_i**	**Chamber environment**	**Chamber conditions for He**		**Chamber conditions for N_2**	
					$\frac{P_{chamber}}{P_{c,He}}$	$\frac{T_{chamber}}{T_{c,He}}$	$\frac{P_{chamber}}{P_{c,N_2}}$	$\frac{T_{chamber}}{T_{c,N_2}}$
Sub- to high subcritical conditions	0.85	0.97	0.71	He	6.95	82.47		
	1				8.18			
	1.2				9.81			
Subcritical to supercritical conditions	0.85	1.07	0.71	He	6.95	90.97		
	1				8.18			
	1.2				9.81			
High subcritical to subcritical conditions	0.85	0.72	0.92	N_2 or He	6.95	61.21	0.465	2.521
	1				8.18		0.547	
	1.2				9.81		0.657	
Near critical to subcritical conditions	0.85	0.85	1	N_2 or He	6.95	72.42	0.465	2.97
	1				8.18		0.547	
	1.2				9.81		0.657	
Supercritical to subcritical conditions	0.85	0.87	1.06	N_2 or He	6.95	73.96	0.465	3.045
	1				8.18		0.547	
	1.2				9.81		0.657	
Supercritical to supercritical conditions	0.85	1.04	1.05	N_2 or He	6.95	88.42	0.465	3.641
	1				8.18		0.547	
	1.2				9.81		0.657	

Table 4.3 Pressure and temperature conditions of chamber and the injected fluid chosen for subcritical and supercritical experiments with N_2 or He as the ambient fluid. The T_c and P_c are the critical properties of fluoroketone.

pressure and temperature conditions with respect to the ambient fluid, nitrogen or helium, is provided in the table 4.3.

4.7 Liquid jet at supercritical chamber condition with He as ambient fluid

The helium is chosen in this study since it has the critical pressure of 2.27 bar which is lower than the critical pressure of fluoroketone. The conditions chosen for sub to supercritical experiments in this section are similar to those investigated in section 4.4. The experiments in section 4.4.1 were performed by injecting subcritical elliptical jet into sub to supercritical conditions with nitrogen as surrounding gas; thus this was a binary component system. The presence of axis switching phenomena was observed for the case with nitrogen as ambient environment that indicated the presence of surface tension; also the experiments were conducted at the chamber condition that is always subcritical for the nitrogen gas though the conditions are supercritical for the fluoroketone.

In the present section, helium is used as the ambient environment, the high pressure chamber is purged with helium gas prior to the experiment. The chamber is heated to the temperature just below the critical temperature and three different pressures ranging from sub to supercritical are chosen for the experiment as detailed in table 4.3. When a subcritical fluoroketone jet is injected into high subcritical environment, the axis switching behavior is observed and it indicates the effect of surface tension. Beyond certain downstream distance, the jet undergoes breakup and droplet formation is also observed from fig. 4.8(a-c). To conduct the sub to supercritical experiment, the chamber is heated to a supercritical temperature of about T_r=1.07. The pressure and temperature condition of the chamber are supercritical for both fluoroketone and helium. It is observed that the injected jet exhibits axis switching behavior even at supercritical temperature condition as is evident from fig. 4.8 (d-f). It is also noted that for all the pressure range from subcritical to supercritical, the jet undergoes axis switching followed by breakup after certain downstream distances. This also indicates that pressure does not play a significant role in altering the behavior of the subcritical jet. A similar behavior is discussed in section 4.4. Also it is observed that when a subcritical jet is injected into a supercritical environment, the jet undergoes axis switching for the situation when the jet and the ambient fluids are different. The measured axis switching length is shown in fig. 4.8. It is to be noted that the observed differences in the axis switching length of the cases in fig. 4.8(d-f) are due to their differences in injection Weber number (We_i).

The axis switching length of the subcritical jet injected into supercritical condition with helium as the ambient fluid is compared with that of section 4.4 where nitrogen is used as ambient fluid. The non-dimensional axis switching (λ_n)

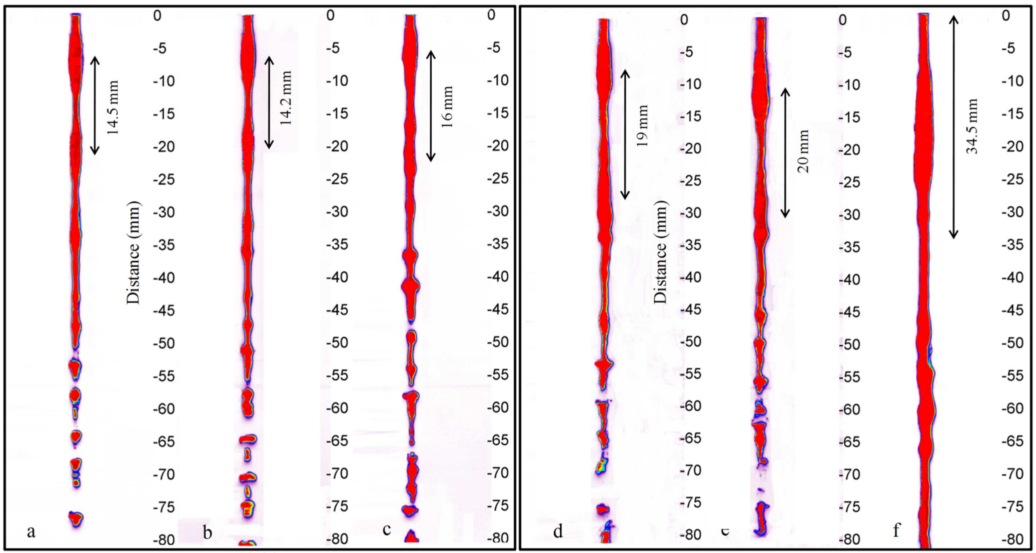

P_r=0.84
T_r=0.97
T_i=0.71
Re_i=1083
We_i=13.9
λ_n=7.25

P_r=0.99
T_r=0.97
T_i=0.71
Re_i=1072
We_i=13.7
λ_n=7.1

P_r=1.12
T_r=0.97
T_i=0.71
Re_i=1124
We_i=14.9
λ_n=8

P_r=0.91
T_r=1.07
T_i=0.71
Re_i=1751
We_i=36.3
λ_n=9.5

P_r=1.02
T_r=1.07
T_i=0.71
Re_i=1770
We_i=37
λ_n=10

P_r=1.32
T_r=1.07
T_i=0.71
Re_i=1971
We_i=51.7
λ_n=17.25

Fluoroketone injected into Helium environment

Figure 4.8 Injection of subcritical fluoroketone jet into high subcritical condition (a-c) and supercritical condition (d-f) in helium environment. The subscript i denotes the injection condition.

length, defined as λ_{as}/D_{eq} is plotted against the square root of Weber number as shown in fig. 4.9. For both N_2 and He environments, the measured axis switching length is found to be similar. Moreover, the axis switching length of sub to supercritical conditions for both fluoroketone-N_2 and fluoroketone-He system is only slightly greater than the values corresponding to the case in which the fluoroketone jet is injected into ambient nitrogen environment at 1 bar and 300 K as reported in section 4.4. Since the fluoroketone-N_2 and fluoroketone-He systems exhibit axis switching, which is a direct indication of the presence of surface tension, it can very well be concluded that the jet has not completely undergone the thermodynamic transition to its critical state. This direct observation would have been nearly impossible if a circular jet was employed for investigating the thermodynamic transition of the jet. As perceived from fig. 4.9 the axis switching length for sub to supercritical injection is independent of the ambient gas when the fluids are different in the jet and the ambient. Though the helium environment is at supercritical state, the results suggest that it does not possess sufficient enthalpy to cause the thermodynamic transition of the injected subcritical jet to supercritical state instantaneously. However, for a single component system, the results of section. 4.4.2 reveal that for subcritical fluoroketone jet injected into its own supercritical environment, the injected jet behaved like a gaseous jet, and demonstrated gas-gas like mixing characteristics.

From fig. 4.9, in the presence of helium environment, the axis switching length of fluoroketone jet is independent of the supercritical pressure and temperature condition. This reveals that there are hardly any changes in the surface tension. The jet behavior in this case is similar to that in the nitrogen environment case of fig. 4.3 discussed in the section 4.4.1; it indicates that the jet has not reached thermal equilibrium with the surrounding supercritical environment. This could also be due to the reason that the enthalpy of surrounding gas is not sufficient for the interface to achieve thermal equilibrium with the surrounding gas. Similar arguments could be found from the analysis of Dahms and Oefelein (2013) where it is demonstrated that for a binary component system, in many cases, the enthalpy of ambient fluid is not sufficient for the interface to reach the critical temperature.

For fig. 4.8f, it can be noted from table 4.3 that the chamber pressure and temperature conditions are supercritical for both the fluoroketone jet and the ambient He; however, the combined fluoroketone-He system does not exhibit transition to gaseous jet behavior as similar to the single component case of fig. 4.7. This also suggests that even at chamber conditions that are supercritical for the individual species, either fluoroketone or helium, the fluoroketone-He mixture at the jet interface would not have reached the critical pressure and temperature conditions to expect gaseous jet-like behavior.

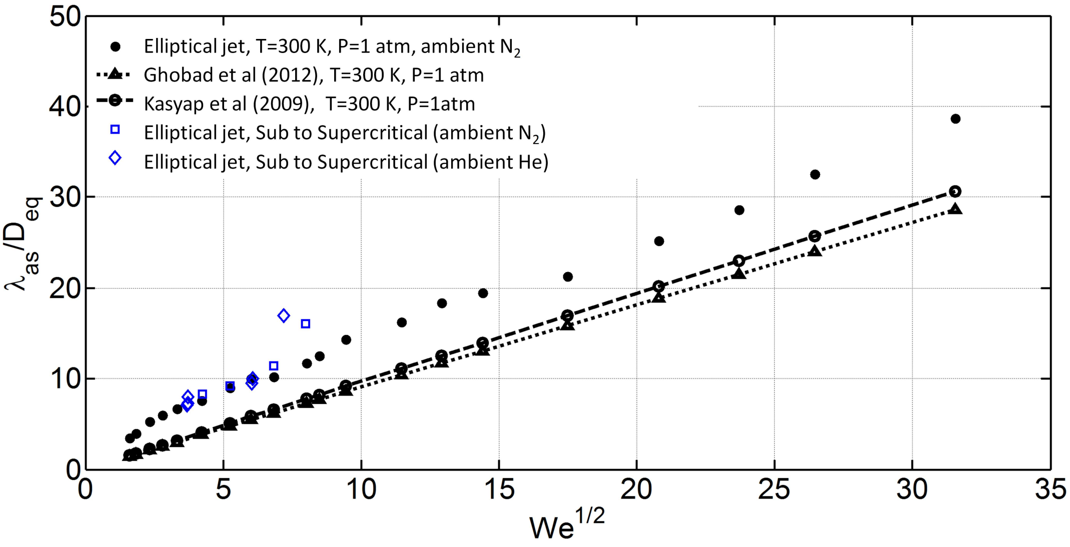

Figure 4.9 Variation of non-dimensional axis switching length with Weber number.

4.8 High subcritical jet injected into subcritical conditions with N_2 or He as ambient fluid

The term high subcritical has been used to refer to the temperature of the fluid which is significantly higher than the atmospheric temperature but below the critical temperature of the injected fluid. In the present section, the injection of high subcritical jet into subcritical environment is shown in fig. 4.10. In fig. 4.10 (a-c), nitrogen gas is used as the chamber environment and in fig. 4.10 (d-f) the chamber environment is constituted by supercritical helium. Under high subcritical temperature (T_r=0.92), the injected jet from the elliptical orifice exhibits axis switching behavior. This suggests the presence of surface tension. The increase in axis switching length is observed and this could be due to the decrease in surface tension of the jet. While keeping the chamber temperature constant, the study is carried out by increasing the pressure from subcritical to supercritical. It is clear from fig. 4.10 (a-c) that the effect of pressure does not seem to affect the axis-switching wavelength of the jet. Also the breakup characteristics of the jet remain the same for chosen pressures. From fig. 4.10(d-f), it is also clear that the chamber pressure

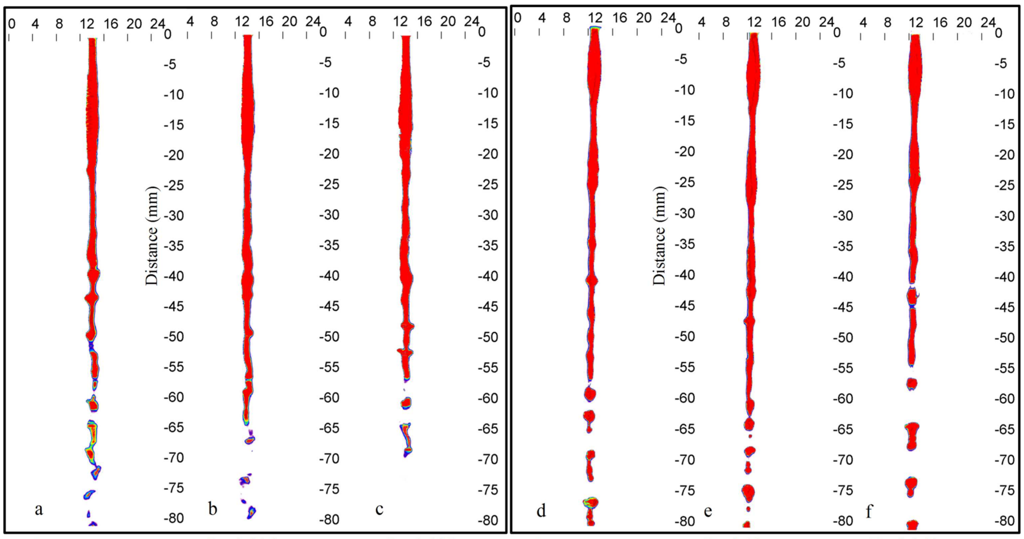

$P_r=0.92$
$T_r=0.71$
$T_i=0.92$
M=0.99 g/s

$P_r=1.016$
$T_r=0.72$
$T_i=0.924$
M=0.95 g/s

$P_r=1.125$
$T_r=0.71$
$T_i=0.93$
M=0.91 g/s

Fluoroketone injected into N2 environment

$P_r=0.90$
$T_r=0.72$,
$T_i=0.915$
M=0.79 g/s

$P_r=1.10$
$T_r=0.727$
$T_i=0.92$
M=0.85 g/s

$P_r=1.341$
$T_r=0.725$
$T_i=0.92$
M=0.80 g/s

Fluoroketone injected into Helium environment

Figure 4.10 High subcritical temperature fluoroketone jet in subcritical environment.

does not play a major role in influencing the axis switching wavelength of the jet.

4.9 Jet at near-critical condition injected into subcritical condition with N_2 or He as ambient fluid

At the critical temperature and pressure, the effect of surface tension is considered to be negligible, the distinction between the liquid and the vapor phase ceases to exist; this is seen from the phase-space diagram in fig. 3.15. The near critical fluoroketone jet injected into nitrogen and the helium environment is shown in fig. 4.11 (a-c) and fig. 4.11 (d-f) respectively. It can be noticed that as the jet at near critical temperature is injected into subcritical chamber conditions, it does not exhibit any axis switching characteristics. This confirms that at the critical temperature, the effect of surface tension of the fluid has significantly reduced. On close observation of the near critical jet injected into the subcritical chamber condition, it is found that the jet disintegrates, and also leads to formation of fluoroketone vapor and droplets. At critical chamber pressure, the fluoroketone droplet formation is more evident as observed from fig. 4.11 (b,e). As the chamber pressure is increased to supercritical condition, the injected jet is in liquid phase as noticed from fig. 3.15 and there is no evidence of vapor phase formation.

As observed from fig. 3.15 of chapter 3, at the critical temperature the density of the fluid is very sensitive to the changes in pressure. The increase in pressure around the critical point from around 15 bar to 20 bar causes large changes in density from 200 to 750 kg/m^3 as observed from fig. 4.12. This could be the reason for the injected jet at critical conditions to undergo immediate transition to liquid phase as the injection and the chamber pressure reaches the supercritical pressure (P_r=1.306). It is observed that at high supercritical chamber pressure and subcritical chamber temperature, the injected jet at critical temperature instantly undergoes thermodynamic transition to liquid state with reestablishment of the effect of surface tension as observed in fig. 4.11c and 4.11f. It is also noted from fig. 4.11f that the near-critical jet exhibits axis switching and it indicates the existence of surface tension prior to jet disintegration. From fig. 4.11 (a-c) and fig. 4.11 (d-f), it is observed that the fluoroketone-N_2 and fluoroketone-He system possess similar characteristics and the chamber environment/medium does not play a significantly different role in deciding the jet behavior for the case of binary component system.

The density map is obtained for the cases presented in section 4.10 and 4.11. For these cases, the injected jet is at supercritical condition for which the density varies between 200 and 550 kg/m^3 as shown in table 4.4. Since the attenuation of laser for the supercritical injection case is less than 12.5%, the uncertainty in density color map is considered to be of the same order. In table 4.4 the injected fluid density for various injection and chamber condition associated with supercritical injection to sub and supercritical chamber conditions are presented.

The details of the density measurement using the PLIF technique of the present experiment is provided in section 3.8.7. The deviation between the experimentally measured injected fluid density and the predicted density from Maxwell

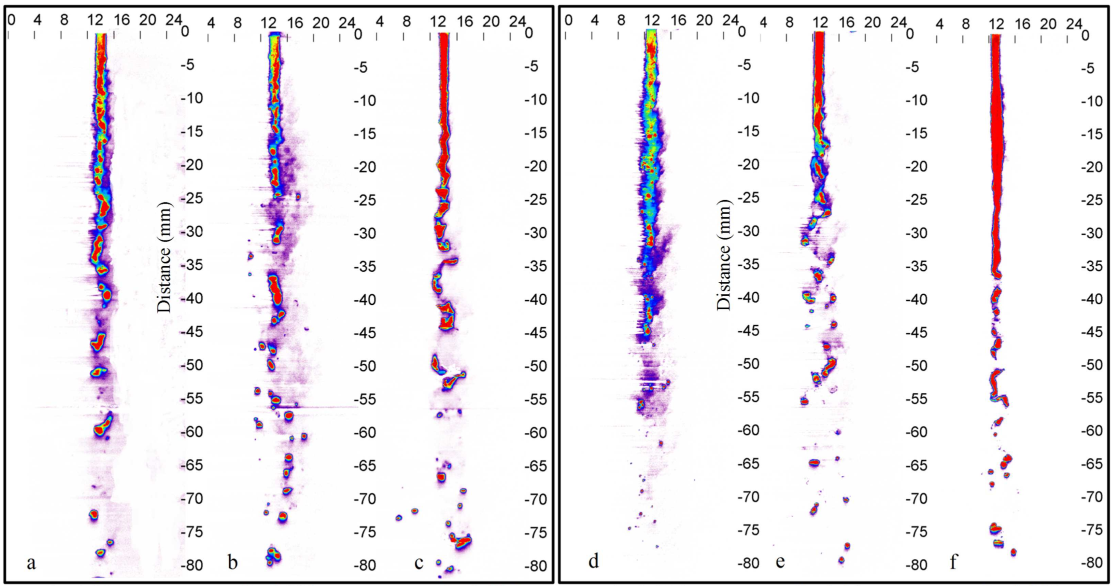

a: P_r=0.92, T_r=0.82, T_i=1.002, M=0.88 g/s

b: P_r=1.001, T_r=0.85, T_i=0.99, M=0.90 g/s

c: P_r=1.225, T_r=0.85, T_i=1.004, M=0.77 g/s

Fluoroketone injected into N2 environment

d: P_r=0.876, T_r=0.857, T_i=1.001, M=1.08 g/s

e: P_r=1.16, T_r=0.85, T_i=1.004, M=0.83 g/s

f: P_r=1.306, T_r=0.857, T_i=1.007, M=0.85 g/s

Fluoroketone injected into Helium environment

Figure 4.11 Near critical fluoroketone jet in subcritical environment.

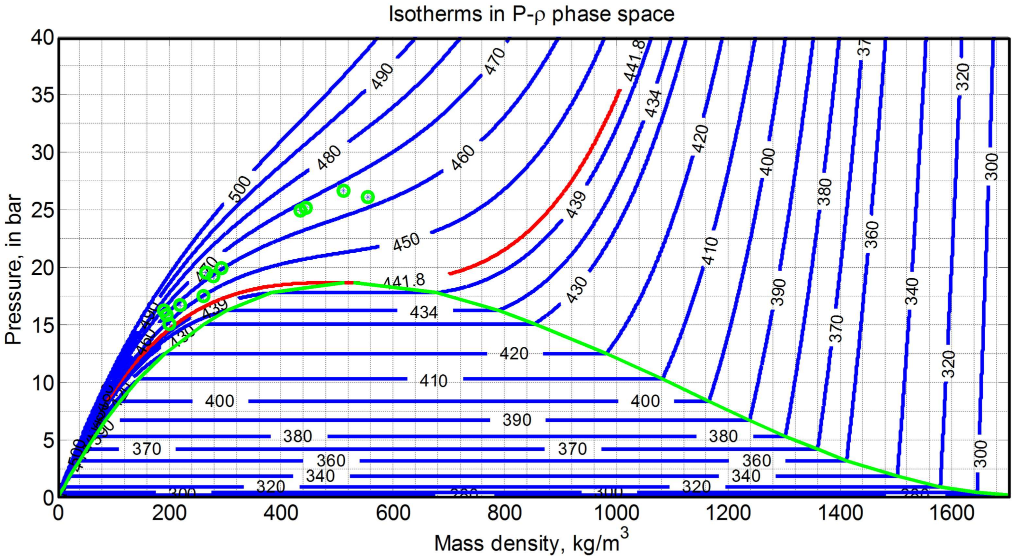

Figure 4.12 Isotherms (temperatures in Kelvin) in P-ρ phase space. The injection condition of cases which corresponds to figs. 4.13, 4.14, 4.15 and 4.16. is marked in green circles.

Injection pressure (bar)	**Injection temperature (K)**	**Chamber temperature (K)**	**Predicted density from Maxwell constructed PRSV equation** Kg/m^3	**Experimentally measured density using PLIF** Kg/m^3	**Calculated temperature at the injection point from Maxwell constructed PRSV plot and measured density (K)**	**Percentage deviation from experimentally measured density and predicted density from Maxwell constructed PRSV plot %**
15.8	460	388	195	219	450	10.9
19.2	464	384	278	321	451	13.3
26.6	468	384	512	569	462	10.02
16.2	468	384	190	218	454	12.8
19.5	468	388	266	312	456	14.7
24.9	471	384	437	508	462	13.9
15.1	451	468	205	210	444	2.4
17.5	452	468	261	220	464	15.7
26	459	477	555	489	466	11.8
16.7	464	460	220	255	443	13.7
19.9	464	462	293	319	457	8.15
25.1	468	468	445	472	465	5.72

Table 4.4 Deviation of the measured density from the predicted density near the injection area.

constructed PRSV plot is also listed in table 4.4. It is noted that the experimentally measured density is higher as compared to the predicted density from PRSV equation.

From table 4.4 the calculated injection temperature corresponding to the measured injectant density of the pixel matrix as represented in fig. 4.13 and the injection pressure is tabulated. It is evident from the table 4.4 that the calculated injection temperature is slightly smaller than the temperature measured prior to the injection.

In the study performed by Roy et al. (2013), the injected fluid density is calculated for the measured injection temperature and pressure, and the density color map for jet is obtained by considering the injected fluid density at injection temperature and pressure as reference. There could be some amount of error in obtaining the density color map in their method though it may not be very significant. In any experiment, the injection temperature can be measured only a few centimeters prior to the injection. At the point where the jet is exposed to the chamber environment, the jet temperature need not be the same as the injection temperature which is typically measured a few centimeters upstream of the injection inlet. In the current study, this error is eliminated in the determination of density, and the density color map is obtained as described in section. 3.8.7.

4.10 Supercritical jet injected into subcritical condition with N_2 or He as ambient fluid

The chamber is kept at subcritical temperature of T_r=0.87 and the injection temperature is at T_i=1.05. The flow characteristics of the fluoroketone-N_2 system and the fluoroketone-He system are shown in fig. 4.13 and fig. 4.14. When the injection temperature is supercritical and the pressure is just below the critical point, the thermodynamic state of the fluoroketone is in gaseous state as in fig. 4.12. This is also observed from figs. 4.13 a and 4.14 a. The dense fluoroketone gaseous jet does not exhibit axis switching behavior, and it is quite clear that the jet does not undergo visible thermodynamic changes as it encounters the subcritical chamber condition.

As the injection and the chamber pressure are increased to slightly above the critical pressure with P_r=1.03 and with temperature T_i=1.05, the injected jet finds itself above the critical region of P-ρ phase space where the changes in density are very sensitive to changes in pressure as shown in fig. 4.12. The pressure and temperature of the chamber correspond to the thermodynamic state where the fluoroketone is in liquid state. As the jet under this condition enters the chamber, it does behave like a gaseous jet with a few droplet formation as shown in figs. 4.13b and 4.14b. The axis switching does not occur and it also indicates that the injected

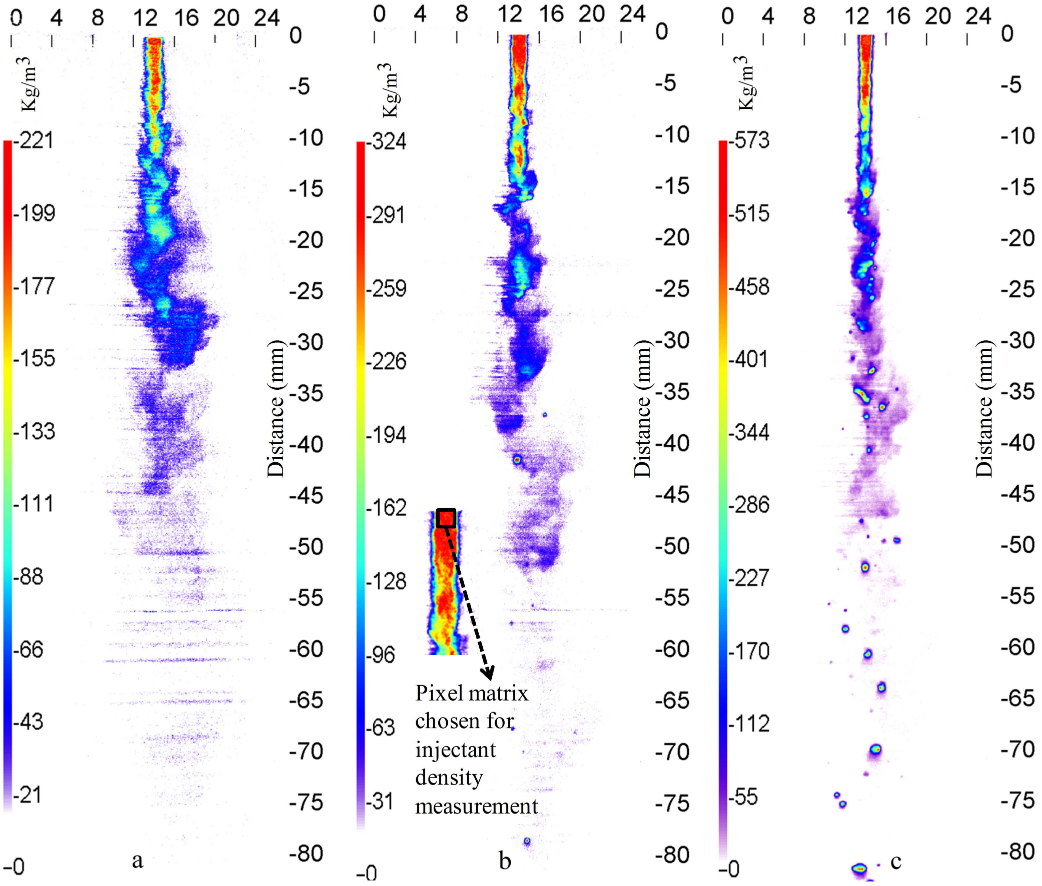

P_r=0.85
T_r=0.88
T_i=1.04
M=0.9 g/s
V_i=1.3 m/s

P_r=1.03
T_r=0.87
T_i=1.05
M=0.82 g/s
V_i=0.81 m/s

P_r=1.43
T_r=0.87
T_i=1.06
M=0.87 g/s
V_i=0.49 m/s

Figure 4.13 Effect of pressure on injection of jet from supercritical to sub-critical temperature condition in Nitrogen environment.

jet expands and mixes with the surrounding environment before the thermodynamic transition into liquid state occurs. There are evidences of some droplet formation and this indicates that some fraction of injected jet fluid has undergone transition to liquid state upon losing some heat.

As the chamber and the injection pressure is increased much beyond the critical pressure with P_r=1.43 and with injection temperature (T_i) being 1.06, the injected fluid is in supercritical state as could be seen from the phase-space diagram in fig. 4.12. As the supercritical jet encounters the chamber at subcritical temperature and supercritical pressure, the jet undergoes thermodynamic changes. It is clear from fig. 4.13c that as the supercritical jet encounters the chamber condition, the droplet formation is quite visible. A large fraction of the injected supercritical jet undergoes a thermodynamic transition to liquid state: for the initial few downstream distances, the jet is continuous and beyond certain downstream distance, the jet disintegrates and droplet formation occurs. The axis switching does not occur in the jet and the reason could be due to the disintegration of the supercritical jet prior to the complete thermodynamic transition to the liquid state. Similar transitional characteristics are also reported by the experimental studies conducted on round jet by Roy et al. (2013). The computational studies carried out by Qiu and Reitz (2014) also indicated the formation of liquid droplets at the boundary of the supercritical jet as it is exposed to the subcritical chamber temperature. The authors reasoned that the droplet formation is due to a strong interaction between the hot injectant fluid and the cold surrounding gas results in heat loss and the entrainment of the ambient N_2 gas into the injectant fluid. The authors also pointed out that the low level of entrainment of ambient gas could significantly change the thermodynamic characteristics of the mixture and affect the transition to liquid state.

From figs. 4.13b, 4.13c and figs. 4.14b, 4.14c, it is quite clear that pressure plays an important role in the thermodynamic transition of the jet behavior. As the pressure is increased from P_r=1.03 to P_r=1.43 and keeping the temperature fixed, the density of the injecting jet varies drastically. As observed from fig. 4.12, the density of injected jet for P_r=1.43 is around 580 kg/m^3 and for P_r=1.03 is around 250 kg/m^3. The reason for the disintegration followed by droplet formation in the case of figs. 4.13c and 4.14c is attributed to the increase in density of the injected jet. The liquid-like high-density fluid having a sudden change in the thermal properties of the jet surface as it encounters the subcritical chamber temperature, undergoes accelerating thermodynamic changes to a liquid state instead of expansion of the jet as seen in figs. 4.13b, 4.14b. Hence, the transition of the supercritical jet into liquid state at subcritical chamber temperatures could be attributed to the following two main reasons: the influence of change in temperature conditions from super to

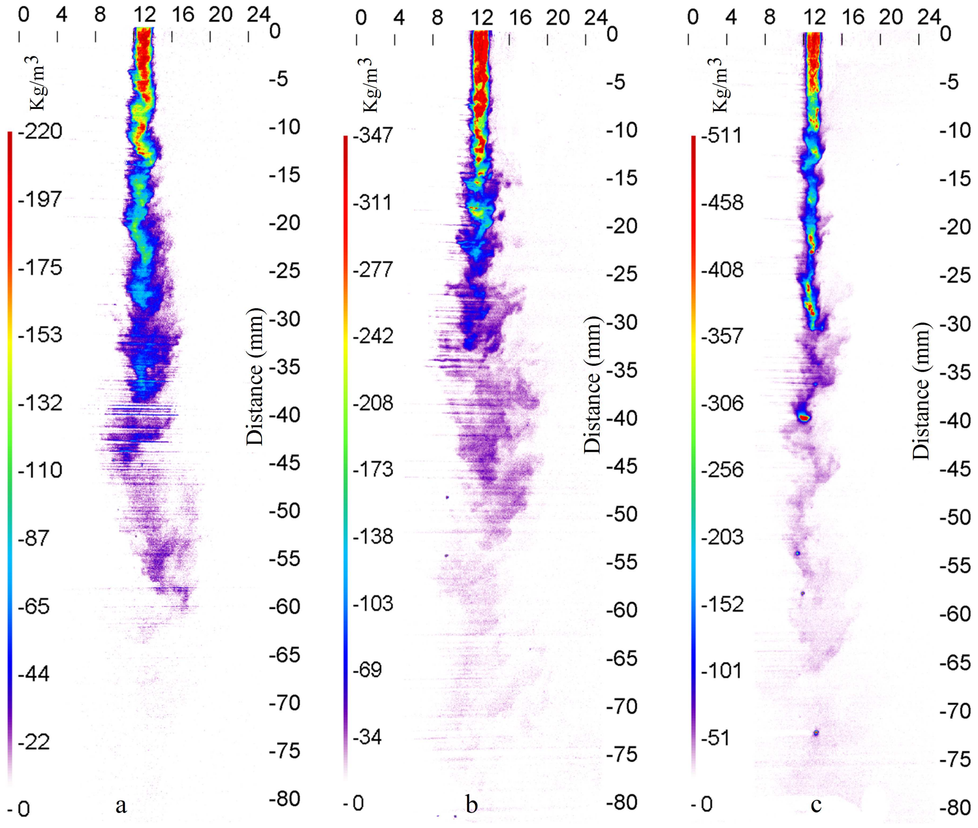

P_r=0.87
T_r=0.87,
T_i=1.06
M=1 g/s
V_i=1.46 m/s

P_r=1.05
T_r=0.87
T_i=1.06
M=0.78 g/s
V_i=0.73 m/s

P_r=1.34
T_r=0.88
T_i=1.07
M=0.86 g/s
V_i=0.54 m/s

Figure 4.14 Effect of pressure on Injection of jet from supercritical to subcritical temperature condition in Helium environment.

subcritical and the other due to the effect of diffusion of the ambient gas into the injected fluid.

4.11 Supercritical jet injected into supercritical condition with N_2 or He as ambient fluid

The chamber temperature as well as the injection temperature is increased to supercritical condition. The effect of pressure on the behavior of the jet is studied. When the injection temperature is supercritical and the pressure is below the critical point, the thermodynamic state of the fluoroketone is gaseous as noticed from fig. 4.12. As the dense gas enters the chamber through an elliptical orifice, it does not switch axis and this clearly indicates the absence of surface tension between surrounding nitrogen or helium environment and the incoming jet. This is observed from figs. 4.15a and 4.16a. There is hardly any formation of the droplets, and the Kelvin-Helmholtz instability or roll up vortices that generally occur in the single phase mixing layer is observed in figs. 4.15a, 4.15b and figs. 4.16a, 4.16b. When the pressure is increased, the state of the incoming jet becomes completely supercritical, as in figs. 4.15c and 4.16c. The dense jet does not exhibit larger roll up vortices. This could be due to the large density difference between the jet fluid and the surrounding medium such that it is more difficult to entrain a denser fluid. For the supercritical fluoroketone jet injected into its supercritical environment with nitrogen or helium as surrounding environment, the jet behaves as variable density gaseous jet, as also reported by Chehroudi et al. (2002a). Also, the jet diffuses into the surrounding environment rapidly.

The transition to liquid state need not occur when a high pressure supercritical jet is injected into supercritical chamber conditions when the jet and the chamber fluids are diffierent. According to Qiu and Reitz (2014), the entrainment of the ambient gas into the injected fluid is identified as one of the reasons for the condensation behavior. The conditions meant to be supercritical for fluoroketone may not be supercritical for either fluoroketone-N_2 system or fluoroketone-He system. Moreover the mixing is first encountered in the interfacial region alone, and since the injected fluid and the surrounding fluid temperature is same, the bulk supercritical jet fluid without losing the heat maintains the supercritical state. Although there is significant entrainment of ambient gas at the jet interface, the expansion and mixing of injected supercritical jet species with the surrounding fluid species diminish the density of the jet. This could be the reason that the jet does not undergo transformation to liquid state. There is no visible droplet formation as observed from figs. 4.15c, 4.16c. However, the process of condensation might have occurred in molecular scale, by beginning the formation of condensation nuclei, provided mix-

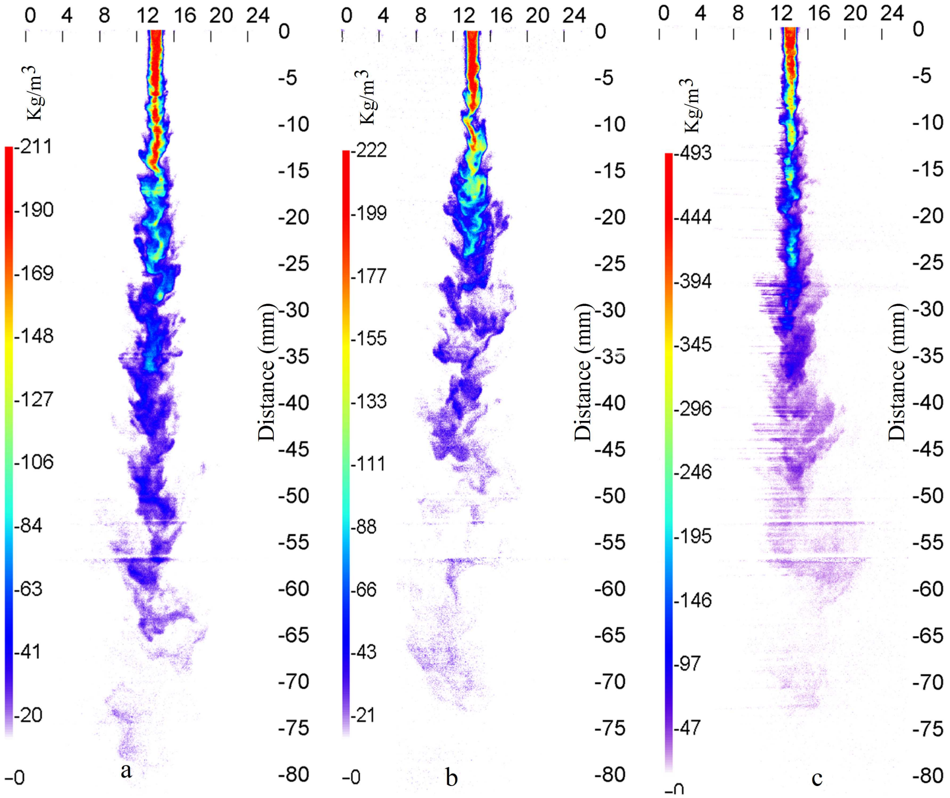

P_r=0.81
T_r=1.06
T_i=1.02
M=1.085 g/s
V_i=1.64 m/s

P_r=0.94
T_r=1.06
T_i=1.02
M=0.873 g/s
V_i=1.26 m/s

P_r=1.40
T_r=1.08
T_i=1.03
M=0.802 g/s
V_i=0.53 m/s

Figure 4.15 Injection of supercritical fluoroketone into supercritical temperature condition in Nitrogen environment.

ing is predominant and thermodynamic conditions are subcritical for the combined fluoroketone-N_2 or fluoroketone-He mixture.

In comparison with fig. 4.15c and fig. 4.16c, the results from figs. 4.13c, 4.14c corresponding to supercritical injection to subcritical chamber temperature condition, revealed the presence of formation of droplets. This could be attributed to the phase transition of the supercritical bulk phase in the jet to near-liquid state that possess higher density than the supercritical fluid. Moreover it also indicates significant loss of enthalpy to the surrounding ambient medium through heat transfer. It is also noticed that when a supercritical fluid is injected into a chamber at

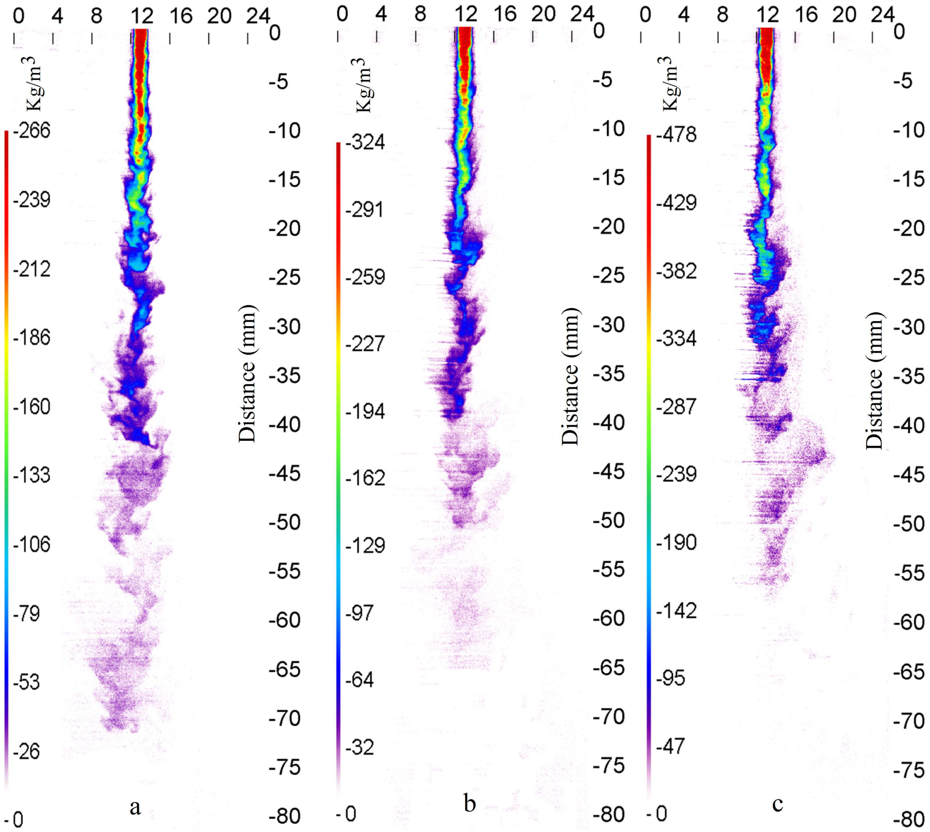

P_r=0.90
T_r=1.04
T_i=1.05
M=0.90 g/s
V_i=1.12 m/s

P_r=1.07
T_r=1.045
T_i=1.05
M=0.90 g/s
V_i=0.90 m/s

P_r=1.35
T_r=1.04
T_i=1.06
M=0.81 g/s
V_i=0.55 m/s

Figure 4.16 Injection of supercritical fluoroketone into supercritical temperature condition in Helium environment.

supercritical pressures, the effect of chamber temperature plays a major role. This can be seen from fig. 4.13c, 4.14c and fig. 4.15c, 4.16c that at supercritical chamber temperatures, the droplet formation is completely absent. However, at subcritical chamber temperatures, the injected supercritical jet undergoes thermodynamic transition with the presence of droplet formation. This suggests that the decrease in chamber temperature in the subcritical regime could lead to formation of larger droplets due to the relatively fast thermodynamic transition of the injected jet.

4.12 Summary

The elliptical jet has been used to investigate the transition in the surface tension of the injected jet at supercritical chamber condition. At atmospheric condition, the elliptical fluoroketone jet exhibits axis-switching due to the effect of surface tension. The experiment is carried out in a nitrogen environment as well as in the environment of the injected jet to understand the possible transition in the surface tension of the injected fluid. A fluoroketone jet injected into a subcritical chamber condition close to the critical point exhibited axis switching when injected in a nitrogen environment. Even at critical and supercritical chamber conditions, the injected liquid jet exhibited axis-switching. The measurement of axis-switch length at supercritical chamber condition deviates less than 10 % of that at subcritical chamber condition. However, when injected in a fluoroketone supercritical environment the injected jet underwent transition to supercritical state and exhibited a misty appearance without axis switching characteristics. The experiment is also conducted in a helium environment because of its difference in the critical pressure from nitrogen. The injection of an elliptical jet into supercritical chamber condition with helium environment also exhibits axis switching similar to that in nitrogen environment. The conclusion is that the molecular mixing between fluoroketone and nitrogen or helium, and the solubility effects altered the critical point of the fluid such that it remains in the liquid state.

For the supercritical injection condition, the experiment is carried out using PLIF technique to obtain the density color map of the two dimensional center plane of the jet. The fluid at the near critical temperature is very sensitive to pressure changes. The near critical jet injected into subcritical chamber condition at subcritical pressures behaves like a gaseous jet. As the injection and the chamber pressure become supercritical, the injected near critical jet behaves like a liquid jet. The characteristics of supercritical jet injection into subcritical chamber condition is also dependent on pressure. At subcritical pressures, the supercritical jet exhibit behavior similar to gaseous jet. However, the jet at supercritical pressure and temperature when injected into subcritical chamber temperature result in formation of fewer droplets. The main reason could be that the higher density injected fluid at supercritical pressure loses significant heat to the surrounding and transforms to liquid state. The injection of a supercritical temperature jet into a supercritical chamber temperature condition possess gaseous jet appearance at pressures ranging from subcritical to supercritical condition.

CHAPTER 5

CIRCULAR JET AT SUBCRITICAL AND SUPERCRITICAL CONDITIONS

In this chapter a detailed investigation is carried out with a circular jet at subcritical to supercritical conditions. The thermodynamic transition associated with the jet fluid significantly influences the fluid dynamic characteristics. The corresponding changes in the stability characteristics is a direct indication of the deviation in fluid properties that determine the mixing characteristics of the jet. In this study the instability waves in a liquid jet injected into subcritical to supercritical chamber conditions for both binary and the single component system are investigated in detail. For the case of supercritical jet injected into subcritical to supercritical chamber temperature condition, density and density gradient field map is obtained using PLIF technique for binary component system. Also fractal analysis of the jet boundary is carried out to analyze the mixing nature of the jet.

5.1 Introduction

Most of the earlier works in round liquid jet at supercritical conditions are performed at high jet Reynolds number. The injected jet is turbulent in many cases, and the generation of the surface disturbances on a laminar jet has not yet been studied in detail. Most of the studies investigated in the past were performed to mimick the injection of fuel in realistic conditions, like rocket engines, where the fuel is injected at higher Reynolds number. Though there are numerous studies that are conducted in the past to understand the characteristics of a liquid jet in supercritical environment, the literature is limited in providing a comprehensive understanding of the interfacial instability of the jet as it encounters the supercritical environments.

In the present experimental study, the injection of a circular liquid jet into subcritical or supercritical condition is performed in N_2 environments as well as in its own vapor at a supercritical condition. For all the cases considered, the injectant is always at atmospheric temperature, and the chamber conditions are varied from subcritical to supercritical temperature. The effect of injection velocity on the fluid dynamic characteristics of the jet is studied. Various regimes of jet instability and breakup characteristics of the liquid jet at subcritical and supercritical condition are analysed. When a liquid jet is injected into its own supercritical environment, the transition in the fluid properties occurs. This transition in the fluid properties could have a significant effect on the characteristics of the disturbance wavelength that forms on the surface of the jet. Various instability regimes as well as the transition in breakup characteristics are investigated. The wavelength of the instability waves on the surface of the injected jet is measured experimentally and compared with those obtained from a dispersion relation that is derived through linear stability analysis for a viscous liquid jet that is injected into an ambient medium.

In addition, fractal dimension of the jet boundary is also determined to comprehend the interfacial corrugations at the jet interface. The fractal dimension increases with the complexity of the jet interface. The gaseous jet possesses more complex interfacial geometry than the liquid jets and hence the fractal dimension of the gaseous jet interface is greater than that of the liquid jet interface. Since the present study is carried out to investigate the transition of the jet from the state of injected fluid to the thermodynamic chamber state, the concept of fractal dimension is used as a tool to identify whether the behavior of the injected jet is similar to that of a liquid jet or a gaseous jet.

The injection of near critical and supercritical fluid jet into subcritical as well as supercritical condition is performed for two binary component systems. The main objective of the work is to investigate the transitional nature of the jet. The study is performed using the PLIF technique to obtain the density and density gradient field map. The fluoroketone is used as the injectant fluid, and the nitrogen and helium are used as chamber fluids to explore the effects of their difference in the critical pressure values. The N_2 has a critical pressure of 33 bar whereas He has a critical pressure of 2.27 bar. The fractal analysis of the supercritical jet is also performed to analyze the jet boundary in detail.

5.2 Linear stability analysis: revisited

The linear stability theory deals with the characteristics of the perturbation that exist on the interface of the jet such as growth rate, underlying physical mechanism, and spatial and temporal instabilities. The governing equation for the perturbation is obtained by linearising the equation that governs the undisturbed flow state/basic state with respect to the perturbations (Lin, 2003). The perturbations are the periodic fluctuations in velocity and pressure field. By solving the resulting governing equation, the dispersion relation is obtained. The form of the Fourier mode perturbation has both the oscillation and exponential growth rate in space as well as in time. Thus, the dispersion equation provides the relation between the wave number/oscillation in space or time and its growth rate. Most of the earlier studies are devoted to the temporal analysis by assuming the frame of reference to be moving with the jet, and only the temporal growth rate is considered. Later Keller et al. (1973) observed that the disturbance grows only in space in the laboratory frame of reference. Also, it is found that both spatial and temporal instability yield similar results for $We >> 1$.

In the present experiment, the injector is circular with an inner diameter of 0.88 mm and the length is nearly 25 mm. In the case of laminar liquid jet near the exit plane of the injector, the flow is fully developed with minor presence of radial velocity distribution, and the velocity is zero at the injector wall, and attains maximum value at the core region. Though the actual flow inside the injector has a radial velocity distribution, once the jet leaves the injector exit it experiences a transition from no-slip situation at injector wall to slip situation which is generally termed as stick-slip situation (Lin, 2003). The velocity distribution relaxes and attains a uniform profile within a distance of few diameters downstream (Lin, 2003) (Scriven and Pigford, 1959). For all the cases discussed in the present experiment, the instabilities develop only at few diameters downstream from the injector exit. From the studies of Ibrahim and Marshall (2000), a jet with uniform velocity profile is more unstable as compared to a jet with parabolic velocity profile, and the assumption is reported to be valid by Segal and Polikhov (2008).

In the present work, the dispersion relation for perturbation on a viscous liquid jet injected into a gaseous medium, as obtained by Segal and Polikhov (2008), is employed. This dispersion equation is similar to the one obtained by Lin (2003). The perturbation is considered only in the longitudinal direction along the jet axis. The perturbation is assumed to be a Fourier mode of the form:

$$F(x,t) = f(x,t)exp[i(kx + m\theta + \omega t)] \tag{5.1}$$

The parameter m corresponds to the azimuthal disturbance mode. The value m=0 indicates axi-symmetric mode. In the present case, the stability analysis is considered only for the axi-symmetric case i.e., with m=0. The parameter m=1 corresponds to sinuous mode or kink mode and m=2 corresponds to screw-like mode as shown in fig. 5.1. The comparison of the experimentally measured disturbance wavelength with those obtained from linear stability analysis is performed only for the axisymmetric case. The parameter $k = (2\pi/\lambda)a$ is a non-dimensional wave number and $\omega = (a/V)\overline{\omega}$ corresponds to non-dimensional temporal oscillation; here V is the velocity of the jet and 'a' is the radius of the jet. The dispersion relation is obtained as:

$$\begin{aligned}(\omega+k)^2\frac{I_0(k)}{I_1(k)} - \frac{2ik^2}{Re_l}(\omega+k)\left[\frac{I_0(k)}{I_1(k)} + \frac{I_1'(k)}{I_1(k)}\right] + \omega^2 Q\frac{K_0(k)}{K_0'(k)} \\ -\frac{4k^3}{Re_l^2}\left[k\frac{I_1'(k)}{I_1(k)} - l\frac{I_1'(l)}{I_1(l)}\right] + \frac{k}{We_l}(1-k^2) = 0\end{aligned} \tag{5.2}$$

where $k = k_r + ik_i$ with k_r being the spatial oscillation and $-k_i$, the spatial growth rate. Also $\omega = \omega_r + i\omega_i$, with ω_r and $-\omega_i$ being the temporal oscillation and temporal growth rate respectively. The liquid jet is susceptible to the disturbances that grow in space as well as in time and hence the parameters k and ω are set to be complex.

Here I and K are the modified Bessel function of the first and the second kind, the subscripts 0, 1 denote the zeroth and the first order of the function, and superscript prime denote their derivative with respect to argument. Also Re, We and Q represent Reynolds number, Weber number and density ratio respectively as shown in equations 5.3, 5.4 and 5.5.

$$Re = \frac{\rho V a}{\mu} \tag{5.3}$$

$$We = \frac{\rho V^2 a}{\sigma} \tag{5.4}$$

$$Q = \frac{\rho_g}{\rho_l} \tag{5.5}$$

The concept of absolute and convective instability is developed to explain the fundamental differences between the various instabilities that typically occur in a wide variety of flows. The theory of absolute and convective instability is developed for the field of plasma physics by Briggs (1964). Huerre and Monkewitz (1985) used the absolute and convective instability concepts to examine the differences between spatial and temporal linear instabilities in shear layers. Based on the theory of absolute and convective instability, Leib and Goldstein (1986) obtained a new mode of instability and is referred to as the absolute instability. In the case of absolute instability, the unstable waves can propagate both upstream and downstream of the jet. Leib and Goldstein (1986) performed the absolute instability analysis by including the viscosity of the jet fluid, and found that there exists a critical We value above which the jet is convectively unstable, and below which the jet is absolutely unstable. Later, Lin and Lian (1989) performed an absolute instability analysis by also incorporating the effect of surrounding gas density, and found that the value of the critical We increases with increasing ambient gas density. In their analysis, the value of critical We is always found to be $We_c \approx 2.5$ for a density ratio $Q = 0.03$. In the present experiments, the value of injectant We is always greater than 2.5.

When the instability occurs near the injector exit or when the velocity dis-

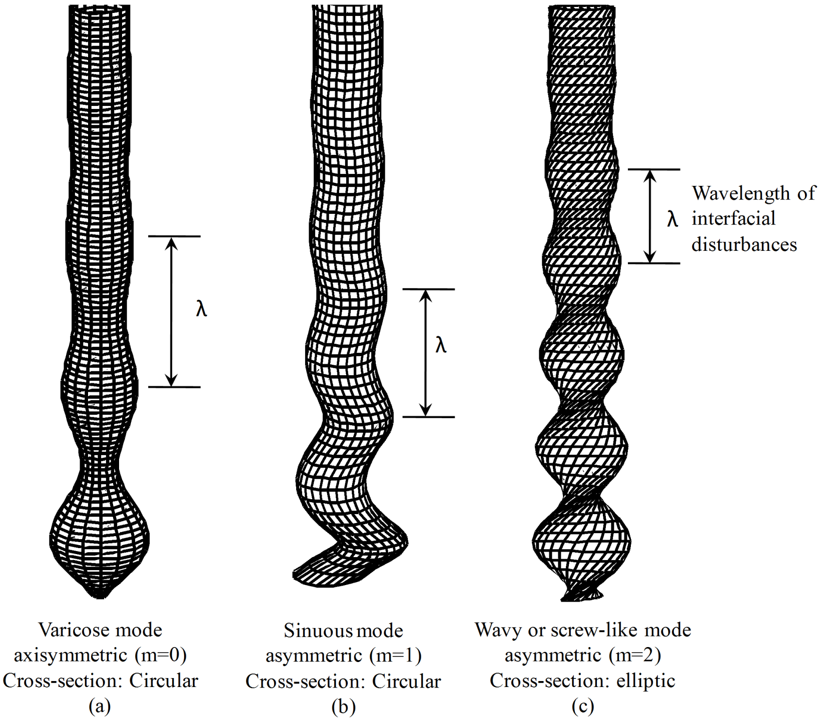

Figure 5.1 Sketch of various instability mode development in a laminar jet.

tribution is non uniform with near zero velocity at the jet surface, the instability waves must propagate both in the upstream and downstream direction, and this instability condition corresponds to absolute instability as reported by Lin (2003). However, in the present experiments, the assumption of uniform velocity profile is appropriate and hence the instability waves are considered to propagate downstream with jet velocity beyond the critical Weber number We_c. This flow instability corresponds to convective instability.

For $We \to \infty$ or large We, the spatial growth rate k_i could be inferred from the temporal growth rate, ω_i by the relation $k_i = \omega_i + O(1/We)$, while the disturbances travel downstream with jet velocity in the laboratory frame. This relation is consistent with Gaster's theorem (Gaster, 1962) which states that, to the first order approximation, the temporal growth rate is represented by the product of the corresponding spatial growth rate and the group velocity of the disturbances. In the present analysis, only the spatial growth rate is considered.

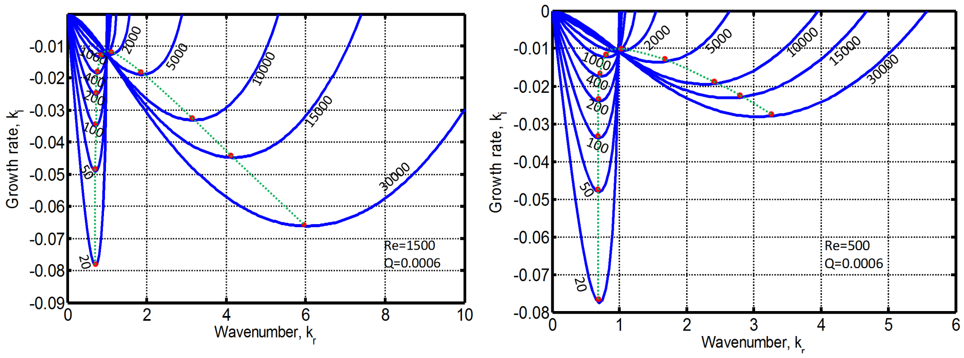

(a) (b)

Figure 5.2 Dependence of the growth rate of the disturbance on its wave number for various Weber number for the density ratio Q=0.0006.

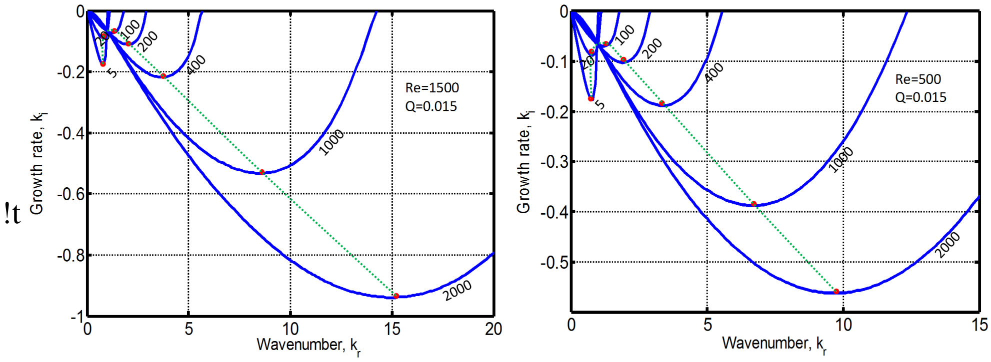

(a) (b)

Figure 5.3 Dependence of the growth rate of the disturbance on its wave number for various Weber number for the density ratio Q=0.015.

The dispersion equation 5.2 is solved for the spatial growth rate k_i for the given spatial disturbances k_r at the onset of spatial instability with temporal growth rate $\omega_i = 0$ and equating $\omega_r \approx k_r$ for the case $We >> 1$. The growth rate dependence on the wave number for various We is shown in fig. 5.2 and fig. 5.3 in which the short wavelength disturbances become more dominant as We is increased. Comparing fig. 5.2 a and fig. 5.2 b, the Reynolds number (Re) is found to have significant effect on the dominant disturbance wave number and its growth rate. As Re is decreased, the effect of viscosity shifts the wavelength of the dominant disturbance towards the longer wavelength. Also viscosity has its role in damping the growth rate of the disturbance as noticed from fig. 5.2. The effect of density of the ambient gas on the instability of the jet is more evident on comparing fig. 5.2 a and fig. 5.3 a. The higher ambient gas density leads to the formation of short wavelength disturbances on the jet surface.

5.3 Experimental conditions for subcritical jet injection

Experiments are performed for binary component systems as well as for a single component system to understand the dynamics of the jet that also depends on the surrounding ambient medium. There were several studies that were performed in the past for both binary component system as well as for a single component system. However the present study is intended to analyse the instability characteristics at the interface of the injected jet. The experiments are performed with an injection velocity that is gradually increased from low velocity corresponding to the Rayleigh regime to high velocities in order to capture the different regimes of instability and breakup processes. The injected fluid employed in the present study is fluoroketone and the injectant is always kept at atmospheric temperature $T_{injection} = 300K$ with reduced injection temperature $T_i = 0.68$. The chamber pressure and temperature are varied from subcritical to supercritical conditions for the injectant fluid, fluoroketone. The injection and the chamber conditions are detailed in table. 5.1. The maximum uncertainty involved in the pressure measurement is ± 0.25 % of the measured value. The maximum temperature achieved in the chamber is less than $215K$ and the maximum uncertainty involved is ± $2.2K$. The maximum uncertainty involved in the velocity measurement is about 0.2 %. The experiment is conducted at steady state flow conditions. To ensure data acquisition in steady state flow conditions, the images are captured along with pressure, temperature and mass flow measurements only after 5 seconds from the start of the injection. The images and the pressure and temperature data are acquired simultaneously for a time period of 10 seconds. Nitrogen is employed as the ambient fluid for the binary component system. For the study of single component system, sufficient quantity of fluoroke-

Injection temperature $\boldsymbol{T_i}$ $\left[\frac{T_{injection}}{T_{critical}}\right]$	**Chamber temperature** $\boldsymbol{T_r}$ $\left[\frac{T_{chamber}}{T_{critical}}\right]$	**Chamber pressure** $\boldsymbol{P_r}$ $\left[\frac{P_{chamber}}{P_{critical}}\right]$	**Surrounding environment**
0.68	0.68	0.054	N_2
0.68	0.68	≈ 1.1	
0.68	1.05	≈ 1.1	
0.68	0.872	≈ 0.2	Fluoroketone
0.68	0.97	≈ 0.7	
0.68	1.03	≈ 0.87	
0.68	1.05	≈ 1.09	

Table 5.1 The pressure and temperature condition chosen for the experiment.

tone is introduced in the chamber to obtain the desired vapor pressure for a given chamber temperature. This chamber condition is achieved prior to the injection of liquid fluoroketone jet. The injectant and the chamber conditions are reduced with respect to the critical properties of injectant fluid, fluoroketone. The abbreviations T_i, T_r and P_r represent the injection temperature, chamber temperature and chamber pressure that are reduced with respect to the critical properties of fluoroketone. The injectant fluid in all the cases is at room temperature, and only the chamber pressure and temperature condition is varied. Also the term subcritical or supercritical refers to the chamber temperature condition that is defined with respect to the critical temperature of the injectant fluid, fluoroketone. For binary component system, the nature of jet instability is investigated for chamber conditions that correspond to atmospheric pressure, supercritical pressure, and supercritical in both pressure and temperature. In the case of single component system, the chamber conditions are selected as follows: 1. subcritical in both temperature and pressure, 2. supercritical temperature and subcritical pressure and 3. supercritical temperature and pressure conditions.

5.4 Liquid jet at subcritical temperature condition

5.4.1 N_2 environment (Binary component system)

The experiments are conducted with nitrogen as the ambient fluid with temperature and pressure conditions corresponding to $29K$ and 1 atm. Initially the chamber is purged with nitrogen gas and the fluoroketone liquid jet is subsequently injected into the chamber. The behavior of the jet is studied from the low We that corresponds to the Rayleigh regime to the high We corresponding to the Taylor regime.

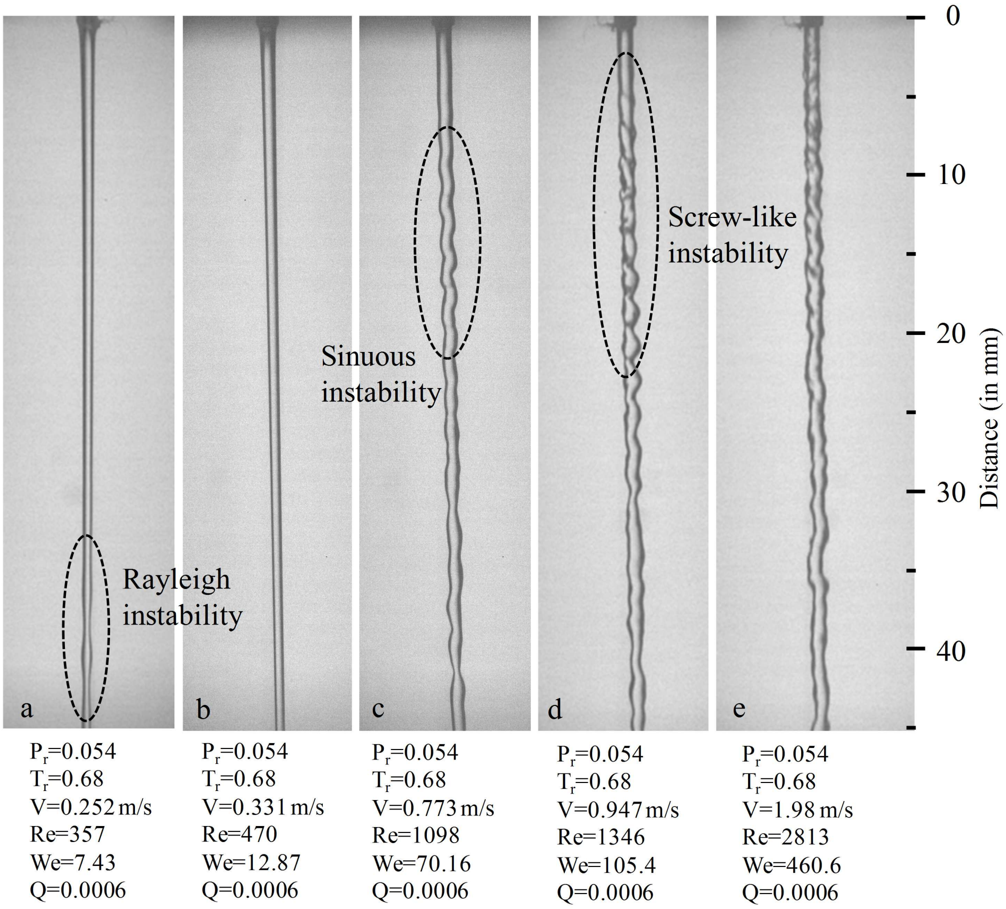

Figure 5.4 Injection of liquid fluoroketone into nitrogen environment at atmospheric temperature and pressure conditions.

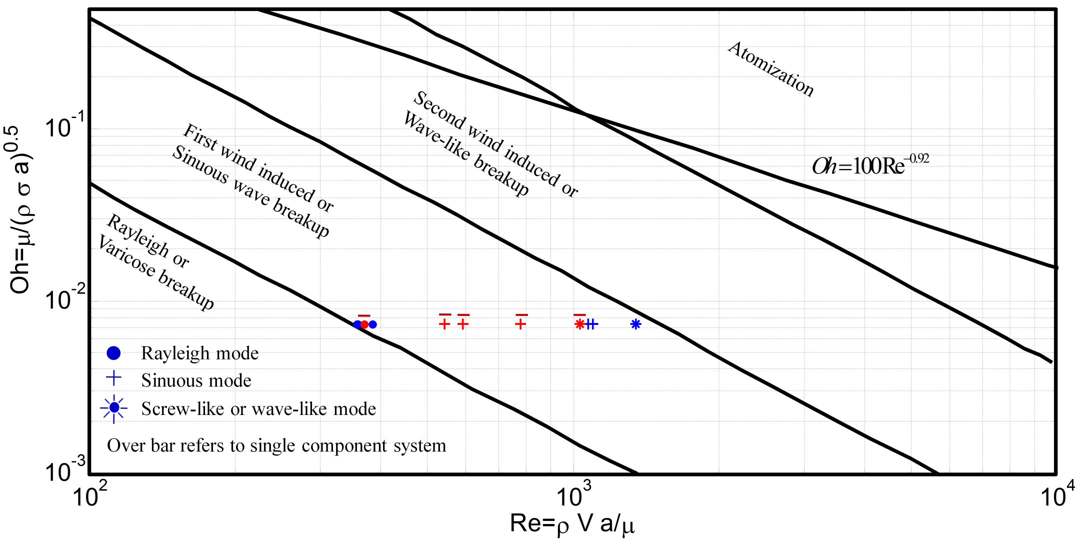

Figure 5.5 Comparison of the experimentally observed mode and various regimes in Ohnesorge chart.

Various regimes of jet characteristics are observed and presented in fig.5.4a. At low Weber number, We=7.43, the development of longer wavelength disturbance is observed. The measurement shows that the disturbance wavelength is 4.3 times the diameter of the jet and it indicates the dominance of the capillary force in causing the instability; this leads to drops of bigger diameter. Within the Rayleigh regime, as We is increased, the breakup length of the jet also increases. As the velocity of the jet is further increased, the transition in the nature of instability is observed for cases corresponding to injection at ambient pressure but with ambient gas to liquid jet density ratio(Q) of 0.0006. As the We_i is increased further, the aerodynamic drag on the jet surface become more prominent and alters the breakup characteristics. It is noted that beyond $Re = 1098$ and $We = 70.16$, a transition in the instability characteristics is observed. At this flow condition, the sinuous mode or snake-like mode is clearly observed as a result of wind induced disturbance on the jet surface. The geometry of the sinuous mode is similar to a stretched spring and it is the first asymmetric mode as shown in fig. 5.1b. At about $Re = 1346$ and $We = 105.4$, the screw-like or helical mode appeared on the injected jet surface at a few diameter distance downstream. The appearance of screw-like disturbance mode was reported earlier by Ohnesorge (1936). The screw-like mode is the second

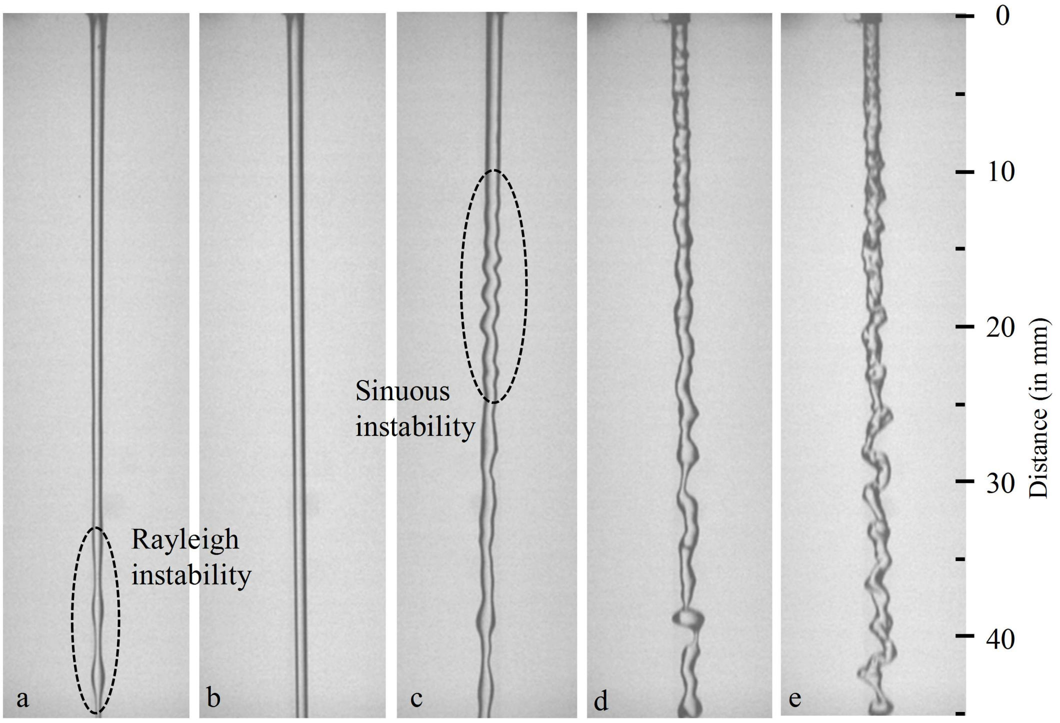

a: P_r=0.995
T_r=0.68
V=0.326 m/s
Re=359
We=7.5
Q=0.013

b: P_r=1.011
T_r=0.68
V=0.596 m/s
Re=656
We=25
Q=0.013

c: P_r=1.14
T_r=0.68
V=0.976 m/s
Re=1074
We=67.5
Q=0.015

d: P_r=1.23
T_r=0.68
V=1.621 m/s
Re=1783
We=185.5
Q=0.016

e: P_r=1.25
T_r=0.68
V=2.5 m/s
Re=2748.5
We=440
Q=0.0162

Figure 5.6 Injection of liquid fluoroketone into nitrogen environment at atmospheric temperature and 20 bar pressure.

asymmetric mode, with a geometry that is similar to a twisted elliptical rod as the disturbance is developed on the jet surface. Beyond $Re = 2813$ and $We = 460.6$, the injected jet is fully turbulent and there is absence of any notable geometrical features on the surface.

It can be observed from table 5.2 that the axisymmetric disturbances are accurately determined by the dispersion relation in equation 5.2. The growth rate of the asymmetric modes of an inviscid liquid jet is analysed by Levich (1962) and Yang (1992). Yang (1992) performed an instability analysis by considering the asymmetric effects in both the surface curvature term due to the surface tension and the gas dynamic interaction term. The analysis made by Yang (1992) shows that the first asymmetric mode/sinuous mode is possible only at $We > 1000$. However, in the present experimental study, the sinuous mode appeared for $We = 70.16$. It has to be noted from fig. 5.4c that the sinuous mode appears in the laminar jet and within a few jet diameter downstream distance it disappears despite the presence of some random interfacial disturbances. This suggests that the sinuous mode might not be a sustaining mode, and the breakup of the jet could be due to the axisymmetric instability. The second mode of the asymmetric disturbance/helical mode is observed to appear at $We = 105.4$.

The various regimes of jet instability associated with the jet breakup are characterised by the Reynolds number and the Ohnesorge number as presented in the Ohnesorge chart in fig. 5.5. For all the cases considered in fig. 5.4, the Oh value is about 0.00734. The Ohnesorge number is a ratio of the viscous force, to the product of surface tension and inertial force. In otherwords, the Ohnesorge number is a ratio of the visco-capillary time scale to the Rayleigh time scale which characterises the thinning dynamics of the viscous threads. The expression for Ohnesorge number is:

$$Oh = \frac{\mu}{\sqrt{\rho a \sigma}} = \frac{\sqrt{We}}{Re} = \frac{\mu a/\sigma}{\sqrt{\rho a^3/\sigma}} \tag{5.6}$$

The Ohnesorge chart presented in this thesis is reproduced from Pan and Suga (2006) with the parameters Re and Oh that are defined based on the characteristic length scale, the radius of jet (a), and is shown in fig. 5.5. Onhesorge did not provide functional relationship in his paper. Later Richardson (1950) and Becher (1990) provided the power law relationship between Re and Oh with exponent $-4/3$. Further, the investigation by McKinley and Renardy (2011) on the Ohnesorge number reported the power law exponent to be close to $-5/4$. Curve fitting the data for transition between Rayleigh and sinuous mode, McKinley and Renardy (2011) reported the relation as $Oh = 125 Re^{-5/4}$. In their work, the diameter of the jet is considered to be the characteristic length scale of the liquid jet; also the selection of the characteristic length scale as either the radius or the diameter of the jet never affects the power law exponent.

However the transitions between the regimes of jet behavior of the Ohnesorge chart that are obtained from Pan and Suga (2006) are curve fitted using power laws and it also indicated that the exponent is $-3/2$ for all the other transitions with similar trend. The transition between Rayleigh-sinuous mode occurs at $Oh = 50Re^{-3/2}$, for sinuous to screw-like mode at $Oh = 440Re^{-3/2}$, and for screw-like mode to atomization at $Oh = 4250Re^{-3/2}$. Based on this power law fit, the relation between We and Re could be obtained and it is found that We is inversely proportional to Re with $We = CRe^{-1}$ where C is the constant factor. This indicates that for practically larger Re otherwise less viscous fluid, the transition from Rayleigh to sinuous mode occurs at lower We. However, the inviscid analysis of Yang (1992) indicates that the appearance of the sinuous mode is possible and it possesses positive growth rate only above $We > 1000$ for the atmospheric pressure conditions. However, the current experimental observation shows the presence of the sinuous mode even for low Weber number. The experimental observations of various regimes such as Rayleigh, sinuous and the screw-like mode is marked in the Ohnesorge chart as shown in fig. 5.5. The flow conditions corresponding to fig. 5.4c is sinuous mode as exactly determined from the Ohnesorge chart.

Experiments are also performed with a round laminar liquid jet at pressure around 20 bar and at room temperature. At this pressure where the density ratio $Q = 0.015$, the jet exhibited capillary instability and transitions to sinuous instability at around $We = 67.5$; this is similar to the case with $Q = 0.0006$ in fig. 5.4c. The aerodynamic shear due to high pressure and density plays a major role only when the Re of the injected jet is beyond 2000 and it also corresponds to the transition to the turbulent regime. The effect of high pressure on the instability of the jet is noticed by comparing fig. 5.4e and fig. 5.6e. It is noted from fig. 5.6e that the turbulent jet possesses more interfacial ruffles at $Q = 0.015$ in comparison with the case in fig. 5.4e where $Q = 0.0006$.

At lower We, the liquid jet injected into a high pressure N_2 environment exhibits the Rayleigh mode. It can be observed from fig. 5.6a and fig. 5.4a that the Rayleigh mode and sinuous mode appeared at almost similar We of around $We \approx 7.5$. The disturbance wavelength of the jet surface for the Rayleigh mode is measured experimentally and compared with the one that is predicted through linear stability analysis as discussed in section 5.2. The measured wavelength of the capillary instability is in good agreement with the predicted wavelength that is 4.3 times the diameter of the jet. This could be perceived from table 5.2 corresponding to fig. 5.4a and fig. 5.6a respectively.

5.4.2 Fluoroketone environment (Single component system)

The experiments are conducted by injecting the laminar liquid fluoroketone jet into its own vapor. To investigate the single component system, the desired ambient vapor pressure is achieved by maintaining the chamber temperature and subsequently introducing sufficient amount of fluoroketone into the chamber. The relationship between the vapor pressure and the temperature is obtained from the Maxwell constructed PRSV equation of state as detailed in fig. 3.15. It is noticed that for subcritical temperatures, the saturated vapor pressure depends only on the chamber temperature and hence the additionally injected fluid mass is in the liquid state at the chamber bottom. Above the critical temperature, the fluid exists in a single homogeneous phase known as the supercritical fluid in which the pressure of the chamber is related to the mass of the fluid in a given volume of the chamber as well as the temperature.

It is to be noted that when a liquid jet is injected into its own saturated vapor, evaporation does not takes place (Cengel et al., 1998). However, the injected jet is subjected to heat transfer from the surroundings and this leads to thermal equilibrium of the jet with the ambient fluid, thereby causing the temperature of the liquid jet to increase. This leads to the changes in the thermodynamic properties like surface tension and viscosity that eventually affects the fluid dynamic process of the jet. At saturated vapor condition, the phase change from liquid to vapor state does not occur and the injected liquid jet always preserves the liquid state at larger downstream distances. When the vapor is not saturated, the injected liquid jet undergoes evaporation that is addition to the changes in the thermodynamic properties. Due to evaporation, the droplet formation, as a result of atomization, promotes the phase change of the liquid jet into vapor state. Since the evaporation process is a slow mass transport process, it is assumed to have negligible effect on the fluid dynamic instability.

When a liquid jet at atmospheric temperature is injected into the vapor environment at higher temperature, the evaporation process takes place in two phases (Jin et al., 2010). In the first phase, the interfacial liquid layer undergoes rapid heating to the temperature T_e that corresponds to the vapor pressure of the ambient vapor. Once the temperature crosses the threshold temperature T_e, the evaporation process is marked by the transition of the molecular layer at the liquid jet surface from liquid to vapor phase. During the process of evaporation, the rate of mass transfer is proportional to the density gradient of the vapor phase. However, the properties such as surface tension and viscosity undergo continual changes with the increase in temperature. In the current set of experiments, the vapor pressure of the ambient vapor is only slightly less than the saturated vapor pressure. As the evaporation is a slow mass transport process, it has negligible effect in altering the fluid dynamic instability.

The injection of fluoroketone jet into its own vapor at pressure around 4 bar is chosen for the study in which the corresponding chamber temperature is 385 K ($T_r = 0.873$). The corresponding density ratio is around $Q = 0.025$. The Reynolds number and Weber number of the jet are defined based on injected jet conditions where the thermodynamic properties are known. When a jet at low Weber number ($We = 2.6$) is injected into its own vapor, the jet exhibits a Rayleigh instability, a fact which is evident from the formation of bigger droplet in fig. 5.7a. The injectant and the chamber conditions are detailed in fig. 3.15. The ambient vapor pressure inside the chamber is slightly lower than the saturated vapor pressure. This suggests that the injected liquid jet could undergo evaporation along with changes in the thermodynamic property such as surface tension, also with changes in the transport

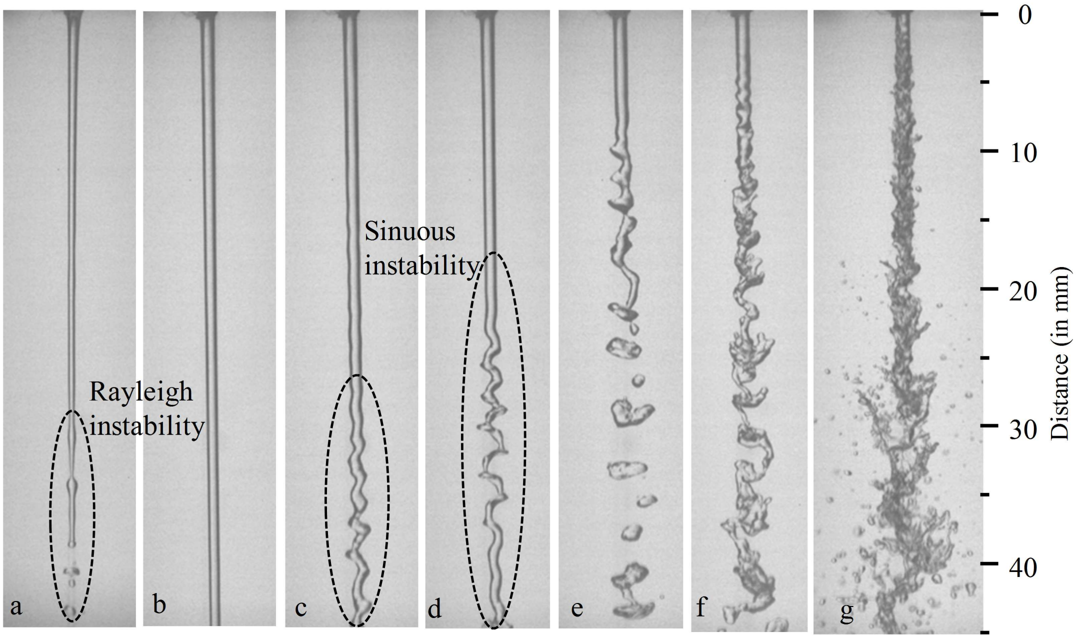

P_r=0.193	P_r=0.193	P_r=0.21	P_r=0.231	P_r=0.21	P_r=0.296	P_r=0.284
T_r=0.873	T_r=0.870	T_r=0.874	T_r=0.871	T_r=0.872	T_r=0.867	T_r=0.893
V=0.191 m/s	V=0.411 m/s	V=0.493 m/s	V=0.54 m/s	V=0.549 m/s	V=0.938 m/s	V=1.762 m/s
Re=210	Re=452.3	Re=543	Re=591	Re=780	Re=1032	Re=1938.5
We=2.6	We=11.91	We=17.14	We=21	We=35.5	We=62	We=218.62
Q=0.026	Q=0.026	Q=0.0287	Q=0.0312	Q=0.0287	Q=0.041	Q=0.04

Figure 5.7 Fluoroketone liquid jet injected into its own vapor environment at $P_r \approx 0.2$ and $T_r \approx 0.875$. The injection temperature is atmospheric, $T_i = 0.68$.

property like viscosity. The changes in the thermodynamic properties could affect the nature of the instability as well as the jet breakup process.

For the present condition, the ambient vapor density is lower and hence the aerodynamic shear due to the ambient vapor on the jet surface could be significantly lower too. The surface of the injected jet is distinctly visible throughout the interrogation window and it indicates that the injected jet did not undergo significant thermodynamic transition to the surrounding. The ambient pressure is slightly lower than that of the saturated vapor pressure, and hence the injected liquid jet might undergo evaporation. However, in the present case, from fig. 5.7, the injected liquid mass is observed to remain intact even at far downstream distances, and that the influence of the evaporation process on jet transition is smaller as compared to

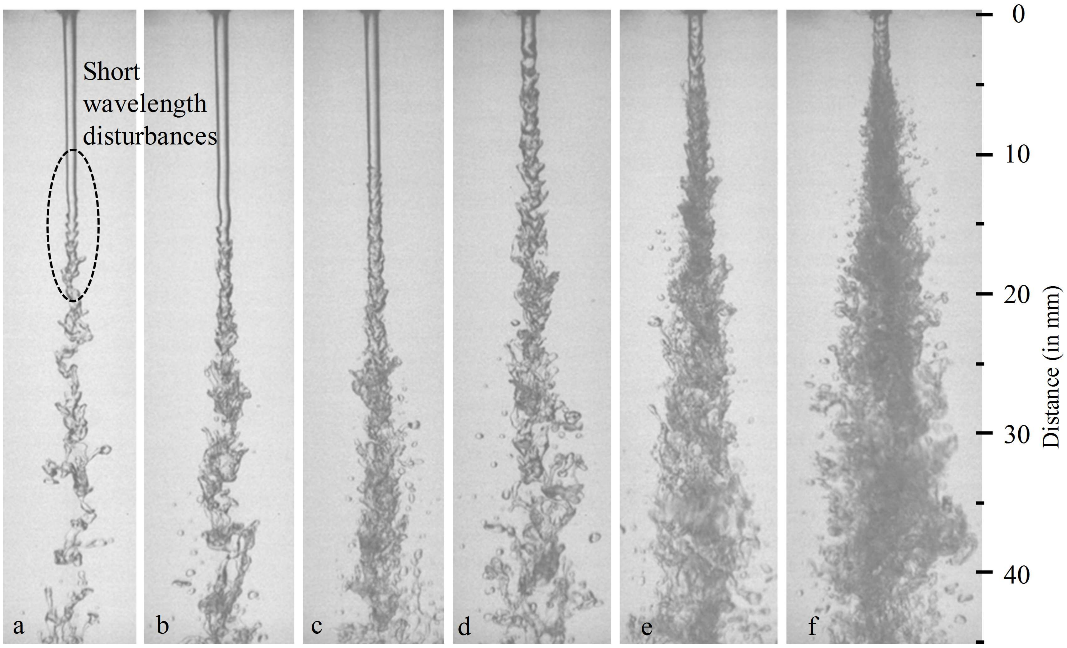

a	b	c	d	e	f
P_r=0.683	P_r=0.657	P_r=0.727	P_r=0.602	P_r=0.726	P_r=0.733
T_r=0.976	T_r=0.976	T_r=0.964	T_r=0.965	T_r=0.96	T_r=0.965
V=0.19m/s	V=0.322 m/s	V=0.34 m/s	V=0.625 m/s	V=0.71 m/s	V=1.06 m/s
Re=210	Re=355	Re=373	Re=687.6	Re=780.4	Re=1165
We=2.6	We=7.3	We=8.1	We=27.51	We=35.4	We=79
Q=0.112	Q=0.106	Q=0.122	Q=0.093	Q=0.123	Q=0.127

Figure 5.8 Fluoroketone liquid jet injected into its own vapor environment $P_r \approx 0.7$ and $T_r \approx 0.97$. The injection temperature is atmospheric, $T_i = 0.68$.

the fluid dynamic process.

Further increase in the jet velocity increases the breakup length, and the injected liquid jet is intact for larger downstream distances. As the velocity of the jet is increased further, the jet exhibits a sinuous mode asymmetric instability at $We = 17.1$ as noticed in fig. 5.7c. This indicates that the cause for interfacial instability is aerodynamic shear. Although, the mechanism of the sinuous instability is not well understood, it was also observed in several of the other previous experiments (Ohnesorge, 1936).

The liquid fluoroketone jet at $We = 62$, $Re = 1032$ is injected into its own vapor at temperature $T_r = 0.867$ and with density ratio $Q = 0.041$ as shown in fig. 5.7f. The jet preserved its laminar nature only for a downstream distance of 8 diameters. In addition to the thermodynamic transition of the fluid properties, the strong aerodynamic shear force due to the dense surrounding vapor causes rapid disturbances to occur and leads to the transition to turbulent regime. The short wavelength disturbance become dominant as the jet velocity is further increased. As a result, fine droplets are pinched out from the jet surface as observed in fig. 5.7g.

As the temperature and the pressure condition of the chamber are increased to 13 bar (P_r=0.683) and 430 K (T_r=0.976), the ambient vapor density increases and the density ratio becomes $Q \approx 0.11$. The short wavelength disturbances are prominent at such condition even at low injectant We and Re as shown in fig. 5.8a. The absence of Rayleigh mode suggests the presence of strong aerodynamic shear stress on the jet interface. In addition, the high chamber temperature causes transition of the interfacial properties that could be responsible for altering the disturbance wavelength and growth rate characteristics. It could be perceived from table 5.2 that the measured wavelength of the interfacial disturbance is much smaller than that determined by stability analysis. The formation of smaller disturbance wavelength could be attributed to the decrease in the surface tension of the jet. The decrease in surface tension leads to an increase in the actual Weber number of the jet, and the actual We is calculated based on the measured interfacial disturbance wavelength and is tabulated in table 5.2.

It is to be noted that as the jet is injected into its own environment at increasingly higher temperatures, both the surface tension and viscosity decreases and hence the actual Weber number and Reynolds number increases; these in turn determine the jet instability. In the present study, only Weber number is predicted based on the measured disturbance wavelength by assuming that the changes in surface tension are more significant than those of viscosity. The effect of surface tension exists only at the jet interface and it undergoes rapid changes as it comes in contact with the surrounding medium. The viscosity of fluid near the jet interface might undergo changes rapidly; however the viscosity of the fluid at the inner core of the jet undergoes slow changes. Although the viscosity at the surface of the jet could be significantly reduced, the bulk of the inner region of the jet could still preserve the injectant jet viscosity and hence the changes in the actual Re could have negligible effects on the instability on the jet surface. Based on the above arguments, by substituting the injectant Re values, density ratio and measured interfacial disturbance in the dispersion relation in equation 5.2, the actual We could be approximately determined.

Figures 5.9 and 5.10 indicate the relation between the dominating disturbance wave number and Weber number for various density ratios and also for two different Reynolds numbers. A significant change in Re does not significantly alter the disturbance wavelength for $We < 500$. However the Weber number plays a crucial role in determining the wavelength of interfacial disturbances. The dominating disturbance wavelength is obtained for various Weber numbers and it shows that at larger We, the aerodynamic shear is more dominant and leads to formation of short wavelength disturbance on the jet surface. It is evident from fig. 5.9 that the increasing density ratio amplifies the aerodynamic shear on the jet surface for a given We.

In the present case for which $Q = 0.11$ and $We = 2.6$, although the injected We is much smaller, the properties of the jet such as surface tension and viscosity undergo continuous changes due to the presence of ambient vapor at higher temperature. The jet is laminar for certain downstream distance, and there could be significant increase in the temperature of the jet surface that could have resulted in the reduction of surface tension. The decrease in surface tension along with the higher ambient density fluid induces short wavelength disturbances on the jet surface. The wavelength of the induced disturbance depends on the value of the surface tension and viscosity.

It is also noticed from fig. 5.9a and fig. 5.10a that for $We \approx 10$ with density ratio ($Q = 0.15$), the dominating disturbance wavelength is of the order of the jet diameter. However, from fig. 5.8, it can be observed that the disturbances

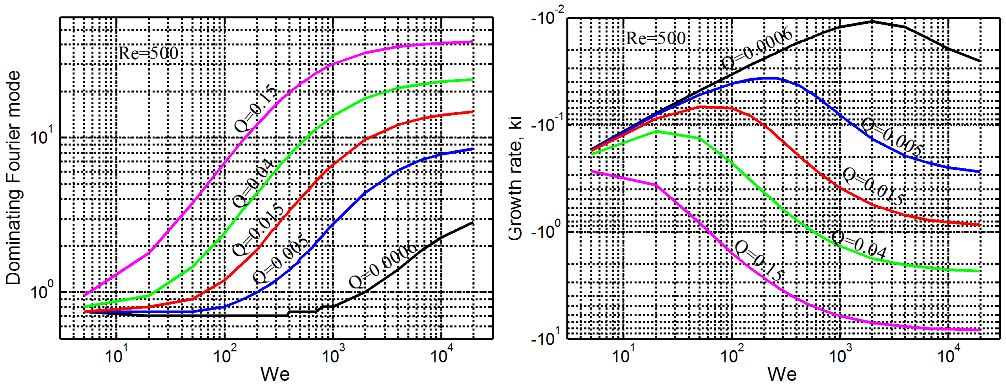

(a) Dominating Fourier mode versus Weber number.

(b) Growth rate versus Weber number.

Figure 5.9 Dominating disturbance wavelength and its growth rate for various ambient fluid to jet density ratio for Re=500.

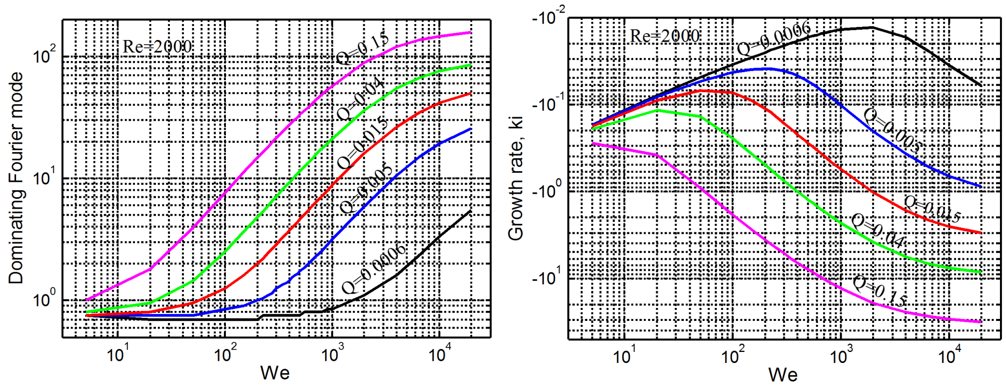

(a) Dominating Fourier mode versus Weber number.

(b) Growth rate versus Weber number.

Figure 5.10 Dominating disturbance wavelength and its growth rate for various ambient fluid to jet density ratio for Re=2000.

formed are of shorter wavelength than those predicted by the dispersion relation. This indicates that the thermodynamic transition of the interfacial properties like surface tension could have played a major role in altering the wavelength of the disturbance. It is also evident from figs.5.9a and 5.10a, that the viscosity does not play a major role in altering the Fourier mode wavelength.

5.5 Fluid jet at supercritical chamber condition

5.5.1 N_2 environment

Results from the injection of fluoroketone liquid jet into supercritical conditions with nitrogen as ambient fluid are presented in fig. 5.11. The injected jet exhibits the classical breakup characteristics. When $We = 8.6$ and $Re = 384$, the jet exhibits the Rayleigh mode instability and the dominant disturbance is of longer wavelength as observed from fig. 5.11a. As the jet Re is increased, the disturbances due to aerodynamic shear play greater role in enhancing the turbulent structures on the jet surface. At $Re > 1500$, the injected jet becomes turbulent as evident from fig. 5.11c, with a distinct interface. The observation shows that the injection of the liquid jet into supercritical conditions, with N_2 as the ambient fluid does not indicate thermodynamic transition.

The study of a binary component system with n-dodecane and nitrogen revealed that the binary component system reaches supercritical state only at higher pressures (Dahms and Oefelein, 2013), (Balaji et al., 2011). At supercritical temperature, the solubility of nitrogen at the surface of n-dodecane liquid surface increases with pressure and at critical pressure, there is hardly any distinct interface. This shows that the n-dodecane-N_2 possess a critical pressure which is larger than either of the components (Balaji et al., 2011). However, in the past, the study conducted by Segal and Polikhov (2008) with fluoroketone-N_2 system revealed that the fluoroketone jet injected into a nitrogen environment at supercritical temperature exhibited the absence of droplet formation, and finger-like projections are reported to appear at the interface. This indicated that the critical conditions of the binary component system of the combined n-dodecane-N_2 mixture (Dahms and Oefelein, 2013) could be very different from the critical conditions of the combined fluoroketone-N_2 system (Segal and Polikhov, 2008). In chapter 4, the study on elliptical liquid jets at its supercritical conditions with ambient N_2 environment revealed that the injected elliptical liquid jet exhibited axis-switching phenomena which is an indicator of surface tension, and did not undergo thermodynamic transition to supercritical state. This shows that the critical pressure of the binary component system could be higher than that of the single component system. However as the results from the previous studies of Segal and Polikhov (2008) have indicated otherwise, there definitely exists a strong reason to investigate the jet transition characteristics of fluoroketone jet at critical condition.

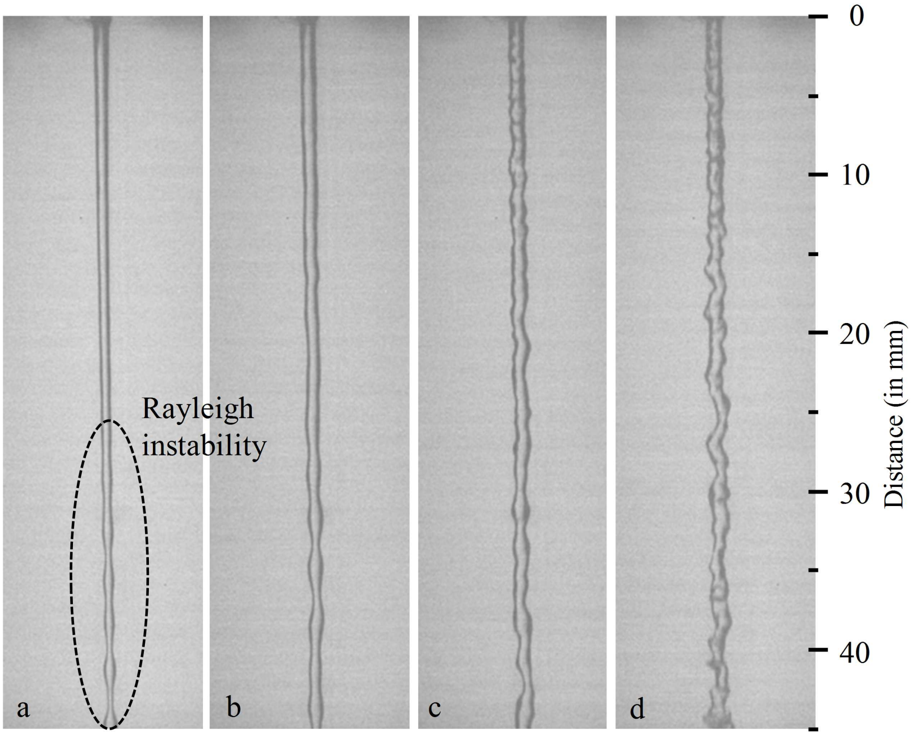

P_r=1.086
T_r=1.058
V=0.349 m/s
Re=384.5
We=8.6
Q=0.0093

P_r=1.16
T_r=1.058
V=0.741 m/s
Re=815.4
We=38.68
Q=0.0097

P_r=1.163
T_r=1.057
V=1.43 m/s
Re=1572
We=143.78
Q=0.0097

P_r=1.25
T_r=1.058
V=2.39 m/s
Re=2623.77
We=400.54
Q=0.0102

Figure 5.11 Injection of liquid fluoroketone into nitrogen environment at supercritical chamber condition. The injection temperature is atmospheric, $T_i = 0.68$.

5.5.2 Fluoroketone environment

Experiments are conducted to investigate the injection at supercritical temperatures ranging from $T_r = 1.02$ to $T_r = 1.06$ at both subcritical and supercritical pressure conditions. When a jet is injected with $We = 2.85$ and $Re = 220$ into high subcritical pressures with density ratio of $Q = 0.131$, the jet maintains laminar behavior only for the downstream distance of about 12 diameters. It is evident from fig. 5.12a that the disturbances are generated in the surface that is accompanied by atomization and is also characterised by the presence of short wavelength disturbances that are responsible for the formation of smaller droplets of the injectant fluid. The dispersion relation suggests that for the We and Re and Q under consideration, even for the high ambient density the jet exhibits instability with wavelength of disturbances larger than the jet diameter. However, it is more evident from the atomization behavior of the jet as observed in fig.5.12a that the surface tension of the jet could have approached a minimum value for which the surface disturbances of shorter wavelength grow quickly and lead to faster atomization. The corresponding injection and chamber conditions are marked in fig. 3.15 where the thermodynamic transition of the injected jet to the chamber condition must follow the constant pressure process and there exists a distinct interface between the injected liquid and the dense fluid surrounding the liquid jet. Since the pressure is subcritical, though the temperature is supercritical, the injected jet must undergo evaporation process to achieve the thermodynamic transition to the chamber condition. Under this chamber condition, as the velocity of the jet is further increased, the instability develops at faster rate and this is evident from the decrease in the intact length of the injected jet. This is clearly evident from fig. 5.12b. Further increase in the jet velocity leads to the formation of droplets that are finer than those corresponding to the first two cases in fig. 5.12a and fig. 5.12b respectively. At $We = 43.55$ and $Re = 866$, the injected liquid jet instantly develops turbulent ruffles on its surface that are followed by atomization of the jet. The atomization is characterised by the formation of fine droplet as could be observed from fig. 5.12e.

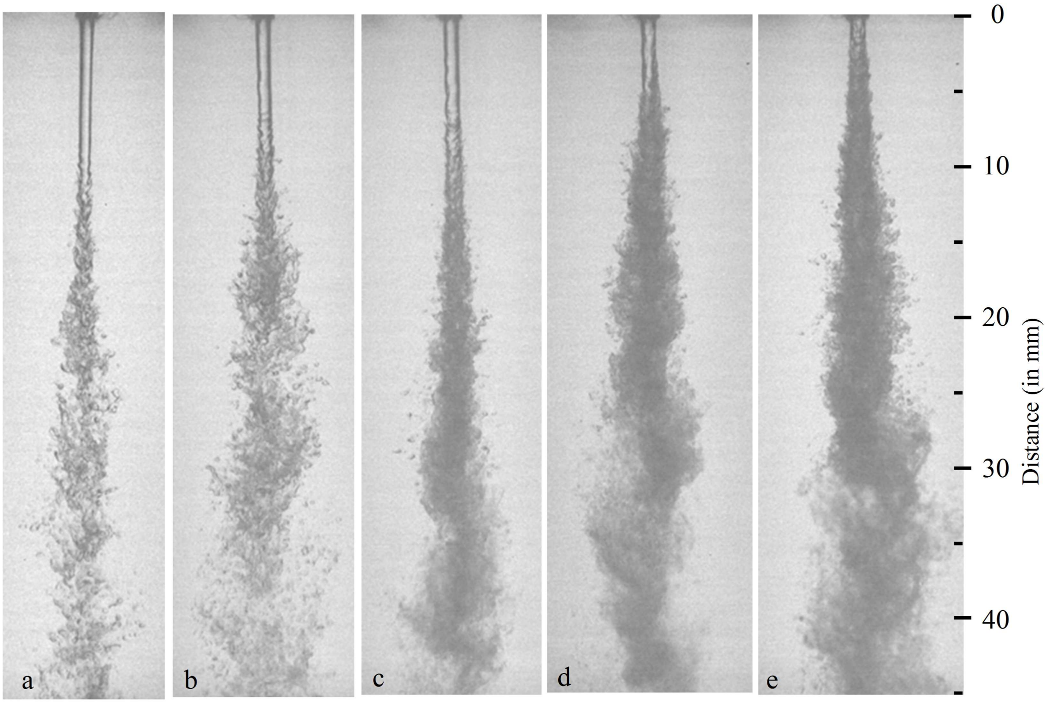

a: P_r=0.855, T_r=1.027, V=0.20 m/s, Re=220, We=2.85, Q=0.131

b: P_r=0.876, T_r=1.039, V=0.282 m/s, Re=310, We=5.6, Q=0.128

c: P_r=0.903, T_r=1.036, V=0.389 m/s, Re=428.3, We=10.7, Q=0.137

d: P_r=0.924, T_r=1.04, V=0.47m/s, Re=515.7, We=15.5, Q=0.14

e: P_r=0.898, T_r=1.04, V=0.78 m/s, Re=866, We=43.55, Q=0.136

Figure 5.12 Fluoroketone jet injected into its own vapor environment at supercritical temperature but at subcritical pressure. The injection temperature is atmospheric, $T_i = 0.68$.

When the chamber condition is supercritical in both pressure and temperature, the transition from liquid into ambient supercritical condition occurs devoid of evaporation. At this condition there is no distinction between the liquid and the surrounding supercritical fluid phase, as it is very evident from P-ρ phase diagram in fig. 3.15. The mixing of injected liquid jet is expected to take place through the diffusion process of species. In many of the previous studies, the liquid jet injected into its supercritical environment is reported to behave as a supercritical jet instantly. This is primarily due to the high jet Re, $Re > 10000$, where the jet is turbulent and the interfacial disturbances rapidly grow and expedite the thermodynamic transition of fluid near the jet interface (Segal and Polikhov, 2008). However, from fig. 5.13a, the injected liquid jet at $We = 24.28$, $Re = 272$ exhibited distinct interface for

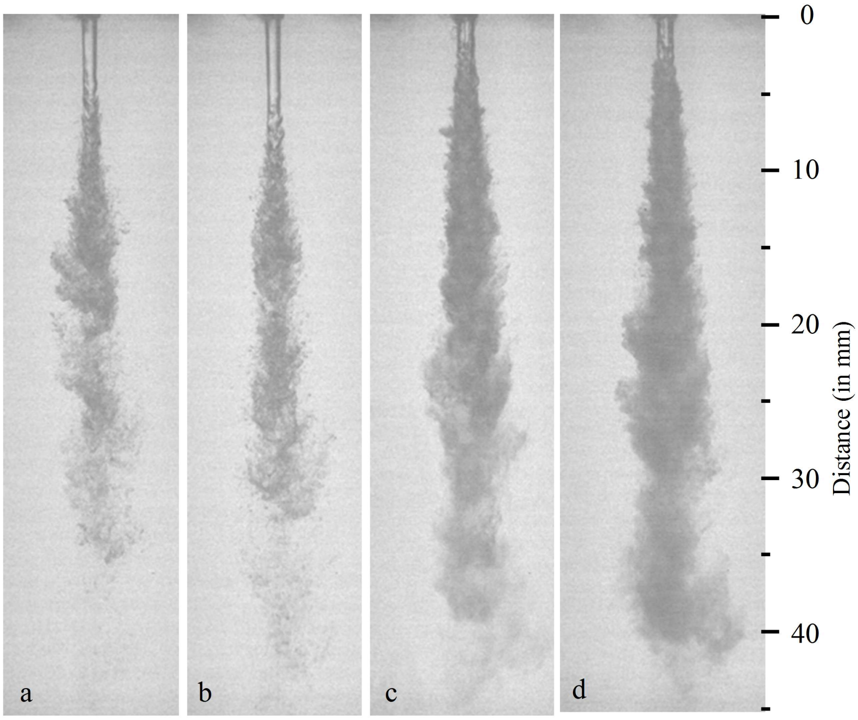

P_r=1.021
T_r=1.05
V=0.247 m/s
Re=272
We=4.28
Q=0.162

P_r=1.02
T_r=1.055
V=0.514 m/s
Re=565.5
We=18.6
Q=0.155

P_r=1.09
T_r=1.057
V=0.617 m/s
Re=679
We=26.8
Q=0.175

P_r=1.022
T_r=1.063
V=0.688 m/s
Re=758
We=33.41
Q=0.156

Figure 5.13 Fluoroketone jet injected into its supercritical environment. The injection temperature is atmospheric, $T_i = 0.68$.

a few downstream distance at its supercritical environment. This reveals that the interface exhibits finite surface tension value and does not instantly reach critical temperature as observed by Dahms and Oefelein (2013). The jet injection and mixing process is considered to be a constant pressure process. It can be also noted that for the case in fig. 5.13a, the injectant temperature is atmospheric with $T_i = 0.68$, and the ambient supercritical temperature is $T_r = 1.05$. The interface of the liquid jet exists between the relatively cold core of the jet and the surrounding hot supercritical environment. This indicates that for the first few diameter downstream distance the interface may not have reached the critical temperature and it could be subcritical and close to the critical temperature. The instability waves develop in the region where the interface is distinct. The development of instability waves result in the increased surface area of the jet and could have expedited the transition to thermal equilibrium of the injected jet with the surrounding fluid.

After certain location downstream, the occurrence of instability leads to the formation of a turbulent surface that rapidly increases the contact area between the injected jet and the surrounding supercritical fluid. At this stage, the interface could have reached the critical temperature as no clear interface is visible. In the absence of surface tension, the laminar jet is no longer intact and the higher ambient density causes significant drag to the jet surface and thus the jet structure exhibit gas-gas like mixing behavior. As the We is increased further, the injected jet is subjected to significant aerodynamic drag and it leads to gas-gas like mixing. The images are captured using backlight method and the jet is identified through the opacity it creates. Normally, for bigger droplets, the opacity is perceived along the surface of the drops, and the smaller droplets are observed as darker points that are separated by some distances. However, for a liquid jet injected into supercritical fluid phase, the droplets are not observed in the boundary of the jet. The opacity of the jet exists only for a certain downstream distance and beyond that it disappears, and also suggests that the jet could have undergone thermodynamic transition to the supercritical fluid phase.

Similar observation is also reported by Woodward and Talley (1996) where liquid nitrogen is injected into gaseous and supercritical N_2. Beyond supercritical pressures, the injected liquid nitrogen undergoes transition to supercritical fluid state within few diameters downstream. Also, experiments were performed by Chehroudi et al. (2002a) to understand the nature of cryogenic shear layers by injecting liquid N_2 into supercritical N_2 at fixed temperature. At subcritical pressures, the injected liquid jet exhibited distinct interface, and as the pressure reaches the critical point, a smoky appearance of the interface is observed and the jet behaved like a variable density gaseous jet. Their experiments were conducted with $Re > 40000$ and the transition of the interface from the atomization regime to a gas-gas like mixing zone is noticed for the increased pressures up to supercritical. Also in the investigation of liquid nitrogen injected into gaseous nitrogen by Mayer et al.

(2000), the interface of the injected jet undergoes transition and exhibits gas-gas like mixing as the pressure is increased to supercritical. The experimental investigation on the effects of density difference on the structure of the shear layer of the jet is performed by Brown and Roshko (1974). In their study, N_2 and helium are used as fluid media, and the study concluded that the density difference affects the spreading angle of the jet. This is attributed to the large momentum possessed by the jet due to its very high density. Even though the jet exhibits single phase mixing characteristics, the potential core length of the jet is found to be larger as compared to the normal gaseous jet due to the higher momentum ratio.

Hence, under supercritical temperature condition the pressure plays major role in determining the behavior of the jet. At subcritical pressures, the mixing of the injected liquid jet into ambient condition takes place through the evaporation process and for supercritical pressures, the thermodynamic transition occurs through diffusion process. From fig. 5.12e and fig. 5.13d, it is evident that at supercritical pressures, the jet becomes transparent after certain downstream distances and it suggests complete transition to supercritical state which is absent at subcritical pressures. The physical mechanism may be explained as follows: At subcritical pressure, the injected liquid jet is atomized into fine droplets through the aerodynamic shear force working against surface tension, and the process of evaporation finally leads to molecular level mixing. However, at supercritical pressures, with very low values of surface tension, there is no resistance to the aerodynamic shear force from the ambient fluid and hence the injected jet fluid diffuses from the interface into the ambient fluid. It is to be noted that the opacity of the injected jet at supercritical pressure and temperature condition is due to the critical opalescence. Since there is no distinct interface and the jet media is continuous, the critical opalescence is attributed to the scattering caused by the density fluctuations that occur in length scales that are of the order of the wavelength of the backlit light source (Gopal, 2000).

The disturbance wavelength predicted by linear stability analysis based on Re and We of the injected jet are compared with the disturbance wavelength

Re	We	Q	**Measured wavelength (λ_m)**	**Predicted wavelength using LSA (λ)**	**Calculated Weber number We_p for λ_m**	**Observed instability mode**	**Corresponding images**	**Ambient fluid**
357	7.43	0.0006	3.29	3.78		R	fig. 5.4a	N_2
1098	70.16	0.0006	1.934			S	fig. 5.4c	N_2
1346	105.4	0.0006	1.92			W	fig. 5.4d	N_2
359	7.5	0.013	3.65	3.68		R	fig. 5.6a	N_2
1074	67.5	0.015	1.55			S	fig. 5.6c	N_2
384	8.6	0.0093	3.11	3.73		R	fig. 5.11a	N_2
370	3.5	0.026	2.91	3.43		R	fig. 5.7a	FK
543	17.14	0.0287	1.74			S	fig. 5.7c	FK
591	21	0.0312	1.87			S	fig. 5.7d	FK
780	35.5	0.0287	1.93			S	fig. 5.7e	FK
1032	62	0.041	0.83			W	fig. 5.7f	FK
210	2.6	0.112	0.442	3.0	140	SA	fig. 5.8a	FK
355	7.3	0.106	0.447	2.89	125	SA	fig. 5.8b	FK
373	8.1	0.122	0.42	2.71	118	SA	fig. 5.8c	FK
220	2.85	0.131	0.46	2.94	112	SA	fig. 5.12a	FK
310	5.6	0.128	0.398	2.91	126	SA	fig. 5.12b	FK
272	4.28	0.162	0.425	2.86	98	SA	fig. 5.13a	FK

Table 5.2 Comparison between experimentally measured wave length and wave length predicted by linear stability analysis. 'FK' denotes Fluoroketone. Abbreviations 'R','S','W','SA' stands for Rayleigh mode, Sinuous mode, wave-like or screw-like mode and short axisymmetric wave respectively. Abbreviation 'LSA' stands for Linear Stability Analysis.

that are measured experimentally at actual chamber conditions in table 5.2. The injected jet temperature condition of all the cases is atmospheric with reduced injection temperature T_i=0.68. It can be noted from table 5.2 that at atmospheric chamber condition, the predicted wavelength is in good agreement with the experimentally measured wavelength. When the chamber conditions are supercritical, the injected fluoroketone jet exhibited Rayleigh instability in the N_2 environment. This suggests that for chamber temperature and pressure conditions considered in the present experiment, the jet characteristics for the binary component system are

P_r	T_r	V m/s	We	Ambient fluid	Corresponding figures	Key observations
0.054	0.68	0.25	7.43	N_2	fig. 5.4a	Rayleigh instability
0.054	0.68	0.77	70.16	N_2	fig. 5.4c	Sinuous instability
0.054	0.68	0.947	105.4	N_2	fig. 5.4d	Screw-like instability
0.995	0.68	0.326	7.5	N_2	fig. 5.6a	Rayleigh instability
1.14	0.68	0.976	67.5	N_2	fig. 5.6c	Sinuous instability
1.086	1.058	0.349	8.6	N_2	fig. 5.11a	Rayleigh instability
0.193	0.873	0.191	2.6	FK	fig. 5.7a	Rayleigh instability
0.21	0.874	0.493	17.14	FK	fig. 5.7c	Sinuous instability
0.683	0.976	0.19	2.6	FK	fig. 5.8a	Short wavelength disturbance followed by turbulent interface that leads to breakup of jet
0.855	1.027	0.20	2.85	FK	fig. 5.12a	Short wavelength disturbance followed by turbulence and formation of droplet clusters
1.021	1.05	0.247	4.28	FK	fig. 5.13a	Short wavelength disturbance leads to smoky like appearance and fine clusters near the the jet edge. At certain downstream, the jet becomes transparent indicating that the jet becomes supercritical.

Table 5.3 Key observations on jet behavior for different chamber and injectant conditions.

independent of pressure and temperature. However, for single component system, the instability characteristics are very much dependent on the chamber pressure and temperature conditions. As noted from table 5.2, the predicted values and measured values of the disturbances differ significantly for the cases of figs. 5.8, 5.12, and 5.13. The formation of small wavelength disturbances on the jet interface suggests that the surface tension of the fluoroketone jet is subjected to significant changes as it is injected into near-critical and supercritical chamber conditions.

The summary of the key observations of the jet behavior and the instability waves are provided in table 5.3. At low jet Re with nitrogen as the ambient fluid, the injected liquid jet remained in liquid state and behaved as a liquid jet even at supercritical chamber condition. For the case of single component system, the liquid jet at subcritical chamber condition exhibited short wavelength formation on its interface; this is mainly due to the higher ambient density and also due to the decrease in surface tension of the jet. As the temperature becomes supercritical, the pressure plays a major role in determining the jet behavior. At subcritical pressure and supercritical temperature the droplet formation is observed. At supercritical pressures and temperatures, the liquid jet transforms to supercritical fluid with smoky like appearance at the intermediate stages.

To further investigate the mixing characteristics of the jet, the fractal analysis is carried out in the following section to understand the jet behavior in detail.

5.6 Fractal geometry of jet boundary

The study of fractal is a branch of mathematics in which objects possess self-similarity in an infinite range of scales. However, the application of fractal concept to the physical objects has its own limitation due to the existence of self-similarity only over certain range of scales. In the early days, Mandelbrot (1983) suggested that the theory of fractals must be applied to the study of turbulence since turbulence possesses the nature of self-similarity over certain range of scales. Later Sreenivasan and Meneveau (1986) studied the fractal nature of the turbulent jet interface in detail. In their study, fractal dimensions are used to analyze the geometry of the turbulent interface of the jet. It was found from their study that the turbulent surface of axisymmetric jet possesses the fractal dimension of 2.33.

Shavit and Chigier (1995) measured the fractal dimension of the liquid-gas interface from the experimental images at various axial locations. The authors found that the fractal dimension of the jet increases sharply from 1 to the peak value at a certain downstream distance, and it again decreases downstream. The concept of fractal analysis was used by Heidorn et al. (2008) to describe the unresolved sub-grid scale of the liquid jet which is obtained from numerical simulation. The authors proposed a dynamic model to predict the fractal dimension of the jet interface. In their simulation results, the fractal dimension of the liquid jet interface spanning three dimensions is found to be within 2.27 for an atomizing jet, for which the corresponding equivalent is 1.27 in the case of the jet boundary.

The fractal nature of the liquid N_2 injected into supercritical nitrogen was investigated by Chehroudi et al. (1999) using Minkowski or box-counting dimension. It is reported that the jet boundary follows a fractal nature with fractal dimension of around 1.35 for the supercritical chamber condition. The evaluation of the fractal nature of the injected jet finds its significance in practical applications as the high fractal dimensions correspond to the larger interfacial area that enhances the mixing process. Turbulent boundaries are fractal objects only up to Kolmogorov scale since there is absence of eddies beyond the Kolmogorov scale.

5.6.1 Box counting method

There are objects which possess a fractal dimension, unlike classical objects which have an integer dimension. Topologically, a curve is a one-dimensional object; and when a hyperspace is space filling, its fractal dimension depends on the degree of space filling nature. Hence a curve possess a dimension between one and two. In the present study the fractal dimension of the injected fluid jet at supercritical conditions is computed using a box-counting algorithm. The iso-density contour of the jet boundary is obtained by selecting a particular threshold intensity value of the visualized jet image. The resulting jet boundary is analyzed for its fractal dimension. To calculate the fractal dimension, the object is overlapped with an evenly spaced grid and the boxes that cover any part of the object are counted. The fractal dimension or the box-counting dimension depends on the number of boxes that cover the fractal set and it changes as the grid size becomes finer. The box-counting dimension is defined as

$$D_f = \lim_{\epsilon \to 0} \frac{Log(N(\epsilon))}{Log(1/\epsilon)} \tag{5.7}$$

Where N(ϵ) is the number of boxes of side ϵ that is required to cover the fractal set. The inbuilt box count algorithm in Matlab software is utilized for computing the fractal dimension.

In this method, a plot between size of the box and dimension of the fractal object is obtained from the expression as detailed in equation 5.7. According to the above expression, the fractal nature of the geometrical object could be revealed by the similarity in the fractal dimension over a few length scales of the grid.

5.6.2 Fractal dimension of subcritical jet injected into subcritical to supercritical chamber condition

The fractal dimension of the liquid jet at subcritical as well as the supercritical chamber condition is investigated in detail for both the single and binary component system. For the N_2 environment, the injected liquid jet exhibits classical behavior at atmospheric chamber condition with fractal dimensions varying between 1.01 and 1.03. Even at supercritical chamber temperature conditions, the existence of the distinct boundary suggests that for a binary component system, the transition to supercritical state does not occur. The fractal dimension of the jet at supercritical condition for N_2 environment is about 1.04. However, for a single component system, the chamber pressure and temperature conditions play a crucial role in determining the transition of the jet to supercritical state. This could be directly perceived through the investigation of the fractal nature of the jet boundary. For the single component case, the injection of the liquid jet into its own vapor at the chamber temperature and pressure at T_r=0.873 and P_r=0.193 resulted in a fractal dimension of the jet boundary of about 1.02, and the value indicates the one dimensional nature. As the velocity of the jet is increased further, the sinuous mode appears with fractal dimension of 1.02. For the case in fig. 5.7f, with chamber condition P_r=0.296 and T_r=0.867, the jet is laminar only for a certain distance and the generation of the random disturbances leads to turbulence, with the overall fractal dimension of the jet being 1.05. When the chamber pressure and temperature are P_r=0.683 and T_r=0.976 (fig. 5.8a), even the jet at low velocity of about 0.19 m/s leads to short wavelength disturbances, thereby resulting in turbulent jet and causes disintegration of the jet into droplets of size of the order of jet diameter. The fractal dimension of the jet for this particular case is 1.08.

The transitional nature of the injected liquid jet into supercritical condition is more evident as the chamber temperature becomes supercritical and the pressure is slightly below the critical point. In the case of the injection of liquid jet at low velocity into the chamber at P_r=0.855 and T_r=1.027 as shown in fig. 5.12a, the jet possess a fractal dimension of 1.11. At similar chamber condition in fig. 5.12c, but with slightly higher jet velocity of V_i=0.389 m/s, the jet is initially laminar for a certain downstream distance, and rapidly develops interfacial corrugations thereby leading to misty-like appearance. A few fine droplets at the interface suggest incomplete transition to supercritical state. The fractal dimension of the overall jet is about 1.21.

When the chamber temperature as well as the pressure become supercritical, the complete transition of the jet is clearly evident from fig. 5.13. At lower velocity of V_i=0.247 m/s, the initially laminar jet develops sudden disturbances at the interface that are followed by misty like appearance, and the jet eventually becomes transparent; this suggests a complete transition of the jet into supercritical state. The fractal dimension of this case in fig. 5.13a is 1.3. When the jet velocity is increased further, the fractal dimension of the jet also increases. The fractal dimension for the cases in fig. 5.13b and 5.13c are 1.35 and 1.4 respectively. The results obtained in the current study are very similar to those reported by Chehroudi et al. (1999) for a liquid jet injected into supercritical chamber condition for a pure component system.

5.7 Jet visualisation using the PLIF technique

5.7.1 Density and density gradient measurement for supercritical jet injection

The density and density gradient fields could be obtained from the fluorescence image of the jet. Since the fluorescence is directly proportional to the density of the jet, the spatial density map could be easily obtained. The optical arrangement of the present experimental study is detailed in fig. 3.7 3. In this arrangement, two laser beams of equal energy are produced using a polarizing beam splitter and a half wave plate. Employing a cylindrical concave lens and a spherical convex lens, two laser sheets are formed. One laser sheet is used to excite the fluid jet injected into the chamber and the other is used to excite the fluoroketone in the reference dye cell. The fluorescence image of fluid jet as well as the dye cell is captured in the same camera sensor using the LaVision image doubler simultaneously.

As the laser beam profile is Gaussian in nature, the laser sheet formed from the beam has a variation in intensity in the vertical direction and must be corrected. The laser sheet is made to pass through the chamber that is filled with fluoroketone vapor. The 2D-fluorescence signal is collected by effectively blocking the elastic scattering using UV filters. The laser sheet profile correction is performed to account for the variation in the intensity along the height of the sheet.

To eliminate the shot-to-shot fluctuation in the laser intensity, the reference dye cell has been employed in the present study. From the laser sheet fluorescence signal, it is found that the maximum percentage deviation in the fluorescence signal due to shot-to-shot fluctuation in the laser intensity is 5.8$\%$. The final expression that relates the density field and the fluorescence is

$$\rho_{jet} = \left[\frac{S_{dyecell(300K,1bar)}}{S_{liqjet(300K,1bar)}}\right]_{\text{Calibration shot}} \left[\frac{S_{jet}}{S_{dyecell(300K,1bar)}}\right]_{\text{experimental shot}} \rho_{liq} \tag{5.8}$$

where S denotes the fluorescence gain and the corresponding subscript $dyecell$ and $liqjet$ denotes the fluorescence imaging from the reference dye cell and the liquid jet respectively. There are various uncertainties in determining the density of the jet that are discussed in detail in section 5.7.2.

The density gradient field is determined to analyze the mixing regions where the density gradients are high and promotes the diffusion of the injectant fluid into the ambient fluid. The density gradient field is obtained using the expression

$$\rho_{grad} = \sqrt{\nabla\rho.\nabla\rho} = \sqrt{\left(\frac{d\rho}{dx}\right)^2 + \left(\frac{d\rho}{dy}\right)^2} \tag{5.9}$$

Uncertainty source	**Percentage error**	**Correction/remarks**
Intensity variation along laser sheet profile	25% deviation	Corrected as detailed in section 3.8.6 using normalized laser sheet profile
Shot-to-shot fluctuation	5.8% deviation	Corrected as detailed in section 3.8.7
Laser sheet profile shape variation	2.9%	Corrected using average laser sheet profile. However shot to shot profile variation will contribute to random error
Laser attenuation	12.5%	Due to absorption by density up to 575 kg/m3
Root Square uncertainty in density prediction	**12.84%**	Due to profile variation and laser attenuation

Table 5.4 List of uncertainties and the possible errors in predicting the density field of supercritical jets.

The density gradient field is obtained from the density matrix using equation 5.9. The derivative at each pixel is calculated using the sixth order approximate central differencing scheme. The density gradient field map is obtained to assess the detailed mixing region of the jet.

5.7.2 Uncertainty analysis

The uncertainties associated with the determination of the density are listed in table 5.4 and it is evident that the largest source of uncertainty of 25% arises due to the variation of laser intensity along the sheet height. This is attributed to the Gaussian nature of intensity distribution of laser beam and is corrected using a normalized laser sheet profile along the length of the jet. However the normalized sheet profile is only an average representation of 50 laser shots and it must be highlighted that there will be minor shot to shot laser sheet profile variations; the uncertainty due to minor deviation from the averaged profile amounts to 2.9%. Similar to the laser sheet profile variation in space, the shot to shot fluctuation in the intensity of the laser sheet amounts to 5.8% and this is eliminated by simultaneously imaging the dye cell fluorescence and jet fluorescence using image doubler. Finally the uncertainty in the laser attenuation due to absorption by fluoroketone with a density of 575 kg/m^3 is estimated to be 12.5%. Based on the error analysis the two factors that contribute to the uncertainty in density measurements include (1) laser sheet profile shape variation of 2.9% and (2) laser attenuation of 12.5%, and the corresponding root square uncertainty in density is estimated as 12.84%.

5.7.3 Experimental conditions for supercritical jet injection

The experimental conditions are detailed in table 5.5. Three different sets of injectant and chamber conditions are selected for the experiments. They are: 1. Near-critical jet injected into subcritical condition, 2. Supercritical jet injected into subcritical condition, and 3. Supercritical jet injected into supercritical condition. The experiments are performed for two different binary component system: 1. Fluoroketone injected into helium environment, and 2. Fluoroketone injected into N_2 environment. The two different ambient fluids are chosen for their difference in critical pressure. The helium is used for its much lower critical pressure as compared to fluoroketone whereas the critical pressure of nitrogen is significantly higher than that of fluoroketone. The chamber and injectant pressures as well as the temperatures are reduced with respect to the critical properties of the injectant fluid, fluoroketone. Also the chamber and the injectant condition are defined based on the temperature conditions of the injectant fluid. The term subcritical or supercritical in the current work implies that the temperature condition is subcritical or supercritical; the pressure could be either subcritical or supercritical, depending on the experimental conditions as detailed in table. 5.5.

A detailed set of experiments on the injection of supercritical jet into its subcritical as well as supercritical conditions are performed to understand the nature of thermodynamic transition of the jet. Also, the fractal dimension of the jet boundary is computed and compared with the previous studies performed by Chehroudi et al. (1999). The density and the density gradient field map are obtained to retrieve the detailed information pertinent to the mixing characteristics of the injected jet. Following are the injection and the chamber conditions selected for carrying out the

Injection temperature to chamber temperature condition	**Chamber pressure P_r**	**Chamber temperature T_r**	**Injection temperature T_i**	**Chamber environment**
Near-critical to subcritical condition	0.79	0.82	0.984	Helium
	0.86	0.82	0.988	
	1.24	0.83	1.0	
Supercritical to subcritical condition	0.806	0.826	1.02	
	0.99	0.82	1.06	
	1.29	0.85	1.07	
supercritical to supercritical condition	0.715	1.034	1.02	
	1.16	1.047	1.022	
	1.34	1.04	1.02	
Near-critical to subcritical condition	0.90	0.82	0.99	Nitrogen
	1.0	0.82	1.0	
	1.21	0.82	0.987	
Supercritical to subcritical condition	0.83	0.83	1.072	
	1.02	0.823	1.032	
	1.344	0.816	1.07	
supercritical to supercritical condition	0.806	1.02	1.07	
	1.02	1.03	1.03	
	1.32	1.03	1.073	

Table 5.5 Pressure and Temperature conditions of chamber and fluid injection chosen for Supercritical to subcritical experiment.

investigation.

1. Near critical to subcritical condition: At near-critical condition, the injectant fluid density is very sensitive to changes in pressure and is expected to affect the behavior of the jet. The study of near-critical injectant jet is necessary to bring out the transitional nature of the jet at different pressures along the near-critical temperatures.

2. Supercritical jet into subcritical chamber condition: As aforementioned the term supercritical jet and subcritical chamber condition implies that the temperature of the injected jet is supercritical whereas the chamber is subcritical. However the pressure will be varied from sub to supercritical conditions.

3. Supercritical jet into supercritical chamber condition: Here the temperature of both jet and chamber are supercritical whereas the pressure will be varied from sub to supercritical conditions

5.8 Near-critical jet into subcritical chamber condition (With N_2 and He as ambient fluids)

The jet at near-critical temperature condition is injected into the subcritical chamber condition for both nitrogen as well as the helium environments, and the results are presented in fig. 5.14 and fig. 5.15. Prior to the conduct of the experiment, the chamber is purged with nitrogen/helium gas and is subsequently filled with N_2 or He to the desired pressure. The injection temperature of the jet is marginally lower than the critical temperature of fluoroketone. As the jet at near critical temperature is injected into the subcritical chamber condition, the chamber pressure plays the crucial role in determining the thermodynamic transition of the injected jet. For the subcritical chamber pressure, the injected near critical jet transforms into vapor and liquid droplets. It is evident from fig. 3.15 that the density of the vapor is close to 300 kg/m^3. As the pressure is beyond the critical point with the jet temperature still maintained at near critical condition, the density change in the fluid is very sensitive to the pressure, as is evident from fig. 3.15. For the changes in the pressure from P_r=0.8 to P_r=1 along the critical isotherm, the density increases from 200 kg/m^3 to 500 kg/m^3, and as the pressure becomes marginally supercritical the fluid is found to exist in the liquid state with density values close to those corresponding to the supercritical fluid. In fig. 5.14c at pressure P_r=1.24, the density of the injectant fluid is 840 kg/m^3 as determined from fig. 3.15, and it indicates that the density values closely correspond to the liquid like state.

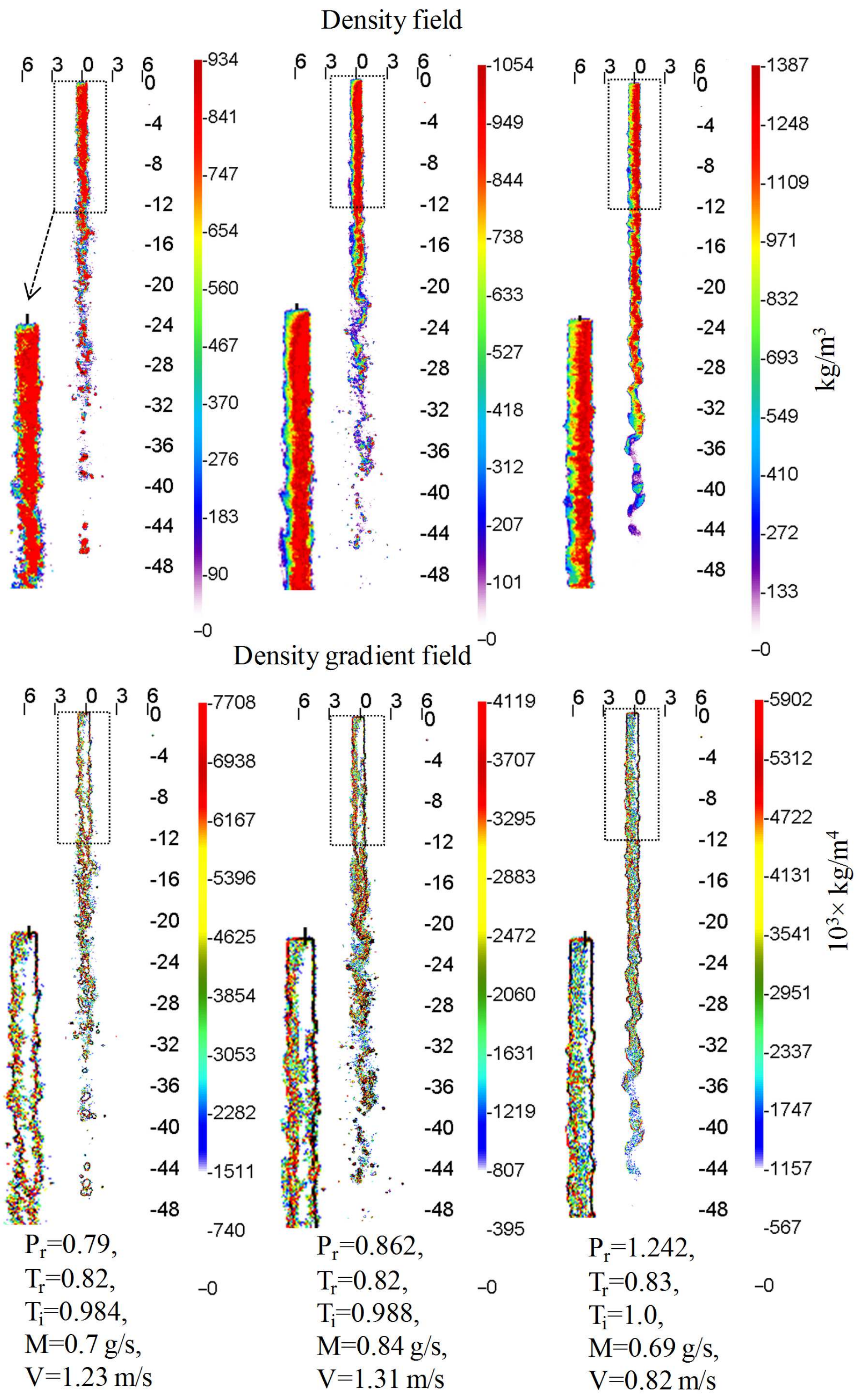

P_r=0.79,
T_r=0.82,
T_i=0.984,
M=0.7 g/s,
V=1.23 m/s

P_r=0.862,
T_r=0.82,
T_i=0.988,
M=0.84 g/s,
V=1.31 m/s

P_r=1.242,
T_r=0.83,
T_i=1.0,
M=0.69 g/s,
V=0.82 m/s

Figure 5.14 Injection of near-critical jet into subcritical condition with helium as ambient fluid.

Density field

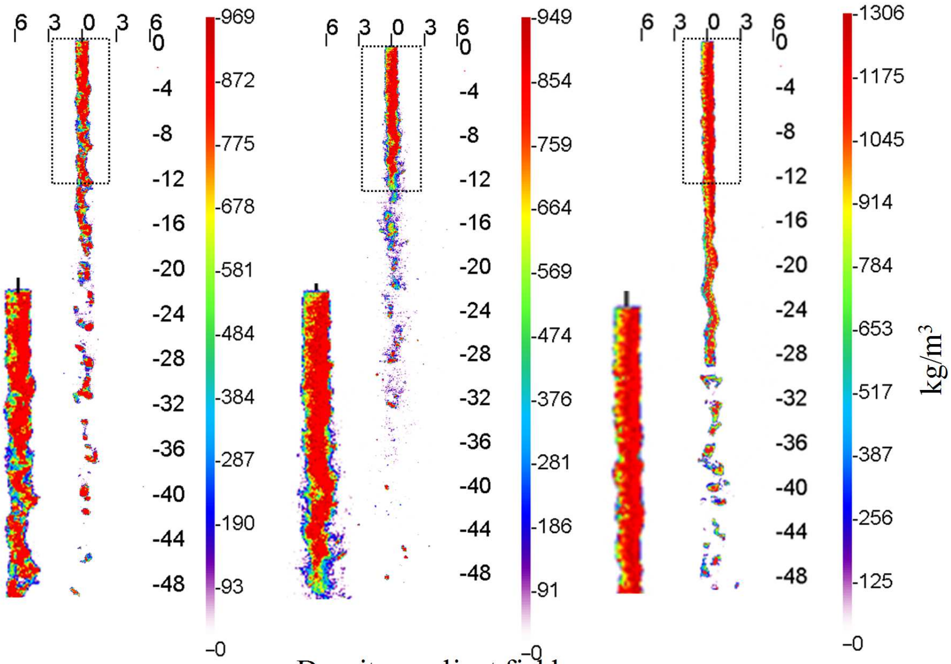

Density gradient field

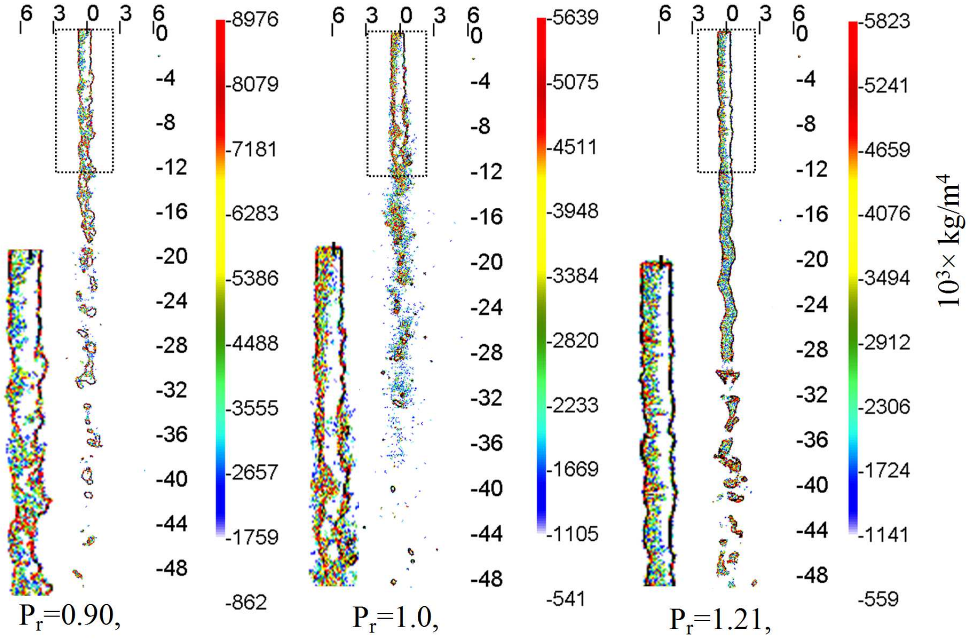

P_r=0.90,
T_r=0.82,
T_i=0.99,
M=0.94 g/s,
V=1.59 m/s

P_r=1.0,
T_r=0.82,
T_i=1.0,
M=0.88 g/s,
V=1.53 m/s

P_r=1.21,
T_r=1.82,
T_i=0.987,
M=0.69 g/s,
V=0.86 m/s

Figure 5.15 Injection of near-critical jet into subcritical condition with nitrogen as ambient fluid.

As the chamber pressure is increased beyond supercritical, the fluid jet prior to injection exists as a compressible liquid as noted from fig. 3.15, and upon injection into a subcritical temperature environment, it behaves like a continuous liquid jet for certain downstream distance; this also indicates that the jet stream is losing its enthalpy to the surrounding nitrogen or helium environment, thereby resulting in a decrease in the jet fluid temperature. This is clearly observed for the nitrogen as well as the helium environments in fig. 5.14 and 5.15. From the structure of the jet, the role of pressure that also determines the density (fig. 3.15) of the injected jet is obvious in determining the transition of a jet at near critical temperature that is injected into the chamber at subcritical temperature condition. The density gradients also reveal further insights on the nature of mixing of the injected jet. It is observed from fig. 5.14 and fig. 5.15 that the boundary of the jet exhibits abrupt density gradients and the core region inside the jet boundary does not exhibit spatial changes in the density for few downstream distances of around 15 mm from the injector exit.

5.9 Supercritical jet into subcritical chamber condition (with N_2 and He as ambient fluids)

The injection of supercritical jet into subcritical chamber conditions is carried out with nitrogen as well as helium as the chamber environments. For all the chamber conditions investigated in the current study, the nitrogen exists in subcritical state whereas helium exists as supercritical fluid. The injected jet is at supercritical temperature and the chamber is at subcritical temperature with three different pressures ranging from subcritical to supercritical. The experimental conditions are detailed in table 5.5 and the results of density and density gradient field are presented in fig. 5.16 and fig. 5.17. When the jet at supercritical temperature is injected into subcritical chamber conditions with helium as the ambient fluid, the injected supercritical jet undergoes mixing, and exhibits characteristics that are similar to single phase mixing. Similar observation is also reported by Roy et al. (2013) where the jet at supercritical temperature is injected into the subcritical chamber

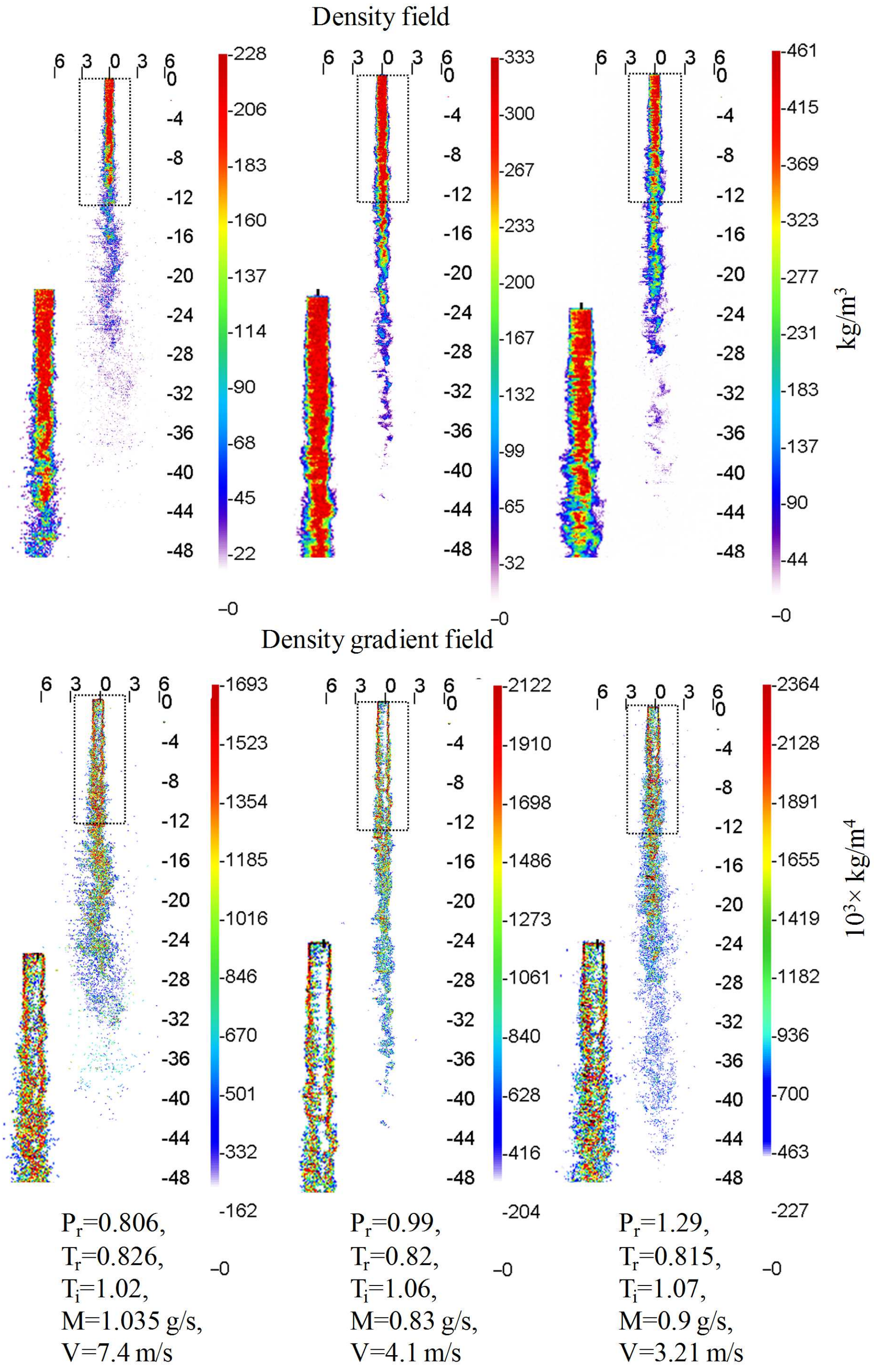

Figure 5.16 Injection of supercritical jet into subcritical condition with helium as ambient fluid.

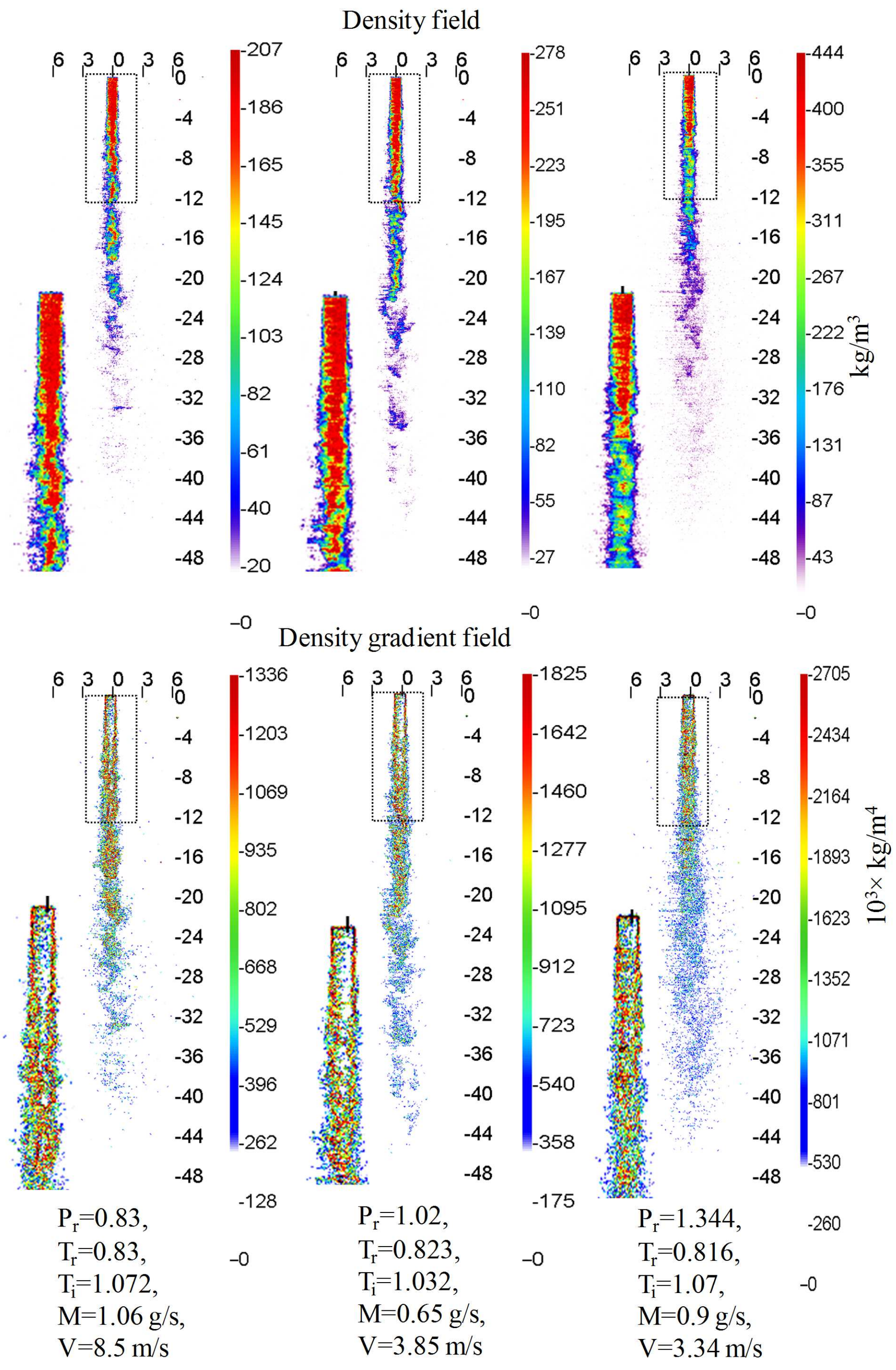

Figure 5.17 Injection of supercritical jet into subcritical condition with nitrogen as ambient fluid.

condition. In their study (Roy et al., 2013) there are indications of formation of spherical droplets at certain downstream distances from the injector exit. Since the study carried out by Roy et al. (2013) never addressed the uncertainty associated with density measurements using PLIF technique, it will be difficult to ascertain the formation of droplets based on the reported values of density measurements. In the current study, it is observed that the injected supercritical jet did not undergo thermodynamic transition to the liquid state at the subcritical chamber conditions. This is evident from density and density gradient fields that are presented in fig. 5.16 and fig. 5.17; the jet exhibits maximum density at the injectant exit, and at downstream distances the density decreases, thereby indicating the presence of diffusional mixing of the injectant fluid into the ambient fluid. Examining the three different cases in fig. 5.16, the influence of pressure is less significant in determining the thermodynamic transition. In the previous study conducted with an elliptical orifice, as in section 4.10, the supercritical jet exhibited the formation of few droplets as the supercritical jet is injected into the subcritical chamber conditions; however the jet did not exhibit axis-switching. This reveals that the transitional behavior of the supercritical jet at subcritical chamber condition is very much dependant on the injectant density that is influenced by injectant pressure. In the case of elliptical jet studies of chapter 4, the injected supercritical jet possessed a density value above 550 kg/m^3. However, in the case of circular jet injection, the injectant density is 460 and 444 kg/m^3 for He and N_2 environments as in fig. 5.16 and fig. 5.17 respectively; this is relatively low as compared to the elliptical jet density of 550 kg/m^3. The injectant density of the supercritical jet plays a crucial role in determining the thermodynamic transition. As the injectant density is higher or close to the liquid-like density, the supercritical jet undergoes thermodynamic transition to liquid state and is also accompanied with a significant loss of enthalpy to the surrounding medium. Also if the dense supercritical jet loses sufficient enthalpy before it mixes or expands, it could lead to droplet formation. For the cases where the injectant density is not sufficiently high, the jet expands and mixes with the ambient fluid and the jet could resemble a gaseous jet, thereby indicating single phase mixing characteristics. It could be observed that the maximum pressure in the present experiment is P_r=1.29 and for the range of pressures considered, the supercritical jet injection into subcritical condition exhibited similar characteristics in mixing. The density gradient field also indicated similar trends. However, the density gradient at the shear layer of the jet for a few downstream distances from the injectant exit varies for different pressures. The shear layer exhibit maximum density gradient of $\rho_{grad} = 2710 \times 10^3 kg/m^4$ at P_r=1.29 than at P_r=0.99 where $\rho_{grad} = 2122 \times 10^3 kg/m^4$ as evident from fig. 5.16.

The supercritical injection into subcritical condition with N_2 as the ambient fluid is presented in fig. 5.17. Experiments are conducted with the pressures ranging from subcritical to supercritical, and the results indicate that the injected jet exhibits similar features at all pressure without the formation of the droplets at the subcritical condition. It can be noted that the injectant density at supercritical pressure is 444 kg/m^3 and is not sufficiently high for the injected jet to transition to a liquid state. The density gradient field map provides the detailed characteristics of the mixing region. It is noted from fig. 5.17 that at short downstream distance from the orifice, the inner core of the jet did not exhibit a density gradient. The inner core possess density gradient of less than 358 $\times 10^3 kg/m^4$ which is smaller than that at shear layer with a value of around 1835 $\times 10^3 kg/m^4$.

5.10 Supercritical jet into supercritical chamber condition (with N_2 and He as ambient fluids)

The jet at supercritical temperature is injected into supercritical temperature chamber condition for nitrogen as well as for helium environments and the results are presented in fig. 5.18 and fig. 5.19 respectively. The corresponding injectant and chamber conditions are detailed in table 5.5. In the current set of experiments the chamber pressure is varied from subcritical to supercritical. For the case of the helium environment in fig. 5.18, the mixing nature of the injected supercritical jet with the ambient fluid resembles that of turbulent gaseous jet. The unmixed region of the inner core region of the jet is evident from both fig. 5.18 and fig. 5.19 for downstream distances upto 10 mm, and is referred to as the potential

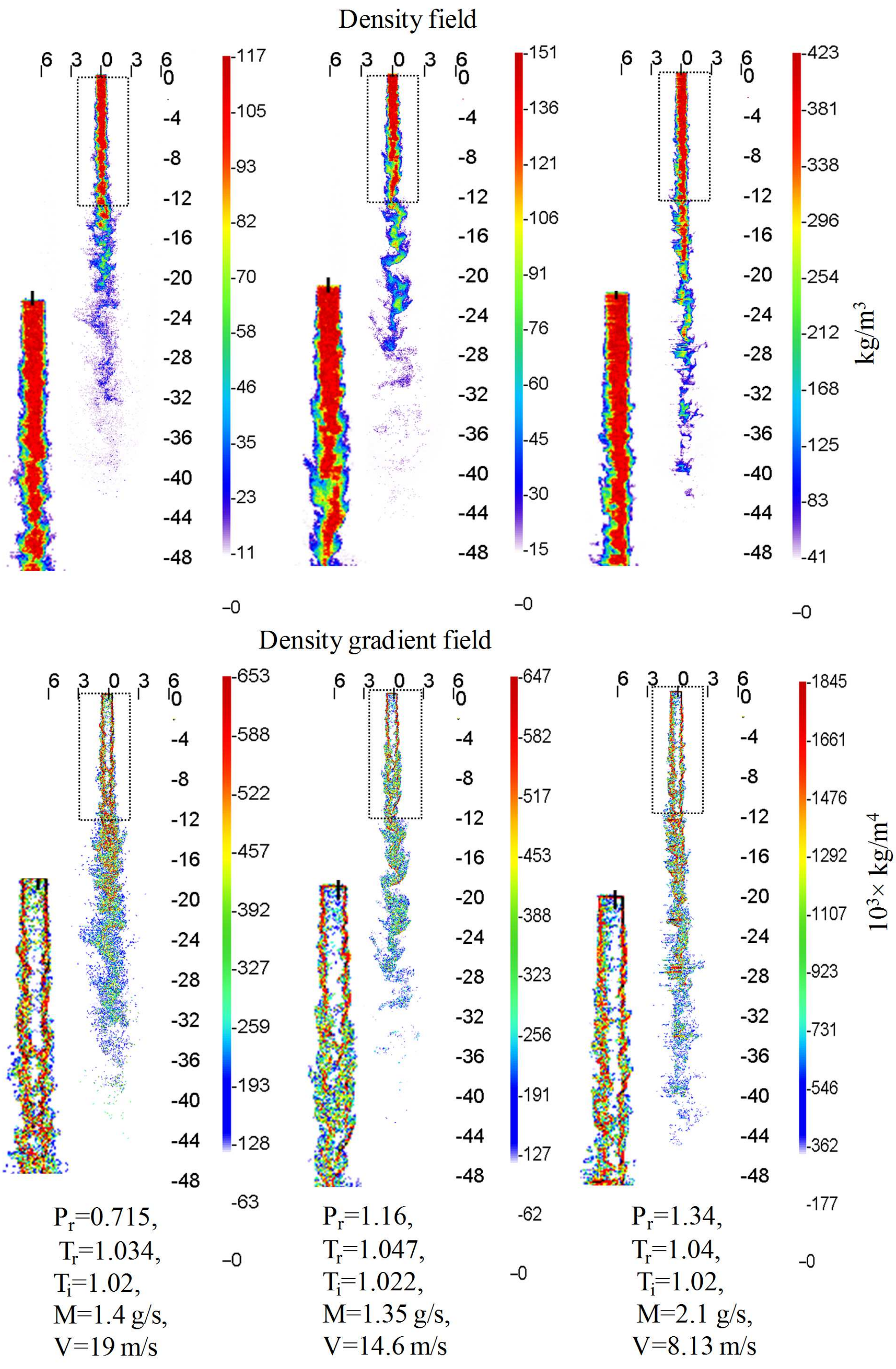

P_r=0.715, T_r=1.034, T_i=1.02, M=1.4 g/s, V=19 m/s

P_r=1.16, T_r=1.047, T_i=1.022, M=1.35 g/s, V=14.6 m/s

P_r=1.34, T_r=1.04, T_i=1.02, M=2.1 g/s, V=8.13 m/s

Figure 5.18 Injection of supercritical jet into supercritical condition with helium as ambient fluid.

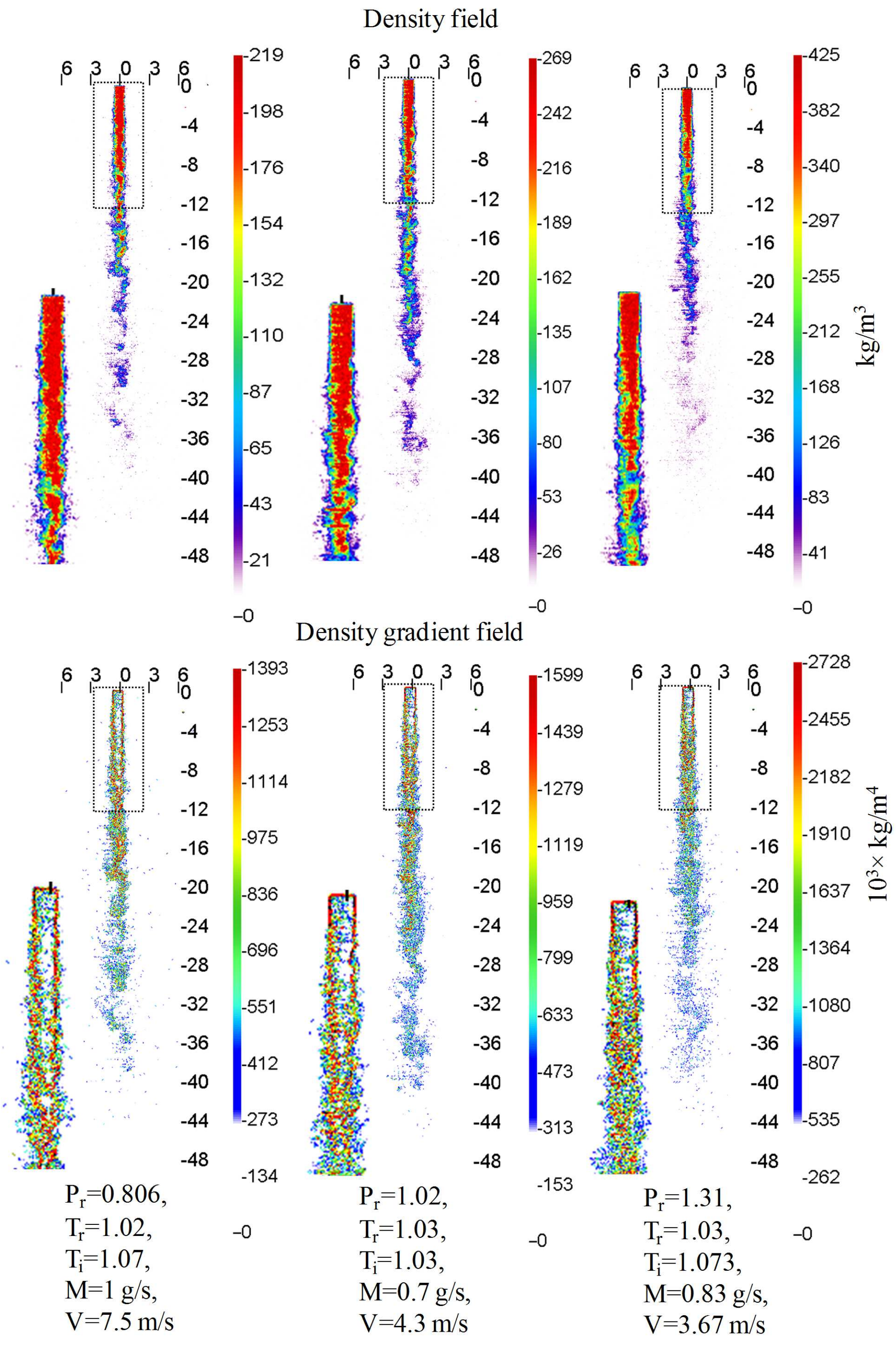

Figure 5.19 Injection of supercritical jet into supercritical condition with nitrogen as ambient fluid.

core of the jet. From fig. 5.18 the density gradient within the potential core is found to be less than 327 $\times 10^3 kg/m^4$ whereas the density gradient at the shear layer is of the order of 1845 $\times 10^3 kg/m^4$.

Similar results are obtained for the case with nitrogen environment as in fig. 5.19; it also reveals that the jet characteristics are similar to those obtained in the case with helium environment. Thus, for the binary component systems investigated in the current study, the ambient fluid does not play a significant role in the thermodynamic transition of the jet that is injected at lower supercritical pressures. However in the present study, the comparison between fig. 5.18a and fig. 5.18c also reveals that the potential core of the jet at supercritical pressure could penetrate for larger downstream distances in the helium environment than at subcritical pressure. The corresponding value of jet density at downstream distance of 15 mm is about 90 kg/m^3 in fig. 5.18a as compared to 330 kg/m^3 in fig. 5.18c at the same distance.

Several investigations performed by Chehroudi et al. (2002a) Chehroudi (2012) also reveal that the jet at supercritical condition behaves as a variable density gaseous jet. The features exhibited by a supercritical jet at supercritical condition are much similar to a gaseous jet though there is a large difference in the injectant and ambient fluid density. It is evident from figs. 5.16, 5.17, 5.18 and 5.19, that the behavior of the supercritical jet is similar at subcritical or supercritical chamber conditions. This is primarily due to the absence of thermodynamic transition of the supercritical jet to liquid state due to the insufficient injectant density. In the absence of significant thermodynamic transition of the supercritical jet, the mixing nature of the jet with the ambient is very similar to those of a gaseous jet.

5.11 Fractal dimension of supercritical jet injected into subcritical and supercritical conditions

The study carried out by Sreenivasan and Meneveau (1986) employed illuminating-thin-light sheet to obtain the boundary of the jets to find out its fractal dimension. However, Lovejoy (1982) evaluated the fractal dimension of the clouds using the projection of the boundary of a cloud onto the horizontal plane. The projected boundary is nothing but the superposition of a few adjacent boundaries of a turbulent structure. Sreenivasan and Meneveau (1986) found that these two techniques offer similar fractal dimension and the corresponding reason as discussed by Sreenivasan and Meneveau (1986) is attributed to the two different effects of superposition: one is attributed to the decrease in fractal dimension because of the decrease in fragmentation due to superposition and the second is attributed to the increase in fractal dimension due to the increase in interfacial corrugations. These two opposite effects are found to negate each other, and the fractal dimension of the planar boundary and the projected boundary is found to be quite similar. In both the cases, the fractal dimension of an axisymmetric turbulent jet is found to be around 1.33.

It is found that the axisymmetric turbulent jet surface that spans the three dimensional space possess a fractal dimension of 2.33 (Sreenivasan and Meneveau, 1986). It also implies that the jet boundary of the turbulent axisymmetric jet must possess a fractal dimension of 1.33. Later Chehroudi et al. (1999) carried out the work to investigate the fractal dimensions of liquid N_2 jet that is injected into ambient N_2 and the pressures are varied from sub to supercritical condition. From the study, (Chehroudi et al., 1999) it is evident that the liquid jet exhibited two phase mixing characteristics for chamber pressures below the critical regime; at critical pressure the liquid N_2 jet mixes with the ambient fluid and exhibits gas-gas like mixing characteristics. However it must be noted that the case corresponding to liquid N_2 injection into the chamber with nitrogen as the chamber environment represents the single component system. The fractal dimension of the jet at various chamber conditions are presented by Chehroudi et al. (1999), and it indicates that the fractal dimensions of the jet injected into subcritical chamber pressure conditions is close to 1.2. The jet injected into the chamber at critical pressure is found to possess the fractal dimension of around 1.33 and for supercritical chamber pressure the fractal dimension is found to lie between 1.35 and 1.4. To the present date, fractal geometry of the jet at supercritical condition is investigated only for subcritical injectant conditions for a single component system (Chehroudi et al., 1999). In the current study, the fractal dimensions are determined for the binary component systems corresponding to those in figs. 5.14, 5.15, 5.16, 5.17, 5.18 and 5.19 where the injected jet condition is supercritical in temperature. The fractal dimensions are computed at the jet boundary from the injector exit plane to various downstream distances. The fractal dimension of the near field region of the jet and also along the full length of the jet is computed.

The fractal dimension of the injected supercritical jet primarily lies between 1.25 and 1.35. Findings from the fractal dimension also indicate that the injected supercritical jet exhibits features similar to the turbulent gaseous jet that are reported earlier by Sreenivasan and Meneveau (1986), Sreenivasan (1991). The fractal dimensions of the various cases corresponding to the near critical jet injected into subcritical chamber conditions are presented in fig. 5.20. The fractal dimension of the full jet is found to be always greater than those determined at the near field region. The fractal dimension of the jet boundary at various downstream distances is plotted in fig. 5.20. At lower chamber pressure, the fractal dimension of

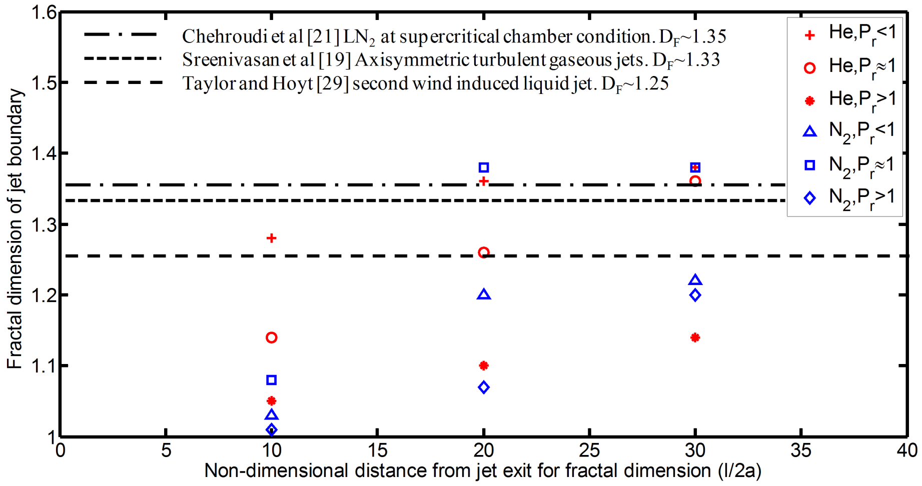

Figure 5.20 Fractal dimension of the jet boundary for various lengths of the jet from the orifice exit for injection from near-critical to subcritical condition.

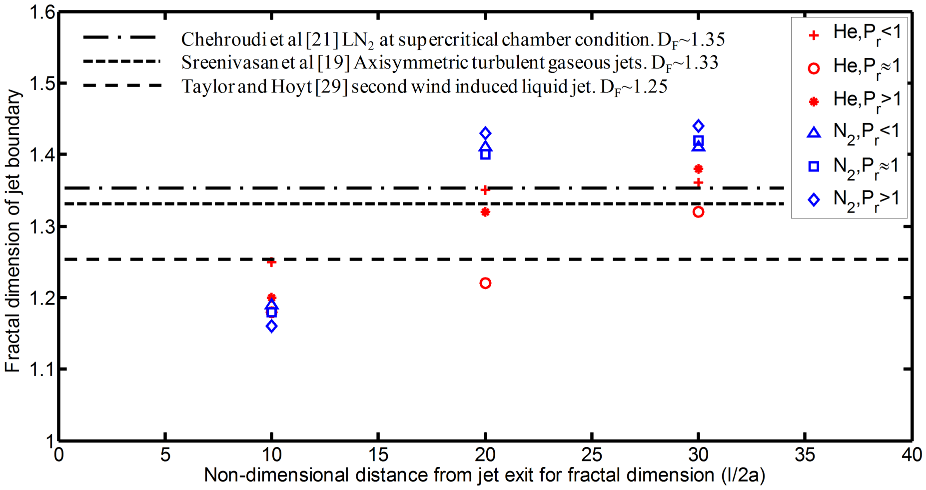

Figure 5.21 Fractal dimension of the jet boundary for various lengths of the jet from the orifice exit for injection from supercritical to subcritical condition.

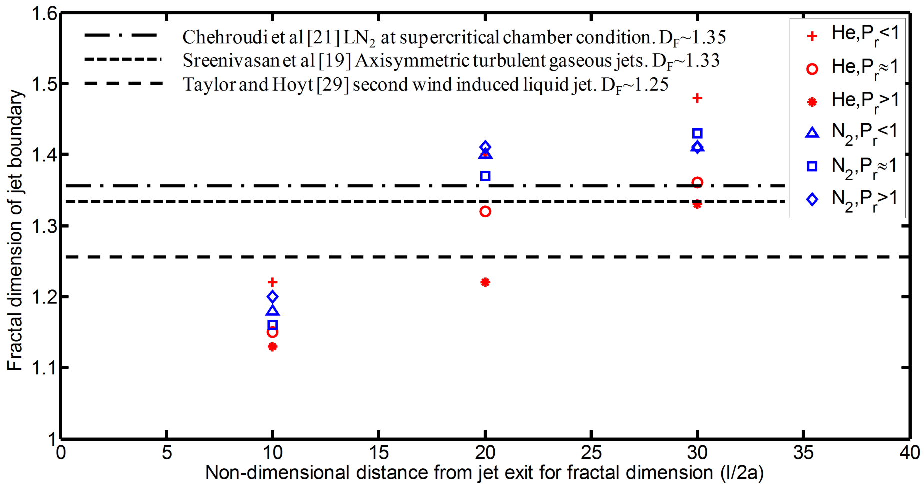

Figure 5.22 Fractal dimension of the jet boundary for various lengths of the jet from the orifice exit for injection from supercritical to supercritical condition.

the near critical full length jet is found to vary between 1.2 and 1.4. The larger fractal dimension indicates the presence of corrugated interface that exists between the injected jet and the ambient fluid. As the pressure is increased to supercritical, the fractal dimension of the interface decreases as observed from fig. 5.20. For the case of supercritical jet injected into the subcritical as well as the supercritical chamber condition, the fractal dimension of the full length jet is found to vary between 1.3 and 1.4 as evident from fig. 5.21 and fig. 5.22. Also there is absence of droplet formation as the supercritical jet is injected into subcritical chamber condition. The close examination of the fractal dimensions of the full length jet suggests that the structure of the supercritical jet injected at very low Reynolds number into subcritical or supercritical chamber conditions remain unaffected for binary component systems and is evident from fig. 5.21 and 5.22.

It could be observed that the fractal dimension of the near critical injectant jet into subcritical chamber condition is slightly less than that of the supercritical injectant condition. Also from figs. 5.14 and 5.15 it could be observed that the injected near critical jet quickly transforms itself into a mixture of liquid and vapor fragments that is also accompanied by the presence of significant amount of droplets. At higher pressures, the near critical jet transforms to the liquid state at the respective chamber conditions. Also, it is very evident from figs. 5.14, 5.15 that the near critical jet exhibits two phase mixing characteristics that is evident from the formation of droplets, and hence the fractal dimensions are less than 1.2 at the near field region; moreover the values are found to lie between 1.2 and 1.4 for the full jet. However, when the injectant condition becomes supercritical, the injected jet behaves like a gaseous jet with larger regions of interfacial corrugations that are evident from the fractal dimensions of the jet of 1.3 and higher as observed from figs. 5.21 and 5.22.

5.12 Summary

Experiments are conducted with a circular jet at thermodynamic supercritical conditions for both binary and a single component system. Linear stability analysis is used to study the disturbance wavelength that is generated at the jet interface. The natural disturbance wavelength formed on the jet interface is determined by the surface tension and the viscosity. During the injection of liquid jet into supercritical chamber condition, the changes in the thermodynamic properties are expected to occur and result in changes in disturbance characteristics. For the case of the nitrogen environment, the liquid jet injected into a subcritical chamber condition revealed the existence of various regimes such as Rayleigh regime, the sinuous mode, the screw-like mode and the atomization regime at different velocities of the jet. The injection of a liquid jet into the supercritical condition also exhibited various regimes that existed at subcritical conditions. The linear stability analysis indicates the absence of thermodynamic transition to supercritical state as in the case of nitrogen environment. The injection of a liquid jet into fluoroketone environment at chamber conditions ranging from high subcritical to supercritical exhibited changes in the structure of the jet. At subcritical chamber temperature, the liquid jet exhibited transition from Rayleigh mode to sinuous mode instability as the jet velocity is increased from 0.2 to 0.5 m/s. A short wavelength disturbance becomes more evident even at low jet velocity as the chamber condition is increased to near critical temperature T_r=0.96 and subcritical pressure P_r=0.65. At supercritical chamber temperature of T_r=1.03 and subcritical chamber pressure of P_r=0.86, the injected jet at low velocity of 0.2 m/s possesses a distinct interface for a few diameter downstream distance. The sudden appearance of the short wavelength disturbance results in the disintegration of the jet and leads to formation of droplets that are smaller than the jet diameter. Even at a moderate velocity of 0.78 m/s with Re=866, the injected jet undergoes atomization, with the presence of fine droplets at the interface.

Once the chamber temperature and pressure become supercritical, the injected jet transitions to supercritical condition after a certain downstream distance. The fractal dimension of the jet boundary is investigated to understand the thermodynamic transition and the mixing nature of the jet. The fractal dimension of the jet boundary remained less than 1.05 at supercritical chamber conditions in a N_2 environment. For the fluoroketone environment, the fractal dimension of the injected jet exceeds 1.2 at supercritical chamber temperature with subcritical chamber pressure. When the chamber pressure and temperature becomes supercritical, the fractal dimension of the jet boundary becomes 1.3 for the single component system.

The experiment is also conducted with the PLIF technique to investigate the two dimensional density field of the injected jet. The experiment is conducted with N_2 as well as helium as the chamber environment. The injection of a supercritical jet into subcritical chamber condition with either helium or N_2 as chamber fluid exhibited the behavior similar to that of a gaseous jet without formation of the droplets. This is due to the low injectant density of the jet. The supercritical jet injected into supercritical condition also behaved like a variable density gaseous jet. Investigation of the fractal geometry of the jet indicates that the fractal dimension of the jet exceeds 1.3.

CHAPTER 6

SUMMARY AND CONCLUSIONS

The injection of fluid jets at subcritical and supercritical conditions is carried out. The experiments are performed with circular as well as elliptical jet. For the case of the elliptical jets, the axis switching characteristics of the jet is investigated in detail as a diagnostic of the existence of the surface tension. The density field map of the jet is obtained using PLIF technique. The interfacial instability of the circular jet is studied to investigate the changes in the surface tension of the jet at supercritical conditions. Also, the fractal dimension of the jet is determined for circular jets to investigate the interfacial corrugations and mixing nature of the jet. For the case of binary species system, nitrogen or helium is used as the chamber environment, and for the pure component system, fluoroketone medium is used as the ambient environment. The major conclusions from the current study are following:

- The subcritical elliptical liquid jet injected into supercritical chamber condition exhibited axis-switching behavior for a binary component system. For supercritical chamber condition with the N_2 environment, the non-dimensional axis-switch length (λ_{as}/D_{eq}) is found to be 11.85 for $We = 46.4$, and for atmospheric condition, $(\lambda_{as}/D_{eq}) = 10.75$ for $We = 46.5$. The axis switch length is independent of the chamber conditions. This indicates that the subcritical elliptical jet fluid does not undergo significant thermodynamic transition to the supercritical state at supercritical chamber conditions for the binary component system.
- For the single component system, the injected subcritical elliptical jet did not undergo axis-switching at supercritical chamber conditions. This is due to the

reduction in the surface tension of the jet. The injected jet completely transitioned to supercritical fluid within the downstream distance of 26 diameters for $P_r = 1.39$ and $T_r = 1.12$.

- At subcritical pressures of about $P_r = 0.92$, the injected near critical elliptical jet exhibited the formation of small droplets that is surrounded by dense injectant vapor. At supercritical pressures $P_r = 1.22$, the near critical elliptical jet exhibited liquid like behavior with presence of surface tension in a binary component system. Examining the behavior of the near critical elliptical jet at subcritical chamber condition revealed the influence of pressure in the transitional nature of the jet from near critical state to liquid droplets for binary component system. The transition occurred due to the changes in the density of the jet that is very sensitive to the changes in pressure near the critical temperature.

- The density measurement in a binary component system using the PLIF technique of the supercritical elliptical jet revealed that the jet behaved like a variable density gaseous jet with K-H instabilities at the interface.

- For the case of elliptical jet, at $P_r = 1.43$, the droplet formation occurred for the supercritical jet ($P_r = 1.43$ and $T_i = 1.06$) at subcritical chamber condition ($T_r = 0.87$) for a binary component system. At high supercritical pressure, the pressure plays a major role in jet transition due to its profound influence on the injectant density. The droplet formation could be due to the high density of the supercritical jet which upon its injection into subcritical condition might lose significant enthalpy and transitions to the liquid state.

- The stability analysis of the binary component system in conjunction with the experimental observations indicate that the subcritical circular jet obeys classical stability theory for the N_2 environment even at supercritical chamber conditions.

- Performing linear stability analysis on the circular jet revealed that there is an increase in the actual Weber number of the jet from the injected conditions.

This indicates a significant reduction in the surface tension that leads to the formation of small wavelength disturbances.

- The measured wavelength of the instability at the jet interface for the binary component system at supercritical chamber condition is $\lambda_m = 2.64mm$ and for the case of pure component system the wavelength is $\lambda_m = 0.425mm$ for similar chamber condition with $P_r \approx 1.05$ and $T_r \approx 1.05$. Also for the binary component system at low injected jet Re=372, the Rayleigh instability could be observed even at supercritical condition whereas it is absent for the single component system.

- For the case of a single component system, instability waves are observed at the circular jet interface even at supercritical chamber condition with high subcritical pressures ($T_r = 1.027$ and $P_r = 0.855$). The actual Weber number of the jet increased to $We = 112$ from $We = 2.85$ thereby indicating the drastic reduction in the surface tension of the injected fluid.

- For a single component system, even at supercritical chamber condition, the injected liquid jet did not undergo instant transition to the supercritical fluid state. Instead, the injected jet interface is distinct for about 10 jet diameter downstream distance. Beyond a certain downstream distance, the instability waves developed at the interface generate turbulence, and then complete transition of the jet to a supercritical fluid phase occurs.

- For the single component system at supercritical chamber temperature, the fractal dimension of the injected liquid jet is strongly dependent on velocity as well as chamber pressure. At supercritical pressure and temperature, the fractal dimension exceeds $D_f = 1.4$ at larger injected Re whereas for low Re the D_f is always greater than 1.28.

- The density and density gradient field map of the supercritical circular jet at supercritical chamber condition for a binary component system indicate gaseous jet behavior. The injection of a supercritical jet into subcritical as well as the supercritical chamber condition in the near field region correspond to the density gradient of the order of $\rho_{grad} \approx 2000 \times 10^3 kg/m^4$. The near critical jet injected into subcritical chamber condition exhibited droplet formation with sharp density gradients $\rho_{grad} \approx 6000 \times 10^3 kg/m^4$, whereas the lower value of the density gradients within the supercritical jet near its interface suggests that the mixing behavior of a supercritical jet corresponds to variable density gaseous jets for binary component system.

- The injection of a circular jet that is supercritical in pressure and temperature into a chamber at subcritical temperature does not result in droplet formation. The injectant pressure significantly influences the injectant density. However, in this case, even at supercritical pressure, the transition of jet fluid to liquid state does not occur due to the lower injectant density. In this study, for a binary component system, the supercritical circular jet characteristics are very similar to a variable density gaseous jet at subcritical as well as at supercritical chamber conditions for binary component system.
- The supercritical circular jet does exhibit similar features for the nitrogen and the helium environments up to the supercritical pressure of $P_r \approx 1.3$. This indicates that the effect of different ambient fluids at identical chamber conditions on the injected jet is not significant for these binary component systems. The jet at supercritical temperature that is injected into supercritical chamber temperature condition exhibited features similar to those of turbulent jets. The central region or potential core has negligible density gradient, of around 350 $\times 10^3 kg/m^4$, as compared to the maximum density gradients of 1825 $\times 10^3 kg/m^4$ in the shear layer of the jets. The observed trend is similar for all the cases of circular jets that are investigated as part of the current study. The fractal dimension of the supercritical circular jet obtained for all the cases primarily lies between 1.25 and 1.35; this fractal dimension corresponds to turbulent gaseous jets. Hence a supercritical circular jet injected at low velocities exhibits behavior similar to the variable density turbulent jets in a binary component system, and the jet behavior is unaffected by the chamber conditions, whether subcritical or supercritical due to the low injectant density.

The summary of the major conclusions from the current study is detailed in table 6.1.

Injection temperature to chamber temperature condition	**Chamber fluid**	**Conclusions**
Injection from subcritical to subcritical and supercritical chamber temperature conditions	N_2 or He	The subcritical liquid jet preserves the injected liquid state with hardly any changes in surface tension even at supercritical chamber temperature and also for the chamber pressure conditions that range from subcritical to supercritical.
	FK	At subcritical temperature, by increasing the vapor pressure, the jet begins to exhibit atomization with the formation of small droplets. At supercritical temperature and subcritical pressure, the initially laminar jet exhibited short wavelength disturbances at the interface and is followed by a highly turbulent region with fine droplet formation. At supercritical temperatures and pressures, the laminar liquid jet which is initially distinct becomes turbulent with misty appearance and soon transforms to supercritical state at larger downstream distances.
Injection from near-critical to subcritical chamber temperature	N_2 or He	At subcritical pressures, the near-critical jet comprises of liquid and vapor mixture. At supercritical pressures, the jet behaves as a liquid jet. The near critical temperature jets are very sensitive to pressure changes near the critical region.
Injection from supercritical to subcritical and supercritical chamber temperature conditions	N_2 or He	At subcritical chamber temperature, the supercritical jet behaves like a gaseous jet at both subcritical and critical pressures. At subcritical chamber temperature and high supercritical pressures, a fraction of supercritical jet could transform to liquid droplets due to high injected jet density along with chemical composition changes at the interface and decrease in jet temperature. At lower supercritical pressures, the supercritical injected jet behaves like a gaseous jet without any droplet formation. At supercritical chamber temperature, the injected supercritical temperature jet exhibits gaseous behavior at all chamber pressures.

Table 6.1 Summary of main conclusions for the various injection and chamber conditions from the present experimental study.

APPENDIX A

Details of the injectors

The elliptical and the circular orifices have been used in the present experimental study. The fluid jet to be injected is fed to the elliptical/circular injectors through a 3 mm OD supply SS supply tube with 2 mm ID. The elliptical orifice used in the present experiment is having an equivalent diameter of 2 mm with an aspect ratio of 4. The elliptical injector element has an elliptical hole from one side of the element for about 30 mm and after this it becomes circular with 3 mm diameter where the supply tube can be connected. For the case of circular jet, hypodermic needle with 0.88 mm ID is used as the injector and is connected to the main supply tube as shown in fig. A.1.

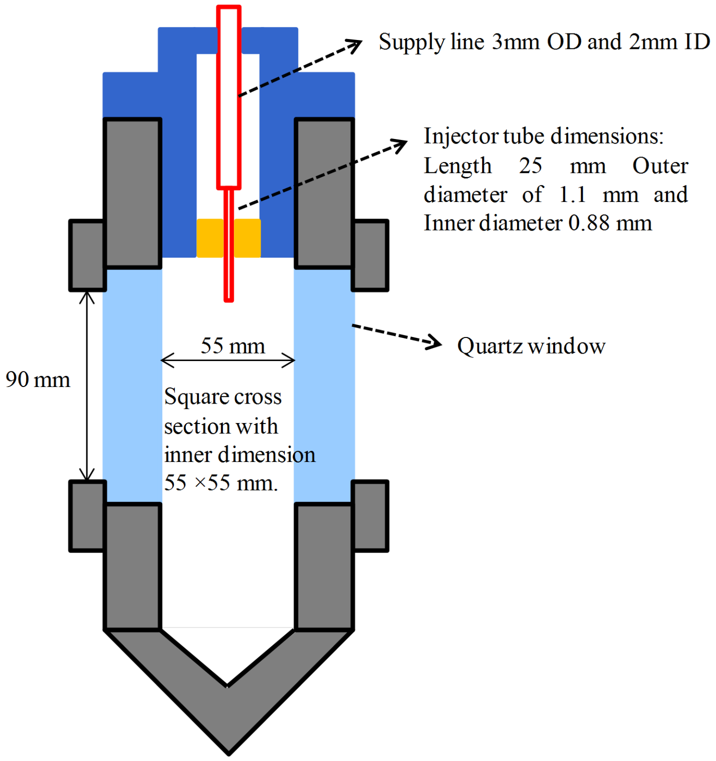

Figure A.1 Schematic of cross section of the high pressure chamber.

APPENDIX B

MATLAB SCRIPTS

B.1 Matlab script of PRSV equation of state, Maxwell construction

The following script file use PRSV equation of state to obtain the density of the fluoroketone at various pressure and temperature. All the parameters are adopted from Gustavsson and Segal (2008). The detailed description of equation of state is provided in chapter. 3. The script file plots the various isotherm in p-v and p-ρ phase diagram.

Maxwell construction is applied to PRSV equation to resolve the discrepancy that the original PRSV equation has three density values at given pressure and temperature. The Maxwell construction is validated with Antoine model and also with the equation provided by 3M company to determine the saturated vapor pressure at given temperature.

```
clear all
close all
clc
Tc=441.8;
Pc=1.8646E6;
w=0.471;
k1=0.052;
R=8.3144;
mw=0.316046;%kg/mol
t=[6.2 26.2 46.2 66.2 86.2 96.2 106.2 116.2 126.2 136.2 146.2 156.2...
 160.2 165.2 168 176.2 186.2 196.2 206.2 216.2 226.2];
```

```
 % Temperature in degree Celsius.
for i=1:length(t)
   rho=0.1:0.05:1700;
   v=mw./rho;
   lv=log10(v);
T(i)=t(i)+273.8;
Tr=T(i)/Tc;
k0=0.378893+(1.4897153*w)-(0.17131848*(w^2))+(0.0196554*(w^3));
k=k0+(k1*(1+(Tr^0.5))*(0.7-Tr));
alpha=(1+(k*(1-(Tr^0.5))))^2;
a=(0.457253*((R^2)*(Tc^2))/Pc)*alpha;
b=0.077796*(R*Tc)/Pc;
P=((R*T(i))./(v-b))-(a./((v.^2)+(2*b*v)-b^2));
pb=P/1E5;
figure(1)
if Tr==1
    h=plot(v,pb,'r','LineWidth',3);
else
    h=plot(v,pb,'LineWidth',3);
end
clabel([t(i)+273.8 v;length(pb) pb],h,'FontSize',14,'LabelSpacing',200)
axis([0 0.035 -50 50])
hold on
set(gca,'Fontsize',18) ;
set(gca,'LineWidth',3);
xlabel('Specific volume, in m^3/mol','fontsize',18);
ylabel('Pressure, in bar','fontsize',18);
title('Isotherms in P-V phase space')
figure(2)
if Tr==1
    h=plot(rho,pb,'r','LineWidth',3);
else
    h=plot(rho,pb,'LineWidth',3);
end
clabel([t(i)+273.8 rho;length(pb) pb],h,'FontSize',14,'LabelSpacing',200)
axis([0 1800 -50 50])
hold on
```

```
set(gca,'Fontsize',18) ;
set(gca,'LineWidth',3);
xlabel('Mass density, kg/m^3','fontsize',18);
ylabel('Pressure, in bar','fontsize',18);
title('Isotherms in P-\rho phase space')
if Tr<1.01
rho4=rho(length(rho));
v4=v(length(rho));
pb4=pb(length(rho));
for k3=1:(length(rho))
    if pb(length(rho)-k3)>pb(length(rho)-k3+1)
        break
    end
end
rho3=rho(length(rho)-k3);
v3=v(length(rho)-k3);
pb3=pb(length(rho)-k3);
for k2=1:(length(rho))
    if pb(k2)>pb(k2+1)
        break
    end
end
rho2=rho(k2);
v2=v(k2);
pb2=pb(k2);
rho1=rho(1);
v1=v(1);
pb1=pb(1);
%%%%%%% Applying Maxwell's equal area rule and finding the saturation
%%%%%%% pressure and the specific volume of the liquid and the vapor phases.
F1=1;
F2=0.5;
while abs(F1-F2)>0.00001
    pbi=(pb1+pb2)/2;
for j12=1:k2
    if pb(j12)>pbi
        break
```

```
    end
end
for j23=k2:(length(rho)-k3)
    if pb(j23)<pbi
        break
    end
end
for j34=(length(rho)-k3):length(rho)
    if pb(j34)>pbi
        break
    end
end
pbi;
v12=v(j12);
pb12=pb(j12);
v23=v(j23);
pb23=pb(j23);
v34=v(j34);
pb34=pb(j34);
fpb=@(v)((((R*T(i))./(v-b))-(a./((v.^2)+(2*b*v)-b^2)))/1)-pbi*1E5;
F1=integral(fpb,v23,v12);
F2=-(integral(fpb,v34,v23));
if F1>F2
pb1=pbi;
elseif F2>F1
pb2=pbi;
end
end
pb(j12:j34)=pbi;
vs1(i)=v(j12);
vs2(i)=v(j34);
lvs1(i)=lv(j12);
lvs2(i)=lv(j34);
rhos1(i)=rho(j12);
rhos2(i)=rho(j34);
pbs(i)=pbi;
else
```

```
P=((R*T(i))./(v-b))-(a./((v.^2)+(2*b*v)-b^2));
pb=P/1E5;
end
%%%%% Construction of Maxwell's line in the P-V phase diagram and P-rho
%%%%% phase diagram.
figure(3)
if Tr==1
    h=plot(lv,pb,'r','LineWidth',3);
else
    h=plot(lv,pb,'LineWidth',3);
end
clabel([t(i)+273.8 lv;length(pb) pb],h,'FontSize',14,'LabelSpacing',200);
axis([-4 1 0 30]);
hold on
plot(lvs1,pbs,'g','LineWidth',3);
hold on
plot(lvs2,pbs,'g','LineWidth',3);
hold on
set(gca,'Fontsize',18) ;
set(gca,'LineWidth',3);
xlabel('log of specific volume, m^3/mol','fontsize',18);
ylabel('Pressure, in  bar','fontsize',18);
title('Isotherms in P-V phase space')
figure(4)
if Tr==1
    h=plot(v,pb,'r','LineWidth',3);
else
    h=plot(v,pb,'LineWidth',3);
end
clabel([t(i)+273.8 v;length(pb) pb],h,'FontSize',14,'LabelSpacing',200);
axis([0 0.03 0 25])
hold on
plot(vs1,pbs,'g','LineWidth',3);
hold on
plot(vs2,pbs,'g','LineWidth',3);
hold on
set(gca,'Fontsize',18) ;
```

```
set(gca,'LineWidth',3);
xlabel('specific volume, m^3/mol','fontsize',18);
ylabel('Pressure, in  bar','fontsize',18);
title('Isotherms in P-V phase space')
figure(5)
if Tr==1
    h=plot(rho,pb,'r','LineWidth',3);
else
    h=plot(rho,pb,'LineWidth',3);
    clabel([t(i)+273.8 rho;length(pb) pb],h,'FontSize',14,'LabelSpacing',200);
end
axis([0 1700 0 30])
hold on
plot(rhos1,pbs,'g','LineWidth',3);
hold on
plot(rhos2,pbs,'g','LineWidth',3);
hold on
set(gca,'Fontsize',18) ;
set(gca,'LineWidth',3);
xlabel('Mass density, kg/m^3','fontsize',18);
ylabel('Pressure, in bar','fontsize',18);
title('Isotherms in P-\rho phase space')
end
% Validation of Maxwell construction with Antoine equation and equation
provided by 3M company for determining saturated vapor pressure.
pba=(10.^(10.205-(1861.01./(t(1:15)+273.8+34.883))))/10^5;
% Antoine equation for predicting saturated vapor pressure (used by Gustavsson)
pba3m=(exp((-3545.3./(t(1:15)+273.8))+22.492))/10^5;
% Equation provided by 3M company (Manufacturer of fluoroketone)
figure(6)
plot(t(1:15)+273,pba,'.')
hold on
plot(t(1:15)+273,pba3m,'+')
hold on
plot(t(1:15)+273,pbs,'*')
hold on
plot(441.8,18.6,'-')
```

```
set(gca,'Fontsize',18) ;
xlabel('Temperature, K','fontsize',18);
ylabel('Saturated vapor Pressure, in bar','fontsize',18);
```

B.2 Matlab script for solving dispersion equation

The following script file numerically solves the dispersion equation detailed in equation. 5.2. The code solves for spatial growth rate K_i of spatial disturbance wavelength K_r for different Weber number and Reynolds number using secant method.

```
clear
clc
wea=110;
wea=[20 50 100 200 400 1000 2000 5000 10000 15000 30000];
for p=1:length(wea);
we=wea(p);
R=384;
pr=0.0093; % ambient to injectant fluid density ratio
% % % % % plotting dispersion relation using secant method.
% % % % % finding root ki for every kr (doing spatial instability analysis),
% % % % % setting wi=0
kr=0:0.01:10;
dk=0.002+(1i*0.002);
% we=50;
% R=1000;
% pr=0.000625;
for m=1:length(kr);
    ki=[-0.05 -0.5];
    iter=50;
    for n=1:iter
k=kr(m)+1i*ki(n);
w=-kr(m); %setting wr=-kr according to Gaster's theorem........
l=((k^2)+(1i*R*w))^0.5;
dl=((dk^2)+(1i*R*w))^0.5;

i0=besseli(0,k);
i1=besseli(1,k);
k0=besselk(0,k);
```

```
i1l=besseli(1,l);

k1=(k-(0.5*dk));
k2=(k+(0.5*dk));
l1=((k1^2)+(1i*R*w))^(1/2);
l2=((k2^2)+(1i*R*w))^(1/2);

di1=(besseli(1,k2)-besseli(1,k1))/dk;
dk0=(besselk(0,k2)-besselk(0,k1))/dk;
di1l=(besseli(1,l2)-besselk(0,l1))/dl;

f(n)=(((w+k)^2)*(i0/i1))-((((2*1i*(w+k)*k^2))/R)*((i0/i1)+(di1/i1)))...
-((w^2)*pr*(k0/dk0))-(((4/R^2)*k^3)*((k*(di1/i1))-(l*(di1l/i1l))))...
+((k/we)*(1-k^2));

k=kr(m)+1i*ki(n+1);
l=((k^2)+(1i*R*w))^0.5;
dl=((dk^2)+(1i*R*w))^0.5;

i0=besseli(0,k);
i1=besseli(1,k);
k0=besselk(0,k);
i1l=besseli(1,l);

k1=(k-(0.5*dk));
k2=(k+(0.5*dk));
l1=((k1^2)+(1i*R*w))^(1/2);
l2=((k2^2)+(1i*R*w))^(1/2);

di1=(besseli(1,k2)-besseli(1,k1))/dk;
dk0=(besselk(0,k2)-besselk(0,k1))/dk;
di1l=(besseli(1,l2)-besselk(0,l1))/dl;

f(n+1)=(((w+k)^2)*(i0/i1))-((((2*1i*(w+k)*k^2))/R)*((i0/i1)+(di1/i1)))...
-((w^2)*pr*(k0/dk0))-(((4/R^2)*k^3)*((k*(di1/i1))-(l*(di1l/i1l))))...
+((k/we)*(1-k^2));
```

```
     ki(n+2)=((ki(n)*f(n+1))-(ki(n+1)*f(n)))/(f(n+1)-f(n));
     diff=abs(ki(n+2)-ki(n+1));
     if diff<0.0000005;
         break
     end
     end
kim(m)=real(ki(n+2));
end
figure(1);
h=plot(kr,kim,'b','LineWidth',3);
grid on;
hold on;
% axis([0 4 -0.2 0]);
set(gca,'Fontsize',18,'LineWidth',3);
xlabel('Non-dimensional wavenumber, kr=k(d/2)','fontsize',16);
ylabel('Growth rate, ki','fontsize',16);
end
```

B.3 Matlab script for obtaining density and density gradient colormap

The following script file is used to obtain the density and density gradient field of the jet with corresponding color map.

```
clc
close all
clear all
%%%%%%%%%%%%%%%%%%%    Laser sheet correction
%%%%%%%%%%%%%%%%%%%%%%%%%%
% % % 1mm = 70 pixels in reference dye cell
% % % 1mm = 22 pixels in test area
cg=imread('C:\All datas\png images\301014\301014-01_301014-01\B00010.png');
bg=imread('C:\All datas\png images\030714-sheet_bg_01\B00002.png');
a=imread('C:\All datas\png images\131114\131114-03_131114-03\B00002.png');
row=950;
col=460;
lim1=170;
lim2=570;
vlim1=385;
vlim2=1500;
reflim=1950;

v1=15;  %%%%%%%
v2=25;  %% selected pixels in jet near field in liquids for July experiments
h1=200; %%%%%%%
h2=205; %%%%%%%

bgf=0.85;    % factor for background correction
rf=25;       % factor for right side correction
lf=25;       % factor for left side correction
bf=9000;     % factor for bottom side correction
cbf=4;      % factor for color bar correction
ccbf=50;     %factor for density grad and its color bar correction
```

```
fitf=0.0058; % constant for attenuation fit
ex=1;
rat=1;
%%%%%%%%%%%%%%%%%%%%%%%%%%%%%%%%%%%%%%%%%%%%%%%%%%%%%%%%%%%%%%%%%%%%%%%%%%%
ag=double(rgb2gray(a));
bgg=double(rgb2gray(bg));
cgg=double(rgb2gray(cg));
imshow(uint8(ag));
figure(2);
imshow(uint8(bgg));
figure(3);
vect1=(cgg(vlim1:vlim2,col:col+5));
vect2=(mean(vect1'))';
vect3=vect2.^ex; % for supercritical jets
or=100*ones(length(vect2),1);
vector=(or-vect2).^ex;
plot(vect2*1);
hold on
plot(vect3,'r');
%%%%%%%%%%%%%%%%%%%%%%      figure properties
%%%%%%%%%%%%%%%%%%%%%%%%
set(gca,'Fontsize',18) ;
xlabel('Pixel distance','fontsize',18);
ylabel('Pixel index','fontsize',18);
title('Variation of fluorescence intensity');
legend('Intensity variation', 'Exponential fit','fontsize',10);
grid on
%%%%%%%%%%%%%%%%%%%%%%%%%%%%%%%%%%%%%%%%%%%%%%%%%%%%%%%%%%%%%%%%%%%%%%%%%%%
jetim=(ag(vlim1:vlim2,lim1:lim2));
% jetimbg=(bgg(vlim1:vlim2,(lim1-40):(lim2-40)));
jetimbg=30*ones(size(jetim));
%%%%%
sz=size(jetimbg);
cf=linspace(1,1.5,sz(2));
cfy=((((80.^(cf-1))-1)/rf)+1);
flipcfy=fliplr((((80.^(cf-1))-1)/lf)+1);
cfcf=(cfy+flipcfy)/2;
```

```
f=linspace(0,1,sz(1));
ff=((1000.^f)/bf)+1;
figure(4)
plot(cfcf)
hold on
plot(ff,'r')
for i=1:sz(2);
jetimbg(:,i)=jetimbg(:,i).*(ff)';
end
for j=1:sz(1)
    jetimbg(j,:)=jetimbg(j,:).*cfcf;
end
%%%%%
jetimbgc=(jetim-(jetimbg*bgf));
figure(5)
imshow(uint8(jetim))
for i=1:length(vect2)
   njetim(i,:)=(jetimbgc(i,:)/vect3(i))*mean(vect3);
end
figure(6)
imshow(uint8(njetim))
figure(7);
mat1=ones(size(njetim))*120;
mat2=(mat1-njetim)*1.5;
imshow(uint8(mat2));
%%%%%%%%%%%%%%%%%%%%%%%%%%%%%%%%%%%%%%%
[m,ind]=max(double(ag(row,1201:1940)));
Ind=ind+1200;
flipag=fliplr(double(ag(row,1250:Ind)));
figure(8)
plot(double(ag(row,1:2000)));
figure(9)
plot((1:length(flipag))/70,(flipag)/m,'r','LineWidth',3);
hold on
plot((1:length(flipag))/70,exp(-fitf*(1:length(flipag))),'b','LineWidth',3);
hold on
plot((1:length(flipag))/70,exp(-(fitf/1600)*1200*(1:length(flipag))),'g'...
```

```
,'LineWidth',3);
hold on
plot((1:length(flipag))/70,exp(-(fitf/1600)*400*(1:length(flipag))),'g'...
,'LineWidth',3);
grid on
plot((1:length(flipag))/70,exp(-(fitf/1600)*550*(1:length(flipag))),'g'...
,'LineWidth',3);
grid on
axis([0 8 0 1.2])
set(gca,'Fontsize',18) ;
xlabel('Distance (mm)','fontsize',18);
ylabel('Pixel intensity','fontsize',18);
% near the jet edge (for liquids)
jetinmat=njetim(v1:v2,h1:h2);  % near the jet edge (for supercritical jets)
bginmat=jetimbg(v1:v2,h1:h2);
liqrefmat=ag(row:row+1,Ind-3:Ind-2);
jetin=mean(mean(jetinmat));
bgin=(mean(mean(bginmat))*bgf)*(mean(vect3)/mean(vect3(v1:v2)));
liqref=(mean(mean(liqrefmat)));
nliqref=liqref*exp(fitf*(reflim-Ind+2));
ratio=jetin/liqref;
%%%%%%%%%%%%%%%%%%%%% Generating RGB matrices %%%%%%%%%%%%%%%%%%%%
% mxim=max(max(njetim));
% mxim=max(max(njetim(1:200,215:260)));
mxim=max(max(njetim(1:200,:)));
a=(njetim*(255/(jetin*1)));
bw=[-4 0 cbf 55 95 130 175 230 255 265 280 300];
r=([255 255 255 0 0 70 255 255 200 200 250 655]);
g=([255 255 255 0 190 230 255 0 -100 -200 -300 -300]);
b=([255 255 255 255 255 70 0 -100 -200 -300 -400 -400]);
ln=length(bw);
[ro co]=size(njetim);
rmat=zeros(ro,co);
gmat=zeros(ro,co);
bmat=zeros(ro,co);
rgb=ones(ro,co,3);
for i=1:ln
```

```
u=ones(ro,co,1);
v=ones(ro,co,ln);
for j=1:ln
  if i==j
v(:,:,i)=1*u;
  else
v(:,:,i)=((a-bw(j))/(bw(i)-bw(j))).*u(:,:,1);
  end
u(:,:,1)=v(:,:,i);
end
rmat=(r(i)*v(:,:,i))+rmat;
gmat=(g(i)*v(:,:,i))+gmat;
bmat=(b(i)*v(:,:,i))+bmat;
end
rgb(:,:,1)=rmat;
rgb(:,:,2)=gmat;
rgb(:,:,3)=bmat;
figure(10)
imshow(uint8(rgb))
for i=0:88:ro-1
text(335,i+14,num2str(convergent(-i/22)),'Fontsize',14);
end
for i=198:66:396
text(i,-26,num2str(convergent((i-198)/22)),'Fontsize',14);
end
for i=0:66:132
text(i,-26,num2str(convergent(9-(i/22))),'Fontsize',14);
end
%%%
for i=0:66:co-1
text(i-5,-4,'|','Fontsize',8);
end
grid on;
% set(gcf, 'PaperUnits', 'inches');
% set(gcf, 'PaperSize', [4.6 12.70])
% set(gcf, 'PaperPosition', [-1.74 -6.4 7 23.52]);
saveas(gcf,strcat('C:\All datas\circularjetprocessed\density.png'))
```

```
figure(11)
imshow(uint8(a))
grid on
% set(gcf, 'PaperUnits', 'inches');
% set(gcf, 'PaperSize', [4.6 12.70])
% set(gcf, 'PaperPosition', [-1.74 -6.4 7 23.52]);
saveas(gcf,strcat('C:\All datas\circularjetprocessed\den-bw.png'))
%%%%%%%%%%%%%%%%%%%%%%%%%%%%%%%%%%%%%%%%%%%%%%%%%%%%%%%%%%%%%%%%%%%%
colbar1=ag(40:2040,2130:2143);
colbar=[colbar1 colbar1];
cmxim=max(max(colbar));
[row,col]=size(colbar);
c=((colbar*255)/cmxim);
bw=[-4 0 cbf 55 95 130 175 230 255 265 280 300];
r=([255 255 255 0 0 70 255 255 200 200 250 655]);
g=([255 255 255 0 190 230 255 0 -100 -200 -300 -300]);
b=([255 255 255 255 255 70 0 -100 -200 -300 -400 -400]);
ln=length(bw);
[ro co]=size(colbar);
rmat=zeros(ro,co);
gmat=zeros(ro,co);
bmat=zeros(ro,co);
rgb=ones(ro,co,3);
for i=1:ln
u=ones(ro,co,1);
v=ones(ro,co,ln);
for j=1:ln
  if i==j
v(:,:,i)=1*u;
  else
v(:,:,i)=((c-bw(j))/(bw(i)-bw(j))).*u(:,:,1);
  end
u(:,:,1)=v(:,:,i);
end
rmat=(r(i)*v(:,:,i))+rmat;
gmat=(g(i)*v(:,:,i))+gmat;
bmat=(b(i)*v(:,:,i))+bmat;
```

```
end
black=zeros(4,co);
rgb(1:ro,1:co,1)=rmat;
rgb(ro+1:ro+4,1:co,1)=black;
rgb(1:ro,1:co,2)=gmat;
rgb(ro+1:ro+4,1:co,2)=black;
rgb(1:ro,1:co,3)=bmat;
rgb(ro+1:ro+4,1:co,3)=black;
figure(12)
imshow(uint8(rgb))
cc=c(:,1);
intf=1;
dens=convergent(-1*(cc/nliqref)*(1600/rat)...
*(mean(mean(jetim(v1:v2,h1:h2)))/255)*intf);
for i=0:200:length(cc)-1
text(30,i,num2str(dens(i+1)),'Fontsize',12);
end
grid on
saveas(gcf,strcat('C:\All datas\circularjetprocessed\den-colbar.png'))
figure(13)
imshow(uint8(c))
for i=0:200:length(cc)-1
text(30,i,num2str(dens(i+1)),'Fontsize',12);
end
for i=1:sz(1)-6
    for j=1:sz(2)-6
        grada(i,j)=((((((45*(au(i+2,j+3)-au(i+4,j+3)))-(9*(au(i+1,j+3)...
        -au(i+5,j+3)))+(au(i,j+3)-au(i+6,j+3)))/60)^2)+...
        ((((45*(au(i+3,j+2)-au(i+3,j+4)))-(9*(au(i+3,j+1)-au(i+3,j+5)))...
        +(au(i+3,j)-au(i+3,j+6)))/60)^2))^0.5)/((1/25)*0.001);
         % this is sixth order central differential scheme..
    end
end
dengrad=convergent((grada/nliqref)*(1600/rat)*...
(mean(mean(jetim(v1:v2,h1:h2)))/255));
% mdengrad=max(max(dengrad(10:300,150:240)));
mdengrad=mean(mean(dengrad(18:24,180:186)))*1.4;
```

```
ndengrad=dengrad*(255/mdengrad);
figure(16);
imshow(uint8(ndengrad));

bw=[-4   0    ccbf 60   85   115  155   210   245   265   280
300];
r=([255  255  255  0    0    70   255   285   285   285   280
2500]);
g=([255  255  255  0    190  230  255    0    -100  -200  -300
-300]);
b=([255  255  255  255  255  70   0    -100  -200  -300  -400
-400]);
ln=length(bw);
[ro co]=size(ndengrad);
rmat=zeros(ro,co);
gmat=zeros(ro,co);
bmat=zeros(ro,co);
rgb=ones(ro,co,3);
for i=1:ln
u=ones(ro,co,1);
v=ones(ro,co,ln);
for j=1:ln
  if i==j
v(:,:,i)=1*u;
  else
v(:,:,i)=((ndengrad-bw(j))/(bw(i)-bw(j))).*u(:,:,1);
  end
u(:,:,1)=v(:,:,i);
end
rmat=(r(i)*v(:,:,i))+rmat;
gmat=(g(i)*v(:,:,i))+gmat;
bmat=(b(i)*v(:,:,i))+bmat;
end
rgb(:,:,1)=rmat;
rgb(:,:,2)=gmat;
rgb(:,:,3)=bmat;
figure(17)
```

```
imshow(uint8(rgb))
for i=0:88:ro-1
text(335,i+14,num2str(convergent(-i/22)),'Fontsize',14);
end
%%%
for i=198:66:396
text(i,-26,num2str(convergent((i-198)/22)),'Fontsize',14);
end
for i=0:66:132
text(i,-26,num2str(convergent(9-(i/22))),'Fontsize',14);
end
%%%
for i=0:66:co-1
text(i-4,0,'|','Fontsize',8);
end
grid on;
saveas(gcf,strcat('C:\All datas\circularjetprocessed\dengrad.png'));
grid on
%%%%%%%%%%%%%%%%%%%%%%%%%%%%%%%%%%%%%%%%%%%%%%%%%%%%%%%%%%%%%%%%%%%%%%%%%%%%
% color bar for density gradient field
colbar1=ag(40:2040,2130:2143);
colbar=[colbar1 colbar1];
cmxim=max(max(colbar));
[row,col]=size(colbar);
c=((colbar*255)/cmxim);
bw=[-4   0    ccbf 60   85   115  155   210   245   265   280
300];
r=([255  255  255  0    0    70   255   285   285   285   280
2500]);
g=([255  255  255  0    190  230  255    0    -100  -200  -300
-300]);
b=([255  255  255  255  255  70   0    -100  -200  -300  -400
-400]);
ln=length(bw);
[ro co]=size(colbar);
rmat=zeros(ro,co);
gmat=zeros(ro,co);
```

```
bmat=zeros(ro,co);
rgb=ones(ro,co,3);
for i=1:ln
u=ones(ro,co,1);
v=ones(ro,co,ln);
for j=1:ln
  if i==j
v(:,:,i)=1*u;
  else
v(:,:,i)=((c-bw(j))/(bw(i)-bw(j))).*u(:,:,1);
  end
u(:,:,1)=v(:,:,i);
end
rmat=(r(i)*v(:,:,i))+rmat;
gmat=(g(i)*v(:,:,i))+gmat;
bmat=(b(i)*v(:,:,i))+bmat;
end
black=zeros(4,co);
rgb(1:ro,1:co,1)=rmat;
rgb(ro+1:ro+4,1:co,1)=black;
rgb(1:ro,1:co,2)=gmat;
rgb(ro+1:ro+4,1:co,2)=black;
rgb(1:ro,1:co,3)=bmat;
rgb(ro+1:ro+4,1:co,3)=black;
figure(18)
imshow(uint8(rgb))
cc=c(:,1);
densgrad=convergent(-1*(cc/255)*mdengrad*(1/1000));
% since the digit is longer it is
divided by 1000 and will be written as E3 in color bar
for i=0:200:length(cc)-1
text(30,i,num2str(densgrad(i+1)),'Fontsize',12);
end
grid on
saveas(gcf,strcat('C:\All datas\circularjetprocessed\dengrad-colbar.png'))
```

APPENDIX C

DRAWINGS OF HIGH PRESSURE CHAMBER

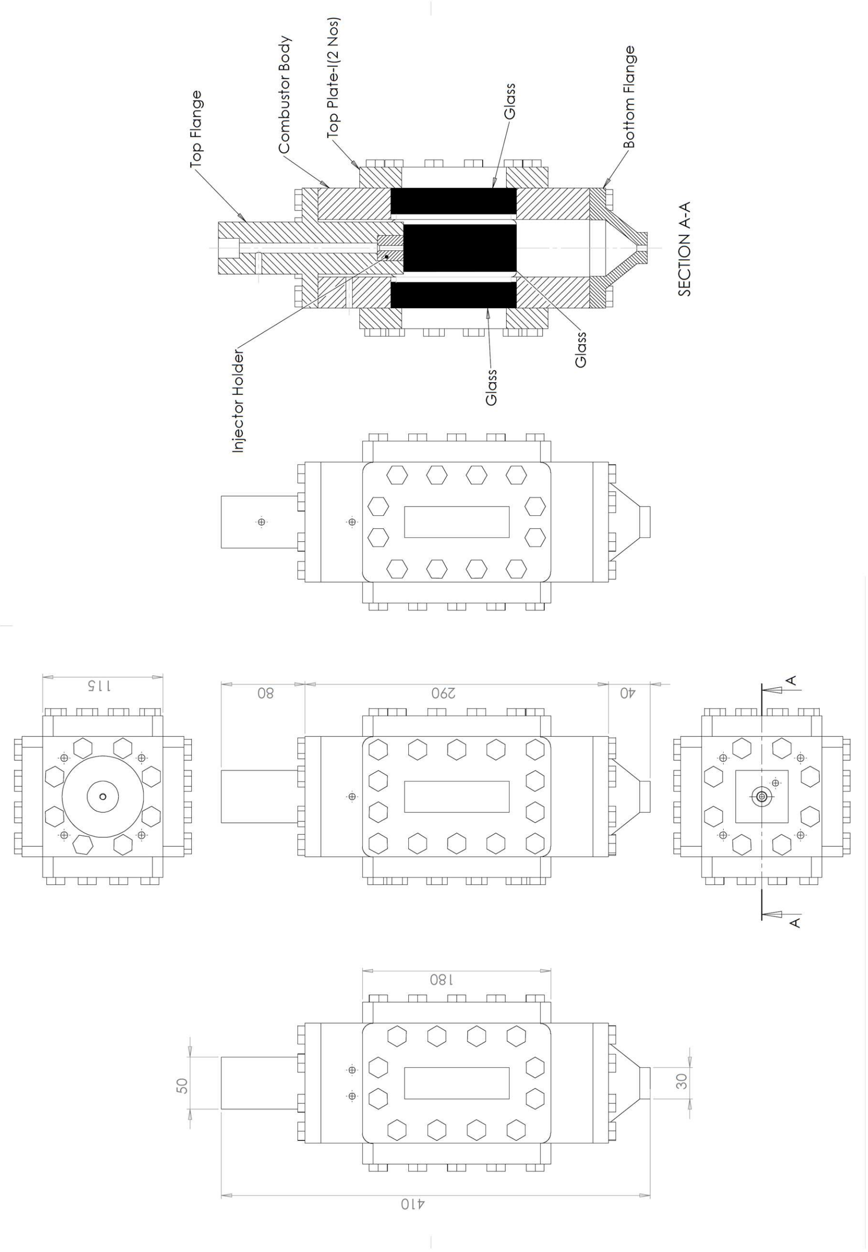

Figure C.1 High pressure chamber assembly.

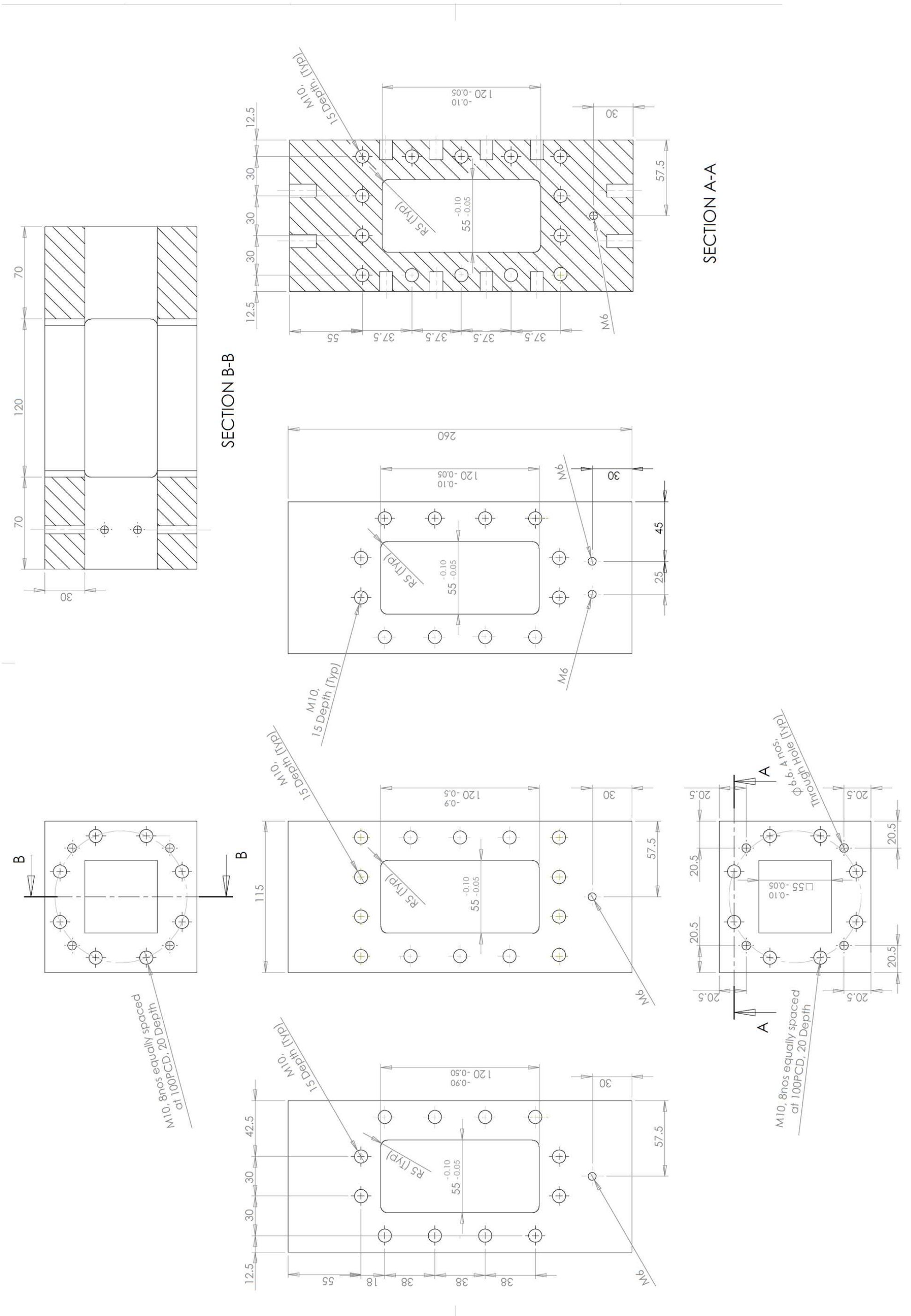

Figure C.2 Main body of the high pressure chamber.

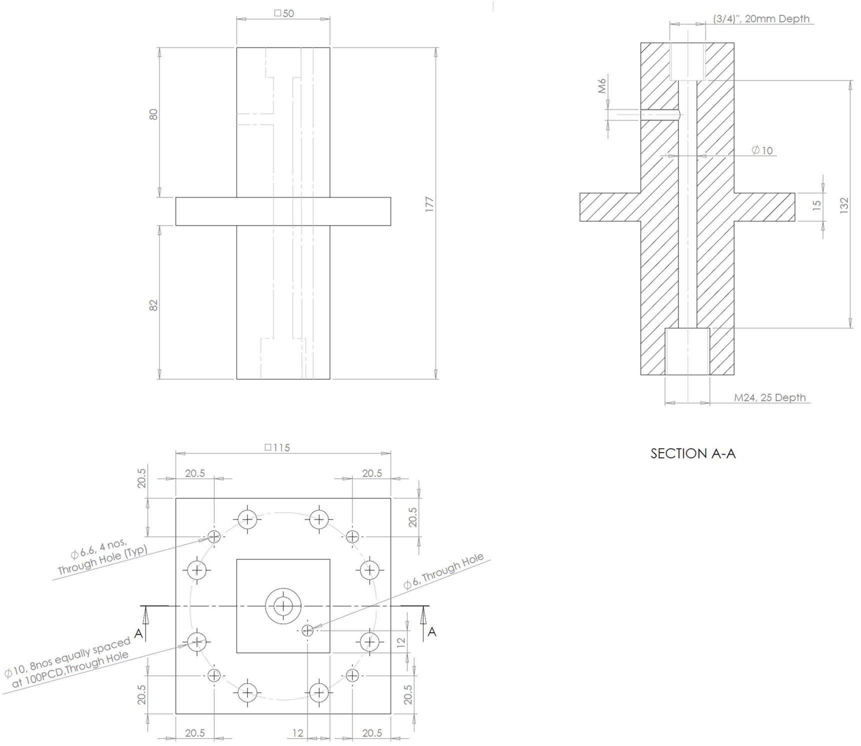

Figure C.3 Injector head of the high pressure chamber.

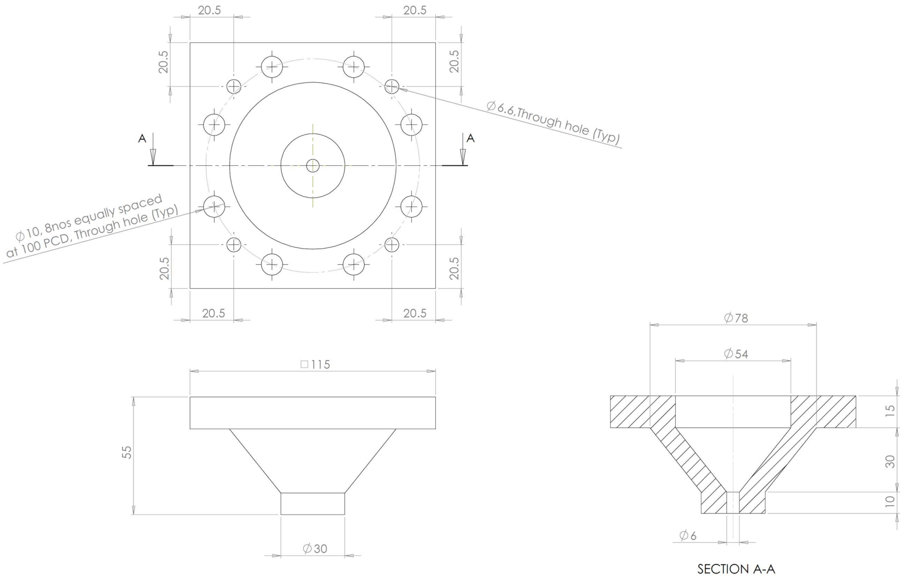

Figure C.4 Bottom flow exit of the high pressure chamber.

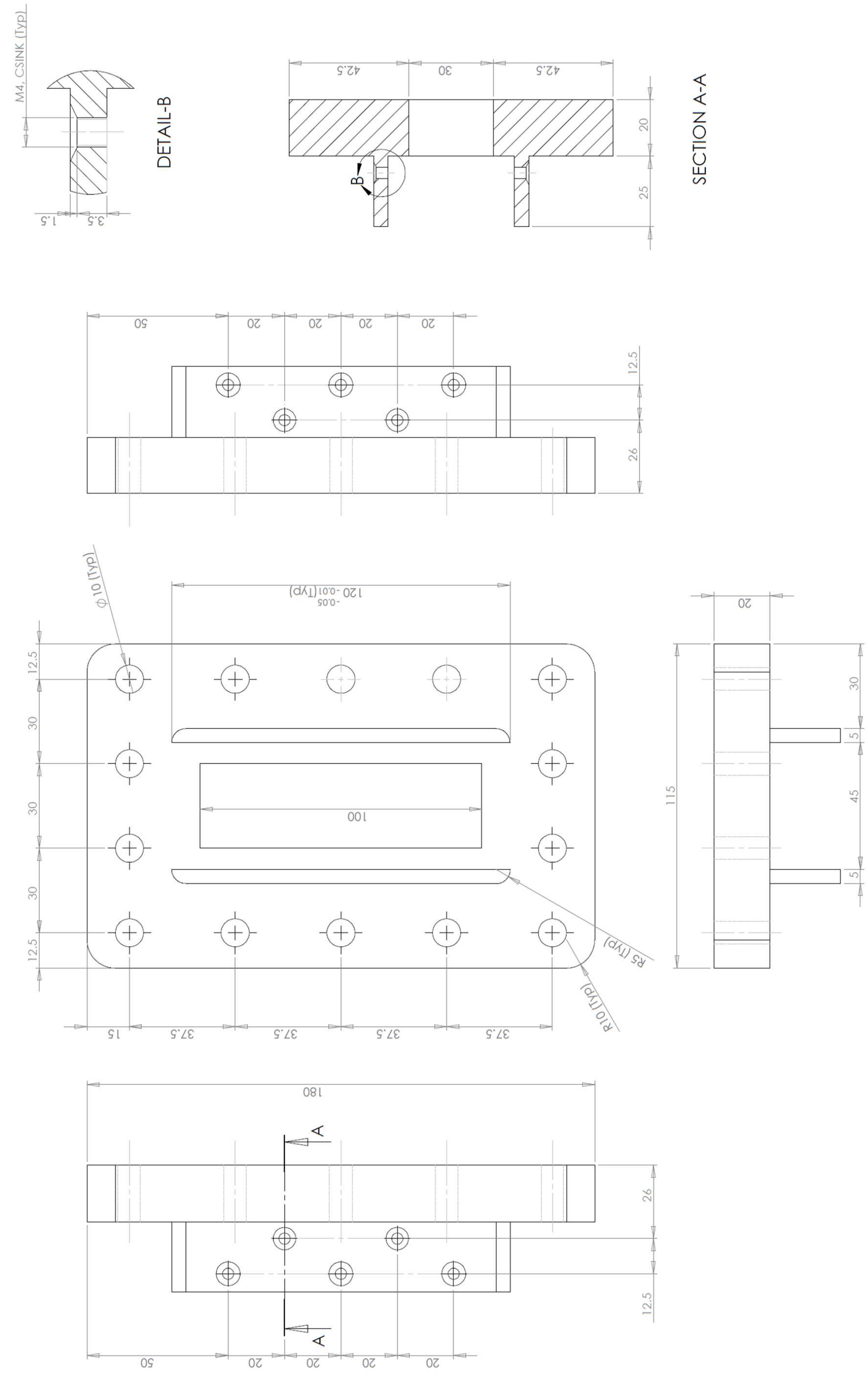

Figure C.5 Side flange of the chamber with provision for optical access.

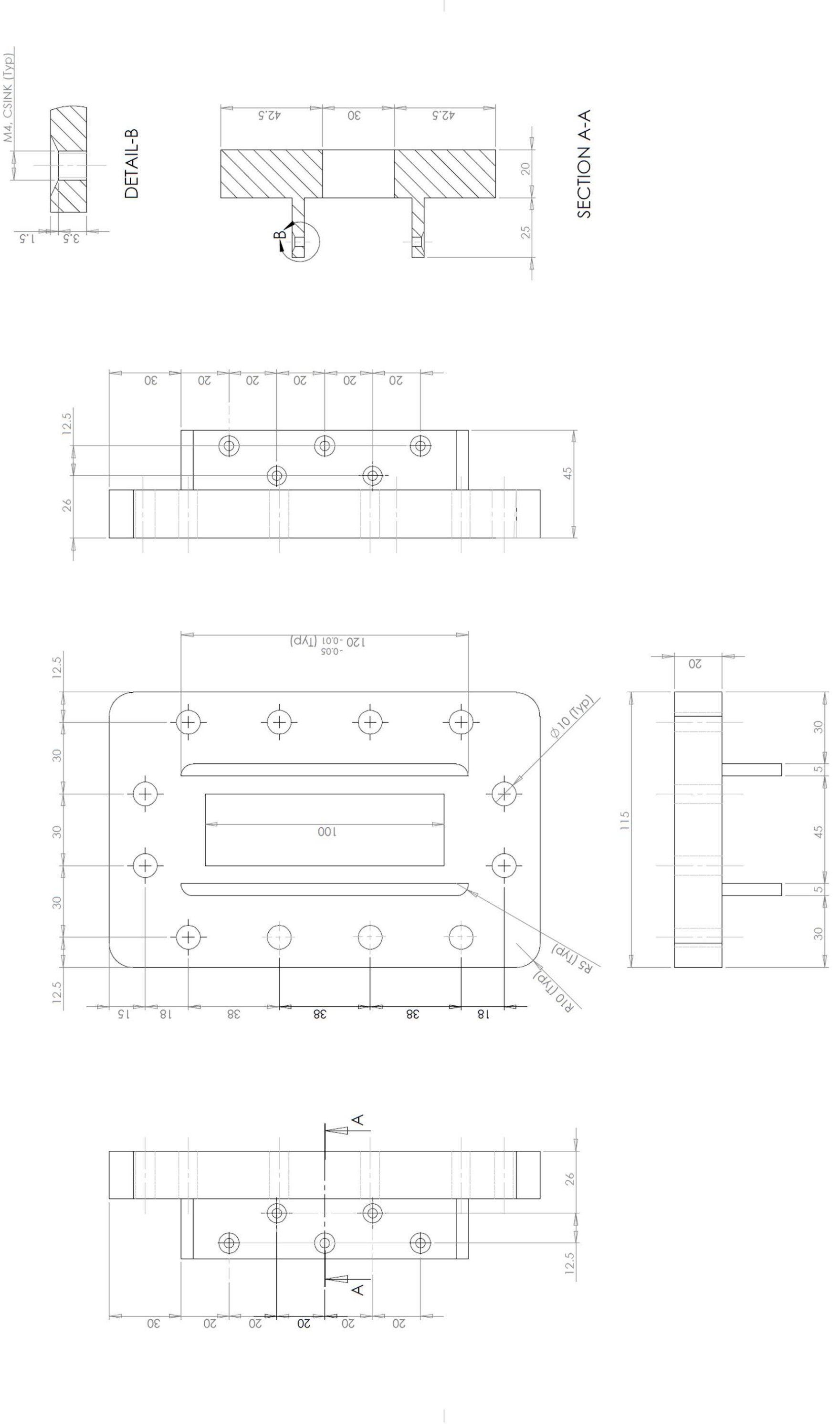

Figure C.6 Side flange of the chamber with provision for optical access.

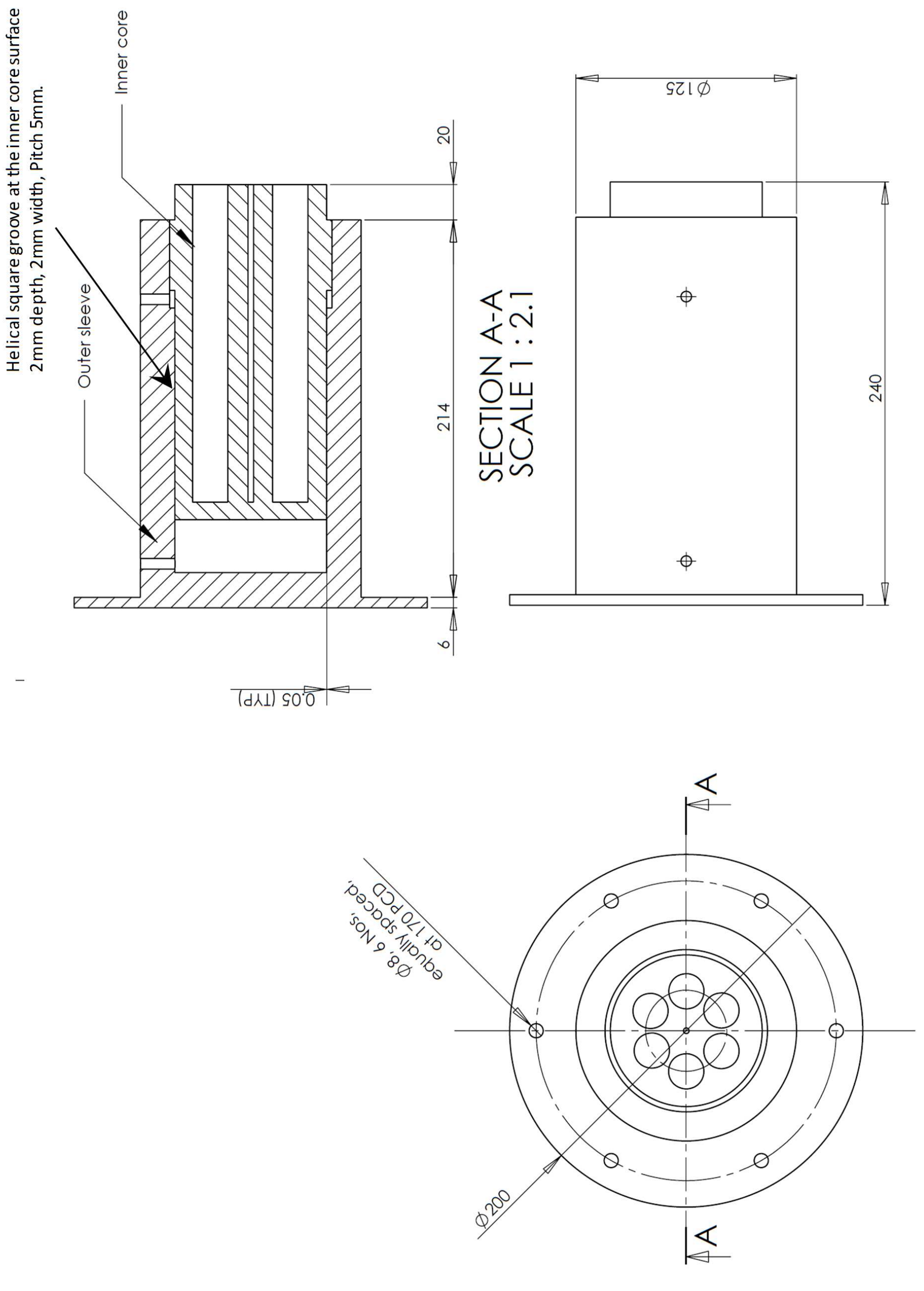

Figure C.7 Liquid heater assembly.

REFERENCES

1. Abdel-Hameed, H. and Bellan, J. (2002). Direct numerical simulations of two-phase laminar jet flows with different cross-section injection geometries. *Physics of Fluids (1994-present)*, 14(10):3655–3674.

2. Aifantis, E. C. and Serrin, J. B. (1983). The mechanical theory of fluid interfaces and maxwell's rule. *Journal of colloid and interface science*, 96(2):517–529.

3. Ambravaneswaran, B., Subramani, H. J., Phillips, S. D., and Basaran, O. A. (2004). Dripping-jetting transitions in a dripping faucet. *Physical review letters*, 93(3):034501.

4. Amini, G. and Dolatabadi, A. (2012). Axis-switching and breakup of low-speed elliptic liquid jets. *International Journal of Multiphase Flow*, 42:96–103.

5. Anderson, W. and Yang, V. (1995). *Liquid rocket engine combustion instability*, volume 169. Aiaa.

6. Balaji, B., Raghavan, V., Ramamurthi, K., and Gogos, G. (2011). A numerical study of evaporation characteristics of spherical n-dodecane droplets in high pressure nitrogen environment. *Physics of Fluids (1994-present)*, 23(6):063601.

7. Becher, P. (1990). The so-called ohnesorge equation. *Journal of colloid and interface science*, 140(1):299–301.

8. Bechtel, S. E. (1989). The oscillation of slender elliptical inviscid and newtonian jets: Effects of surface tension, inertia, viscosity, and gravity. *Journal of applied mechanics*, 56(4):968–974.

9. Bechtel, S. E., Cooper, J. A., Forest, M. G., Petersson, N. A., Reichard, D. L., Saleh, A., and Venkataramanan, V. (1995). A new model to determine dynamic surface

tension and elongational viscosity using oscillating jet measurements. *Journal of Fluid Mechanics*, 293:379–403.

10. Bellan, J. (2000). Supercritical (and subcritical) fluid behavior and modeling: drops, streams, shear and mixing layers, jets and sprays. *Progress in energy and combustion science*, 26(4):329–366.

11. Bohr, N. (1889). Determination of dynamic surface tension by the method of jet vibration. *Phil. Trans. R. Soc. London*, 209:281–317.

12. Briggs, R. J. (1964). Electron-stream interaction with plasmas.

13. Brown, G. L. and Roshko, A. (1974). On density effects and large structure in turbulent mixing layers. *Journal of Fluid Mechanics*, 64(04):775–816.

14. Cengel, Y. A., Boles, M. A., and Kanoglu, M. (1998). *Thermodynamics: an engineering approach*, volume 1056. McGraw-Hill New York.

15. Chandrasekhar, S. (1970). *Hydrodynamic and hydromagnetic stability*, volume 196. Clarendon Press Oxford.

16. Chaté, H., Villermaux, E., and Chomaz, J. M. (2012). *Mixing: chaos and turbulence*, volume 373. Springer Science & Business Media.

17. Chehroudi, B. (2012). Recent experimental efforts on high-pressure supercritical injection for liquid rockets and their implications. *International Journal of Aerospace Engineering*, 2012.

18. Chehroudi, B., Cohn, R., and Talley, D. (2002a). Cryogenic shear layers: experiments and phenomenological modeling of the initial growth rate under subcritical and supercritical conditions. *International journal of heat and fluid flow*, 23(5):554–563.

19. Chehroudi, B., Talley, D., and Coy, E. (1999). Fractal geometry and growth rate changes of cryogenic jets near the critical point, aiaa 99-2489. In *35th Joint Propulsion Conference, Los Angeles, CA*.

20. Chehroudi, B., Talley, D., and Coy, E. (2002b). Visual characteristics and initial growth rates of round cryogenic jets at subcritical and supercritical pressures. *Physics of Fluids (1994-present)*, 14(2):850–861.

21. Chigier, N. and Reitz, R. D. (1996). Regimes of jet breakup and breakup mechanisms- physical aspects. *Recent advances in spray combustion: Spray atomization and drop burning phenomena.*, 1:109–135.

22. Clerk-Maxwell, J. (1875). On the dynamical evidence of the molecular constitution of bodies. *Nature*, 11:357–359.

23. Crighton, D. G. (1973). Instability of an elliptic jet. *Journal of Fluid Mechanics*, 59(04):665–672.

24. Dahms, R. N. and Oefelein, J. C. (2013). On the transition between two-phase and single-phase interface dynamics in multicomponent fluids at supercritical pressures. *Physics of Fluids (1994-present)*, 25(9):092103.

25. Davidson, P. A. (2015). *Turbulence: an introduction for scientists and engineers*. Oxford University Press, USA.

26. Davis, H. T. and Scriven, L. E. (1982). Stress and structure in fluid interfaces. *Adv. Chem. Phys*, 49:357–454.

27. Donnelly, R. J. and Glaberson, W. (1966). Experiments on the capillary instability of a liquid jet. In *Proceedings of the Royal Society of London A: Mathematical, Physical and Engineering Sciences*, volume 290, pages 547–556. The Royal Society.

28. Dumouchel, C. (2008). On the experimental investigation on primary atomization of liquid streams. *Experiments in fluids*, 45(3):371–422.

29. Essick, J. (2012). *Hands-on introduction to LabVIEW for scientists and engineers*. Oxford University Press.

30. Faeth, G. M. (1977). Current status of droplet and liquid combustion. *Progress in Energy and Combustion Science*, 3(4):191–224.

31. Gaster, M. (1962). A note on the relation between temporally-increasing and spatially-increasing disturbances in hydrodynamic stability. *Journal of Fluid Mechanics*, 14(02):222–224.

32. Geer, J. F. and Strikwerda, J. C. (1983). Vertical slender jets with surface tension. *Journal of Fluid Mechanics*, 135:155–169.

33. Givler, S. D. and Abraham, J. (1996). Supercritical droplet vaporization and combustion studies. *Progress in Energy and combustion Science*, 22(1):1–28.

34. Gopal, E. S. R. (2000). Critical opalescence. *Resonance*, 5(4):37–45.

35. Greiner, W., Neise, L., and Stöcker, H. (1995). *Thermodynamics and statistical mechanics*. Springer.

36. Gustavsson, J. and Segal, C. (2008). Characterization of a perfluorinated ketone for lif applications. In *46th AIAA Aerospace Sciences Meeting and Exhibit*, pages 7–10.

37. Gustavsson, J. P. and Segal, C. (2007). Fluorescence spectrum of 2-trifluoromethyl-1, 1, 1, 2, 4, 4, 5, 5, 5-nonafluoro-3-pentanone. *Applied spectroscopy*, 61(8):903–907.

38. Gutmark, E. and Grinstein, F. F. (1999). Flow control with noncircular jets. *Annual review of fluid mechanics*, 31(1):239–272.

39. Gutmark, E. and Ho, C. M. (1986). Visualization of a forced elliptic jet. *AIAA journal*, 24(4):684–685.

40. Hanson, R. K., Seitzman, J. M., and Paul, P. H. (1990). Planar laser-fluorescence imaging of combustion gases. *Applied Physics B*, 50(6):441–454.

41. Harstad, K. and Bellan, J. (2001). Evaluation of commonly used assumptions for isolated and cluster heptane drops in nitrogen at all pressures. *Combustion and flame*, 127(1):1861–1879.

42. Heidorn, D., Steiner, H., and Brenn, G. (2008). Modelling of the fractal dimension in the primary atomization of high-speed liquid jets. In *ILASS08-P-8 2008 Como, Italy*.

43. Ho, C. M. and Gutmark, E. (1987). Vortex induction and mass entrainment in a small-aspect-ratio elliptic jet. *Journal of Fluid Mechanics*, 179:383–405.

44. Hoyt, J. W. and Taylor, J. (1978). Elliptical water jets. *AIAA Journal*, 16(1):85–87.

45. Huerre, P. and Monkewitz, P. (1985). Absolute and convective instabilities in free shear layers. *Journal of Fluid Mechanics*, 159:151–168.

46. Hussain, F. and Husain, H. S. (1989). Elliptic jets. part 1. characteristics of unexcited and excited jets. *Journal of Fluid Mechanics*, 208:257–320.

47. Ibrahim, E. A. and Marshall, S. O. (2000). Instability of a liquid jet of parabolic velocity profile. *Chemical Engineering Journal*, 76(1):17–21.

48. Instruction Manual, DG535 digital delay generator, Stanford research systems (http://www.thinksrs.com).

49. Instruction Manual, Imager Pro X 4M CCD camera, Lasion (http://www.lavision.de).

50. Instruction Manual, Micromotion Coriolis Elite sensor, Emerson process management (http://www.emersonprocess.com).

51. Instruction Manual, Mixed signal oscilloscope DLM2000 Yokogawa (http://www.yokogawa.com).

52. Instruction Manual, National Instruments (http://www.ni.in).

53. Instruction Manual, Pulsed Nd-YAG laser for PIV, Spectra-Physics (http://www.spectra-physics.com).

54. Jin, G., Tian, R., Song, X., and Wu, W. (2010). Theoretical and experimental studies of droplet evaporation in high-temperature air.

55. Kasyap, T. V., Sivakumar, D., and Raghunandan, B. N. (2009). Flow and breakup characteristics of elliptical liquid jets. *International journal of multiphase flow*, 35(1):8–19.

56. Keller, J. B., Rubinow, S. I., and Tu, Y. O. (1973). Spatial instability of a jet. *Physics of Fluids*, 16(12):2052–2055.

57. Law, C. K. (1982). Recent advances in droplet vaporization and combustion. *Progress in energy and combustion science*, 8(3):171–201.

58. Lefebvre, A. (1988). *Atomization and sprays*, volume 1040. CRC press.

59. Leib, S. J. and Goldstein, M. E. (1986). Convective and absolute instability of a viscous liquid jet. *Physics of Fluids (1958-1988)*, 29(4):952–954.

60. Levich, V. G. (1962). *Physicochemical hydrodynamics*, volume 689. Prentice-hall Englewood Cliffs, NJ.

61. Lin, K. C., Cox-Stouffer, S. K., and Jackson, T. A. (2006). Structures and phase transition processes of supercritical methane/ethylene mixtures injected into a subcritical environment. *Combustion science and technology*, 178(1-3):129–160.

62. Lin, S. P. (2003). *Breakup of liquid sheets and jets*. Cambridge University Press.

63. Lin, S. P. and Creighton, B. (1990). Energy budget in atomization. *Aerosol Science and Technology*, 12(3):630–636.

64. Lin, S. P. and Kang, D. J. (1987). Atomization of a liquid jet. *Physics of Fluids (1958-1988)*, 30(7):2000–2006.

65. Lin, S. P. and Lian, Z. W. (1989). Absolute instability of a liquid jet in a gas. *Physics of Fluids A: Fluid Dynamics (1989-1993)*, 1(3):490–493.

66. Lin, S. P. and Reitz, R. D. (1998). Drop and spray formation from a liquid jet. *Annual Review of Fluid Mechanics*, 30(1):85–105.

67. Lovejoy, S. (1982). Area-perimeter relation for rain and cloud areas. *Science*, 216(4542):185–187.

68. Mandelbrot, B. B. (1983). *The fractal geometry of nature*, volume 173. Macmillan.

69. Mandelbrot, B. B. and Blumen, A. (1989). Fractal geometry: What is it, and what does it do?[and discussion]. In *Proceedings of the Royal Society of London A: Mathematical, Physical and Engineering Sciences*, volume 423, pages 3–16. The Royal Society.

70. Manrique, J. A. and Borman, G. L. (1969). Calculations of steady state droplet vaporization at high ambient pressures. *International Journal of Heat and Mass Transfer*, 12(9):1081–1095.

71. Martin, G. D., Hoath, S. D., and Hutchings, I. M. (2008). Inkjet printing-the physics of manipulating liquid jets and drops. In *Journal of Physics: Conference Series*, volume 105, page 012001. IOP Publishing.

72. Matson, D. W., Fulton, J. L., Petersen, R. C., and Smith, R. D. (1987). Rapid expansion of supercritical fluid solutions: solute formation of powders, thin films, and fibers. *Industrial & engineering chemistry research*, 26(11):2298–2306.

73. Mayer, W., Schik, A., Sch-aring, M., ffler, and Tamura, H. (2000). Injection and mixing processes in high-pressure liquid oxygen/gaseous hydrogen rocket combustors. *Journal of Propulsion and Power*, 16(5):823–828.

74. McKinley, G. H. and Renardy, M. (2011). Wolfgang von ohnesorge. *Physics of Fluids (1994-present)*, 23(12):127101.

75. Newman, J. A. and Brzustowski, T. A. (1971). Behavior of a liquid jet near the thermodynamic critical region. *AIAA journal*, 9(8):1595–1602.

76. Ohnesorge, W. V. (1936). Formation of drops by nozzles and the breakup of liquid jets. *Z. Angew. Math. Mech*, 16(4):355–358.

77. Oschwald, M., Smith, J. J., Branam, R., Hussong, J., Schik, A., Chehroudi, B., and Talley, D. (2006). Injection of fluids into supercritical environments. *Combustion Science and Technology*, 178(1-3):49–100.

78. Owens, J. G. (2002). Physical and environmental properties of a next generation extinguishing agent. In *proceedings of 12th Halon Options Technical Working Conference, R. Gann and P. Reneke, editors, National Institute of Standards and Technology, US Department of Commerce, Gaithersberg, MD*.

79. Pan, Y. u. and Suga, K. (2006). A numerical study on the breakup process of laminar liquid jets into a gas. *Physics of Fluids (1994-present)*, 18(5):052101.

80. Peng, D. Y. and Robinson, D. B. (1976). A new two-constant equation of state. *Industrial & Engineering Chemistry Fundamentals*, 15(1):59–64.

81. Plateau, J. (1873). Experimental and theoretical statics of liquids subject to molecular forces only.

82. Product information, High performance pressure transducer, Omega engineering (http://www.omega.com).

83. Qiu, L. and Reitz, R. D. (2014). Simulation of supercritical fuel injection with condensation. *International Journal of Heat and Mass Transfer*, 79:1070–1086.

84. Rayleigh, L. (1878). On the instability of jets. *Proc. London Math. Soc*, 10:4–13.

85. Rayleigh, L. (1879). On the capillary phenomena of jets. In *Proc. R. Soc. London*, volume 29, pages 71–97.

86. Rayleigh, L. (1889). On the tension of recently formed liquid surfaces. *Proceedings of the Royal Society of London*, 47(286-291):281–287.

87. Rayleigh, L. (1892). Xvi. on the instability of a cylinder of viscous liquid under capillary force. *The London, Edinburgh, and Dublin Philosophical Magazine and Journal of Science*, 34(207):145–154.

88. Reitz, R. D. and Bracco, F. V. (1982). Mechanism of atomization of a liquid jet. *Physics of Fluids (1958-1988)*, 25(10):1730–1742.

89. Richardson, E. G. (1950). The formation and flow of emulsion. *Journal of Colloid Science*, 5(4):404–413.

90. Rosner, D. E. (1967). On liquid droplet combustion at high pressures. *AIAA Journal*, 5(1):163–166.

91. Roy, A., Gustavsson, J. P., and Segal, C. (2011). Spectroscopic properties of a perfluorinated ketone for plif applications. *Experiments in fluids*, 51(5):1455–1463.

92. Roy, A., Joly, C., and Segal, C. (2013). Disintegrating supercritical jets in a subcritical environment. *Journal of Fluid Mechanics*, 717:193–202.

93. Roy, A. and Segal, C. (2010). Experimental study of fluid jet mixing at supercritical conditions. *Journal of Propulsion and Power*, 26(6):1205–1211.

94. Scriven, L. E. and Pigford, R. L. (1959). Fluid dynamics and diffusion calculations for laminar liquid jets. *AIChE Journal*, 5(3):397–402.

95. Segal, C. and Polikhov, S. A. (2008). Subcritical to supercritical mixing. *Physics of Fluids (1994-present)*, 20(5):052101.

96. Sengers, J. V. (1985). Transport properties of fluids near critical points. *International journal of thermophysics*, 6(3):203–232.

97. Shavit, U. and Chigier, N. (1995). Fractal dimensions of liquid jet interface under breakup. *Atomization and Sprays*, 5(6):525–543.

98. Shen, Y. B. and Poulikakos, D. (1998). Impinging jet atomization at elevated and supercritical ambient temperature and pressure conditions. *EXPERIMENTAL HEAT TRANSFER An International Journal*, 11(1):23–40.

99. Sirignano, W. A. and Delplanque, J. P. (1999). Transcritical vaporization of liquid fuels and propellants. *Journal of Propulsion and Power*, 15(6):896–902.

100. Sirignano, W. A. and Mehring, C. (2000). Review of theory of distortion and disintegration of liquid streams. *Progress in energy and combustion science*, 26(4):609–655.

101. Sreenivasan, K. R. (1991). Fractals and multifractals in fluid turbulence. *Annual Review of Fluid Mechanics*, 23(1):539–604.

102. Sreenivasan, K. R. and Meneveau, C. J. (1986). The fractal facets of turbulence. *Journal of Fluid Mechanics*, 173:357–386.

103. Sterling, A. M. and Sleicher, C. A. (1975). The instability of capillary jets. *Journal of Fluid Mechanics*, 68(03):477–495.

104. Stryjek, R. and Vera, J. H. (1986). Prsv: An improved peng-robinson equation of state for pure compounds and mixtures. *The canadian journal of chemical engineering*, 64(2):323–333.

105. Taniguchi, N., Wallington, T. J., Hurley, M. D., Guschin, A. G., Molina, L. T., and Molina, M. J. (2003). Atmospheric chemistry of c2f5c (o) cf (cf3) 2: Photolysis and reaction with cl atoms, oh radicals, and ozone. *The Journal of Physical Chemistry A*, 107(15):2674–2679.

106. Taylor, G. (1960). Formation of thin flat sheets of water. In *Proceedings of the Royal Society of London A: Mathematical, Physical and Engineering Sciences*, volume 259, pages 1–17. The Royal Society.

107. Taylor, G. I. (1940). Generation of ripples by wind blowing over a viscous fluid. *The Scientific Papers of GI Taylor, edited by G. K. Batchelor*, 3:244–254.

108. Thomson, G. W. (1946). The antoine equation for vapor-pressure data. *Chemical reviews*, 38(1):1–39.

109. Tomotika, S. (1935). On the instability of a cylindrical thread of a viscous liquid surrounded by another viscous fluid. In *Proc. Roy. Soc. A*, volume 150, pages 322–337.

110. Turcotte, D. L. (1988). Fractals in fluid mechanics. *Annual review of fluid mechanics*, 20(1):5–16.

111. Vaidyanathan, A., Gustavsson, J. P., and Segal, C. (2009). Oxygen/hydrogen-planar-laser-induced fluorescence measurements and accuracy investigation in high-pressure combustion. *Journal of Propulsion and Power*, 25(4):864–874.

112. Valeur, B. and Berberan-Santos, M. N. (2012). *Molecular fluorescence: principles and applications*. John Wiley & Sons.

113. Weber, C. (1931). Zum zerfall eines flüssigkeitsstrahles. *ZAMM-Journal of Applied Mathematics and Mechanics/Zeitschrift für Angewandte Mathematik und Mechanik*, 11(2):136–154.

114. Woodward, R. D. and Talley, D. G. (1996). Raman imaging of transcritical cryogenic propellants. *AIAA paper*, 468:1996.

115. Wu, P. K., Shahnam, M., Kirkendall, K. A., Carter, C. D., and Nejad, A. S. (1999). Expansion and mixing processes of underexpanded supercritical fuel jets injected into superheated conditions. *Journal of Propulsion and Power*, 15(5):642–649.

116. Yang, H. Q. (1992). Asymmetric instability of a liquid jet. *Physics of Fluids A: Fluid Dynamics (1989-1993)*, 4(4):681–689.

117. Yang, J. R. and Wong, S. C. (2001). On the discrepancies between theoretical and experimental results for microgravity droplet evaporation. *International journal of heat and mass transfer*, 44(23):4433–4443.

118. Yang, V. (2000). Modeling of supercritical vaporization, mixing, and combustion processes in liquid-fueled propulsion systems. *Proceedings of the Combustion Institute*, 28(1):925–942.

119. Zaman, K. B. M. Q. (1996). Axis switching and spreading of an asymmetric jet: the role of coherent structure dynamics. *Journal of Fluid Mechanics*, 316:1–27.

120. Zappoli, B. (2003). Near-critical fluid hydrodynamics. *Comptes Rendus Mécanique*, 331(10):713–726.

121. Zhang, H., Raghavan, V., and Gogos, G. (2009). Subcritical and supercritical droplet evaporation within a zero gravity environment; on the discrepancies between theoretical and experimental results. *International Journal of Spray and Combustion Dynamics*, 1(3):317–338.

LIST OF PAPERS BASED ON THESIS

PAPERS IN REFEREED INTERNATIONAL JOURNALS

1. **Muthukumaran, C. K.**, Vaidyanathan, A (2014). Experimental study of elliptical jet from sub to supercritical conditions. ***Phys. of Fluids***, 26(4), 044104.
2. **Muthukumaran, C. K.**, Vaidyanathan, A (2015). Experimental study of elliptical jet from supercritical to subcritical conditions using planar laser induced fluorescence. ***Phys. of Fluids***, 27(3), 034109.
3. **Muthukumaran, C. K.**, Vaidyanathan, A (2016). Initial instability of round liquid jet at subcritical and supercritical environments. ***Phys. of Fluids***, 28(7), 074104.
4. **Muthukumaran, C. K.**, Vaidyanathan, A (2016). Mixing nature of supercritical jet in subcritical and supercritical conditions. ***accepted for publication in Journal of Propulsion and Power***.

PRESENTATIONS IN CONFERENCES

1. **Muthukumaran. C K.**, Aravind Vaidyanathan (2014). Flow characteristics of elliptical jet from subcritical to supercritical conditions, *22nd National and 11th international symposium on heat and mass transfer conference (ISHMT-ASME 2013).* IIT Kharagpur, December 28-31, 2013.
2. **Muthukumaran, C K.**, Kamalakannan, K, Aravind Vaidyanathan (2014). Transition in the elliptical jet characteristics from supercritical to subcritical conditions, *5nd international and 41st National conference on Fluid Mechanics and Fluid Power (FMFP).* IIT Kanpur, December 12-14, 2014.

3. **Muthukumaran, C K.**, Aravind Vaidyanathan (2015). Interfacial instabilities in laminar liquid jet at its subcritical and supercritical environments, *International heat and mass transfer conference (IHMTC 2015).* LPSC Valiyamala, December 2015.